Charles University

Faculty of Science

Department of Physical Geography and Geoecology

Doctoral thesis

Soil water dynamics in context of soil properties and climate change impact

Dynamika půdní vody v kontextu půdních vlastností a změny klimatu

Mgr. Jiří Kocum

Supervisor: RNDr. Lukáš Vlček, Ph.D.

Prague 2025

Declaration

I hereby declare that I have written this thesis independently and that I have cited all sources of information and literature used. This thesis, or any substantial part of it, has not been submitted for the award of any other or the same academic degree.

In Prague,

…….

Mgr. Jiří Kocum

Acknowledgements

I would like to express my sincere gratitude to Dr. Lukáš Vlček not only for his role as my supervisor, but also for his guidance in shaping the direction of this research, and for his valuable advice and insightful comments throughout the work on this thesis and related tasks. I am also grateful to the Institute of Hydrodynamics of the Czech Academy of Sciences, whose financial and material support was essential for the completion of this thesis. Finally, I would like to thank my family, friends and colleagues, whose unwavering support made it possible for me to complete this work.

Abstract

Soil drought has become increasingly frequent and severe due to ongoing climate change, significantly affecting hydrological and ecohydrological processes. A comprehensive understanding of soil water dynamics is essential for improving predictions of runoff generation, groundwater recharge, and vegetation responses under drought conditions. This study investigates soil water behavior across multiple spatial scales, from a pan-European perspective, through catchment and sub-catchment levels, down to the soil profile, focusing on interactions between mobile (macropore) and tightly bound (capillary) soil water. The research combined both direct and indirect methods, including conventional approaches such as measurements of soil moisture and stream temperature, as well as advanced techniques such as stable isotope analysis of hydrogen and oxygen in soil and xylem water. In addition to existing methods, novel methodological procedures were developed to improve accuracy and to allow the separation of soil water components that were previously indistinguishable. The resulting findings, often generated in collaboration with domestic and international researchers and institutions, provide valuable insights for improving hydrological predictions in headwater catchments, understanding soil–vegetation interactions, and refining isotope-enabled ecohydrological models under future climate scenarios.

Abstrakt

Půdní sucho se v důsledku probíhajících klimatických změn stává čím dál častějším a závažnějším jevem, který významně ovlivňuje hydrologické a eko-hydrologické procesy. Pro zlepšení predikcí odtoku, doplňování podzemních vod a reakce vegetace na období sucha je nezbytné komplexní porozumění dynamice půdní vody. Tato studie zkoumá chování půdní vody v různých prostorových měřítkách, a to od celoevropského pohledu, přes úroveň povodí, jeho části, až po samotný půdní profil, se zaměřením na interakce mezi mobilní (makropórovou) a pevně vázanou (kapilární) půdní vodou. Výzkum kombinuje přímé i nepřímé metody, včetně konvenčních přístupů, jako je měření vlhkosti půdy a teploty vodních toků, a pokročilých technik, jako je analýza stabilních izotopů vodíku a kyslíku v půdní a xylémové vodě. Kromě využití stávajících metod byly vyvinuty i nové metodické postupy s cílem zvýšit přesnost a umožnit oddělení dříve nerozlišitelných složek půdní vody. Získané výsledky, často vytvořené ve spolupráci s domácími i zahraničními výzkumníky a institucemi, přinášejí nové poznatky pro zlepšení predikce hydrologického chování v pramenných povodích, porozumění interakcím mezi půdní vodou a vegetací a zpřesnění eko-hydrologických modelů využívajících izotopová data v podmínkách budoucího měnícího se klimatu.

Table of Contents

1 Introduction 8

2 Climate change impact on drought 10

2.1 Drought indices 11

2.1.1 Seasonal soil moisture drought definition 11

2.1.2 Standardized Precipitation Index 11

2.1.3 Standardized Precipitation−Evapotranspiration Index 11

2.1.4 Standardized Runoff Index 12

3 Soil water dynamics 13

3.1 Artificial tracers 13

3.2 Natural tracers 13

3.3 Soil−plant−atmosphere continuum 14

3.4 Ecohydrological separation 14

4 Stable isotope analyses in ecohydrological research 16

4.1 Stable isotopes of hydrogen and oxygen 16

4.2 Fractionation factors 18

4.3 Application of stable isotopes analyses 20

4.4 Soil water extraction methods 21

5 Study sites 24

5.1 Rokytka catchment 25

5.2 Liz catchment 26

5.3 Trhové Dušníky 27

5.4 Zvěřínek 28

6 Methodology 29

6.1 Using stream water temperature as a natural tracer 29

6.2 Soil water balance model 29

6.3 Soil water extraction 29

6.3.1 Mobile soil water extraction 30

6.3.2 Tightly bound soil water extraction 31

6.4 Measurement of stable isotope composition 32

6.5 Stable isotope analysis and calculations 33

6.5.1 Line−conditioned excess 33

6.5.2 Seasonal trends and the mean residence time calculations 34

6.5.3 Seasonal Origin Index 35

7 Results 36

7.1 Dynamics of soil moisture under two dominant tree species....38
7.2 Temperature−based analysis of runoff formation dynamics in various soil types....69
7.3 Stable isotope−based analysis of seasonal runoff dynamics in a mountain peat bog 84
7.4 A new laboratory approach to extract soil water 125
7.5 Pan−European dataset of soil and stem xylem water isotopes 144
7.6 Partitioning and dynamics of mobile and tightly bound soil water 178
8 Conclusions 209
9 References....211

1 Introduction

Ongoing climate change, characterized by an increasing frequency and severity of hydroclimatic extremes, exerts profound impacts on both human societies and ecosystems, as well as on the processes governing their functioning. Observable manifestations include rising air temperatures and a reduction in snow cover (Musselman et al., 2017; Marty et al., 2017; Jenicek et al., 2018; Willibald et al., 2020), a shift from snowfall to rainfall during the winter season (Safeeq et al., 2016; Harpold et al., 2017), and alterations in the total amount of precipitation and its intra-annual distribution (Samaniego et al., 2018; Gebrechorkos et al., 2025). Such hydrological changes influence not only the availability of water for vegetation and human consumption (Wheeler and von Braun, 2013; Padrón et al., 2013), but also water quality, with potentially severe ecological consequences (Whitehead et al., 2009; van Vliet et al., 2013). Equally critical are effects on plant-available water in lowland ecosystems, particularly during the latter part of the growing season when drought stress is most pronounced (Mankin et al., 2019; Qin et al., 2020). This has heightened interest in the role of snowpack water storage and runoff generation in snow-dominated catchments, which are essential for groundwater recharge and the replenishment of soil moisture (Jenicek et al., 2016, 2020, 2021; Musselman et al., 2017; Šípek et al., 2021).

The hydrological cycle is projected to intensify with ongoing global warming, likely leading to increased intensity of extreme precipitation events and a heightened risk of flooding (Tabari, 2020; Peleg et al., 2025), as well as more frequent and intense drought periods (Qin et al., 2020). Drought is among the most prevalent and complex natural hazards, with far-reaching effects on the environment, economies, and populations worldwide (Sheffield at el., 2012; Trenberth et al., 2014; Pokhrel et al., 2021; Chiang et al., 2021). Over the past three decades, droughts have contributed to a persistent decline in vegetation-accessible water (Jiao et al., 2021), and concerns about potential future water shortages are increasing across many regions (Iglesias et al., 2007; Roudier et al., 2014; Mancosu et al., 2015; Gosling and Arnell, 2016; Mekonnen and Hoekstra, 2016). A comprehensive understanding of these climate changes is therefore essential for predicting runoff formation, soil water dynamics, and groundwater recharge, as well as vegetation responses and adaptive strategies under increasingly frequent and severe drought conditions.

This thesis aims to contribute to a more comprehensive understanding of soil water dynamics. The investigation initially employed conventional soil moisture monitoring

techniques. This was subsequently complemented by tracer-based approaches, including the use of water temperature and, later, the stable isotope analysis of hydrogen and oxygen, which formed the methodological basis for the majority of this thesis. These methods were applied at both the catchment scale, to investigate large-scale hydrological responses, and at a finer spatial resolution within the soil profile, with particular emphasis on the dynamics of water movement through macropores versus capillary pores, and on distinguishing mobile from tightly bound soil water fractions.

The submitted thesis is structured around the following specific objectives:

a) Assess seasonal variation in soil water regime under two dominant tree species in a montane forest ecosystem of Central Europe (section 7.1).
b) Investigate the dynamics of runoff generation on slopes with mineral and peat soils, employing tracer experiments utilizing water temperature and stable isotopes of hydrogen and oxygen as tracers (section 7.2 and 7.3).
c) Develop a new approach to extract soil water for stable isotope analysis (section 7.4).
d) Contribute to the establishment of a comprehensive pan-European database containing isotope data of soil and xylem water (section 7.5).
e) Evaluate the annual course of the isotopic composition of mobile and tightly bound soil water across the elevation gradient with regard to the decrease in snow cover and precipitation in general (section 7.6).

2 Climate change impact on drought

Anthropogenic warming intensifies soil moisture droughts by accelerating the terrestrial water cycle, thereby posing substantial risks to food security, freshwater availability, and ecosystem resilience (Tabari, 2020; Chen and Yuan, 2024; Peleg et al., 2025). Droughts and heatwaves, particularly when manifesting as compound events, have been linked to severe agricultural losses (Mankin et al., 2019; Qin et al., 2020), widespread forest mortality (Zhang et al., 2017; McMahon, et al., 2019; Liu et al., 2023), and drinking water shortages (Iglesias et al., 2007; Roudier et al., 2014; Mancosu et al., 2015; Gosling and Arnell, 2016; Mekonnen and Hoekstra, 2016). Their onset is often associated with persistent anticyclonic circulation patterns that promote low relative humidity, elevated air temperatures, and reduced cloud cover (Karl et al., 2012). These conditions increase atmospheric evaporative demand, initially enhancing soil water loss through evaporation and stimulating plant transpiration (Karl et al., 2012; Teuling et al., 2013; Liu et al., 2015).

The precipitation deficits (*meteorological drought*) and raising potential evapotransporation can result in a sustained depletion of soil water storage (*agricultural drought*), with subsequent adverse effects on hydrological systems (*hydrological drought*) (Liu et al., 2015). As meteorological droughts or heatwaves progress, the evaporative response of ecosystems becomes less straightforward: once soil moisture falls below a critical threshold, evaporation rates may decline (Seneviratne et al., 2010). The influence of soil water storage on land evaporation, particularly transpiration, has been the subject of extensive investigation for decades (Jarvis, 1976). However, despite its central role in land–atmosphere coupling, the fundamental controls governing this relationship remain insufficiently understood (Powell et al., 2013; Verhoef and Egea, 2014; Combe et al., 2016).

Both elevated temperatures and extreme precipitation events adversely affect soil water storage. Increased temperatures enhance evapotranspiration during the summer season, while a shift from snowfall to rainfall in winter alters the seasonal water input. Intense rainfall events frequently exceed the soil's infiltration capacity, resulting in rapid surface runoff rather than groundwater recharge. These hydrological alterations impact not only water availability for vegetation and human consumption (Wheeler and von Braun, 2013; Padrón et al., 2013) but also degrade water quality, potentially leading to severe ecological consequences (Whitehead et al., 2009; van Vliet et al., 2013). To monitor, analyze, and quantify drought severity related to these changes, several indices have been developed.

2.1 Drought indices

2.1.1 Seasonal soil moisture drought definition

The drought index used to identify seasonal soil moisture droughts is calculated from the percentile of total column soil moisture. For each calendar month, the soil moisture values from the same month over a preceding 30-year period are used to establish the baseline climatology for percentile computation. This climatology is derived from a 360-month record (30 years × 12 months). A seasonal drought event is defined as a period during which the soil moisture percentile remains below a specified threshold for at least three consecutive months. Thresholds of 30%, 20%, and 10% correspond to moderate, severe, and extreme drought, respectively (Yuan and Wood, 2013; Chen and Yuan, 2024).

2.1.2 Standardized Precipitation Index

The standardized precipitation index (SPI), developed by McKee et al. (1993), relies solely on precipitation data. A distinctive feature of the SPI is its applicability across multiple temporal scales, enabling its use in both short-term and long-term hydrological assessments. The SPI quantifies drought and wetness conditions relative to a historical baseline, with positive values indicating wetter-than-average conditions and negative values corresponding to drier-than-average conditions. SPI values are expressed in terms of standard deviations from the mean precipitation. For instance, an SPI value of -1.0 corresponds to a drought event one standard deviation below the mean, whereas an SPI value of +1.0 represents a wet period one standard deviation above the mean.

2.1.3 Standardized Precipitation-Evapotranspiration Index

The standardized Precipitation-evapotranspiration index (SPEI), developed by Vicente-Serrano et al. (2010), is a multiscalar drought index that integrates both precipitation and potential evapotranspiration (PET) to quantify dry and wet periods. Unlike traditional precipitation-based index SPI, the SPEI accounts for the temperature-driven component of the water balance, making it more sensitive to climate change, particularly global warming. This index enables the detection of drought events caused not only by precipitation deficits but also by increased evaporative demand associated with higher temperatures.

2.1.4 Standardized Runoff Index

The standardized runoff index (SRI), developed by Shukla and Wood (2008), is derived by transforming streamflow data into a standardized normal distribution, analogous to the SPI, but with a focus on runoff rather than precipitation. The SRI facilitates the assessment of the severity and duration of hydrological droughts. As a critical tool for water resource management, especially in drought-prone regions, the SRI quantifies dryness based on streamflow anomalies, thereby identifying periods of water scarcity. The SRI is frequently applied alongside other drought indices, such as the SPI and the SPEI, to enable a more comprehensive evaluation of drought conditions.

3 Soil water dynamics

To investigate soil water dynamics, including the extent and rate of infiltration, water retention capacity, and residence time in the soil, and thus the generation of runoff from a given area, researchers increasingly employ tracer experiments. These are now commonly used in conjunction with traditional methods such as the assessment of soil hydraulic properties through soil water retention curves (pF curves; van Genuchten, 1980; Groenevelt and Grant, 2004) and direct measurements of soil moisture (Trnka et al., 2015; Zelíková et al., under review; Yang et al., 2024).

3.1 Artificial tracers

Sprinkling experiments using sorptive dye tracers are frequently applied. Among these, Brilliant Blue FCF (BB) is arguably the most widely used dye tracer in hydrological studies. Such techniques enable the detailed investigation of runoff formation processes, including infiltration and the initiation of vertical preferential flow through macropores (Weiler and Flühler, 2004), as well as the influence of soil structure, soil type, and land use on infiltration pathways (Weiler and Flühler, 2004; Bachmair et al., 2009). They are also effective for exploring lateral preferential flow through subsurface soil pipe networks (Anderson et al., 2009; Wienhöfer et al., 2009; Vlček et al., 2017) and through organic topsoil layers or biomats (Schneider et al., 2014).

In situations where the use of artificial dye tracers is not feasible, natural tracers are commonly employed. These include stable isotopes of hydrogen and oxygen that naturally occur in the environment, as well as water temperature, which can serve as an effective tracer.

3.2 Natural tracers

The use of water temperature as a tracer was first introduced as a tool for monitoring groundwater flow (Keys and Brown, 1987; James et al., 2000). Since then, it has been widely applied in a variety of hydrological contexts, including studies of karst systems (Genthon et al., 2005; Lüthi, 2019), hyporheic exchange processes (Bianchin et al., 2010; Bhaskar et al., 2012), surface water dynamics, and runoff generation (Shanley and Peters, 1988; Brown and Hannah, 2007; Birkinshaw and Webb, 2010; Zajíček et al., 2016; Falátková et al., 2024).

Currently, the most widely used method for studying soil water dynamics involves the analysis of stable isotopes of hydrogen (^{1}H, ^{2}H) and oxygen (^{16}O, ^{17}O, ^{18}O). This trend has been largely driven by technological advances, including the widespread availability of isotope ratio mass spectrometers and, more recently, laser-based spectroscopic instruments in hydropedological laboratories worldwide.

Stable isotope analysis allows for the quantification of key hydrological metrics such as the mean residence time of water in catchments (Soulsby et al., 2000), the fraction of young water contributing to runoff (Kirchner, 2016a, 2016b), and the seasonal origin of water using indices such as the seasonal origin index (SOI, Allen et al., 2019). Moreover, isotope-based approaches are essential to ecohydrological research and play a key role in advancing our understanding of the soil–plant–atmosphere continuum.

3.3 Soil-plant-atmosphere continuum

The soil–plant–atmosphere continuum (originally introduced by Gradmann (1928), and later formalized by van den Honert (1948)) describes the movement of water from the soil, through plants, and into the atmosphere, thereby providing a more detailed representation of the hydrological cycle. Only in recent decades, however, driven by technological advances and the widespread application of stable isotope analyses of hydrogen and oxygen, has research on soil water dynamics advanced substantially beyond traditional measurements of soil moisture and assessments of soil retention and hydraulic properties to explicitly investigate this continuum. These developments have fostered the emergence of ecohydrology as a distinct interdisciplinary field. With ongoing methodological improvements, and with the discipline becoming more accessible due to reduced costs, there is increasing effort to predict runoff formation, soil water dynamics, groundwater recharge, and vegetation responses and adaptive strategies under more frequent and severe drought conditions.

3.4 Ecohydrological separation

The relationship between plant water use and local hydrology has been studied since the early 20th century (Bates et al., 1921). Pioneering studies on water transport through soils and plants were subsequently summarized in comprehensive reviews (e.g., Tinker, 1976; Weatherley, 1976; Molz, 1981). A major shift in perspective occurred when Dawson and Ehleringer (1991) demonstrated that some riparian trees primarily access deeper groundwater, rather than the

more readily available stream water. However, later work by Bond et al. (2002) appeared to challenge this finding by demonstrating diel fluctuations in stream baseflow attributable to plant transpiration, implying that plants might directly use stream-derived water. Despite this apparent contradiction, Brooks et al. (2010) showed that mobile water (represented by stream water) and tightly bound soil water (represented by the plant water) are isotopically distinct. Their results suggested that, especially during the dry season, mobile water traveling through macropores or pipes bypasses tightly bound soil water, which is instead more likely to be taken up by plants and not contribute to streamflow.

This conceptual breakthrough formed the basis for the ecohydrological separation framework, later termed the "Two Water Worlds" (TWW) hypothesis (McDonnell, 2014). Since then, the TWW hypothesis has stimulated widespread debate, with numerous studies supporting (e.g., Goldsmith et al., 2012; Evaristo et al., 2015; Hervé-Fernandez et al., 2016) or contesting (e.g., Geris et al., 2015; Vargas et al., 2017; Dubbert et al., 2019) the existence of isotopically distinct water pools for vegetation use and runoff generation. Despite ongoing refinements, the hydrological connectivity between plant-accessed water and mobile water remains a central, unresolved question in ecohydrology.

However, the study of soil water dynamics using stable isotopes requires the extraction of water from soil samples in a manner that preserves the natural isotopic composition. While obtaining isotopic signatures from liquid water sources such as precipitation, groundwater, or streamflow is relatively straightforward, the extraction of soil water remains a methodological challenge. Despite a variety of techniques that have been developed to extract water from soils it is well established that no method is universally applicable across all soil types and moisture conditions without introducing some degree of isotopic fractionation or bias (Sprenger et al., 2015a; Orlowski et al., 2018). This limitation poses a substantial challenge for the interpretation of isotope data and complicates cross-study comparisons of soil water isotope dynamics.

4 Stable isotope analyses in ecohydrological research

4.1 Stable isotopes of hydrogen and oxygen

In the observation of the hydrological cycle and its associated processes, the isotope ratios of oxygen ($^{18}O/^{16}O$) and hydrogen ($^{2}H/^{1}H$) are most commonly used. The ratio of stable isotopes in water changes due to the influence of local conditions such as air and soil temperature, humidity or soil moisture. Hence, this method is suitable for the evaluation of changes in water balance and hydrological processes within a soil profile forced by changes in climate. The isotope ratio R (Eq. 1) is the fundamental quantity defined for the quantification of stable isotopes. However, to facilitate interpretation and comparison of isotope data, the δ-notation is commonly employed (Eq. 2; Craig, 1961). This notation expresses the relative enrichment or depletion of a given sample in the heavier isotope compared to a reference standard. For water, the reference standard is Standard Mean Ocean Water (SMOW), characterized by $\delta^{18}O$ and $\delta^{2}H$ values equal to 0‰, meaning no enrichment or depletion. SMOW represents the average isotopic composition of ocean water unaffected by fractionation processes.

This standard is now synthetically produced by the International Atomic Energy Agency (IAEA) in Vienna. Therefore, it is often referred to as Vienna Standard Mean Ocean Water (VSMOW or V-SMOW). Due to the depletion of the original standard, a replacement standard (VSMOW2) was developed with isotopic compositions as close as possible to those of the original standard for both hydrogen and oxygen isotopes.

$$R = \frac{abundance\ of\ the\ minor\ isotope}{abundance\ of\ the\ major\ isotope} \quad (1)$$

e.g.: R = abundance ^{18}O / abundance ^{16}O

$$\delta^{H}X = \left(\frac{R_{sample}}{R_{standard}} - 1\right) \cdot 1\,000\ [‰] \quad (2)$$

where $\delta^{H}X$ represents the delta notation of the given element, X stands for the element and H indicates its nucleon (mass) number.

The relationship between $\delta^{2}H$ and $\delta^{18}O$ is linear and defines the so-called Global Meteoric Water Line (GMWL) (Fig. 1; Eq. 3). When this linear relationship is derived from a local series

of precipitation, it is referred to as the Local Meteoric Water Line (LMWL), which differs from the GMWL depending on the geographical location of the site.

$$\delta^2 H = 8 \cdot \delta^{18} O + d \ [‰] \quad (3)$$

where $\delta^2 H$ and $\delta^{18} O$ is the isotopic composition of meteoric water and d represents the deuterium excess, which is typically around 10 for the GMWL.

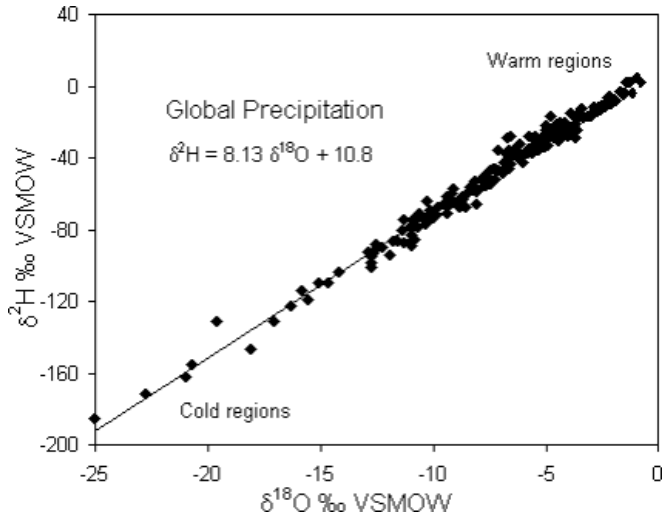

Figure 1. The relationship between $\delta^{18}O$ and δ^2H in meteoric waters. The data represent weighted annual mean precipitation values collected from monitoring stations within the IAEA's Global Network (Rozanski et al., 1993).

The GMWL was originally established by Craig (1961) based on approximately 400 samples of precipitation, river water, and lake water. This relationship has since been revisited using weighted monthly precipitation means with near-global coverage (Dansgaard, 1964; Rozanski et al., 1993), as well as stream water samples from the United States (Kendall and Coplen, 2001). While the resulting regression lines exhibited slightly different slopes, they were statistically indistinguishable from Craig's original line, confirming that the $\delta^{18}O$–δ^2H relationship is robust and accurately represents global variations in the isotopic composition of meteoric water (Gat, 1996).

The slope of the GMWL, approximately 8, reflects the different extents of isotopic fractionation affecting oxygen and hydrogen isotopes. The degree of fractionation increases

with the mass difference between isotopes of the same element. Deuterium (^{2}H or D) is roughly twice as heavy as protium (^{1}H), whereas the relative mass difference between ^{16}O and ^{18}O is about 13%. As a result, hydrogen isotopes undergo isotopic fractionation to a degree approximately eight times greater than oxygen isotopes (Craig, 1961).

The Local Meteoric Water Line is often evaluated in relation to the GMWL, which is considered to represent the expected equilibrium relationship between $\delta^{2}H$ and $\delta^{18}O$. An LMWL with a slope deviating from the canonical value of 8 may indicate equilibrium fractionation processes occurring under different temperatures or isotopic ranges (Dütsch et al., 2017), or that part of the annual precipitation is influenced by non-equilibrium processes (Dansgaard, 1964). Non-equilibrium processes can be assessed using the deuterium excess (D-ex; Eq. 3; Froehlich et al., 2002). For precipitation aligning with the GMWL, D-ex typically equals 10‰.

One common non-equilibrium process is diffusive exchange across humidity gradients, such as the evaporation of falling raindrops in dry air. In this case, the precipitation reaching the ground becomes relatively enriched in heavy isotopes, leading to a lower D-ex (Stewart, 1975), while the evaporated vapor shows a higher D-ex. If this recycled vapor contributes to subsequent rainfall, the resulting precipitation may then exhibit an elevated D-ex (Noone, 2013). This mechanism is especially relevant in tropical regions (Worden et al., 2007).

Another key non-equilibrium process is condensation within mixed-phase clouds, which contain both liquid droplets and ice particles. In such systems, ice crystals grow at the expense of supercooled water droplets. The vapor that supplies the growing ice phase is enriched in ^{2}H, which becomes reflected in the isotopic composition of precipitation derived from these clouds (Jouzel and Merlivat, 1984). As a result, higher D-ex values are often observed in solid precipitation originating from mixed-phase clouds.

4.2 Fractionation factors

Due to differences in atomic mass among isotopes, phase transitions and transport processes induce isotopic partitioning—referred to as fractionation. Isotopic fractionation encompasses a range of physico-chemical processes that cause spatial and temporal shifts in the relative abundances of isotopes within a sample. The extent to which fractionation occurs during these processes can be described by the fractionation factor, α (Eq. 4).

$$\alpha = R_A/R_B \quad (4)$$

where *R* represents the isotopic ratio of the substance prior to (A – reactant) and following (B – product) its passage through a different medium.

Two types of effects influence isotope fractionation (Thiemens et al., 2012; Bao et al., 2016):

a) Non-mass-dependent effects, and

b) Mass-dependent effects.

Non-mass-dependent processes primarily include chemical mechanisms such as photochemical reactions, nuclear spin effects, redox transitions, and molecular symmetry (Thiemens and Heidenreich, 1983; Criss and Farquhar, 2008). These effects can lead to significant deviations in the isotopic ratios, which have proven useful in atmospheric chemistry studies, cosmochemical investigations, and in identifying biological activity in plants (Blunier et al., 2002, 2012; Bao et al., 2009).

Mass-dependent fractionation includes equilibrium and kinetic fractionation, which arise due to differences in bonding energies, chemical reactivities, and thermal diffusivities of isotopically distinct molecules (Matsuhisa et al., 1978; Young et al., 2002).

Equilibrium fractionation ε^* (Eq. 5) predominantly affects evaporation processes. Heavier water isotopologues require more energy to transition into the vapor phase compared to lighter ones. Consequently, the evaporated vapor is relatively depleted in heavy isotopes, whereas the remaining liquid becomes enriched. During condensation in clouds, heavy isotopes preferentially partition into the liquid phase and precipitate more readily (Šantrůček et al., 2018).

$$\varepsilon^* = (\alpha - 1) \cdot 1000 \quad (5)$$

At 20 °C, the equilibrium fractionation factors are $\varepsilon^{*2}H$ = 84 ‰ and $\varepsilon^{*18}O$ = 9.8 ‰, indicating that water vapor is depleted in deuterium and oxygen by 84 ‰ and 9.8 ‰, respectively, compared to the source water (Majoube, 1971).

Kinetic fractionation ε_k (Eq. 6) occurs during unidirectional transport processes such as the diffusion of water vapor across boundary layers into the free atmosphere, uptake by plant

leaves, or water diffusion through plant tissues. It is governed by the ratio of molecular diffusion coefficients (D), where heavier isotopologues diffuse more slowly due to their lower mean velocities between molecular collisions at a given temperature (Šantrůček et al., 2018).

$$\varepsilon_k = \left(\frac{D_{H_2O}}{D_{HDO}} - 1\right) \cdot 1000 \quad (6)$$

In recent decades, stable water isotopes have been widely adopted as natural tracers in ecological, soil, and hydrological research. Isotopic fractionation during evaporation and condensation results in measurable shifts in isotopic composition, enabling water to serve as a natural tracer of hydrological processes (Araguás-Araguás et al., 1995; Unkovich et al., 2001). This approach is particularly valuable for studying, for example, the soil water dynamics. Alternative methods include artificial tracers (Käss, 1998) and noble gas tracers (Jankovec et al., 2017).

4.3 Application of stable isotopes analyses

Thanks to the increased accessibility of technologies for measuring stable isotopes of hydrogen and oxygen, driven by advances in laser spectroscopy, declining costs, and the corresponding shift away from mass spektrometry, their applications in ecohydrology have expanded significantly. These isotopes serve as powerful natural tracers, enabling the study of flow processes in the vadose zone (Weiler et al., 2003; Garvelmann et al., 2012; Mueller et al., 2014). They facilitate the identification of precipitation source water, characterization of runoff generation, estimation of water residence time in catchments, and determination of water age (McDonnell et al., 2010; Penna and van Meerveld, 2019; Sprenger et al., 2019). Further applications include the investigation of connectivity within lake systems (Falátková et al., 2020), as well as hydrograph separation and hydrological model calibration (McGuire et al., 2006; Birkel et al., 2014; Sprenger et al., 2015b).

Stable isotopes are also extensively applied in plant ecology. They represent a robust method for determining seasonal changes in plant water uptake (Corbin et al., 2005; Eggemeyer et al., 2009), assessing intra- and inter-specific competition for water resources (Williams and Ehleringer, 2000; Yang et al., 2011), partitioning evaporation versus transpiration (Wang and Yakir, 2000; Rothfuss et al., 2012), tracing water source allocation among plant species (Stratton et al., 2000; Rossatto et al., 2012; Plavcová et al., 2018), and reconstructing past

hydrological cycles via cellulose analysis (Voelker et al., 2014). Plant water uptake is considered a non-fractionating process under non-saline conditions (Wershaw et al., 1966; Walker and Richardson, 1991; Lin and Sternberg, 1993), meaning that the isotopic signature of source water is preserved during root water uptake and xylem transport (White et al., 1985). It can thus be used to trace the origin of water in non-transpiring plant tissues, e.g. to determine the depth from which water was absorbed.

In forest ecosystems, isotope-based analyses have been used to determine shifts in root water uptake depths in response to drought (Brinkmann et al., 2018; Gessler et al., 2022), to assess whether trees primarily utilize summer or winter precipitation (Allen et al., 2019; Floriancic et al., 2024), to distinguish between soil water, groundwater, and streamwater sources (Bowling et al., 2017; Engel et al., 2022), and to evaluate competitive or complementary water-use strategies among species (Penna et al., 2020; Kinzinger et al., 2024). Such advancements aim to improve the prediction of extreme events such as droughts and flash floods and to support more effective water resource management under evolving hydroclimatic conditions.

To utilize stable isotopes in these applications, proper sampling design is essential (Ceperley et al., 2024). Representative sampling locations must be selected carefully, and sample handling (during transport, storage, and processing) must prevent evaporation or contamination. In addition to direct water sampling (precipitation, streamflow, mobile soil water, groundwater), indirect sampling via plant and soil matrices is common. In such cases, water must be extracted from these matrices in a manner that minimally alters its isotopic signature.

4.4 Soil water extraction methods

To determine the isotopic signature of soil water, it is necessary to extract it from the the sample soil matrix. Over the past decades, several extraction methods have been developed using:

a) various chemical compounds or elements like toluene for azeotropic distillation (Revesz and Woods, 1990; Thorburn et al., 1993), dichloromethane for accelerated solvent extraction (Zhu et al., 2014) and zinc for micro-distillation (Kendall and Coplen, 1985);
b) microwave water extraction (Munksgaard et al., 2014);
c) force in terms of mechanical squeezing (White et al., 1985; Wershaw et al., 1996; Böttcher et al. 1997) or centrifugation with or without the use of immiscible heavy

liquids (Mubarak and Olsen, 1976; Batley and Gites, 1979; Barrow and Whelan, 1980; Peters and Yakir, 2008);

d) equilibration methods such as in situ equilibration (Garvelmann et al., 2012; Rothfuss et al., 2013, 2015; Volkmann and Weiler, 2014; Gaj et al., 2016), CO_2 and H_2 equilibration (Jusserand, 1980; Scrimgeour, 1995; Hsieh et al., 1998; McConville et al., 1999; Koehler et al., 2000; Kelln et al., 2001) and the direct liquid-vapour equilibrium laser spectroscopy (DVE-LS) method (Wassenaar et al., 2008; Hendry et al., 2015);

e) cryogenic vacuum extraction (CVE; Dalton, 1988; West et al., 2006; Koeniger et al., 2011; Goebel and Lascano, 2012; Orlowski et al., 2013, 2016a; Gaj et al., 2017), the modified CVE-He-purging method (Ignatev et al., 2013), and the automatic cryogenic vacuum distillation (ACVD) system LI-2100 (Lica United Technology Limited Inc.; Yang et al., 2023)

The two most common techniques for extracting water for stable isotope analysis are cryogenic vacuum extraction (CVE) and the direct liquid-vapour equilibrium laser spectroscopy (DVE-LS). CVE requires an apparatus consisting of two interconnected containers, one heated and the other cooled (typically using liquid nitrogen), under vacuum conditions (Fig. 2). Given that CVE is not a commercial instrument but rather a custom-built laboratory setup, many configurations exist, and one could say that each laboratory operates a unique system. Although the underlying principle is generally consistent, some systems use helium, nitrogen, or other inert gases instead of vacuum. Other differences include materials used, apparatus design, and extraction capacity. Despite these similarities, actual extraction procedures vary widely across laboratories in terms of temperature, vacuum strength, and extraction duration.

A comparative study involving approximately 16 laboratories (Orlowski et al., 2018), in which identical soil samples saturated with the same water were analyzed (once using each lab's standard procedure and once using a standardized protocol), revealed significant variability in results. This underscores that if CVE must be outsourced due to lack of equipment, samples should not be distributed across multiple laboratories, as this could compromise the comparability of results.

The second most widely used and user-friendly technique is the DVE-LS method developed by Wassenaar et al. (2008). In this approach, a soil sample is sealed in an airtight bag filled with dry air and left at room temperature for 1-2 days (Fig. 3). During this time, water evaporates from the sample. In this closed system with constant temperature, the isotopic

composition of the resulting vapor is assumed to be in equilibrium with the liquid water in the sample. The vapour is then extracted via syringe and analyzed.

Figure 2. The CVE apparatus at Forschungszentrum Jülich, Germany, used to extract water from soil samples. The sample is heated in a sand bath, and the resulting water vapour is condensed in blue thermos flasks cooled with liquid nitrogen.

Figure 3. Sample preparation for soil and xylem water analysis using the DVE-LS method during the WATSON COST Training School on isotopic techniques for plant water use investigation, held at Forschungszentrum Jülich, Germany, in 2023.

5 Study sites

The primary research sites included the experimental Rokytka catchment in the Bohemian Forest National Park (Faculty of Science, Charles University in Prague) and the Liz catchment located in the Bohemian Forest foothills (Institute of Hydrodynamics, CAS). These two long-term monitored sites were complemented by the Trhové Dušníky and Zvěřínek sites (both managed by the Faculty of Environmental Sciences, Czech University of Life Sciences in Prague), situated in Central Bohemia (Fig. 4). The study sites span a broad elevation gradient—from the fertile agricultural lowlands of the Elbe River Basin (Zvěřínek; 185 m a.s.l.), through the highlands and foothills (Trhové Dušníky; 430 m a.s.l., and the Liz catchment; 870 m a.s.l.), to the upper montane zone of the Bohemian Forest (Rokytka catchment; 1,260 m a.s.l.). These sites represent a range of elevations and differing precipitation regimes, both in terms of amount and phase (liquid vs. solid), while maintaining similar soil textural properties. The forest soils of the mountain catchments were selected due to their substantial annual inputs of both liquid and solid precipitation, as well as the unique combination of soil types in the Rokytka catchment (mineral soils vs. peat bogs), offering a high potential for advancing understanding of runoff generation processes. The lowland experimental sites were selected to capture changes associated with the decreasing proportion of solid precipitation and the altered seasonal distribution of rainfall.

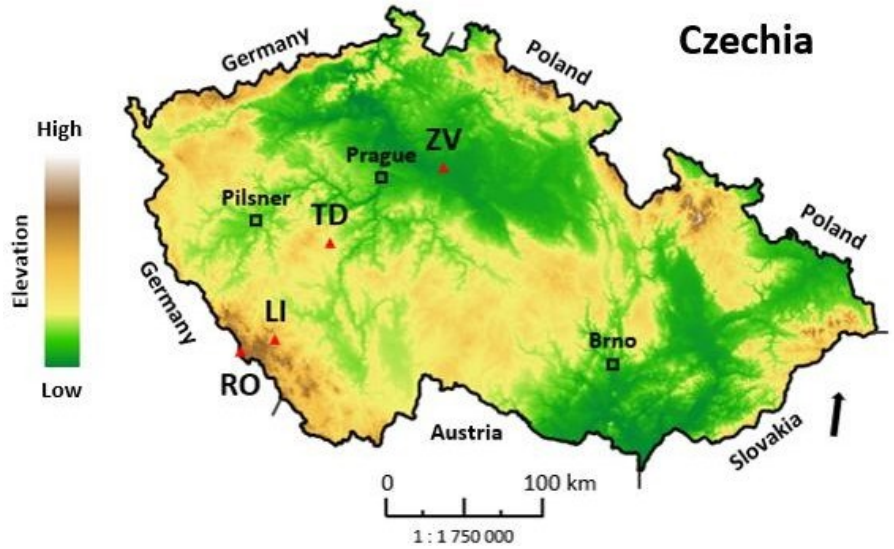

Figure 4. Distribution of research sites within Czechia. Abbreviations denote individual areas: ZV – Zvěřínek, TD – Trhové Dušníky, LI – Liz, and RO – Rokytka. Map data: Digital Vector Database of the Czech Republic ArcČR® version 4.3 (ARCDATA PRAHA, s.r.o., 2024).

5.1 Rokytka catchment

The Rokytka catchment (49° 1' 22" N, 13° 24' 23" E), a sub-catchment of the Modrava basin, is situated at an elevation of approximately 1,200 m a.s.l. and covers an area of 3.8 km², of which one-third is occupied by peatlands and other hydromorphic soils (Fig. 5). The remaining area consists of mineral soils (Podzols) covered predominantly by Norway spruce (*Picea abies* L.) stands, with occasional occurrences of European beech (*Fagus sylvatica* L.). According to the Köppen climate classification, the area falls within the Dfc zone (Tolasz et al., 2007), characterized as a subarctic climate with relatively evenly distributed precipitation throughout the year. Between 1981 and 2010, the mean annual precipitation was 1,695 mm (Starostová, 2012), and the mean daily air temperature was 4.8 °C. A detailed description of the locality is provided in Vlček et al. (2021).

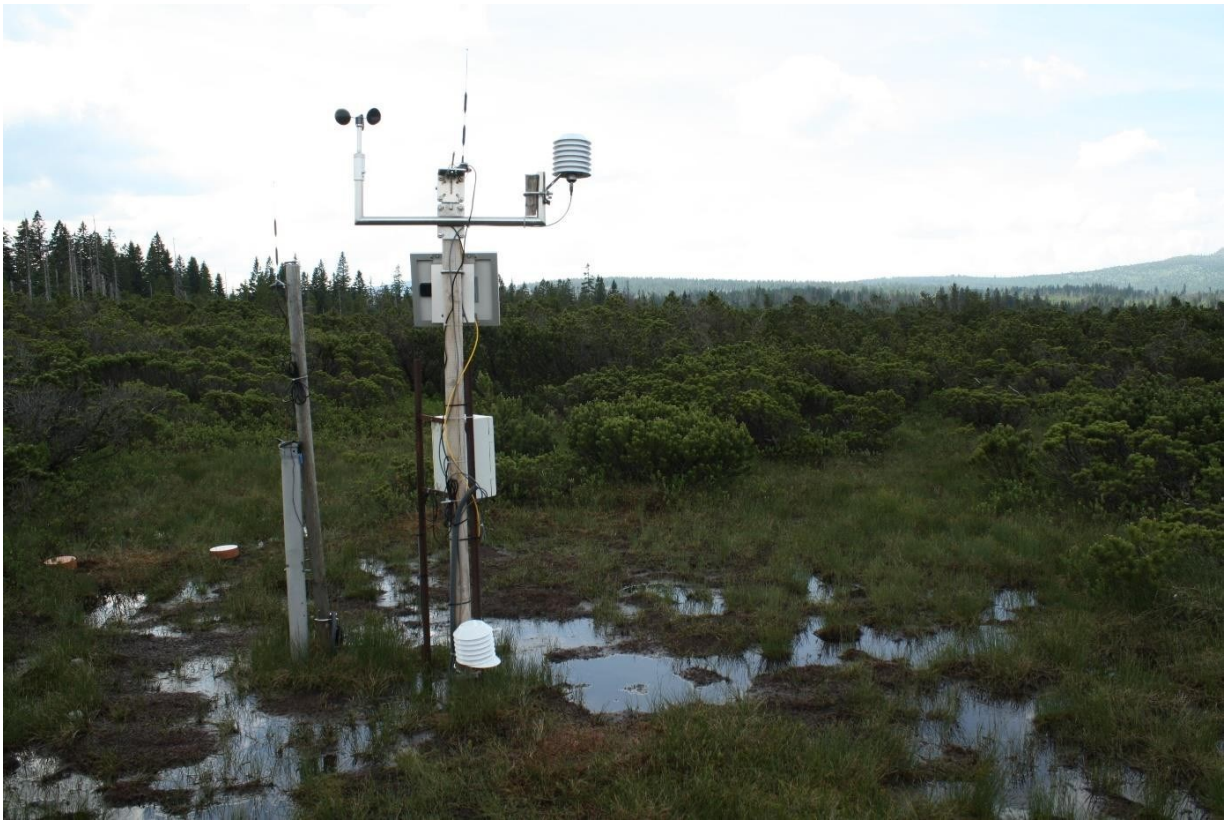

Figure 5. Climate station located on a peat bog at the Rokytka research site in Bohemian Forest.

5.2 Liz catchment

The experimental Liz catchment is located in the foothills of the Bohemian Forest in the southwestern part of Czechia (49° 4' 0.2" N, 13° 40' 49" E). The mean elevation of the catchment is 941 m a.s.l., ranging from 828 to 1,074 m a.s.l. and covers an area of 0.99 km^2 (Fig. 6). The catchment is forested predominantly with Norway spruce (*Picea abies* L.), with occasional occurrences of European beech (*Fagus sylvatica* L.), and is underlain by mineral soils (Podzols). According to the Köppen climate classification, the area lies within the Dfb zone (Tolasz et al., 2007), which is characterized as a humid continental climate with warm summers and relatively evenly distributed precipitation throughout the year. The long-term mean annual air temperature is approximately 6.7 °C, and the mean annual precipitation totals 847 mm (1975–2022). For a detailed description of the locality, see Zelíková et al. (under review).

Figure 6. Monitoring area in a spruce stand at the Liz research site.

5.3 Trhové Dušníky

The experimental site Trhové Dušníky (49°43′12″ N, 14°00′46″ E) is located 2 km north of the town of Příbram, in the flat floodplain of the Litavka River, at an elevation of 430 m a.s.l. (Fig. 7). The area was previously used primarily for grazing. After the confirmation of heavy metal contamination (Žák et al., 2009), the site was taken out of agricultural use and has since been left fallow. The soil is classified as a sandy Gleyic Fluvisol. According to the Köppen climate classification, the area falls within the Cfb zone (Tolasz et al., 2007), characterized by mild winters, cool summers, and relatively uniform precipitation throughout the year. The site receives an average annual precipitation of 650–750 mm and has a mean annual air temperature of 7 °C (Šípek et al., 2019).

Figure 7. Monitoring station at the experimental site Trhové Dušníky used for soil moisture and meteorological data collection.

5.4 Zvěřínek

The experimental site Zvěřínek (50°09′20″ N, 15°00′37″ E) is located in the Elbe River Basin in Central Bohemia, at an elevation of 184 m a.s.l. (Fig. 8). The site is situated on agricultural land and is characterized by loamy sand Regosol. According to the Köppen climate classification, the area falls within the Cfb zone (Tolasz et al., 2007), which is characterized by mild winters, cool summers, and relatively uniform precipitation throughout the year. The site receives an average annual precipitation of 550–600 mm and has a mean annual air temperature of 10 °C. A detailed description of the site is provided in Seyedsadr et al. (2022).

Figure 8. Monitoring station at the experimental site Zvěřínek used for soil moisture and meteorological data collection.

6 Methodology

6.1 Using stream water temperature as a natural tracer

To analyze the water temperature regime of a peat bog and a mineral soil hillslope, and to evaluate the contribution of the peat bog to streamflow during baseflow and rainfall-runoff events, a simple mixing model based on water temperature was applied. The following equation were used:

$$Q_3 = Q_1 + Q_2 \tag{7}$$

$$T_3Q_3 = T_1Q_1 + T_2Q_2 \tag{8}$$

$$\%PS = \frac{Q_2}{Q_3} \cdot 100 \tag{9}$$

where Q_1, Q_2, and Q_3 represent the discharge ($m^3\ s^{-1}$) at the respective sampling points—i.e., the mineral hillslope stream, the peat bog stream, and the downstream channel formed by their confluence. T_1, T_2, and T_3 denote the corresponding water temperatures (°C), and *%PS* refers to the proportion (%) of total streamflow originating from the peat bog hillslope.

6.2 Soil water balance model

The conceptual model used in Zelíková et al. (unpublished results) study was a modified form of the soil water balance model (SWBM), developed by Brocca et al. (2008, 2014). The modification is based on the replacement of the infiltration parameter (the Green-Ampt equation) by throughfall, as surface runoff is not generated in the experimental catchment and all water directly infiltrates into the soil. The original SWBM does not include a snow module; hence, snow accumulation and snowmelt was considered, as the experimental catchment lies in an area with regular snow cover. The degree-day method (Gupta, 2001) was chosen for this purpose because it has been proven to be efficient in the Central Europe (Lopez et al., 2020).

6.3 Soil water extraction

To distinguish tightly bound soil water (representing water held in capillaries) from mobile soil water (representing water in macropores), and to compare both with the potential composition

of bulk soil water (representing the total soil water pool), a novel experimental approach was employed.

6.3.1 Mobile soil water extraction

For the extraction of mobile water, the tensiometer-controlled vacuum system (VS-Pro, UMS, Germany) was employed with a maximum applied tension of -60 kPa (Brooks et al., 2010; Berry et al., 2017; Sprenger et al., 2018). The extraction was conducted from two depths, specifically 20 cm and 40 cm (Fig. 9, left), which often play a significant role in root water uptake (Hackmann et al., 2025). The extracted samples represented a composite of water collected over the preceding two weeks.

Figure 9. On the left: the installed VS-Pro system for sampling mobile soil water at the Bohemian Forest National Park site. On the right: pressure plate apparatus for extracting the mobile soil water fraction from soil samples (Institute of Hydrodynamics, CAS).

6.3.2 Tightly bound soil water extraction

For the extraction of tightly bound soil water, a modified approach utilizing the pressure plate apparatus, as described by Orlowski et al. (2020), was employed. Undisturbed soil cores (100 cm^3) were collected from the same two depths, with five replicates per depth. The soil cylinders were wrapped in Parafilm® and stored in a portable refrigerator for transport to the laboratory. The soil cores were then inserted into the pressure plate apparatus for retention curve determination (5 Bar Pressure Plate Extractor, Soil Moisture Equipment Corp., CA, USA, Fig. 9, right) with a 1 bar pressure plate cell was used. A pressure of 60 kPa (~ pF 2.4) for a two-week period was chosen to get rid of the mobile soil water fraction. Then, the top and bottom of the soil core were removed, and for further soil water extraction, only the inner soil core was used (approx. 50 g of soil sample).

For the subsequent extraction of tightly bound soil water, the mass balance mixing method was selected due to its accessibility, simplicity and high throughput. Briefly, the soil sample was placed in a glass vial (volume of 60 mL) with a plastic cap and silicone sealing. Roughly 20-25 mL of a traced water was added to the sample, and the remaining space was filled with glass balls (5 mm in diameter) to remove the presence of air. Then, the samples were placed on a laboratory-constructed rotating device (Fig. 10) and continuously spun for 16 hours at a fixed speed of 15 rpm. Subsequently, they were stored in a refrigerator to allow sedimentation, after which 0.75 mL of the mixture was collected and filtered through a 0.45 µm mixed cellulose ester membrane. The rest of the sample was dried at 105 °C for 48 hours and weighed to calculate the soil water content of the soil sample.

Figure 10. Laboratory-constructed rotating devices for the tightly bound soil water extraction (Institute of Hydrodynamics, CAS).

The isotopic composition of tightly bound soil water was then calculated according to the mass balance mixing model (Eq. 10, 11).

$$\delta^{18}O_M = \frac{m_S}{m_M} \cdot \delta^{18}O_S + \frac{m_T}{m_M} \cdot \delta^{18}O_T \quad (10)$$

$$\delta^{2}H_M = \frac{m_S}{m_M} \cdot \delta^{2}H_S + \frac{m_T}{m_M} \cdot \delta^{2}H_T \quad (11)$$

where the sub-indices represent mixture (M), tightly bound soil water (S), and traced water (T), m is the weight of those waters and $\delta^{18}0$ and $\delta^{2}H$ represent the stable isotopic composition of the sample.

Following the estimation of tightly bound soil water, the same mass-balance mixing model was applied to calculate the potential stable isotopic composition of bulk soil water. In this approach, bulk water was represented as a mixture of mobile water, obtained from suction lysimeters, and tightly bound water, as derived in the previous step. The relative proportions of these two components were determined based on measurements from the pressure plate apparatus.

6.4 Measurement of stable isotope composition

Stable isotope analyses were conducted across three institutions using two different instruments, depending on the specific study. The study by Lehmann et al. (under review) was carried out at the Swiss Federal Institute for Forest, Snow and Landscape Research (WSL), Switzerland, using cavity ring-down spectroscopy (CRDS) with a Picarro L2140-*i* laser spectrometer (Picarro Inc., Santa Clara, USA). The same instrument was also used for both studies by Kocum et al. (2025, submitted) and Vlček et al. (submitted), with analyses performed at the Institute of Hydrodynamics of the Czech Academy of Sciences. Additional data were analyzed using off-axis integrated cavity output spectroscopy (OA-ICOS) on a Los Gatos Research Liquid-Water Isotope Analyzer 2 (LGR LWIA2; ABB – Los Gatos Research, California, USA) at the Faculty of Civil Engineering, Czech Technical University in Prague. These measurements were primarily used to verify the functionality of a prototype apparatus developed for the study by Kocum et al. (2025).

6.5 Stable isotope analysis and calculations

Beyond the fundamental calculations, including delta notation (Eq. 2) and deuterium excess (D-ex, Eq. 3), several additional analyses were conducted to aid in the visualization and interpretation of the acquired isotopic data.

6.5.1 Line-conditioned excess

Given that the Global Meteoric Water Line (GMWL) and deuterium excess (D-ex; Eq. 3) are based on the global relationship between $\delta^{18}O$ and $\delta^{2}H$, the use of a Local Meteoric Water Line (LMWL) is more appropriate for site-specific studies. The LMWL is derived from the local isotopic composition of precipitation. As a local counterpart to D-ex, the Line-conditioned excess (Lc-ex; Landwehr and Coplen, 2006) is commonly used to evaluate the offset between the LMWL and other water samples. Negative values of Lc-ex indicate the presence of evaporation, whereas positive values suggest mixing with isotopically distinct water (e.g., resulting from condensation processes).

To establish the LMWL, reduced major axis (RMA) regression was applied (Harper, 2016) instead of conventional linear regression. This approach was selected because uncertainties in both $\delta^{2}H$ and $\delta^{18}O$ measurements are equally significant, whereas ordinary least squares regression assumes all error is confined to the y-axis and ignores uncertainty in the x-axis.

The slope (Eq. 12) of the RMA regression was calculated as the ratio of the standard deviations of $\delta^{2}H$ and $\delta^{18}O$, scaled by the sign of their Pearson correlation coefficient. The intercept was then calculated according to Eq. 13:

$$\beta_{RMA} = sign(r) \cdot \frac{\sigma_{\delta^2 H}}{\sigma_{\delta^{18} O}} \tag{12}$$

$$\alpha_{RMA} = \overline{\delta^2 H} - \beta_{RMA} \cdot \overline{\delta^{18} O} \tag{13}$$

where α_{RMA} and β_{RMA} are the intercept and slope of the RMA, respectively, r is Pearson correlation coefficient between $\delta^{2}H$ and $\delta^{18}O$, and $\sigma_{\delta^2 H}$, $\sigma_{\delta^{18}0}$ are their standard deviations. This method minimizes the orthogonal distances between data points and the fitted line, making it more suitable for hydrological isotope data where both variables are subject to analytical and natural variability.

To calculate the Lc-excess the slope and intercept of the RMA is used. The Lc-ex can be calculated according to Eq. 14:

$$lc - excess = \delta^2H - \beta_{RMA} \cdot \delta^{18}O - \alpha_{RMA} \quad (14)$$

where α_{RMA} and β_{RMA} are the coefficients of the LMWL derived from Eq. 13.

6.5.2 Seasonal trends and the mean residence time calculations

Seasonal trends in δ²H values in precipitation and other water sources were modeled using an iteratively reweighted least squares (IRLS) regression method with moving time windows to determine the amplitude and phase of individual isotopic signals. Prior to sine-wave fitting in the case of several years‘ series, a detrending correction was applied following Xia et al. (2024) to account for linear trends in isotopic composition potentially induced by climate change. This step was necessary to prevent biased estimates of the seasonal amplitudes. The isotopic increase at each sampling date was calculated using the following equation:

$$\Delta\delta^2H = \Delta T \times Sen's\ slope \quad (15)$$

$$\delta^2H_c = \delta^2H - \Delta\delta^2H \quad (16)$$

where ΔT represents the time elapsed since T_0. The resulting $\Delta\delta^2H$ values were then adjusted by subtracting the observed δ^2H values, yielding the corrected δ^2Hc values (Eq. 16). A sinusoidal function was subsequently fitted to the full time series of δ^2Hc using the IRLS method with a moving time window (the length of the window was adjusted to the length and nature of the data), providing corrected seasonal amplitudes for precipitation and other water sources (Eq. 17).

$$\delta^2H = mean(\delta^2H_c) + A * sin\left[\left(\frac{2\pi t}{b}\right) + c\right] \quad (17)$$

where $mean(\delta^2Hc)$ represents the average δ^2Hc value, A is the seasonal amplitude, b is the period of the seasonal cycle (with a 1-year period equivalent to 2π), t (in months) denotes time, and c (in radians) indicates the phase shift.

The obtained amplitudes were then used to estimate the mean residence times (MRT) of individual water sources, following the approach of Soulsby et al. (2000) (Eq. 18).

$$T = \omega^{-1}\left[\left(\frac{A2}{A1}\right)^{-2} - 1\right]^{0.5} \tag{18}$$

where $A1$ is the amplitude of the initial water (precipitation), $A2$ is the amplitude of the resulting water (streamflow, groundwater, etc.), and ω is the radial frequency of annual fluctuations (2π).

6.5.3 Seasonal Origin Index

To characterize whether the obtained water sample have a predominant contribution of winter or summer precipitation, a seasonal origin index (SOI) was calculated (Eq. 19; Allen et al., 2019).

$$SOI = \begin{cases} \dfrac{\delta_x - \delta_{annP}}{\delta_{summerP} - \delta_{annP}}, if\ \delta_x > \delta_{annP} \\ \dfrac{\delta_x - \delta_{annP}}{\delta_{annP} - \delta_{winterP}}, if\ \delta_x < \delta_{annP} \end{cases} \tag{19}$$

where δ_x are the $\delta^{18}O$ isotopic values of soil water, and δ_{annP}, $\delta_{winterP}$, and $\delta_{summerP}$, are the $\delta^{18}O$ isotopic values of volume-weighted annual precipitation, typical winter (δ_{annP} – fitted amplitude), and typical summer (δ_{annP} + fitted amplitude) precipitation. The SOI values ranges from -1 to 1, where values close to -1 represent water predominantly derived from winter precipitation, and values approaching 1 reflecting a dominant contribution from summer precipitation.

7 Results

Soil drought is increasingly prevalent as a consequence of ongoing climate change. A thorough understanding of these changes is essential for improving predictions of runoff generation, soil water dynamics, and groundwater recharge, as well as vegetation responses and adaptive strategies under increasingly frequent and severe drought conditions.

Building upon this context, the following studies were conducted to advance the understanding of these processes:

1st study (section 7.1)

Zelíková, N., Toušková, J., **Kocum, J**., Vlcek, L., Tesar, M., Bouda, M., and Sipek, V.: Divergent water balance trajectories under two dominant tree species in montane forest catchment shifting from energy- to water-limitation. Hydrology and Earth System Sciences. https://doi.org/10.5194/hess-2024-244, 2024. [under review]

2nd study (section 7.2)

Falátková, K., Šípek, V., Vlček, L., **Kocum, J**., and Pivokonský, M.: Hydrological balance and runoff from a montane peat bog traced by water temperature. Hydrological Science Journal, 69, 4, 393–406. https://doi.org/10.1080/02626667.2024.2320392, 2024.

3rd study (section 7.3)

Vlček, L., Falátková, K., **Kocum, J.**, Ledvinka, O., Su, Y., Pivokonský, M., and Šípek, V.: Tracing Water Sources in a Mountain Catchment Using Stable Isotopes: Insights from Peat and Mineral Soils, Journal of Hydrology, 2025. [submitted]

4th study (section 7.4)

Kocum, J., Haidl, J., Gebousky, O., Falatkova, K., Sipek, V., Sanda, M., Orlowski, N., and Vlcek, L.: Technical note: A new laboratory approach to extract soil water for stable isotope analysis from large soil samples. Hydrology and Earth System Sciences, 29, 13, 2863–2880, https://doi.org/10.5194/hess-29-2863-2025, 2025.

5th study (section 7.5)

Lehman, M. M., Geris, J., van Meerveld, I., Penna, D., Rothfuss, Y., Verdone, M., Ala-Aho, P., Arvai, M., Babre, A., Balandier, P., Bernhard, F., Butorac, L., Carrière, S. D., Ceperley, N. C., Chen, Z., Correa, A., Diao, H., Dubbert, D., Dubbert, M., Ercoli, F., Floriancic, M. G., Gimeno, T. E., Gounelle, D., Hagedorn, F., Hissler, C., Huneau, F., Iraheta, A., Jakovljević, T., Kazakis, N., Kern, Z., Knaebel, K., Kobler, J., **Kocum, J.**, Koeber, C., Koren, G., Kübert, A., Kupka, D., Le Gall, S., Lehtonen, A., Leydier, T., Malagoli, P., di Villahermosa, F. S. M., Marchina, C., Martínez-Carreras, N., Martin-StPaul, N., Marttila, H., Oliveira, A. M., Monvoisin, G., Orlowski, N., Palmik-Das, K., Persoiu, A., Popa, A., Prikaziuk, E., Quantin, C., Rinne-Garmston, K. T., Rohde, C., Sanda, M., Saurer, M., Schulz, D., Stockinger, M. P., Stumpp, C., Venisse, J. S., Vlcek, L., Voudouris, S., Weeser, B., Wilkinson, M. E., Zuecco, G., and Meusburger, K.: Soil and stem xylem water isotope data from two pan-European sampling campaigns. Earth System Sciences Data. https://doi.org/10.5194/essd-2024-409, 2025. [under review]

6th study (section 7.6)

Kocum, J., Falatkova, K., Sipek., V., Patek, K., Hnilica, J., Jenicek, M., Sanda, M., Trakal, L., and Vlcek, L.: Isotopic insight into the dynamics of soil water pools along an elevation gradient, Hydrology and Earth System Sciences, 2025. [submitted]

7.1 Dynamics of soil moisture under two dominant tree species

The study *Divergent water balance trajectories under two dominant tree species in a montane forest catchment shifting from energy- to water-limitation* (Zelíková et al., under review) investigates the impacts of ongoing climate change on the transition from energy- to water-limited conditions and the resulting shifts in tree species composition within European forests. Utilizing a 22-year dataset of soil water potential measurements, the study examines changes in evapotranspiration and groundwater recharge beneath Norway spruce (*Picea abies* L.) and European beech (*Fagus sylvatica* L.) stands at the Liz experimental site.

The findings indicate that, under intensifying water-limitation, forest stands composed of deeper-rooted and more anisohydric species will increasingly deplete soil water disproportionately. This, in turn, may exacerbate summer soil drought and further reduce groundwater recharge. Conversely, an increased representation of deciduous species may enhance winter recharge due to reduced canopy interception during leaf-off periods.

Given that climate–vegetation interactions remain a significant source of uncertainty in forecasting ecosystem responses to climate change, the insights gained from this study are expected to inform the development of next-generation ecosystem models and hydrological projections. These advancements are critical for improving both forest and water resource management under ongoing hydroclimatic shifts.

Manuscript review stage

The manuscript was submitted to Hydrology and Earth System Sciences on 5 August 2024 and is currently, as of August 2025, undergoing minor revisions following the second round of peer review. Acceptance is anticipated in the coming months.

Divergent water balance trajectories under two dominant tree species in montane forest catchment shifting from energy- to water-limitation

Nikol Zelíková[1,2], Jitka Toušková[1], Jiří Kocum[1,3], Lukáš Vlček[1], Miroslav Tesař[1], Martin Bouda[4,5], Václav Šípek[1]

[1] Institute of Hydrodynamics of the Czech Academy of Sciences, Pod Patankou 30/5, Prague, 160 00, Czech Republic
[2] Department of Water Resources and Environmental Modelling, Faculty of Environmental Sciences, Czech University of Life Sciences Prague, Kamýcká 129, Praha-Suchdol, 165 00, Czech Republic
[3] Department of Physical Geography and Geoecology, Faculty of Science, Charles University in Prague, Albertov 6, Prague, 120 00, Czech Republic
[4] Department of Plant Ecophysiology, University of Hohenheim, Garbenstraße 30, Stuttgart 70599, Germany
[5] Institute of Botany of the Czech Academy of Sciences, Zámek 1, Průhonice, 252 43, Czech Republic

Correspondence to: Václav Šípek (sipek@ih.cas.cz)

Abstract.

Vegetation interacts with both soil moisture and atmospheric conditions, contributing to water flow partitioning at the land surface. Therefore, changes in both climate and land cover with vegetation affect the availability of water resources. This study aimed to determine the differential effects of climate change on the soil water regime of two common Central European montane forest types: Norway spruce (Picea abies L.) and European beech (Fagus sylvatica L.). A unique dataset, including 22 years (2000–2021) of measured soil water potentials, was used with a bucket-type soil water balance model to investigate differences in evapotranspiration and groundwater recharge both between the forest types and across years. Results revealed an accelerating transition from a fully energy-limited state towards water-limitation, with evidence of strict water-limitation in recent outlier years, unprecedented in this system. While long-term column-averaged pressure heads indicated drier soil at the spruce site overall, this was driven by the wettest years in the dataset. Seasonal and interannual variability of meteorological conditions drove complex but robust differences between the flow partitioning of the two forest types, which diverged further with increasing water-limitation. Higher snow interception by spruce (27 mm season^{-1}) resulted in drier soil below the spruce canopy in the cold season. Higher transpiration by beech (100 mm season^{-1}) led to increasingly drier soils over the warm seasons causing lower ground water recharge (34 mm season^{-1}). Low summer precipitation inputs exacerbated soil drying under beech more than under to spruce. These suggest that expected trends in regional climate and forest species composition may interact to produce a disproportionate shift of recharge from the summer to the winter season.

1 Introduction

Making ecohydrological predictions in a non-stationary state of the Earth system requires detailed process understanding that remains elusive. A major obstacle to advancing process understanding is the lack of long-term observations of variables with direct mechanistic relevance, such as water potential (or hydraulic head). Water potential in soil and plants suffers from a noted information gap despite being key to our understanding of land-atmosphere interactions (Novick et al. 2022). Soil moisture status integrates the fluxes of the entire hydrological cycle and in turn exerts significant control over key Earth system processes (Legates et al., 2011; Humphrey et al. 2021). As water potentials directly drive the soil-plant-atmosphere water flows that are tightly coupled with other land-atmosphere fluxes, addressing this gap offers a promising pathway to resolving major uncertainties in ecosystem fate and functioning (Trugman et al. 2018, Green et al., 2019) during the transition to previously unobserved hydroclimatic regimes. After centuries of relative climatic stability (Brázdil et al., 2022), a clear rise in average and maximum air temperatures has been affecting Central Europe since the last part of the 20th century (Zahradníček et al., 2020). Increased air temperature has induced higher atmospheric water demand contributing to the severity of recent droughts (Možný et al., 2020). Although, long-term annual precipitation sums have not changed in the past (Brázdil et al., 2021) and are not expected to change significantly in near future (Svoboda et al., 2017), the occurrence of seasonal precipitation deficits causing severe soil drought is projected to increase (Hari et al., 2020). Increased water demand combined with seasonally reduced water supply is expected to shift the region from energy- toward water-limitation of evapotranspiration over the coming decades (Denissen et al., 2022).

One of the less well understood consequences of ongoing climatic changes is a shift in forest species composition, which has the potential to further affect water fluxes in the soil-plant-atmosphere system (Maxwell et al., 2018). The two most frequent tree species in central European forests are beech (*Fagus sylvatica* L.) and spruce (*Picea abies* L.). As spruce thrives in colder and moisture-rich conditions, its stands are increasingly being replaced by beech (Daněk et al., 2019). This climate-induced transformation of montane forests has potential implications for ecosystem ecohydrological function. Each of these species has distinctive physiological and architectural properties such as leaf morphology and phenology, rooting depth (Jost et al., 2012), xylem structure and function (Tyree & Zimmermann, 2002), or stomatal control during dry periods (Gebhardt et al., 2023). Their specific ecohydrological characteristics and strategies may not only determine their fates under hydroclimatic change but also yield divergent effects on the water balance through contrasting rates of interception (Savenije, 2004), soil water fluxes, water storage dynamics, and thus soil water regimes (Schume et al., 2004).

At present, available studies comparing soil moisture regimes under these common tree species provide ambiguous results due to their limited duration. Schume et al. (2004) and Šípek et al. (2020) reported a stronger drying of the soil profile during the growing season at beech sites. By contrast, Schwärzel et al. (2009), Rötzer et al. (2017), and Kuželková et al. (2024) observed greater soil drying under spruce than under beech. Some of these differences may partly be explained by contrasting soil hydraulic properties at the sites compared. The main limitation shared by such studies; however, is their limited temporal extent. The periods of the observation range from one day (e.g., Jost et al., 2012) to several years (Schume et al., 2004;

Schwärzel et al., 2009; Zucco et al., 2014; Korres et al., 2015; Huang et al., 2016; Rötzer et al., 2017). The longest periods of analyses so far lasted from 4 to 5 years (Wang et al., 2018; Šípek et al., 2020; Gebhardt et al., 2023). The results of short-term studies are difficult to interpret as they provide only a partial insight into the role of individual water fluxes. They are limited by the variability of climatic conditions during the study period. Moreover, short-term studies cannot capture long-term changes in the characteristics of droughts, such as higher temperatures (Groissord et al., 2021) and flash droughts (Qing et al., 2022) and therefore their second-order effects via the given species. Hence, the availability of a long-term data series is crucial not only to observe trends, but also as a tool to better understand processes and natural variability in a period of changing climate and land cover (Huntingford et al., 2014; Milly et al. 2015).

This study aims to advance process understanding by disentangling the effects of climate and forest composition on water fluxes as these ecosystems transition from energy- to water-limitation. We focused on the impact of two forest types, monospecific Norway spruce and European beech, on the soil water regime in an experimental montane catchment in Bohemian Forest, Czechia. The study benefits from a unique 22-year-long dataset of measured soil water potential in the two forest types that enables us to make robust interannual comparisons for the first time. Long-term observations of the experimental catchment allow us to impose closure on the hydraulic balance to estimate individual fluxes and to compare the current evapotranspiration regime with previous decades. Together with its depth coverage over the rooting zone in each stand, these advantages allow the present dataset to yield comprehensive insight into the studied forests' ecohydrological function during the ongoing hydroclimatic transition. To reveal how climatic drivers interact with vegetation processes to produce hydrologic flux partitioning, we: (1) analyse seasonal differences in measured soil water potential between the two forest types, (2) estimate the soil water balance components (evapotranspiration and drainage) at the two sites using a process-based soil water balance model, and (3) determine the main climate dependency of the soil water regime under both tree species.

2 Data and Methods

The study is based on extensive field measurements of soil moisture regime and necessary hydrometeorological variables in a Central European montane catchment including spruce and beech covered sites. The water balance of both sites was estimated using the bucket type soil water balance model. The workflow of the study is presented in Supplementary material (Fig. S1).

2.1 Study site

The Liz experimental catchment, Czechia (49°04′N, 13°41′E) (Fig. 1), served as the experimental area for this study. It is located in the Bohemian Forest on the border between Czechia and Germany. The catchment area is approximately 1 km^2. Its elevation ranges from 828 m a. s. l. (at the outlet) to 1,070 m a. s. l. It is located in the cold region (unit C7 of the Quitt Climatic Classification, Vondrakova et al., 2013) of an otherwise humid continental climate (unit Dfb of the Köppen Climatic Classification (Tolasz et al., 2007 according to Köppen, 1936). During the study period 2000–2021 (and the preceding period of catchment measurements, 1975–1999) it had an average annual air temperature of 7.2 (6.4) °C and an average annual

precipitation of approximately 847 (842) mm. The monthly average maximum temperature is 16.5 (15.5) °C in July, and the minimum is −1.9 (-2.3) °C in January. More precipitation arrives during the May-October growing season than the rest of the year: 515.7 (471.2) mm compared with 331.9 (370.9) mm, respectively. Mean annual snow cover duration is 133 (147) days. The annual potential evapotranspiration (PET) determined by the air temperature-based method (Oudin et al., 2005) is 560.7 (521) mm. The annual runoff height from the catchment is approximately 352 (317) mm, representing ~40% of the total precipitation.

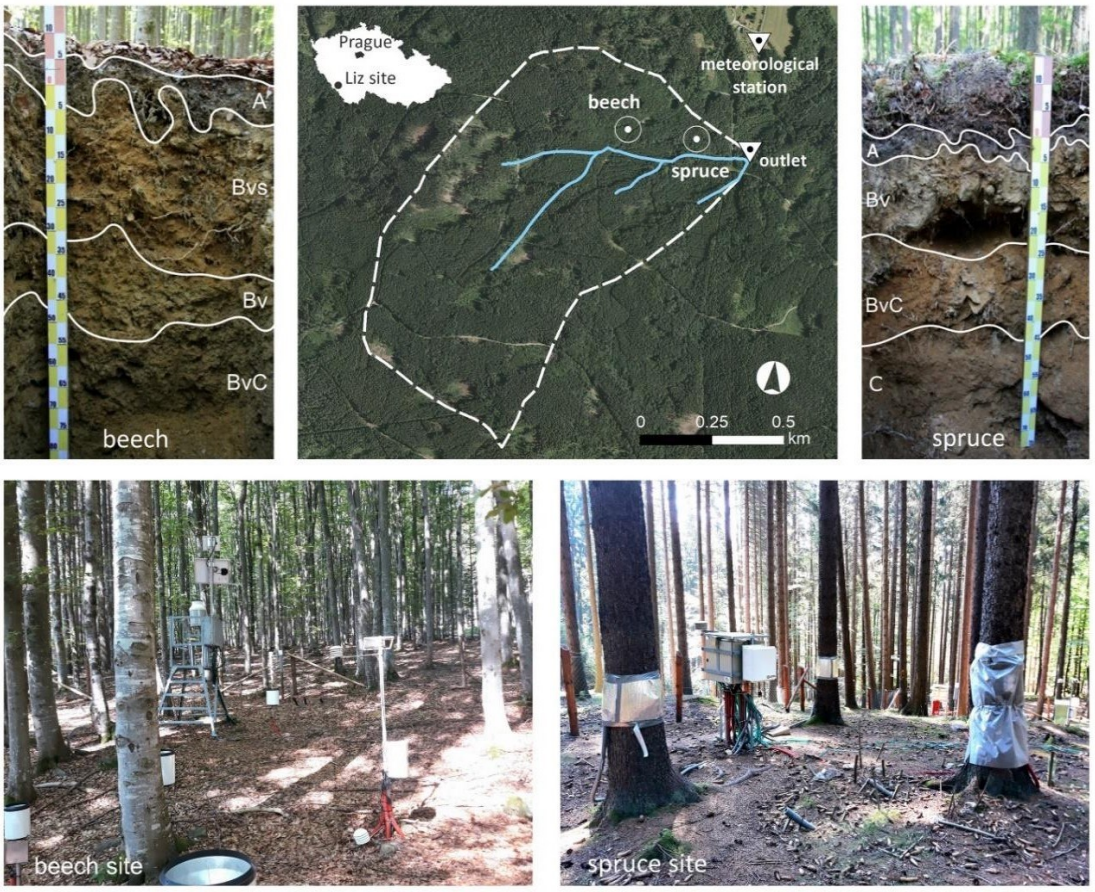

Figure 1: Overview of the experimental site (© CUZK 2024) and soil profiles (© Přemysl Fiala).

Crystalline bedrock in the catchment only allows water circulation in the weathered zone and does not communicate with adjacent catchments, such that the hydrological catchment corresponds fully to the hydrogeological catchment (Hrkal et al., 2009). This observation underpins a fundamental assumption of our modelling framework: that all water from precipitation generates measurable runoff at the gauging station, which is well supported by the hydrogeological survey. The majority of the area is covered by nearly pure spruce forest, with a dominance of 120–140-year-old Norway spruce (*Picea abies* L.) (>

85% of the canopy cover). In several places, the spruce forest is penetrated by 100–120-year-old beech stands (*Fagus sylvatica* L.).

Two experimental sites within the Liz experimental catchment were chosen for this study: one with Norway spruce (*Picea abies* L.) and the other with European beech (*Fagus sylvatica* L.). The elevation difference between the two sites is approximately 30 m: the spruce site is located at 855–860 m a.s.l., and the beech site is located at 885–890 m a. s. l., both with a slope of 7.5° and an eastern aspect. Both spruce and beech canopies tend to suppress understory vegetation, which was accordingly absent at both sites (Fig. 1). The leaf area index (LAI) was measured throughout the 2022 season on a monthly basis and showed a seasonally stable value with an average of 3.7±0.5 in the spruce site and seasonally variable values in beech ranging from 1.1±0.2 at the beginning and end of growing season (May and September) to 4.7±0.5 in the middle of the growing season. A visual inspection of the root depth distribution (when excavating the soil) revealed that the roots were present only in the upper 40 cm of the spruce site and down to 100 cm of the beech site.

The soil at both sites can be classified as moderately deep loamy sand dystric Cambisol (IUSS, 2015), with an average soil depth of approximately 100 cm. The percentages of sand-silt-clay fractions are 73.2%–24.2%–2.6% at the spruce-covered site and 80.2%–18.1%–1.7% at the beech-covered site. The soil water permeability is relatively high ranging from 518 cm.day^{-1} at the bottom of the soil profile to 1700 cm.day^{-1} in the topsoil horizon. The humus A horizon (0–10 cm), together with surface organic horizon O (5–10 cm thick at beech stand and 10–15 cm at spruce stand), is followed by a Bvs/v horizon (down to 50 cm at beech site and to 30 cm at spruce site) and finally by a BvC horizon with a significant amount of larger than sandy particles (>50%). Both soil profiles are presented in Fig. 1.

2.2 Field measurements

The meteorological variables used in this study were air temperature (Fiedler RV12/RK5, Czech Republic) and precipitation (Meteoservis MRW 500, Czech Republic), which were measured at 10-minute intervals during the entire twenty-two-year period (2000−2021). The meteorological station is located circa 400 meters away from two experimental plots outside the forest. Moreover, the experimental catchment is instrumented with discharge and groundwater level measurements. Discharge was also measured at the 10-min time step, and the groundwater level was recorded manually every week throughout the entire investigated period. Average daily air temperatures, precipitation sums and discharges were collected from 1975. The snow water equivalent (SWE) was measured manually three times per week since 2000. Soil water potential data were acquired from permanently installed soil tensiometers (Adolf Thies GmbH, Germany, see Fig. S2) measuring pressure heads at five depths (15, 30, 45, 60 and 90 cm). Soil water potentials were recorded manually three times a week during the growing season (mid-May to mid-October) from 2000 to 2021. The measuring range of these tensiometers included pressure heads ranging from 0 cm to −865 cm (−85 kPa). Up to four tensiometers were available for each measuring depth at each site over the entire measurement period (at least 2 measurements 93 % of the time), and we used their average for a particular depth as the site-representative value. Given the fully closed, even, monospecific canopies at our sites, the representativeness of the measurements was ensured by avoiding placing sensors at micro-sites subject to preferential flows. We used measurement

points representing average site slope and distance between the trees (3.6/2.7 m from tree in spruce/beech forest when the average distance in between two adjacent trees is 5.4/4.5 m). This resulted in same order of spatial variability of LAI (coefficient of variation was 12.8/8.9 % for spruce and beech) and soil moisture (coefficient of variation was 2.3/6.3 % for spruce and beech) in both forests and good correspondence of soil water potentials with another three profiles equipped with UMS T8 tensiometers located nearby (Sipek et al., 2020). The average soil column pressure head was estimated as a weighted mean of five soil layers (each represented by one measurement depth). The soil profile was considered to have a uniform depth of 100 cm. The measured pressure heads were used to determine differences in soil water regimes between the stands, as they better demonstrate the differences in soil water energy states during dry conditions, which were of interest to the study.

2.3 Soil water balance model

The conceptual model used in this study was a modified form of the soil water balance model (SWBM), developed by Brocca et al. (2008, 2014). The bucket-type of the model was used as (1) it is sufficient to answer questions posed (soil column water balance) without adding more complexity, (2) it uses "Feddes" type of equation for the estimation of plant water use, (3) it is more convenient for the simulation of longer periods, (4) the soil column is represented by one unified domain with column average soil hydraulic properties, which is beneficial especially when the soil encompasses a lot of rock fragments. Moreover, several widely used hydrological models use similar bucket/reservoir modelling approaches for the determination of soil water regimes (e.g., the Soil Water Assessment Tool (Arnold et al., 2012), the HBV model (Seibert and Vis, 2012) or the VIC model (Liang et al., 1994)). The modification for this study is based on the replacement of the infiltration parameter (the Green-Ampt equation) by throughfall *(P_{TF})*, as surface runoff is not generated in the experimental catchment and all water directly infiltrates into the soil. Therefore, the following soil water balance Eq. (1) was used:

$$\frac{d\Theta(t)}{dt} = P_{TF}(t) - S(t) - D(t) \quad (1)$$

where *$\theta(t)$* is the average volumetric soil water content at a day (t), *$P_{TF}(t)$* is the throughfall (mm day^{-1}), *$S(t)$* is the actual evapotranspiration rate (mm day^{-1}) and *$D(t)$* is the drainage rate (mm day^{-1}). The Eq. (2) for *$P_{TF}(t)$* is given as:

$$P_{TF}(t) = P_{OAR}(t) - P_{INT}(t) \quad (2)$$

where P_{OAR} represents the measured open area precipitation (mm day^{-1}) and P_{INT} is the estimated interception (mm day^{-1}) for a given location. Spruce interception in the summer season (May to October) was estimated based on the deduction of the interception capacity from every single precipitation event. The interception capacity of 2.2 mm was derived by Kofroňová et al. (2021) for the same experimental site. In the case of beech stands, the summer interception capacity was calculated using a general formula by von Hoyningen-Hüne (1983) and Braden (1985) applying seasonal variation in the leaf area index (LAI):

$$P_{INT} = a \cdot LAI \left(1 - \frac{1}{1+\frac{b \cdot P_{OAR}}{a \cdot LAI}}\right) \quad (3)$$

where a is an empirical coefficient (-) and b is the soil cover fraction (=LAI/3.0) (-). Daily values of LAI were acquired from linear interpolation between monthly measured values (May−September) conducted by a LI-COR 2000 Plant Analyser in 2022 (Toušková et al., unpublished results). The calibration of a parameter was performed so that the fraction of intercepted precipitation was allowed to range between 15 and 20%, which is an ordinary interception loss of beech canopies (Gerrits et al., 2010). For the winter season (November to April), linear regression functions linking open area snow water equivalent to that below the forest canopy were used (Šípek and Tesař, 2014). The regression equations are based on the measured snow water equivalents in the forest openings and below the spruce (Eq. 4) and beech (Eq. 5) canopies for a period of ten years and are in the form:

$$SWE_{TF}(t) = SWE_{OAR}(t) \cdot 0.595 \quad (4)$$
$$SWE_{TF}(t) = SWE_{OAR}(t) \cdot 0.679 \quad (5)$$

where SWE_{OAR} is the snow water equivalent (mm day^{-1}) in the open area and SWE_{TF} is the snow water equivalent under the forest canopy (mm day^{-1}).

Potential evapotranspiration (PET) was estimated using the Oudin et al. (2005) approach, which offers reliable estimates of PET for long-term water balance studies in the Central European region (Toušková et al., 2025). This approach provided a consistent PET estimate based on data available for the entire observation period (1975–2021), whereas data needed for more sophisticated approaches are not available for the first decades. The actual evapotranspiration (*AET*) was found as the sum of P_{INT} and soil evapotranspiration rate S (comprising soil evaporation and plant transpiration) was then estimated based on the linear decrease in its potential rate with decreasing effective soil water content as proposed by (Feddes and Rijtema, 1972) according to the following Eq. (6) and Eq. (7):

$$S(t) = \frac{LAI}{LAI_{max}} \cdot PET(t) \cdot \Theta_e \quad (6)$$

$$\Theta_e = \left[\frac{\Theta_{(t-1)} - \Theta_r}{\Theta_s - \Theta_r}\right] \quad (7)$$

where PET is the potential evapotranspiration (mm day^{-1}),Θ_e is the effective water content (–), and $\Theta_{r,s}$ are the residual and saturated soil water contents (mm), respectively and $\theta_{(t-1)}$ is modelled volumetric water content at previous day (*t-1*). The drainage component $D(t)$ is a nonlinear function of Θ_e:

$$D(t) = K_s \Theta_e^{\,3+\frac{2}{\lambda}} \quad (8)$$

where K_s is the saturated hydraulic conductivity (mm day^{-1}) and λ is the pore size distribution index (-) linked to the textural structure of the soil layer, which was set to 0.5. In this case, the flow is assumed to be gravity driven, with drainage consisting of deep percolation.

The original SWBM does not include a snow module; hence, snow accumulation and snowmelt had to be considered first, as the experimental catchment lies in an area with regular snow cover. The degree-day method (Gupta, 2001) was chosen for this purpose because it has been proven to be efficient in the Central Europe (Girons Lopez et al., 2020).

2.4 Model parameterisation, validation, and forward simulation

The model was calibrated with the genetic algorithm in two separate steps: one focused on the additional snow module and the second on the original SWBM parameters using fixed values of snow parameters from the first step. In each case, the RMSE of the model response variable (snow water equivalent and soil water content, respectively) was used as the objective function. All model parameters which were subject of calibration are described in Table 1. Four parameters of the snow module were calibrated separately for each winter season so that the input for the soil water model was as accurate as possible. The remaining model parameters were calibrated against the soil water content at both the beech and spruce sites. To obtain soil water content for calibration, the measured pressure heads were used to calculate the volumetric soil water content by means of the van Genuchten (1980) function. The function parameters were retrieved from the measured retention curves specific for each site and depth (see Table S3 in Supplementary material). For more information about the determination of the soil water retention curves, we refer to Šípek et al. (2020). In addition to the minimisation of the RMSE, the model was calibrated with three boundary conditions: (1) simulated drainage from both sites must be approximately 360 mm y^{-1}, which is a value obtained from the long-term measured runoff from the area, (2) higher reported transpiration of beech (Brinkmann et al., 2016, Gebhardt et al., 2023) and (3) beech summer interception loss will be within 15–20% of the open area rainfall, which corresponds to the range reported by Gerrits et al. (2010).

To evaluate model fit, we first split the period of interest into 4 sub-periods for cross-validation, each covering 5 years (2000–2004, 2005–2009, 2010–2014, 2015–2019) and calibrated the model separately for each of these periods using the remaining three sub-periods as unseen datasets for cross-validation. In each case, we constrained drainage to fit the measured runoff by omitting the parameter sets resulting in differences in runoff volume higher than 5 %. Model error in cross-validation was on the same order as measurement error (max. RMSE <3%, see Fig. S4) and parameters did not change substantially when all sub-periods were used. We thus chose to calibrate a single set of model parameters for the entire period so that the water balance (i.e., discharge) could be maintained as close as possible to the measured long-term mean. Using mean drainage estimated from the water balance for the whole period as a constraint led to only minor deterioration of the objective function compared with parameters fitted to the separate four 5-year sub-periods.

Following validation, we thus only used the model fitted to the entire period of available data (2000–2021). Besides the model run in the period of available soil water potential measurements (2000–2021), the calibrated model was run also from 1975 to

1999 when soil water potential measurements were not available in order to quantify annual *AET* and runoff for the period spanning to the beginning of the meteorological measurements.

Table 1. Model parameters. SWE stands for measured snow water equivalent and SWC for soil water content.

Parameter	Abbreviation	Data used for calibration	Objective function
Snowfall correction factor	*SFCF*	SWE	RMSE
Snowfall occurrence temperature	T_{snow}	SWE	RMSE
Snowmelt occurence temperature	T_{melt}	SWE	RMSE
Degree-day factor	*DDF*	SWE	RMSE
Saturated soil water content	θ_s	SWC	RMSE
Residual soil water content	θ_r	SWC	RMSE
Saturated hydraulic conductivity	K_s	SWC	RMSE
Beech interception coefficient	*a*	SWC	RMSE

2.5 Analysis

Meteorological data and soil water contents trend analysis was conducted using trend-free pre-whitening Mann-Kendall approach (Yue et al., 2002). We also calculated annual and 5-yr evaporative ratio (*AET*/*P*) and aridity index (*PET*/*P*) values from our model results to evaluate energy versus water limitation of our sites using the Budyko framework (Renner et al., 2014; Mianabadi et al., 2020). For the analysis of the vertical distributions of pressure heads we utilized a principle of flow-duration curves describing the fraction of time that the magnitude of a given variable is exceeded (Dingman, 2015).

3 Results

3.1 Analysis of the measured soil water regime

The climate conditions of all investigated summer and winter seasons are depicted in Fig. 2. One wet and one dry year were chosen to demonstrate differences among pressure heads between the spruce and beech sites influenced by extreme meteorological conditions (Fig. 3). Specific years were then categorized according to soil wetness régime based on the seasonal distribution of measured pressure heads from May to August.

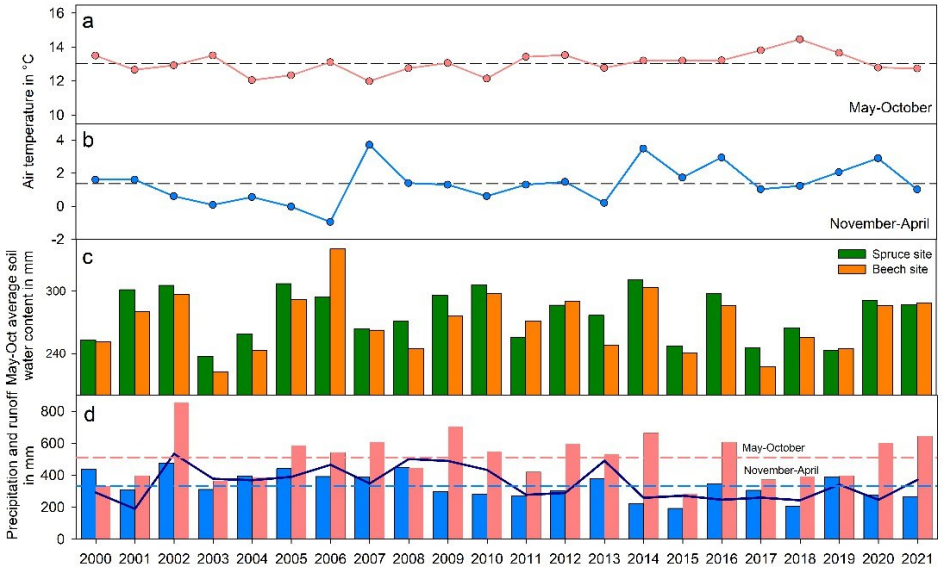

Figure 2: Average air temperatures in summer (a) and winter seasons (b), May-October average soil water content (c) and precipitation sums and runoff (d). The red columns represent the summer seasons (May–October), and the blue columns represent the winter seasons (November–April), dashed lines represent season average values, and dark blue line represents runoff.

3.1.1 Vertical distribution of pressure heads

Pressure-head values were higher at the beech site, with a long-term median of −155 cm compared to −255 cm for the spruce site. However, despite the higher median pressure-head values recorded at the beech site, the occurrence of low pressure-heads was more frequent here as reflected by higher exceedance of pressure values lower than –400 cm from the depth of 30 cm and deeper (Fig. 3). Differences in the vertical distribution of pressure heads were visible, namely, in the topsoil layer (depth of 0–15 cm), where soil under spruce reached permanently lower pressure head values than that under beech. The overall depth distribution of the pressure heads was more uniform under spruce – documented with flatter slope of curve describing the exceedance of pressure heads in all depths (Fig. 3). In contrast, the pressure head depth distribution under beech trees exhibited greater propensity to drying, especially in the bottom soil layers. The slope of exceedance curve is steeper namely between pressure heads of –200 cm and –400 cm. As the soil gets drier then the soil water potential is lower under beech. The beech site, despite having higher pressure heads on average, was therefore more susceptible to more intensive drying than the spruce site.

The differences between the beech and spruce site were less pronounced during the wet years (e.g., year 2020 represented by long-dashed lines in Fig. 3) but the soil under beech was noticeably drier in dry years (see example dry year 2015 represented by short-dashed lines in Fig. 3). Although the differences among the sites were small in wet years, lower pressure heads were observed at the spruce site at all depths. In contrast, during the dry year of 2015, the soil under spruce site was wetter (reached

a higher column average median pressure head) than at the beech site even in the top soil layer (depth of down to 15 cm). Below the depth of 45 cm the pressure head of −850 cm was exceeded in more than 50 % of records under beach and only up to 10 % in the case of soil under spruce canopy. Hence, the differences in pressure heads might be even greater, as the tensiometer data reached their limit more frequently at the beech site than at the spruce site; thus, even lower pressure heads were likely to occur at the beech site. If the number of dry years increase in the future, the soil under beech will therefore become drier during the growing seasons.

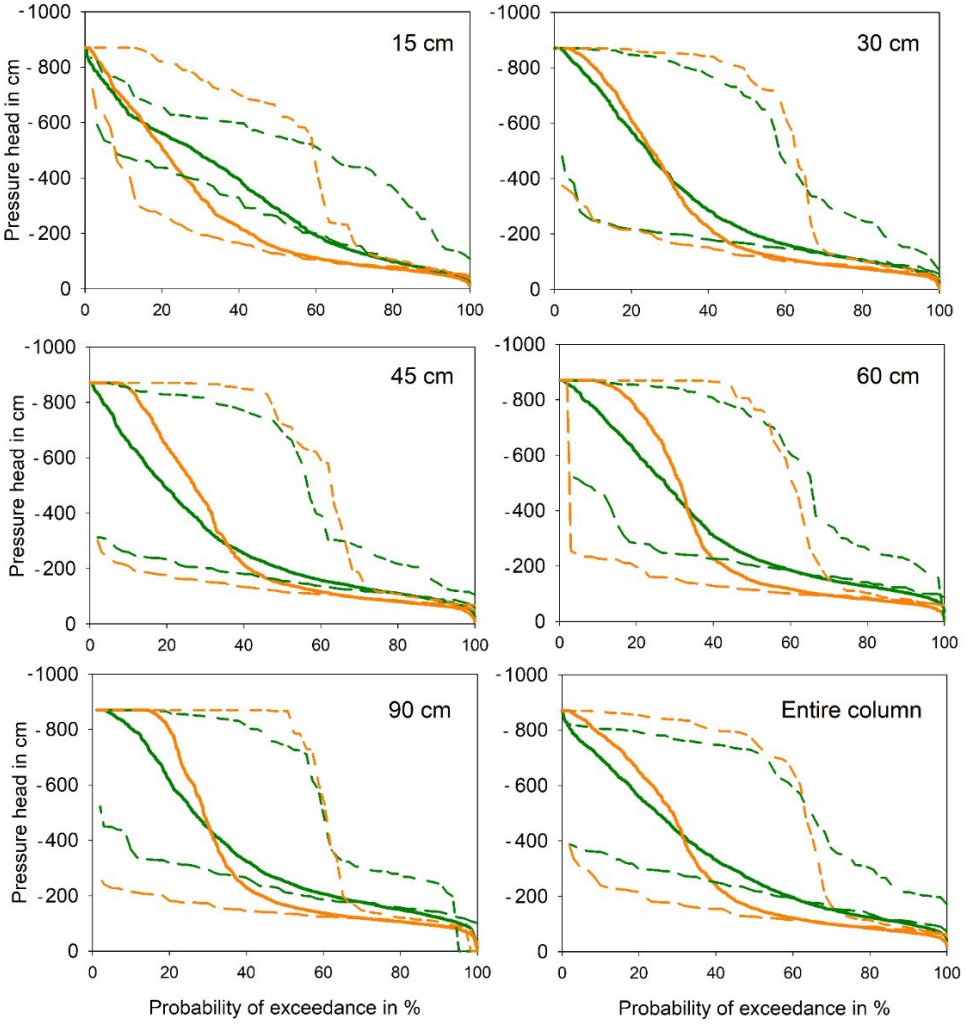

Figure 3: Exceedance probabilities of pressure head for particular depths for averaged the entire period (thick solid lines), dry season 2015 (short dashed lines) and wet season 2020 (long dashed lines). Green colour represents spruce and orange beech forest.

3.1.2 Soil wetness trend and categories

We found significant negative trends in both daily soil moisture time-series, 0.7 mm yr^{-1} in beech (p-value 0.001), 0.2 mm yr^{-1} in spruce (p-value 0.0015), documenting gradual changes in soil water regime which correspond to the increasing occurrence of water limited seasons. Looking closer, we divided years into four soil wetness categories based on the typical seasonal development of their measured pressure heads.

We have used four categories of soil moisture regime for further analysis:

- category A - spruce retained lower pressure heads throughout most of the season
- category B - only one single event when the beech site attained lower pressure heads than spruce
- category C - the pressure head decreased more pronouncedly at the beech site for a significant part of the summer season
- category D - refers to the seasons when the tensiometer measurement limit of –865 cm was reached (mostly at the beech site)

The evolution of average pressure heads for each month of the summer season over the measured period (2000–2021) is depicted in Fig. 4. At both sites, a similar pattern of decreasing pressure heads from the onset of the summer season can be observed. However, there are noticeable differences between the two sites. At the beginning of every summer season (May), the spruce site reached lower pressure head values than did the beech site (the average difference in pressure heads was 130 cm). Typically, as the season progresses, the pressure heads at the beech site decrease more than those at the spruce site. However, this was not valid for the wet seasons of 2002, 2005, 2020, and 2021, when spruce retained lower pressure heads throughout most of the season (see Fig. 4), as no precipitation deficit was observed (category A). For those seasons, the difference between the two sites was negligible, with their average values fluctuating between −100 and −200 cm. In the other few years, when above average precipitation seasonal sums were reached (category B, including the years 2006, 2010, 2012, 2014, and 2016), there was only one single event when the beech site reached lower pressure heads (below −400 cm), which was usually ended by rainfall higher than 50 mm·day^{-1}. In contrast, in the periods with below average precipitation, the pressure head decreased more pronouncedly at the beech site for a significant part of the summer season (category C included, e.g., years 2007, 2012 or 2019, as shown in Fig. 4). With even more prominent precipitation deficits (in 2003, 2008, 2015 and 2017), the beech site was the first and often only site to reach the tensiometer measurement limit of –865 cm (category D) – up to ten times more often than the spruce site, especially in the bottom soil layers. Real pressure head values were likely significantly lower. As lower pressure heads cannot be recorded at the beech site with tensiometer measurements (measuring limit was reached) and pressure heads at the spruce site only seldom approached this limit, the differences between both sites were higher than documented by sensors. The effect on our analysis was likely insignificant as the implied differences in the amounts of water retained would be rather small. By the end of the season, pressure head values slowly increased, with beech still maintaining lower pressure head values than spruce.

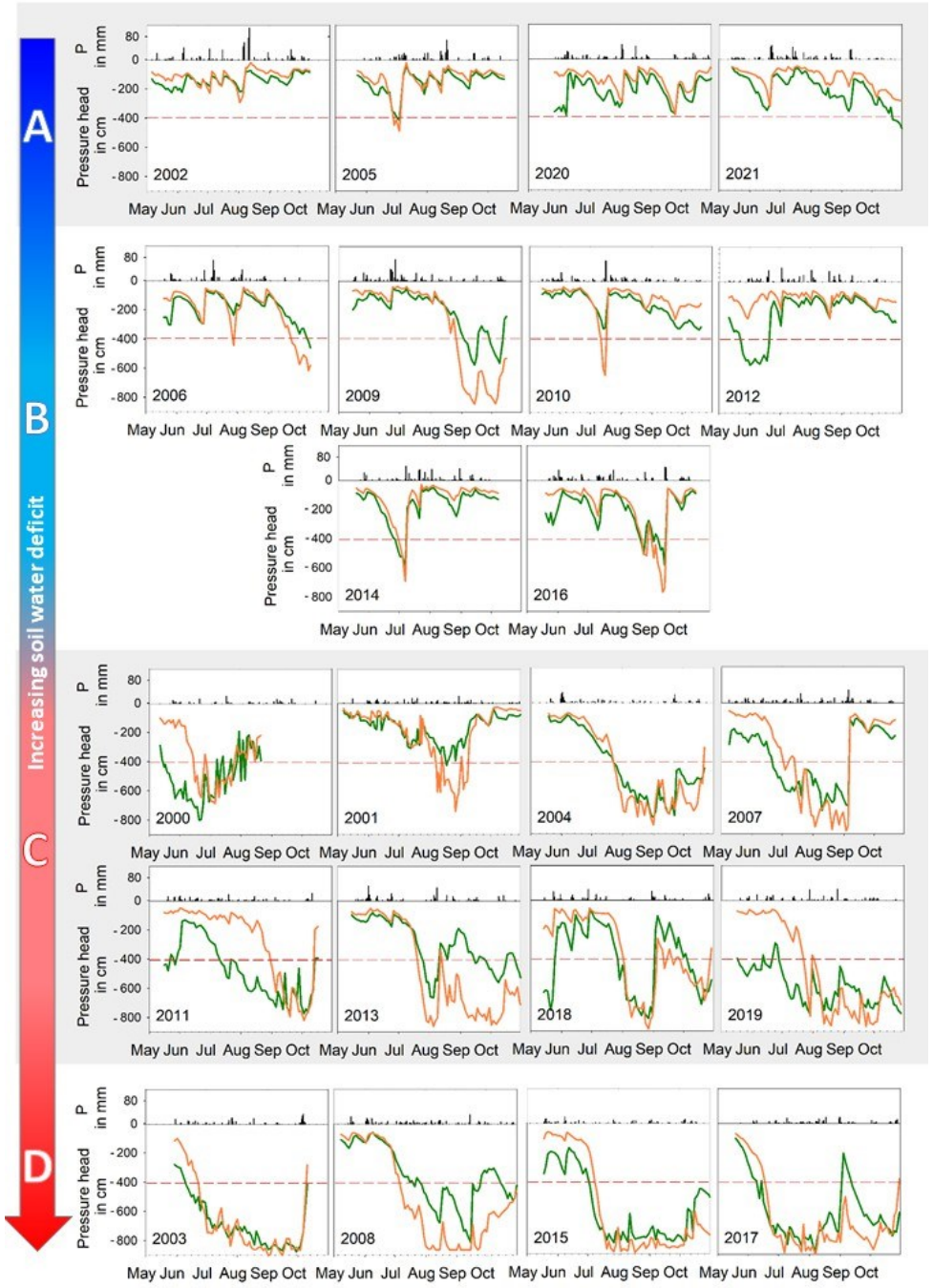

315

Figure 4: Daily precipitation (P) (black columns) and soil column average pressure heads at beech (orange line) and spruce (green line) sites in all investigated years divided into four wetness categories (A–D) defined by pressure head values. The red dashed line represents the pressure head of −400 cm used for the division of categories A and B.

3.2 Modelling of evapotranspiration and drainage

3.2.1 Model calibration result

The modified SWBM model was used to obtain evapotranspiration and drainage fluxes over a period of twenty-two years (2000–2021) at both spruce and beech sites. The mean RMSE values (2000–2021) for the snow module were 7.1 mm (beech) and 9.5 mm (spruce), which are in accordance with Šípek and Tesař (2017), who modelled snow cover dynamics from 2009 to 2014 and reached an RMSE value of 9.1 mm in a spruce stand. An example of the modelled cumulative snow precipitation fitted to the measured SWE is shown in Fig. S5a.

The resulting mean RMSE (2000–2021) were 2.5% and 2.9% for the spruce and beech sites, respectively. The modelled long-term drainage was 369 mm year^{-1} for beech and 365 mm year^{-1} for spruce. The average annual discharge for the experimental Liz catchment was 360 mm, which was very close to the modelled values. The final parameters of the SWBM (θ_s, θ_r, K_s, λ) for each site are documented in Table 2. Examples of modelled and observed volumetric water contents are depicted in Supplementary material (Fig. S5b).

Table 2. Calibrated model parameters

	a	θ_s	θ_r	K_s	λ	*RMSE*
Spruce	-	514.4	79.8	165.9	0.50	2.5 %
Beech	0.50	401.0	0.0	6.7	0.50	2.9 %

3.2.2 Simulated Water balance

The total actual evapotranspiration (AET; encompassing transpiration and soil evaporation (S) and interception (P_{int})) and drainage attain similar values at both plots on average. The total average AET is approximately 540 mm year^{-1}, and the drainage is between 350 and 360 mm year^{-1} (Table 3). The beech reaches on average almost 80 mm year^{-1} more S than the spruce stand, on the other hand, the evaporation from the interception storage in the spruce stand exceeds that of the beech stand to the same extent. The resulting AET values therefore do not differ greatly from each other because S and interception tend to compensate for each other between stands, which is hence also reflected in similar drainage.

Even though the winter seasons are characterised by lower precipitation sums than the summer seasons (approximately 1/3 of the annual precipitation), the spruce forest had, on average, a higher rate of interception (133 mm season^{-1}) due to defoliated beech forest (106 mm season^{-1}) (Table 3). From the AET perspective, the difference in interception is further raised by slightly higher transpiration and soil evaporation under the spruce canopy (11 mm season^{-1}). Nevertheless, the interception rate and winter transpiration at the spruce site resulted in a lower amount of water available for infiltration and therefore a lower modelled soil water content during the winter months. The drier soil in spruce forests regularly represents an initial condition for the summer season. A higher soil water content below the beech canopy was a reason for higher modelled drainage during the winter season at the beech site (by 34 mm season^{-1} on average).

Table 3: Modelled soil water balance components (mm) at the spruce and beech sites. S represents transpiration and soil evaporation from the soil column. AET stands for actual evapotranspiration.

	2000–2021		WET 2020		DRY 2015		Winter season		Summer season	
	SPR	BEE	SPR	BEE	SPR	BEE	SPR	BEE	SPR	BEE
Precipitation	901		923		499		340		561	
S	261	340	270	353	221	288	46	25	213	314
Interception	275	204	270	194	201	139	133	106	143	103
AET	536	545	540	547	422	427	179	132	356	417
Drainage	365	370	352	337	145	190	162	196	205	174

In the summer, transpiration flux significantly affected the water balance at both sites but it was noticeably higher in the beech forest (see Table 3). The interception pattern of both stands was preserved, with spruce having higher interception (143 mm season^{-1}) than beech (103 mm season^{-1}). The differences in the soil water content were therefore caused by the transpiration in the beech stands (by 101 mm season^{-1} on average). Hence, soil under spruce trees retained (with the ongoing summer season) more water than soil under beech trees, where soil moisture was more effectively used for higher transpiration of beech trees, especially during dry spells. The wetter soil under spruce (in the majority of summer seasons) resulted in higher drainage by 34 mm season^{-1} on average.

3.3 Interannual comparison of climatic drivers of seasonal soil water regime and soil water fluxes

Figure 5 shows the relative rankings of individual study years according to snow cover duration, air temperature, summer precipitation (May-October), and their classification into the four wetness categories according to the resulting pressure head dynamics, shown in Fig. 4.

The dominant factor controlling the soil water regime in the growing season was the amount of summer precipitation. A significant soil moisture deficit could develop even following a winter with abundant snow. Fig. 5 clearly shows the direct link between pressure head and summer precipitation, where lower pressure heads are linked mainly to years with lower seasonal precipitation, and higher pressure heads are linked to years with abundant precipitation. The correlation coefficient between summer precipitation and soil moisture regime category was 0.80 (significant at 0.05 probability level). Two marginal

categories (A and D) were always linked to specific climatic conditions (see Fig. 5). Category A, denoting wet soil (hence small differences between beech and spruce sites), was always determined by above average precipitation amounts and below average air temperatures observed in the summer season. Category D, representing the very dry soil moisture regime, was always accompanied by low observed precipitation amounts in the summer season. Two middle categories (wetter B and drier C) tend to be connected primarily with above (in the case of B) and below (category C) average precipitation sums. The influence of preceding winter snow cover and summer season air temperatures was ambiguous, as seen in the frequently strongly mismatched placement of particular seasons along these axes in Fig. 5, compared to the resulting soil wetness category. The correlation coefficient with soil moisture regime were 0.30 and 0.08 for summer air temperature and snow cover duration, respectively. Higher correlation coefficient was also observed for the summer vapour pressure deficit (VPD) attaining the value of 0.61 (not shown in the Fig. 5).

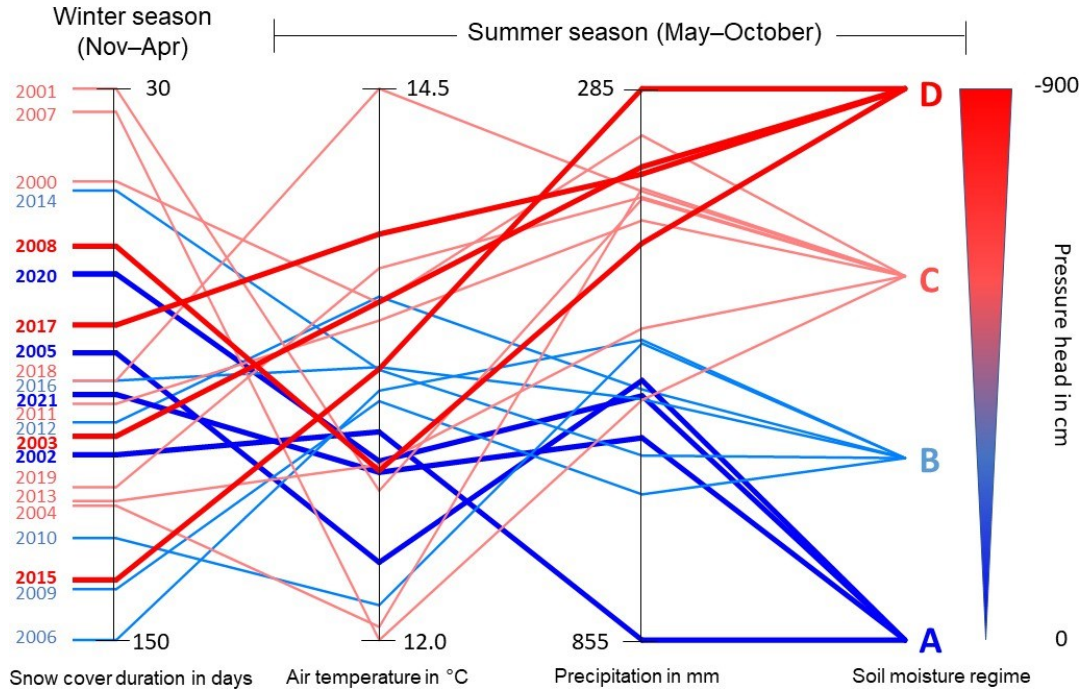

Figure 5: Average air temperature and precipitation sums for each summer season (represented by one horizontal line) encompassing the preceding winter snow cover duration. Each season is ultimately linked to a specific wetness category (A–D), as shown in Fig. 4.

The most pronounced deviations from the observed link between summer precipitation sums and the soil moisture regime were in the 2013 and 2007 seasons, with above average precipitation but a drier soil moisture regime. This was caused by a near absence of snow cover observed in the winter of 2006/2007, accompanied by the highest recorded winter air temperature (Fig. 2), and by the extreme floods in 2013, when the catchment received 1/3 of all summer precipitation in June but saw below

average precipitation amounts during the rest of the season. These two factors caused a drier soil moisture regime even when above average precipitation sums were recorded. These results therefore document how different rainfall conditions influence the development of soil moisture content and the different behaviours of beech and spruce in growing season (Fig. 4).

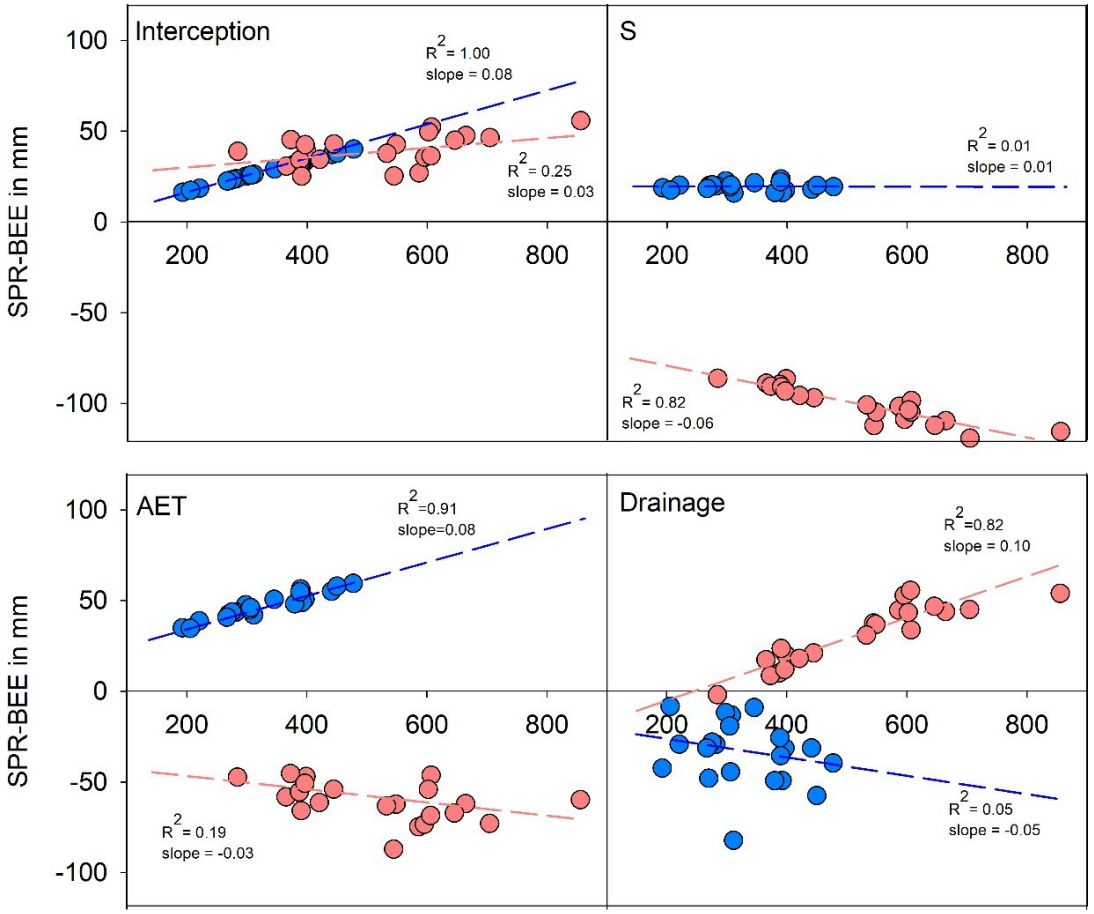

Figure 6: Differences between spruce and beech modelled soil water fluxes (AET, D) during summer (May to October, orange colour) and winter (November to April, blue colour) in relation to precipitation. AET can also be divided into INT and S (upper panel).

Seasonal precipitation also had a major influence on the differences between beech and spruce sites in particular water fluxes (Fig. 6). Differences in all fluxes could be positively or negatively related to seasonal precipitation sums with the exception of winter transpiration and soil evaporation (S). The differences in winter and summer interception, winter actual evapotranspiration (governed mainly by interception) and summer drainage increased with increasing precipitation. By contrast, summer transpiration and soil evaporation, summer actual evapotranspiration (governed by transpiration) and winter drainage were negatively related to precipitation sums. The largest absolute differences in water fluxes between the stands were recorded during wet summer seasons. The most pronounced discrepancies were in the rates of transpiration and soil

evaporation (higher for beech plots; up to 120 mm season^{-1}), summer interception (higher for spruce plots; up to 55 mm season^{-1}) and drainage (higher for spruce plots; up to 55 mm season^{-1}). The lowest differences occurred during the dry winter seasons. The differences in the winter seasons were generally less prominent, usually below 40 mm season^{-1}.

4 Discussion

4.1 Transition from energy and water limitation

The studied catchment falls within a montane system classically thought of as energy-limited not just under "baseline" (1961–1990) climate but over previous millennia (Schafstall et al., 2024). Our results show gradual soil drying following an accelerating shift in the balance between atmospheric water supply and demand (Fig 7). The transition from energy- toward water-limitation predicted for the coming decades (Denissen et al., 2022) is in fact already apparent over our measurement period. Incipient water limitation at the annual-scale was first observed for the drought year 2003 and four times since, with entirely unprecedented examples of outright water-limitation over the years 2015 and 2018. Our dataset thus offers some of the first observations of the hydrologic functioning of these previously cold and humid montane forest types under water limitation.

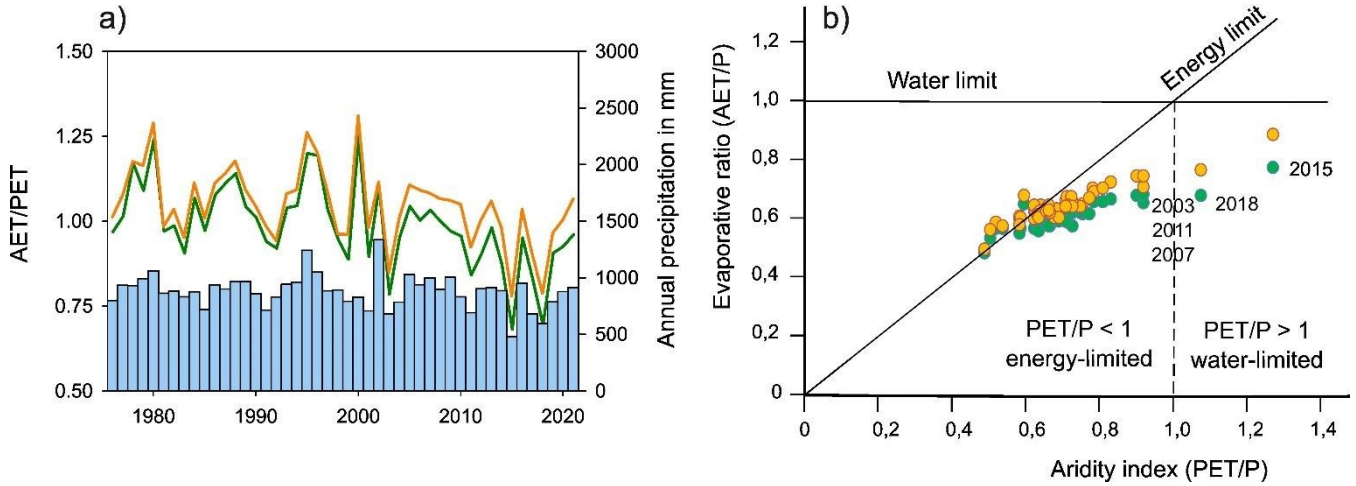

Figure 7. Long-term evolution of ration of AET to PET ratio (1975–2021) in the comparison with annual precipitation sums (a), and ratios of actual and potential evapotranspiration to precipitation from the experimental watershed covering the period 2000 to 2021 shown within the Budyko curve reference frame (b). Green lines/points represent the spruce site and orange lines/points beech. Ratios of AET/PET higher than 1.0 are given by the winter snow interception as its estimation is not based on the PET.

We found that increased water limitation enhances differences in annual evaporative ratio between beech and spruce forest, indicating divergence of their water balance in a drier climate. The differences in soil moisture were strongly dependent on the

seasonal precipitation sums. Even though, observed trends in the catchment over the period 1975–2021 show that significantly increasing annual atmospheric demand (*PET*) (slope 1.6 mm y^{-1}, p-value 1.91E-06) rather than insignificant changes in precipitation supply (*P*) drives increased aridity over the long term, the differences in flux partitioning in the driest years were strongly dependent on the seasonal precipitation sums (Figs. 5-6). With increasing water limitation, the trend of atmospheric demand will cease to exert direct control over the water balance (*P-AET*), while interactions between seasonal precipitation patterns and vegetation processes will become increasingly important drivers.

4.2 Vegetation and climate interactions in the soil moisture regime

Our unique 22-year long dataset of measured soil water potentials, air temperatures and precipitation sums enabled robust comparisons of the soil water regime between dry and wet years (Fig. 8), allowing modelled soil water fluxes under beech and spruce canopy to reveal the interactions between forest cover, climate, and soil moisture. Differences in winter soil moisture regime were determined mainly by the higher interception of the spruce canopy, which resulted in higher pressure heads under beech causing more drainage compared to the spruce site. When the precipitation in the following summer season was high, only minor differences in pressure heads were recorded between stands, even though the spruce site maintained slightly lower pressure heads throughout most of the season (as a winter season legacy effect). The resulting differences remained small as the higher interception of spruce did not exceed the higher rate of transpiration of beech in the growing season.

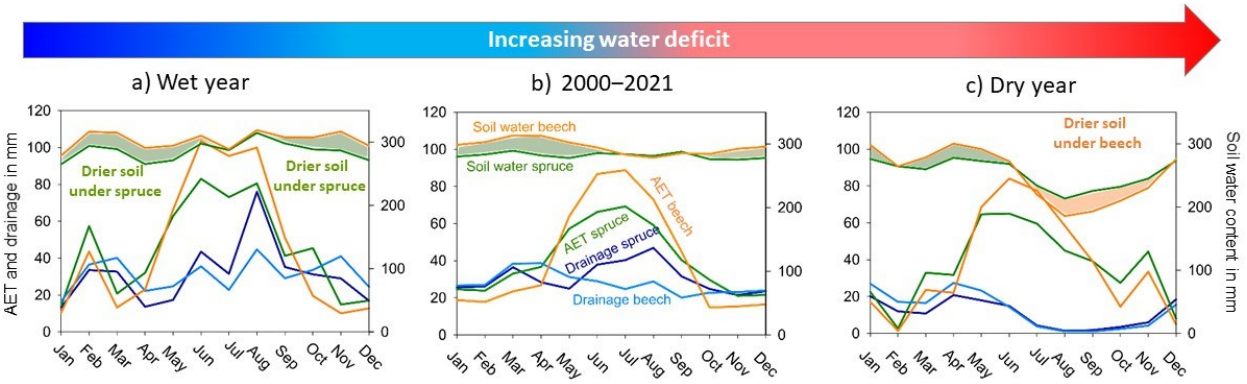

Figure 8. A monthly water budget under spruce and beech canopy in wet (2020) and dry (2015) year and its overall averages

As the growing season advanced, transpiration became an increasingly important factor in the soil moisture regime. The balance between interception and transpiration and soil evaporation resulted in greater drainage under the spruce canopy. In seasons with prominent precipitation deficits (Fig.8c), the soil at the beech site consistently dried out more than at the spruce site. This can be explained by species-specific plant hydraulic traits. Beech has a wider and deeper rooting pattern and thus soil volume and water in its root zone, especially at greater depths (Čermák et al., 1995; Schwärzel et al., 2009; Gebauer et al., 2012). Beech also has a greater tissue-specific hydraulic conductance due to favourable anatomical and morphological traits, allowing it to supply leaves with water more efficiently at a given root-zone water potential (Tyree & Zimmermann, 2002).

As a result, beech behaves more anisohydrically, maintaining transpiration rates in the face of drier soils, in contrast to the more isohydric spruce, whose lower ability to supply water to its foliage requires it to restrict transpiration earlier as the soil dries out (Čermák et al., 1995; Zweifel et al., 2002; Schume et al., 2004; Hochberg et al., 2017; Gebhardt et al., 2023). Schwärzel et al. (2009) and Floriancic et al. (2022) reported higher evaporation from soil and litter under beech stands compared to spruce. Additional factors possibly affecting differences in soil water regimes include lateral flow, which is reportedly more common at beech sites (Jost et al., 2012), and root water redistribution (Burgess et al., 1998). In dry summers, the drainage remained higher under spruce canopy, although the difference between the stands decreased as the difference between interception and transpiration declined.

Robust interannual comparisons of the soil moisture regime under beech and spruce canopies integrated over the entire soil column allow this study to resolve the contradictory results of previous work limited in scope of over space or time. While Schume et al. (2004) and Šípek et al. (2020) observed drier soil during the growing season under a beech canopy, Schwärzel et al. (2009) found the opposite. In the latter case the more prominent drying under spruce was attributed to the nonuniform and rocky soil compared to beech site. Rötzer et al. (2017) and Kuželková et al. (2024) also reported drier soil under spruce but these studies covered only the upper part of the soil profile (0—30 cm). Viewed over two decades and the entire soil profile, the contrasting soil moisture regimes of individual studies prove to be precipitation-driven while differences between the forest types are dominated by depths of 30 cm and more, where the greatest differences arise. The latter finding highlights the need for soil moisture measurement at greater depths, which are too often neglected.

We also found a surprising trend of intra-annual precipitation redistribution in the catchment since 1975. Our observations show significantly decreasing winter (slope -1.7 mm y^{-1}, p-value 0.061) and insignificantly increasing summer *P* (slope 1.7 mm y^{-1}, p-value 0.24), which is entirely contrary to prevailing expectations based on climate model predictions (Kyselý et al., 2011). Given that seasonal *P* sums interact with vegetation processes to affect the overall water balance, the actual direction of this trend will not only determine when water arrives in the system but also how it is partitioned.

A precipitation shift in either direction would reinforce the ecohydrological differences between the two forest types. With a shift to winter precipitation, differences in summer transpiration would be abated by lower growing-season input and groundwater recharge would become increasingly reliant on deciduous forest due to its low winter interception. By contrast, a shift to summer precipitation would decrease ET from winter interception by evergreen forest and increase the importance of montane spruce forest to recharge. The rates of groundwater recharge under the two forest types will thus continue to diverge under increased water limitation in either precipitation seasonality scenario.

Further developments in the forest species composition of montane catchments is also likely to play a role. Given the present dominance of spruce, the precipitation seasonality trend in our catchment is consistent with groundwater recharge shifting to the summer and offsetting overall drying somewhat. Increasing representation of beech would exacerbate higher atmospheric demand, given their ability to consume soil water even during drought periods. A combined trend of wetter winters and increasing representation of beech trees in Central Europe, would lead to even higher winter groundwater recharge and runoff. Overall, these various possible trajectories underscore the key role of climate-vegetation feedbacks in modulating how

hydroclimatic changes actually affect water balance. Given ongoing hydroclimatic shifts, process understanding of these interactions will become increasingly important to detailed projections of water flux partitioning.

4.3 Scope of the study

By focusing on a pair of instrumented sites in a long-term experimental catchment, our study design allows the key processes to be examined in detail at the appropriate scale. Nevertheless, the landscape position of the study system gives it particular significance to projections of future ecological and hydrological dynamics across the region. Through both locally higher inputs and intra-annual storage, forested montane headwater catchments play an outsize role in baseflow generation, supporting regional hydrological stability (Viviroli et al., 2007, Immerzeel et al, 2020). The broader landscape's (i.e., downstream) water regimes will be particularly sensitive to their seasonal functioning under climate change. Furthermore, the observation of an annual-scale switch from energy- to a water-limitation in a montane forest is strongly indicative for large parts of the generally warmer, drier Central European landscape.

On the other hand, the resulting process understanding is only transferable to an extent circumscribed by an adequate consideration of the landscape position of the study system. For example, while summer season temperature did not greatly affect the water balance in our study catchment, this may in part be due to comparatively low a vapour pressure deficit (VPD) at this elevation. As VPD is a strongly nonlinear function of air temperature (Groissord et al., 2021), lower elevation forests will face disproportionately higher summer VPD, potentially increasing its importance in their water balance. This factor may also increase in importance disproportionately across the landscape with further climate warming. Given our findings, we would again expect any increased effects to be stronger in beech rather than spruce stands, due to their relatively anisohydric transpiration, and to shift the state of these systems further towards water limitation.

It should urgently be evaluated how widespread the observed deviation from the predicted trend in the seasonal timing of precipitation is. If it is merely a strong local anomaly, we would expect drier summers to exacerbate overall water-limitation and the importance of winter recharge from deciduous forest to increase over time. If the trend we found is real but limited to catchments with the specific landscape position of ours (e.g., similar exposure and position within the Bohemian Forest), then these catchments may play an offsetting role in the shifting regional water balance, smoothing out shifts in recharge. If, on the other hand, this deviation is due to a general (e.g., orographic) effect not accounted for in climate models, it may generalise to the entire Bohemian Forest and reverse expectations about both the seasonality of future water availability and, through interactions with vegetation, its annual sums in the region.

Measurement limitations

As the measuring limit of the tensiometers is −865 cm (−85 kPa), pressure heads below this limit could not be recorded. Some information was therefore lost, especially at the beech site where periods with a constant limit value were clearly visible.

However, for pressure heads lower than the measurement limit, the loss and gain of the volumetric water content corresponding to the unit change in the pressure head is very small (a 100 cm change in the pressure head accounts for less than 0.002 cm^3 cm^{-3} of the change in the volumetric water content). The same rate was observed for a saturation to a pressure head of −100 cm, which is equal to 0.22 cm^3 cm^{-3}. Hence, the changes in pressure head concerning such low heads have a negligible effect on the volumetric soil water content.

To encompass the influence of soil moisture spatial variability, 2 to 5 tensiometers were used at each depth. As the standard errors of precipitation measurements are 10% in summer and 40% in winter, it can be assumed that these measurements of precipitation can also be biased due to wind eddies around the rain gauge and deposited precipitation (Dingman, 2015). Even though the study sites are located close to the rain gauges (<500 m) and we also checked the open area rainfall data with the raingauges located in the forest, there were occasional episodes in the data where the volumetric water content did not match to the volume measured rainfall, which resulted in a few errors in the soil moisture modelling, especially of the rises in the volumetric soil moisture content.

Modelling limitations

Observations from the above-mentioned periods when soil pressure heads were at or below the measuring range of the tensiometer were not used to constrain or evaluate the soil water balance model. The model was allowed to run freely below this limit, and the error statistics from these periods were not considered. Eliminating this bias did not allow model fitting during dry periods. Another issue arose from the noted episodes of rainfall over- and underestimation. As both issues affected periods with negligible water fluxes, neither was found to affect the long-term water balance. Finally, as shown in Cejpek et al. (2018) and Jačka et al. (2021), different vegetation species growing on the same soil type tend to change soil properties, whether due to different root systems, soil biology or litter. Even though the soil parameters (Ks, $\Theta_{e,r,s}$) that were entered into the balance model have measured equivalents at each site, their values in this study are the result of model calibration.

As we used a simple temperature-based approach for the estimation of PET we compared these estimates with state-of-the-art method of Penman-Monteith (Monteith, 1965) over the period of available data (from 2008). The influence of method selection on the resulting water fluxes was negligible (<2% on seasonal and annual PET, AET, modelled soil water content) (see Fig. S6). The sensitivity of PET to canopy-specific aerodynamic resistance parameterisation (beech vs spruce) in the Penman-Montieth approach was in our case outweighed by the influence of soil water availability (reflected in stomatal resistance). We limited our inferences to seasonal and annual comparisons, at which scales the differences between the PET estimation methods are negligible.

Since the model validation was performed on the average annual discharge value measured for the entire watershed, which is mostly covered by spruce forest, it is possible that these values may not correspond with the discharge that might occur from the beech site alone. This might affect confidence in the balance components (drainage and actual evapotranspiration) at the beech site as compared to the spruce site. However, the modelled high transpiration rates at the beech sites mostly follow from fitting to the high-resolution time series of measured local soil moisture data, which show lower values during the summer

season compared to spruce, and simultaneous observations of no change in groundwater levels. The higher modelled transpiration rates of beech during the summer season presented in this study could also be supported by the higher measured sap flow during the summer season in Switzerland (Brinkmann et al., 2016) or nearby Kranzberg forest in Bavaria (Gebhardt et al., 2023). Moreover, due to the absence of measured soil moisture data below the tensiometer measurement limit, it could be assumed that as soil moisture values could be even lower at beech sites, transpiration will be higher than estimated. To avoid such uncertainties in future research, detailed sap flow measurements might serve for model calibration, which could then show the values of actual evapotranspiration and drainage more precisely.

5 Conclusion

Ongoing climate change is forcing a transition from energy- to water-limitation and altering the species composition of European forests. We analysed a multi-decade record of soil water potential and climatic data to determine which variables have driven water limitation so far and which vegetation processes most exacerbate or dampen it. We found evidence of annual-scale water limitation, unprecedented in Central European montane forest. While increasing atmospheric demand drives progressive water limitation at the broader scale, seasonal water supply interacts with vegetation processes to determine the actual soil water balance in the studied beech and spruce stands. Decreased summer precipitation drove stronger drying in the beech stand compared to spruce. Our water-balance model suggests that beech did not reduce transpiration rates in dry summers but continued to exploit deeper soil water reserves more extensively (by ~100 mm season^{-1} on average), resulting in decreased drainage. During wet summers and all winter seasons, the soil was drier in the spruce stand, due to higher winter interception by its evergreen canopy (by ~40 mm season^{-1} on average). Hence, in wet periods, drainage remained higher in the beech forest.

The results suggest that with progressing water-limitation, soil water will increasingly be disproportionately depleted in by forests composed of deeper-rooted, more anisohydric species. The combined effects of climate and forest composition change may thus increase the severity of summer soil drought and limit groundwater recharge. On the other hand, increasing the proportion of deciduous species should result in increased winter recharge, due to decreased interception by leafless canopies. As climate-vegetation interactions represent key sources of uncertainty in predicting shifts in ecosystem function and composition under climate change, we expect such advances in process understanding will contribute to the next generation of models and projections, facilitating both ecosystem and water management during the ongoing hydroclimatic shift.

Author contribution

VS, MT, LV created the concept and set the methodology; NZ, VS, JT, JK carried the investigation; NZ implemented the model and created visualizations; NZ, VS and MB wrote the manuscript draft; all authors reviewed and edited the manuscript.

Competing interests

The authors declare that they have no conflict of interest.

Acknowledgement

This research was supported by the Czech Science Foundation (GA CR 24-10375S), the institutional support of the Czech Academy of Sciences, Czech Republic (RVO: 67985874, 67985939), and by the programme framework of the Strategy AV21. The authors would like to thank David Pěsta for conducting regular field measurements.

References

Arnold, J. G., Kiniry, J. R., Srinivasan, R., Williams, J. R., Haney, E. B., amd Neitsch, S. L.: Soil and Water Assessment Tool Input/Output Documentation: Version 2012. Texas Water Resources Institute, College Station, 2012.

Braden, H.: Ein Energiehaushalts-und Verdunstungsmodell for Wasser und Stoffhaushaltsuntersuchungen landwirtschaftlich genutzer Einzugsgebiete, Mittelungen Deutsche Bodenkundliche Geselschaft, 42, 294-299, 1985.

Brázdil, R., Dobrovolný, P., Mikšovský, J., Pišoft, P., Trnka, M., Možný, M., and Balek, J.: Documentary-based climate reconstructions in the Czech Lands 1501–2020CE and their European context, Clim. Past, 18, 935–959, doi: 10.5194/cp-18-935-2022, 2022.

Brázil, R., Zahradníček, P., Dobrovolný, P., Štěpánek, P., and Trnka, M.: Observed changes in precipitation during recent warming: The Czech Republic, 1961–2019, Int. J. Climatol., 41, 3881–3902, doi:10.1002/joc.7048, 2021.

Brinkmann, N., Eugster, W., Zweifel, R., Buchmann, N., and Kahmen, A.: Temperate tree species show identical response in tree water deficit but different sensitivities in sap flow to summer soil drying, Tree Physiol., 36, 1508–1519, doi: 0.1093/treephys/tpw062, 2016.

Brocca, L., Melone, F., and Moramarco, T.: On the estimation of antecedent wetness conditions in rainfall-runoff modelling, Hydrol. Process., 2274, 2267–2274, doi:10.1002/hyp.6629, 2008.

Brocca, L., Camici, S., Melone, F., Moramarco, T., Martínez-Fernández, J., Didon-Lescot, J.F., and Morbidelli, R.: Improving the representation of soil moisture by using a semi-analytical infiltration model, Hydrol. Process., 28, 2103–2115, doi:10.1002/hyp.9766, 2014.

Burgess, S. S. O., Adams, M. A., Turner, N. C., and Ong, C. K.: The redistribution of soil water by tree root systems, Oecologia, 115, 306–311, doi:10.1007/s004420050521, 1998.

Cejpek, J., Kuráž, V., Vindušková, O., and Frouz, J.: Water regime of reclaimed and unreclaimed post-mining sites, Ecohydrology, 11, 1–9, doi:10.1002/eco.1911, 2018.

Čermák, J., Cienciala, E., Kučera, J., Lindroth, A., and Bednářová, E.: Individual variation of sap-flow rate in large pine and spruce trees and stand transpiration: a pilot study at the central NOPEX site, J. Hydrol., 168, 17–27. doi:10.1016/0022-1694(94)02657-W, 1995.

Daněk, P., Šmaonil, P., and Vrška, T.: Four decades of the coexistence of beech and spruce in a Central European old-growth forest, Which succeeds on what soils and why? Plant Soil, 437, 254–272, doi :10.1007/s11104-019-03968-4, 2019.

Denissen, J. M. C., Teuling, A. J., Pitman, A. J., Koirala, S., Migliavacca, M., Reichstein, M., Winkler, A. J., Zhan, C., Orth, R.: Widespread shift from ecosystem energy to water limitation with climate change. Nature Climate Change, 12, 677–684. doi:10.1038/s41558-022-01403-8, 2022.

Dingman, S. L.: Physical hydrology, 3. ed. Waveland Press, Inc., Long Grove. doi:10.1177/030913338901300106, 2015.

Feddes, R. A., and Rijtema, P. E.: Water withdrawal by plant roots, J. Hydrol., 17, 33–59. doi:10.1016/0022-1694(72)90065-0, 1972.

Floriancic, M. G., Allen, S. T., Meier, R., Truniger, L., Kirchner, J. W., and Molnar, P.: Potential for significant precipitation cycling by forest-floor litter and deadwood, Ecohydrology, 16, 1–16, doi:10.1002/eco.2493, 2022.

Gebauer, T., Horna, V., and Leuschner, C.: Canopy transpiration of pure and mixed forest stands with variable abundance of European beech, J. Hydrol., 442–443, 2–14, doi: 10.1016/j.jhydrol.2012.03.009, 2012.

Gebhardt, T., Hesse, B. D., Hikino, K., Kolovrat, K., Hafner, B. D., Grams, T. E. E., and Häberle, K. H.: Repeated summer drought changes the radial xylem sap flow profile in mature Norway spruce but not in European beech, Agric. For. Meteorol., 329, 109285, doi:10.1016/j.agrformet.2022.109285, 2023.

Gerrits, A. M. J., Pfister, L., and Savenije, H. H. G.: Spatial and temporal variability of canopy and forest floor interception in a beech forest, Hydrol. Process., 24, 3011–3025, doi:10.1002/hyp.7712, 2010.

Girons Lopez, M., Vis, M., Jenicek, M., Griessinger, N., and Seibert, J.: Complexity and performance of temperature-based snow routines for runoff modelling in mountainous areas in Central Europe, Hydrol. Earth Syst. Sci., 24, 4441–4461, doi:10.5194/hess-24-4441-2020, 2020.

Green, J. K., Seneviratne, S. I., Berg, Am. M., Findell, K. L., Hagemann, S., Lawrence, D. M., and Gentine, P.: Large influence of soil moisture on long-term terrestrial carbon uptake, Nature, 565, 476–479, doi: 10.1038/s41586-018-0848-x, 2019.

Grossiord, C., Buckley, T. N., Cernusak, L. A., Novick, K. A., Poulter, B., Siegwolf, R. T. W., Sperry, J. S., and McDowell, N. G.: Plant responses to rising vapor pressure deficit, New Phytol., 226(6), 1550–1556,doi:10.1111/nph.16485, 2020.

Gupta, R. S.: Hydrology and hydraulic systems. Waveland Press, Long Grove, 2016.

Hari, V., Rakovec, O., Markonis, Y., Hanel, M., and Kumar, R.: Increased future occurrences of the exceptional 2018–2019 Central European drought under global warming, Sci. Rep-UK, 10, 12207, doi:10.1038/s41598-020-68872-9, 2020.

Hochberg, U., Rockwell, F. E., Holbrook, N. M., and Cochard, H.: Iso/Anisohydry: A Plant–Environment Interaction Rather Than a Simple Hydraulic Trait, Trends Plant Sci., 23(2), 112–120, doi:10.1016/j.tplants.2017.11.002, 2018.

Hrkal, Z., Milický, M., and Tesař, M.: Climate change in central Europe and the sensitivity of the hard rock aquifer in the Bohemian Massif to decline of recharge: Case study from the Bohemian Massif. Environ. Earth Sci., 59, 703–713, doi:10.1007/s12665-009-0067-8, 2014.

Huang, X., Shi, Z. H., Zhu, H. D., Zhang, H. Y., Ai, L., Yin, W.: Soil moisture dynamics within soil profiles and associated environmental controls, Catena, 136, 189–196, doi: 10.1016/J.Catena.2015.01.014, 2016.

Humphrey, V., Berg, A., Ciais, P., Gentine, P., Jung, M., Reichstein, M., Seneviratne, S. I., and Frankenberg, C.: Soil-moisture–atmosphere feedback dominates land carbon uptake variability, Nature, 592, 65–69, doi:10.1038/s41586-021-03325-5, 2021.

Huntingford, C., Marsh, T., Scaife, A., Kendon, E. J., Hannaford, J., Kay, A. L., Lockwood, M., Prudhomme, C., Reynard, N. S., Parry, S., Lowe, J. A., Screen, J. A., Ward, H. C., Roberts, M., Stott, P. A., Bell, V. A., Bailey, M., Jenkins, A., Legg, T., Otto, F. E. L., Massey, N., Schaller, N., Slingo, J., and Allen, M. R.: Potential influences on the United Kingdom's floods of winter 2013/14, Nat. Clim. Change, 4, 769–777, doi:10.1038/nclimate2314, 2014

Immerzeel, W.W., Lutz, A. F., Andrade, M., Bahl, A., Biemans, H., Bolch, T., Hyde, S., Brumby, S., Davies, B. J., Elmore, A. C., Emmer, A., Feng, M., Fernández, A., Haritashya, U., Kargel, J. S., Koppes, M., Kraaijenbrink, P. D. A., Kulkarni, A. V., Mayewski, P. A., Nepal, S., Pacheco, P., Painter, T. H., Pellicciotti, F., Rajaram, H., Rupper, S., Sinisalo, A., Shrestha, A. B., Viviroli, D., Wada, Y., Xiao, C., Yao, T., and Baillie, J. E. M.: Importance and vulnerability of the world's water towers, Nature, 577, 364–369, doi:10. 1038/ s41586- 019- 1822-y, 2020.

IUSS: World Reference Base for Soil Resources 2014, Update 2015. World Soil Resources Reports No. 106. FAO, Rome, 2015.

Jačka, L., Walmsley, A., Kovář, M., and Frouz, J.: Effects of different tree species on infiltration and preferential flow in soils developing at a clayey spoil heap, Geoderma, 403, 115372, doi:10.1016/j.geoderma.2021.115372, 2021.

Jost, G., Schume, H., Hager, H., Markart, G., and Kohl, B.: A hillslope scale comparison of tree species influence on soil moisture dynamics and runoff processes during intense rainfall, J. Hydrol., 420–421, 112–124, doi:10.1016/j.jhydrol.2011.11.057, 2012.

Kofroňová, J., Šípek, V., Hnilica, J., Vlček, L., and Tesař, M.: Canopy interception estimates in a Norway spruce forest and their importance for hydrological modelling, Hydrol. Sci. J., 66, 1233–1247, doi:10.1080/02626667.2021.1922691, 2021.

Korres, W., Reichenau, T. G., Fiener, P., Koyama, C. N., Bogena, H. R., Cornelissen, T., Baatz, R., Herbst, M., Diekkrüger, B., Vereecken, H., and Schneider, K.: Spatio-temporal soil moisture patterns - A meta-analysis using plot to catchment scale data, J. Hydrol., 520, 326–341, doi:10.1016/j.jhydrol.2014.11.042, 2015.

Kuželková, M., Jačka, L., Kovář, M., Hradilek, V., and Máca, P.: Tree trait-mediated differences in soil moisture regimes: a

comparative study of beech, spruce, and larch in a drought-prone area of Central Europe, Eur. J. Forest Res., 143, 319–332, doi:10.1007/s10342-023-01628-y, 2024.

Kyselý, J., Gaál, L., Beranová, R., Plavcová, E.: Climate change scenarios of precipitation extremes in Central Europe from ENSEMBLES regional climate models, Theor. Appl. Climatol., 104, 529–542, doi: 10.1007/s00704-010-0362-z.

Legates, D. R., Mahmood, R., Levia, D. F., DeLiberty, T. L., Quiring, S. M., Houser, C., and Nelson, F. E.: Soil moisture: A central and unifying theme in physical geography, Prog. Phys. Geogr., 35, 65–86, doi:10.1177/0309133310386514, 2011.

Liang, X., Lettenmaier, D. P., Wood, E. F., and Burges, S. J.: A simple hydrologically based model of land surface water and energy fluxes for general circulation model, J. Geophys. Res., 99(14), 415–14, 428, doi:10.1143/jjap.39.2063, 1994.

Maxwell, T. M., Silva, L. C. R., and Horwath, W . R.: Integrating effects of species composition and soil properties to predict shifts in montane forest carbon–water relations, PNAS, 115(18), E4219–E4226, doi:10.1073/pnas.1718864115, 2018.

Mianabadi, A., Davary, K., Pourreza-Bilondi, M., Coenders-Gerrits, A.M.J.: Budyko framework; towards non-steady state conditions, J. Hydrol., 588, 125089, doi: 10.1016/j.jhydrol.2020.125089, 2020.

Milly, P. C. D., Betancourt, J., Falkenmark, M., Hirsch, R. M., Kundzewicz, Z. W., Lettenmaier, D. P., Stouffer, R. J., Dettinger, M. D., and Krysanova, V.: On critiques of ‘‘Stationarity is dead: Whither water management?”, Water Resour. Res., 51, 7785–7789, doi:10.1002/2015WR017408, 2015.

Monteith, J. L.: Evaporation and environment, Symposia of the Society for Experimental Biology, 19, 205–234, 1965.

Možný, M., Trnka, M., Vlach, V., Vizina, A., Potopová, V., Zahradníček, P., Štěpánek, P., Hajková, L., Staponites, L., and Žalud, Z.: Past (1971-2018) and future (2021–2100) pan evaporation rates in the Czech Republic, J. Hydrol., 590, 125390, doi:10.1016/j.jhydrol.2020.125390, 2020.

Novick, K. A., Ficklin, D. L., Baldocchi, D., Davis, K. J., Ghezzehei, T. A, Konings, A. G., MacBean, N., Raoult, N., Scott, R. L., Shi, Y., Sulman, B. N., and Wood, J. D.: Confronting the water potential information gap, Nat. Geosci., 15, 158–164, doi:10.1038/s41561-022-00909-2, 2022.

Oudin, L., Hervieu, F., Michel, C., Perrin, C., Andréassian, V., Anctil, F., and Loumagne, C.: Which potential evapotranspiration input for a lumped rainfall-runoff model? Part 2 - Towards a simple and efficient potential evapotranspiration model for rainfall-runoff modelling, J. Hydrol., 303, 290–306, doi:10.1016/j.jhydrol.2004.08.026, 2005.

Qing, Y., Ancell, B. C., and Yang, Z.-L.: Accelerating flash droughts induced by the joint influence of soil moisture depletion and atmospheric aridity, Nat. Commun., 13, 1139, doi:10.1038/s41467-022-28752-4, 2022.

Renner, M., Brust, K., Schwärzel, K., Volk, M., and Bernhofer, V.: Separating the effects of changes in land cover and climate: ahydro-meteorological analysis of the past 60 yr in Saxony, Germany, Hydrol. Earth Syst. Sci., 18, 389–405, doi: 10.5194/hess-18-389-2014.

Rötzer, T., Häberle, K. H., Kallenbach, C., Matyssek, R., Schütze, G., and Pretzsch, H.: Tree species and size drive water consumption of beech/spruce forests - a simulation study highlighting growth under water limitation, Plant Soil, 418, 337–356, doi:10.1007/s11104-017-3306-x, 2017.

Savenije, H. H. G.: The importance of interception and why we should delete the term evapotranspiration from our vocabulary, Hydrol. Process., 18, 1507–1511, doi:10.1002/hyp.5563, 2004.

Schafstall, N., Svitavská-Svobodová, H., Kadlec, M., Gałka, M., Kuneš, P., Bobek, P., Goliáš, V., Pech, P., Nývlt, D., Hubený, P., Kuosmanen, N., Carter, V. A., Florescu, F.: The absence of disturbances promoted Late Holocene expansion of silver fir (Abies alba) in the Bohemian Forest, Palaeogeogr. Palaeoclimatol. Palaeoecol., 635, 111950, doi:10.1016/j.palaeo.2023.111950, 2024.

Schume, H., Jost, G., and Hager, H.: Soil water depletion and recharge patterns in mixed and pure forest stands of European beech and Norway spruce, J. Hydrol., 289, 258–274, doi:10.1016/j.jhydrol.2003.11.036, 2004.

Schwärzel, K., Menzer, A., Clausnitzer, F., Spank, U., Häntzschel, J., Grünwald, T., Köstner, B., Bernhofer, C., and Feger, K. H.: Soil water content measurements deliver reliable estimates of water fluxes: A comparative study in a beech and a spruce stand in the Tharandt forest (Saxony, Germany), Agric. For. Meteorol., 149, 1994–2006, doi:10.1016/j.agrformet.2009.07.006, 2009.

Seibert, J., and Vis, M. J. P.: Teaching hydrological modeling with a user-friendly catchment-runoff-model software package, Hydrol. Earth Syst. Sci., 16, 3315–3325, doi:10.5194/hess-16-3315-2012, 2012.

Šípek, V., and Tesař, M.: Seasonal snow accumulation in the mid-latitude forested catchment, Biologia, 69, 1562–1569,

doi:10.2478/s11756-014-0468-3, 2014.
Šípek, V., and Tesař, M.: Year-round estimation of soil moisture content using temporally variable soil hydraulic parameters, Hydrol. Process., 31, 1438–1452, doi:10.1002/hyp.11121, 2017.
Šípek, V., Hnilica, J., Vlček, L., Hnilicová, S., and Tesař, M.: Influence of vegetation type and soil properties on soil water dynamics in the Šumava Mountains (Southern Bohemia), J. Hydrol., 582, 124285, doi:10.1016/j.jhydrol.2019.124285, 2020.
Svoboda, V., Hanel, M., Máca, P., and Kyselý J.: Characteristics of rainfall events in regional climate model simulations for the Czech Republic, Hydrol. Earth Syst. Sci., 21(2), 963–980, doi: 10.5194/hess-21-963-2017, 2017.
Tolasz, R., et al.: Climate Atlas of Czechia. Czech Hydrometeorological Institute, Prague, 2007.
Toušková, J., Falátková, K., and Šípek, V.: Estimating potential evapotranspiration in a temperate zone: The challenge of model selection, Water Res. Manag., doi.org/10.1007/s11269-025-04233-3, 2025.
Trugman, A. T., Medvigy, D., Mankin, J. S., and Andregg W. R. L.: Soil moisture as a major driver of carbon cycle uncertainty, Geophys. Res. Lett., 45, 6495–6503, doi:10.1029/2018GL078131, 2018.
Tyree, M. T., and Zimmermann, M. H.: Xylem structure and the Ascent of Sap, Springer, Heidelberg, 2002.
Van Genuchten, M. T.: A closed-form equation for predicting the hydraulic conductivity of unsaturated soils, Soil Sci. Soc. Am. J., 44(5), 892–898, doi:10.2136/sssaj1980.03615995004400050002x, 1980.
Viviroli, D., Dürr, H. H., Messerli, B., Meybeck, M., Weingarten, R.: Mountains of the world, water towers for humanity: Typology, mapping, and global significance. Water Resour. Res., 43, 1–13, doi:10. 1029/ 2006W R0056 53, 2007.
von-Hoyningen-Huene, J.: Die interzeption des Niederschlages in landwirtschaftlichen Pflanzenbeständen, DVVVK, 57, 3–51, 1983.
Vondráková, A., Vávra, A., Voženílek, V.: Climatic regions of the Czech Republic, J. Maps, 9(3), 425–430, doi: 10.1080/17445647.2013.800827, 2013.
Wang, H., Tetzlaff, D., and Soulsby, C.: Modelling the effects of land cover and climate change on soil water partitioning in a boreal headwater catchment, J. Hydrol., 558, 520–531, doi:10.1016/j.jhydrol.2018.02.002, 2018.
Yue, S., Pilon, P., Phinney, B., Cavadias, G.: The influence of autocorrelation on the ability to detect trend in hydrological series, Hydrol. Process., 16, 1807–1829, doi: 10.1002/hyp.1095, 2002.
Zahradníček, P., Brázdil, R., Štěpánek, P., and Trnka, M.: Reflections of global warming in trends of temperature characteristics in the Czech Republic, 1961–2019, Int. J. Climatol., 41, 1211–1229, doi: 10.1002/joc.6791, 2020.
Zucco, G., Brocca, L., Moramarco, T., and Morbidelli, R.: Influence of land use on soil moisture spatial-temporal variability and monitoring, J. Hydrol., 516, 193–199, doi:10.1016/j.jhydrol.2014.01.043, 2014.
Zweifel, R., Böhm, J. P., and Häsler, R.: Midday stomatal closure in Norway spruce - Reactions in the upper and lower crown, Tree Physiol, 22, 1125–1136, doi:10.1093/treephys/22.15-16.1125, 2002.

Supplementary Material

Figure S1: Scheme representing the workflow of the study

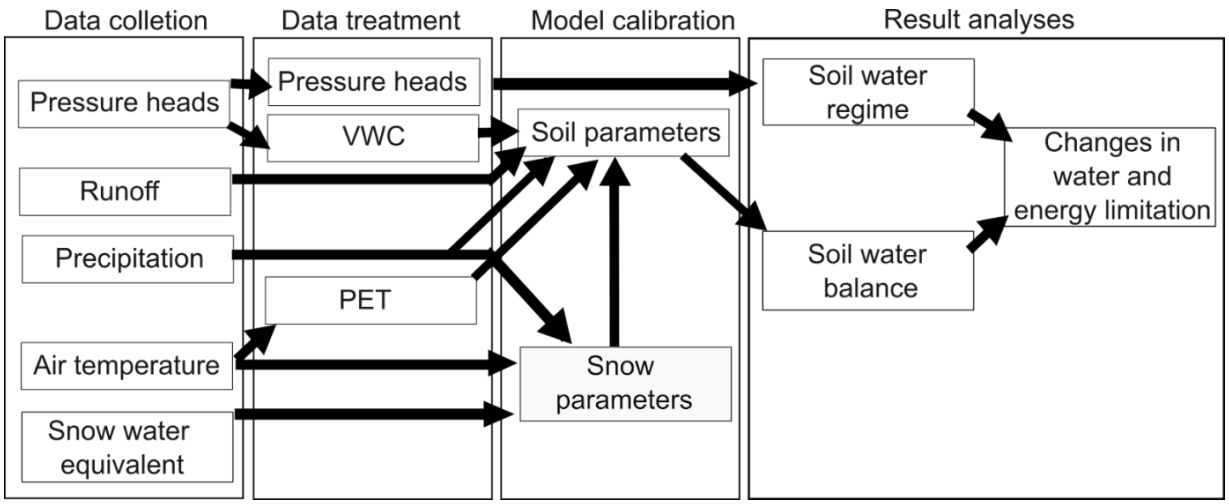

Figure S2. The soil tensiometer with a reading unit (Thies, Germany)

Table S3: Average soil hydraulic parameters of all soil layers derived from direct measurements. Each value is depicted by its mean ± standard deviation.

Measured SHP		θ_r	Θ_s	α	n
Spruce	10 cm	0.32 ± 0.03	0.70 ± 0.04	0.04 ± 0.01	2.10 ± 0.53
	35–45 cm	0.18 ± 0.04	0.52 ± 0.03	0.04 ± 0.01	1.72 ± 0.15
	50 cm	0.15 ± 0.02	0.48 ± 0.02	0.05 ± 0.01	1.58 ± 0.19
	70–75 cm	0.15 ± 0.04	0.50 ± 0.04	0.07 ± 0.03	1.45 ± 0.13
Beech	10 cm	0.17 ± 0.02	0.53 ± 0.02	0.05 ± 0.01	1.36 ± 0.02
	30 cm	0.18 ± 0.01	0.49 ± 0.04	0.05 ± 0.01	1.55 ± 0.21
	45 cm	0.17 ± 0.01	0.47 ± 0.01	0.05 ± 0.01	1.46 ± 0.01
	60 cm	0.13 ± 0.02	0.42 ± 0.01	0.05 ± 0.02	1.48 ± 0.13

Figure S4: Model performance when calibrated in particular periods. Values from first columns represent calibration from 2000 to 2004, the second and following columns represent the following calibration periods (2005-2009, 2010-2014, 2015-2019, and the last column is an overall calibration)

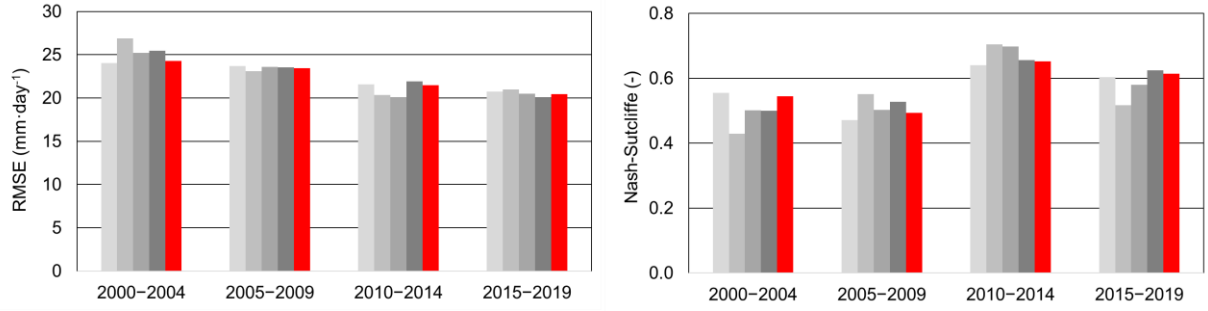

Figure S5: Measured and modelled snow water equivalent (a) and soil water content (b)

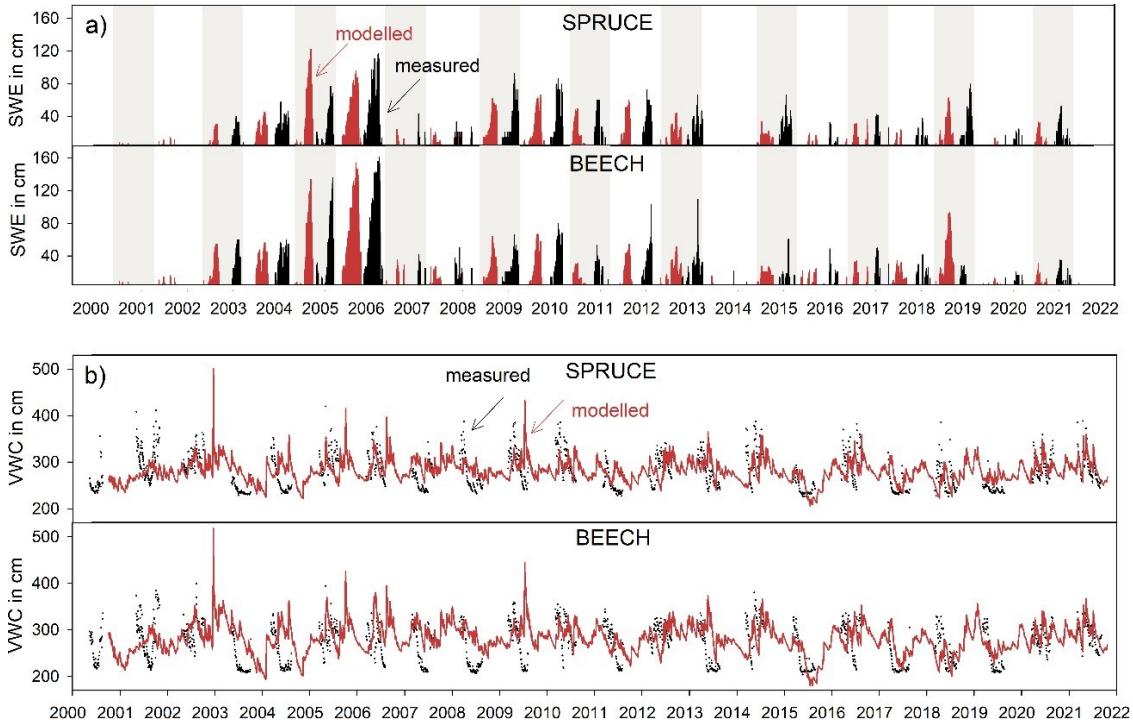

Figure S6. Comparison of estimation of potential evapotranspiration by Penman-Monteith and Oudin approaches (a) and differences in soil water content modelling using both approaches (b)

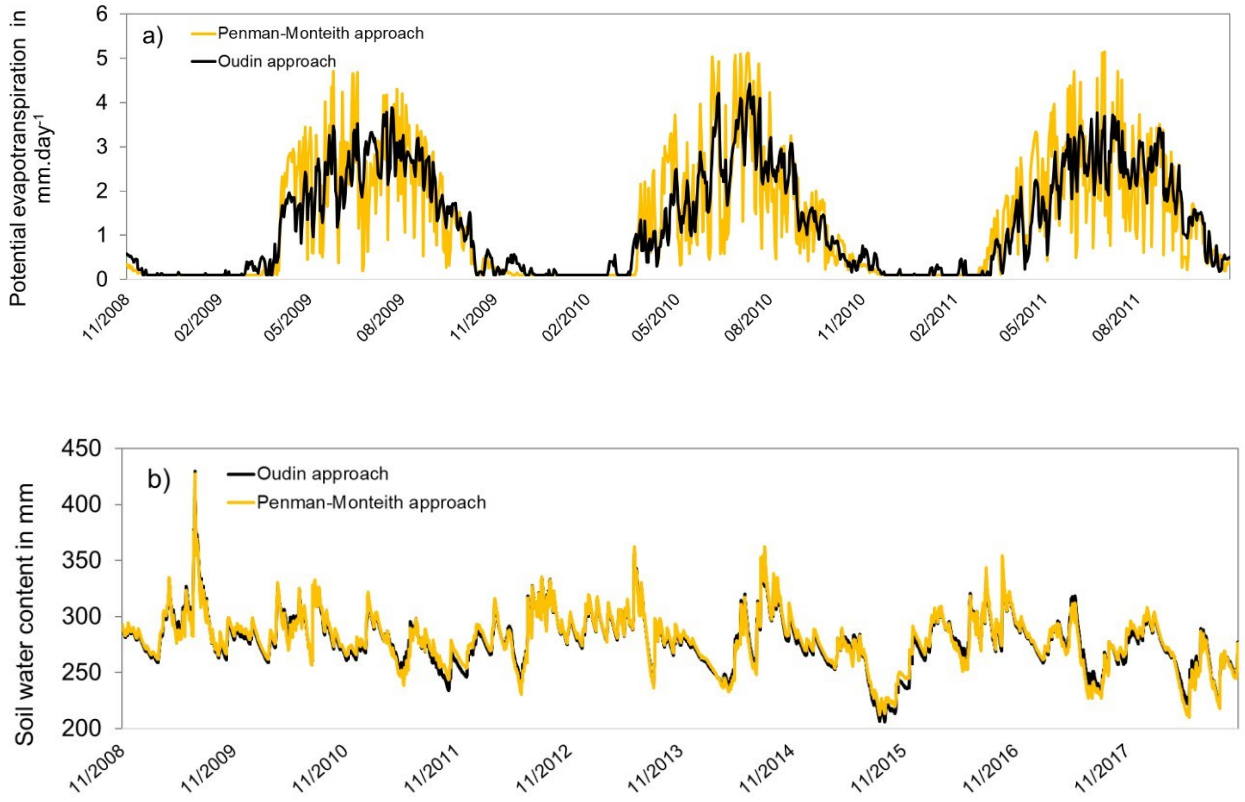

7.2 Temperature-based analysis of runoff formation dynamics in various soil types

The study *Hydrological balance and runoff from a montane peat bog traced by water temperature* (Falátková et al., 2024) investigates the contribution of a montane peat bog to the total runoff of a catchment composed of two hydrologically distinct units: the peat bog and adjacent mineral hillslopes, located at the Rokytka experimental site. To quantify this contribution, water temperature was employed as a natural tracer, offering continuous high-frequency data beyond the temporal limitations of conventional sampling campaigns.

The results revealed significant differences in the peat bog's contribution during baseflow conditions compared to runoff events. These findings improve the accuracy of hydrological models assessing the response of peatland soils to climate change, particularly under scenarios characterized by more frequent drought periods alternating with high-intensity rainfall events or a shortening of snow pack duration during winter. Given that the peatlands' water contribution to runoff formation varies significantly with soil saturation, it can be assumed that the spring yield and water regime of streams in these areas will change.

Moreover, based on the observed hydrological behaviour of the peat bog, future research in peatland hydrology could greatly benefit from a detailed understanding of percolation dynamics and evapotranspiration constraints, as these factors are critical for comprehensively assessing peatland water balance under changing climatic conditions.

HYDROLOGICAL SCIENCES JOURNAL
https://doi.org/10.1080/02626667.2024.2320392

Hydrological balance and runoff from a montane peat bog traced by water temperature

Kristyna Falatkova [a], Václav Šípek [a], Lukáš Vlček [a,b], Jiří Kocum [a,b] and Martin Pivokonský [a]

[a]Institute of Hydrodynamics of the Czech Academy of Sciences, Prague, Czech Republic; [b]Faculty of Science, Charles University, Prague, Czech Republic

ABSTRACT

Peatlands are hydrologically significant landscape units in mountain headwater catchments in Central Europe. In this study, the contribution of a peat bog to runoff and its annual water balance were analysed and compared with those of a forested mineral soil hillslope. A mixing model method using the water temperature as a tracer was applied, and the resulting ratio of peat bog water in streams was incorporated into a hydrological model. The mean peat bog contribution during baseflow ranged from 33.4% during the cold season to 48.9% during the warm season, while during runoff events, the contribution reached over 83%. The simulated water balance results showed a higher actual evapotranspiration on the mineral hillslope, which suggests a higher total runoff from the peat bog (1523 versus 1327 mm/year on the mineral hillslope). The results of this study enable more reliable modelling assessments of peatland reactions to climate change.

ARTICLE HISTORY
Received 25 April 2023
Accepted 24 January 2024

EDITOR
K. Soulis

ASSOCIATE EDITOR
G. Chiogna

KEYWORDS
peatlands; runoff formation; catchment hydrology; water balance; water temperature; tracer

1 Introduction

One of the concerns regarding climate change is its impact on the water availability, a problem relevant in many regions worldwide (Iglesias *et al*. 2007, Roudier *et al*. 2014, Mancosu *et al*. 2015, Gosling and Arnell 2016, Mekonnen and Hoekstra 2016). Discharge in many rivers decreases to low flows in summer months, impacting not only the water availability for human use (agriculture, industry, and transport; Wheeler and Von Braun 2013, Padrón *et al*. 2020) but also the water quality, with potentially severe ecological consequences (Whitehead *et al*. 2009, van Vliet *et al*. 2013).

Under climate conditions with a relatively high water input to the hydrological cycle in the form of precipitation, the main concern is to retain rainfall and snowmelt water in the landscape as long as possible: to enable it to percolate and recharge groundwater, to ensure enough soil moisture for plants, and to cool the local climate by evapotranspiration (Bescansa *et al*. 2006, Scholz 2007, Yang *et al*. 2014). One relevant strategy is to integrate the extension of wetland areas, including revitalization of peatlands, into landscape management (Price *et al*. 2003, Mitsch 2005, Erwin 2009, Kimmel and Mander 2010, Verhoeven 2014). The role of peatlands in the hydrological cycle has been debated for decades (Bacon *et al*. 2017), ranging from imposing a positive effect on stream discharge levels, thus reducing flood peaks and supplying streams during dry periods, i.e. functioning as a sponge (Ingram 1983), to a clearly negative effect, thereby emphasizing both extremes (Bragg 2002, Holden and Burt 2003b, Acreman and Holden 2013).

Existing research, however, primarily focuses on the distinction between the hydrological functions of a degraded (drained or burned) peatland and a pristine or revitalized peatland (Grayson *et al*. 2010, Holden *et al*. 2011, 2015, Ballard *et al*. 2012, Gao *et al*. 2016, Ahmad *et al*. 2020). Unsurprisingly, the latter exhibits overall better conditions in terms of reducing peak discharge levels, e.g. due to a higher surface roughness, than a drained peatland with patches of bare surfaces. Although there is no doubt that peatlands are ecologically invaluable ecosystems, their influence on the hydrological regime of streams remains unclear (Gracz *et al*. 2015, Meriö *et al*. 2019). When peatlands cover a non-negligible part of river headwaters, it is important to understand their role in greater detail, especially in regard to the expected changes in climate (Bechtold *et al*. 2019). As such, a direct comparison with mineral soils is essential, yet very few studies have considered this aspect (Šanda *et al*. 2014, Vlček *et al*. 2021).

Runoff generation from peatlands is controlled by the internal structure, comprising two layers with very different porosities (Holden and Burt 2003a, Rezanezhad *et al*. 2012). The upper layer, the acrotelm, encompasses living plants (*Sphagnum* mosses) and is defined by a fluctuating water table; thus, it is periodically aerated. High porosity indicates it exhibits a relatively high hydraulic conductivity (Rezanezhad *et al*. 2010). Water stored in the acrotelm is mostly mobile water (Staudinger *et al*. 2017) and highly variable over time. The below-lying layer of peat, the catotelm, exhibits permanently anaerobic conditions; therefore, it is completely

CONTACT Kristyna Falatkova falatkova@ih.cas.cz Institute of Hydrodynamics of the Czech Academy of Sciences, Pod Pat'ankou 30/5, Prague 160 00, Czech Republic

Supplemental data for this article can be accessed online at https://doi.org/10.1080/02626667.2024.2320392

saturated, and due to the low porosity, it provides a very low hydraulic conductivity (the hydraulic properties depend on the degree of peat decomposition; Wong *et al.* 2009). Some authors have considered catotelm hydraulic conductivity values to lie close to zero, stating that the decomposed peat occurring at deeper positions burdened with above-lying layers represents an immobile region in terms of water flow (Rezanezhad *et al.* 2016), whereas others have reported low saturated hydraulic conductivity values (up to 0.0001–5 m d^{-1}; Clymo 2004, Quinton *et al.* 2008, Wong *et al.* 2009). Therefore, water is accumulated here for a long period.

Mainly due to the characteristics of catotelm, peatlands are considered to play a relatively minor role in groundwater recharge and to generate very little baseflow (Burt *et al.* 1990, Soulsby *et al.* 2006). The typical high water table in peatlands causes most event water to be transferred by saturation-excess overland flow and interflow in the acrotelm (upper 5–10 cm), while some can be transferred by preferential flow through macropores (Jones 1997, Holden 2006, Holden *et al.* 2008). The general runoff formation mechanisms in peatlands have been extensively described; however, the contribution of peatlands to streams during the dormant (cold) and vegetation (warm) seasons has yet to be determined.

Separating individual water sources (runoff components) and thus achieving a better understanding of the hydrological processes within a catchment has been facilitated by the use of tracers, especially stable isotopes of water (Klaus and McDonnell 2013). Their conservative behaviour (suggesting that they are neither altered nor sorbed by other substances when in contact) is a great advantage (Gat and Gonfiantini 1981). However, this method requires frequent sampling and sometimes costly analyses. The use of water temperature as a tracer first emerged as a useful tool to monitor groundwater flow (Keys and Brown 1987, James *et al.* 2000). Since then, it has been applied in studies of karstic environments (Genthon *et al.* 2005, Lüthi 2019) and as a tracer of fluxes in the hyporheic zone (Bianchin *et al.* 2010, Bhaskar *et al.* 2012), surface waters and runoff generation (Shanley and Peters 1988, Brown and Hannah 2007, Birkinshaw and Webb 2010, Zajíček *et al.* 2016). The main advantages of this method include its simplicity, cost-effectiveness, and continuous data acquisition mode. Although the water temperature is a nonconservative tracer, water has a high specific heat capacity, indicating that the temperature does not rapidly change. However, caution should be exercised concerning the time needed for the source water of a given temperature to migrate to the stream. To successfully employ this streamflow separation method, the condition of a sufficient difference between the individual components must be satisfied.

The main motivation for this study was to describe peat bog behaviour during low-flow periods (drought spells) accompanied by detailed quantification of its contribution to the total runoff during high-flow periods and to establish a hydrological model that accounts for the water balance of two common natural landscape units in the mountainous area of Central Europe. This in turn could provide reliable modelling projections of the water balance under a changing climate. For this purpose, the following specific goals were defined: (1) to analyse the water temperature regime of a peat bog and mineral soil hillslope; (2) to evaluate the contribution of a peat bog to a stream during baseflow and rainfall–runoff events; and (3) to compare the peat bog and mineral soil hillslope in terms of the modelled water balance. To compare the hydrological functions of the peat bog and mineral soil hillslope under the same conditions, we opted for a simple mixing model method based on the water temperature.

2 Material and methods

2.1 Study area

The Bohemian Forest is a mid-altitude mountain range in Central Europe, forming a natural borderline between Germany and Czechia. Its geology is characterized by old, denuded surfaces and elevated platforms formed by metamorphic and igneous rocks (gneiss). The dominant part of the mountain range is covered with spruce forest, alternating with beech and fir trees. In the higher parts (700–1100 m a.s.l.), peatlands have developed due to the suitable climatic and geological conditions, representing one of the typical biotopes of the mountain range. The area is generally well preserved, as it has been protected since 1963, and it became a part of a national park in 1991.

Rokytka (49.0164°N, 13.4165°E; 5.7 km^2) is a typical catchment in the high parts of the Bohemian Forest, with approximately 40% of the area covered with peat and other hydromorphic soils. For the analysis, we selected its northern part: a small sub-catchment of a stream referred to as the northern tributary (NT). It has an area of 0.65 km^2 and an elevation ranging from 1095 m to 1155 m a.s.l. (Fig. 1).

The experimental site covers two opposing hillslopes, which significantly differ in terms of their soil cover, vegetation and hydrological response to a rainfall event (Vlček *et al.* 2021). The southeast-oriented hillslope is covered with mineral soils, mainly entic podzolic soils, with an average slope of 5°. The vegetation catena starts with beech forest in the uppermost parts, followed by a highly disturbed spruce forest mostly comprising dead trees and young seedlings (impact of a bark beetle infestation peaking in 2010–2015 (Fig. 1(c))), and a water-logged spruce patch near the valley bottom. The other hillslope encompasses an ombrotrophic peat bog and is gently sloping (<2°) towards the southwest. The upper part (bog dome) is formed by peat mosses (*Sphagnum*) and cottongrass (*Eriophorum*), followed by a patchy bog pine cover (*Pinus mugo*) in the higher parts and a dense bog pine cover in the lower parts (Fig. 1(d)), and finally grasses and sedges (Cyperaceae) and water-logged spruce in the lagg (i.e. a transitional zone at the edge of an ombrotrophic peat bog, occurring between a bog and mineral slope; Whitfield *et al.* 2006).

Each hillslope constitutes approximately half of the catchment area, and the interface is formed by a lagg – a waterlogged area sometimes recognized as an integral part of a peatland (Fig. 1(b)). The hydraulic properties of each hillslope cover type result in different runoff formation mechanisms: on mineral hillslopes, water easily infiltrates and percolates to reach deeper positions without forming surface flow, whereas in peat bogs, overland and shallow

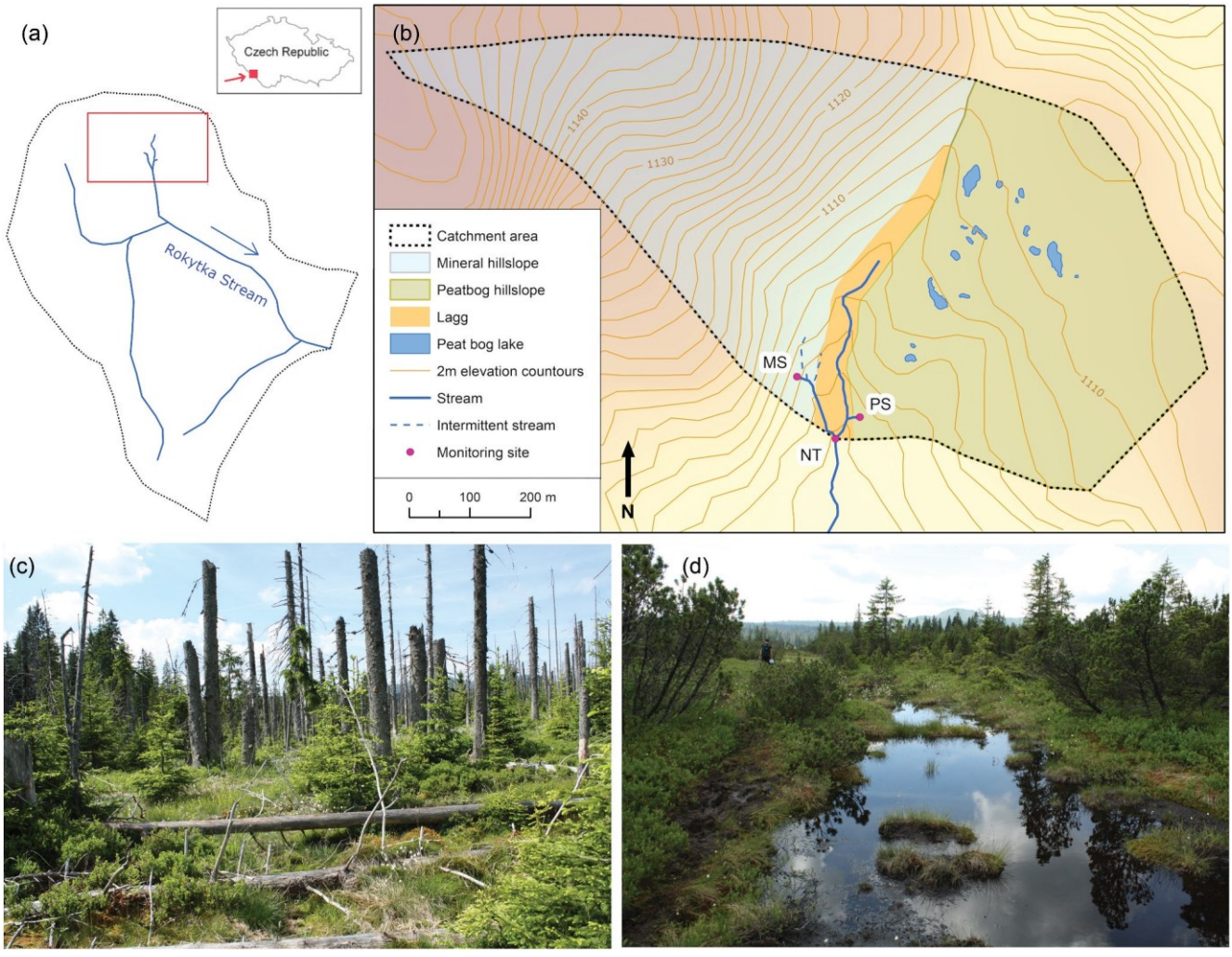

Figure 1. The study site: the northern tributary (NT) stream catchment of the Bohemian Forest, southwest Czechia. (a) Location of the study catchment within the larger Rokytka catchment (marked with a red rectangle); (b) the study catchment, topography of both hillslopes, the approximate extent of the lagg and location of the water temperature and water level sensors (PS – peat bog stream, MS – mineral hillslope stream, NT – northern tributary stream); (c) and (d) photographs of the landscape taken at the mineral and peat bog hillslopes, respectively.

subsurface flows are the dominant routes where water is directed. The NT stream drains the catchment and emerges from the confluence of two streams: one originating at a spring on the mineral hillslope (MS) and the other directing water through the lagg at the valley bottom. A spring emerging in the lower part of the bog is connected with the latter and it contributes water to the peat bog. Here, it is referred to as peat bog stream (PS). The lagg is considered an area where mixing of waters from both the ombrotrophic peat bog and mineral hillslope occurs (Langlois *et al*. 2015).

The fluctuation of the water table exhibits a varying amplitude across the peat bog: lowest typically at the bog dome (10 cm) and higher in the bog pine zone (15–20 cm) and the lagg (up to 30 cm).

The climate of this site is classified as a cold climate with cold summers (Dfc) on the basis of the Köppen-Geiger climate classification (Beck *et al*. 2018). The mean annual air temperature is 4.8°C, with the mean air temperature in the coldest months below 0°C and typically three months (JJA) with a mean monthly air temperature above 10°C. Due to the prevailing westerly winds, the site can be partly subjected to rain shadow effects, yet the conditions are still relatively wet. The mean annual precipitation is 1695 mm (1981–2010; Starostová 2012), with a relatively even distribution throughout the year. Despite its southern exposition, snow cover is present for a substantial part of the year, usually from November until May. The observation period (2020–2021) was unusually cold, with an average air temperature below 4°C, and the precipitation totals were above average. The second analysis year (2021–2022) was slightly colder than the average (4.3°C). The precipitation totals were similar to those in the previous year; however, the maximum value of the snow water equivalent was almost twice as high during a substantial part of the cold season.

2.2 Data

To separate the two water sources, we used data from temperature sensors installed at the springs of PS and MS located on the opposing slopes and the NT stream (Fig. 1(b)). Both springs perennially supply water to the stream year round. To ensure that the sensor at the NT stream was positioned far

enough downstream of the confluence to detect sufficiently mixed water from the two sources, we performed manual water temperature measurements on several occasions during field trips. These campaigns confirmed that the water within the lagg is well mixed and that the waters from the two streams already exhibit the same temperature a few metres upstream of the confluence. The water temperature was supplemented with flow rate data of the NT stream, calculated from the water level measured with a pressure sensor and a rating curve. Both the temperature and water level data are available in 10-minute time steps, and the observation period includes two warm and two cold seasons, covering the two years from June 2020 to May 2022.

Meteorological data, including precipitation totals, air temperature and humidity, were supplied by an automated weather station (AWS) located in the Rokytka catchment (1090 m a.s.l.), supplemented with global radiation, precipitation and wind speed data from an AWS located 6 km away in Modrava village (980 m a.s.l.). Due to soil moisture monitoring on both hillslopes, data from tensiometers (UMS, T8) installed at two depths (30 and 60 cm) were available for the analysis. The volumetric soil water content was inferred from water retention curves determined with a pressure apparatus (Soilmoisture, US) in the laboratory (more details have been provided in Vlček *et al.* 2017). The water table was measured in three shallow boreholes in the lower part of the peatland with a hydrostatic submersible level probe (Fiedler, CZ). For the purpose of model validation, snow cover characteristics (snowpack height and snow water equivalent) of the local snow pillow were utilized, both with daily time steps. The time-series data were corrected by omitting clearly erroneous values and resampled into hourly (for the purpose of establishing the mixing model) and daily series (to be used by the hydrological model) using the zoo package in R software (CRAN).

2.3 Methods

2.3.1 Mixing model

To obtain the contribution of the stream draining the peat bog to the NT stream, we employed a simple mixing model with two components (MS and PS) throughout the entire 2-year period, i.e. to separate the hydrograph not only during events but also during baseflow. The following equations were used:

$$Q_{NT} = Q_{MS} + Q_{PS} \tag{1}$$

$$T_{NT}\, Q_{NT} = T_{MS}\, Q_{MS} + T_{PS}\, Q_{PS} \tag{2}$$

$$\%PS = \frac{Q_{PS}}{Q_{NT}} * 100 \tag{3}$$

where Q_{NT}, Q_{MS}, and Q_{PS} are the flow rates of the northern tributary stream ($m^3\ s^{-1}$), mineral hillslope stream, and peat bog stream, respectively; T_{NT}, T_{MS}, and T_{PS} are the water temperatures (°C) of the NT stream, MS, and PS, respectively; and %PS is the fraction (%) of the NT stream flow rate that originates on the peat bog hillslope.

The use of the water temperature to separate the contributions of several sources is a simple method with the major benefit of inexpensive and continual measurement of the needed data. However, it exhibits certain limitations: separation cannot be achieved when the components (water temperatures) are not sufficiently different. For this reason, we omitted certain periods: autumn, when the water temperature of the peat bog stream plummets and becomes very similar to that of MS, and spring, when the reverse situation occurs (T_{PS} rising towards T_{MS}). The omitted periods are 11 October-20 November 2020, 2 April-5 June 2021, 10 October-18 November 2021, 6 April-30 May 2022.

To analyse the contribution of the peat bog hillslope runoff to the stream during baseflow, we developed a routine to automatically select baseflow periods based on the inclination of the hydrograph (10-min NT stream water level data series). The selection parameters – namely, the window size, i.e. the length of the hydrograph segment, and the hydrograph inclination, i.e. the difference between the first and last points of the given hydrograph segment relative to the window size – were evaluated in R software (CRAN). With the use of the preselected window sizes (3, 6, 8, and 12 h) and hydrograph inclination limits (<4°, <6°, <8°, and <10°), optimal results were achieved with a 6 h window and an inclination limit of 6°. This combination minimized the inclusion of segments just past an event, where the %PS value is still relatively high. Additionally, it ensured continuity of the selected segments – the minimum segment length was set to 48 h. The final set of baseflow segments was divided based on the time of occurrence into warm ($T_{PS} > T_{NT} > T_{MS}$) and cold ($T_{PS} < T_{NT} < T_{MS}$) seasons, and a statistical data analysis was performed.

To examine the peat bog hillslope input to the stream during rainfall events, we manually selected suitable events using hourly data series of the NT stream flow rate. Only single- and double-peak hydrographs with distinctive causal rainfall levels were analysed in detail. Regarding the cold season hydrograph peaks, the two water sources could not be separated as the area was covered with snow and the stormflow thus contained meltwater. In this case, the components could not be separated based on the temperature only. The selected events all occurred between 1 June and 30 September (Table 1). We examined the relationship between the NT stream flow rate and %PS and compared the pre-event conditions, namely the water table (average over the 24 h prior to the start of rainfall) and antecedent soil moisture (based on the sum of precipitation over the past 7 days).

2.3.2 Hydrological model

Rainfall–runoff processes were estimated using the HBV model (Bergström 1992), with the modification introduced by Vlček *et al.* (2021). The modification was tailored for peat bog catchments because it respects the acrotelm–catotelm concept proposed by Ingram (1978) for hydrological processes in peat bog environments. The standard model in the HBV-light scheme (Seibert and Vis 2012) with a soil box MS1 system and two groundwater storage systems (upper MS2 and lower MS3) was used for the mineral hillslope. The model modification, which was utilized only for the peat bog part of the catchment, was grounded in the separation of the subsurface zone into two storage systems (representing the acrotelm and catotelm). The upper acrotelm storage is subject to

Table 1. Characteristics of the selected rainfall–runoff events. Asterisks mark events with a double-peaked hydrograph; the value linked to the second peak is in parentheses. %PS – ratio of peat bog water in stream. Precip. 7-day sum – sum of precipitation recorded during 7 days prior to the start of an event.

Event no.	Start date	Total period (h)	Q pre-event (L/s)	Q peak (L/s)	%PS pre-event (%)	%PS peak (%)	Lag time peak Q-peak %PS (h)	Precip. sum (mm)	Precip. intensity (mm/h)	Precip. 7-day sum (mm)
1	28 June 2020	63	10.7	178.8	40.0	72.0	7	26.7	1.7	16.9
2	11 July 2020	33	10.5	75.1	45.1	70.6	12	16.3	1.6	13.0
3*	3 August 2020	100	9.8	108.0(395.7)	45.9	67.2(96.1)	7 (4)	77.5	2.8	25.9
4*	17 August 2020	89	10.2	368.5(134.0)	40.7	93.8(88.5)	4(1)	43.8	3.7	48.6
5	25 September 2020	131	9.8	289.9	44.4	96.0	6	72.3	1.1	2.1
6	22 June 2021	24	10.3	166.9	40.7	83.7	0	29.1	9.7	0.1
7	23 June 2021	86	10.9	486.7	41.9	93.8	6	39.3	13.1	34.6
8*	8 July 2021	44	11.0	149.4(145.4)	39.3	82.8(83.3)	0(1)	19.8	1.7	27.7
9*	14 July 2021	54	10.9	261.1(97.0)	40.3	88.7(79.3)	3(1)	16.4	2.3	30.7
10	17 July 2021	63	11.7	514.5	40.7	94.8	3	55.2	4.3	24.0
11	2 August 2021	32	11.9	37.9	41.7	63.5	1	4.7	0.9	19.2
12	5 August 2021	56	11.5	146.0	41.0	81.2	3	15.1	0.8	23.4
13	7 August 2021	38	11.6	149.8	41.2	82.9	2	12.7	1.6	33.1

evapotranspiration (utilizing the HBV approach based on potential evapotranspiration (PET) restriction by the available water content) and generated three forms of runoff. First, overland flow and biomat flow occur when the soil is saturated and all rainwater is immediately drained into the stream. Second, water from the acrotelm and upper part of the catotelm feeds springs throughout the year using the linear storage coefficient. The last runoff mechanism from the acrotelm is pipe flow based on an exponential outflow function. Runoff from the lower storage system, the catotelm, was produced as in the original HBV approach. A detailed model description comprising all the governing equations can be found in Vlček *et al*. (2021).

The model was run at daily time steps and requires the air temperature, precipitation sums, and potential evapotranspiration as input data. The temporal resolution of the model is determined by its intended use for estimating the impact of climate change on the water regime of peat bog-dominated areas. PET was estimated for both hillslopes in the same way using the combined Penman-Monteith method (Monteith 1965). For calibration/validation purposes, discharge, groundwater, soil moisture, and snow water equivalent time series were used (for model efficiency details, refer to the Supplementary material). Overall, the model required 22 parameters for both domains, and all of them were determined using the genetic algorithm, with the root mean square error (RMSE) as an objective function. The snow and soil moisture modules were separately calibrated in advance against the measured snow water equivalent and soil moisture measurements. A detailed description of the model parameters and the resulting values are presented in Vlček *et al*. (2021) for the 2014–2016 calibration period. In this study, only the parameters directly influencing runoff generation (i.e. storage coefficients and non-linearity coefficients from all underground storages) were calibrated against the daily averaged results of the mixing model and observed discharge over the 1 June 2020 - 31 May 2021 period (hereinafter referred to as the year 2020). The mixing model provided the ratio of the peat bog hillslope and mineral hillslope in the resulting discharge, and the RMSE value during calibration matched that of the observed discharge. The 1 June 2021 - 31 May 2022 (hereinafter referred to as the year 2021) served as the validation period.

The model could reproduce the discharge at the catchment outlet at the good (Nash-Sutcliffe coefficient (NS) = 0.64 during the calibration period) and satisfactory levels (NS = 0.56 during the validation period) using the model evaluation scheme of Moriasi *et al*. (2007). The largest model simulation differences could be attributed to the estimation of snow accumulation/melt processes (Vlček *et al*. 2021). The observed and simulated values of particular water storage components and fluxes are provided in the Supplementary material.

3 Results

3.1 Water temperature characteristics

The mineral hillslope stream exhibited only slight variations in the flow rate and, more importantly, in the water temperature. The annual fluctuation in the MS water temperature varied between 4.5 and 5.5°C (Fig. 2). The absence of higher daily and seasonal variations in the water temperature confirms our assumptions about the prevailing percolation process on this hillslope (Vlček *et al*. 2021). Most water from precipitation probably percolates, typical of sandy-loam soils, deep enough below the surface so that the air temperature-induced fluctuation is attenuated (Scherrer and Naef 2003, Anderson 2005). The peat bog stream, however, exhibited notably higher fluctuations in both the flow rate and water temperature (Fig. 2). As described in Vlček *et al*. (2021), the dominant runoff process at the site is fast subsurface flow, routing stormwater through shallow positions of the peat acrotelm. The temperature of the water feeding the PS is therefore much more closely linked to the air and surface temperatures.

Throughout the warm season (Fig. 2(a)), the PS water temperature ranges from 8 to 14°C, with daily fluctuations of 2–3°C on clear days with high radiation. It declines to the 3–8°C range during the autumn/spring transition period (Fig. 2(b)) and stabilizes at approximately 1–2°C during the cold season (Fig. 2(c)) when the daily fluctuation is minimized. The MS water temperature remains almost constant throughout the year; however, small differences sporadically occur during both the warm and cold seasons. These were recorded during heavy rainfall or snow melting events and resulted from water directly entering the spring via near-surface flow.

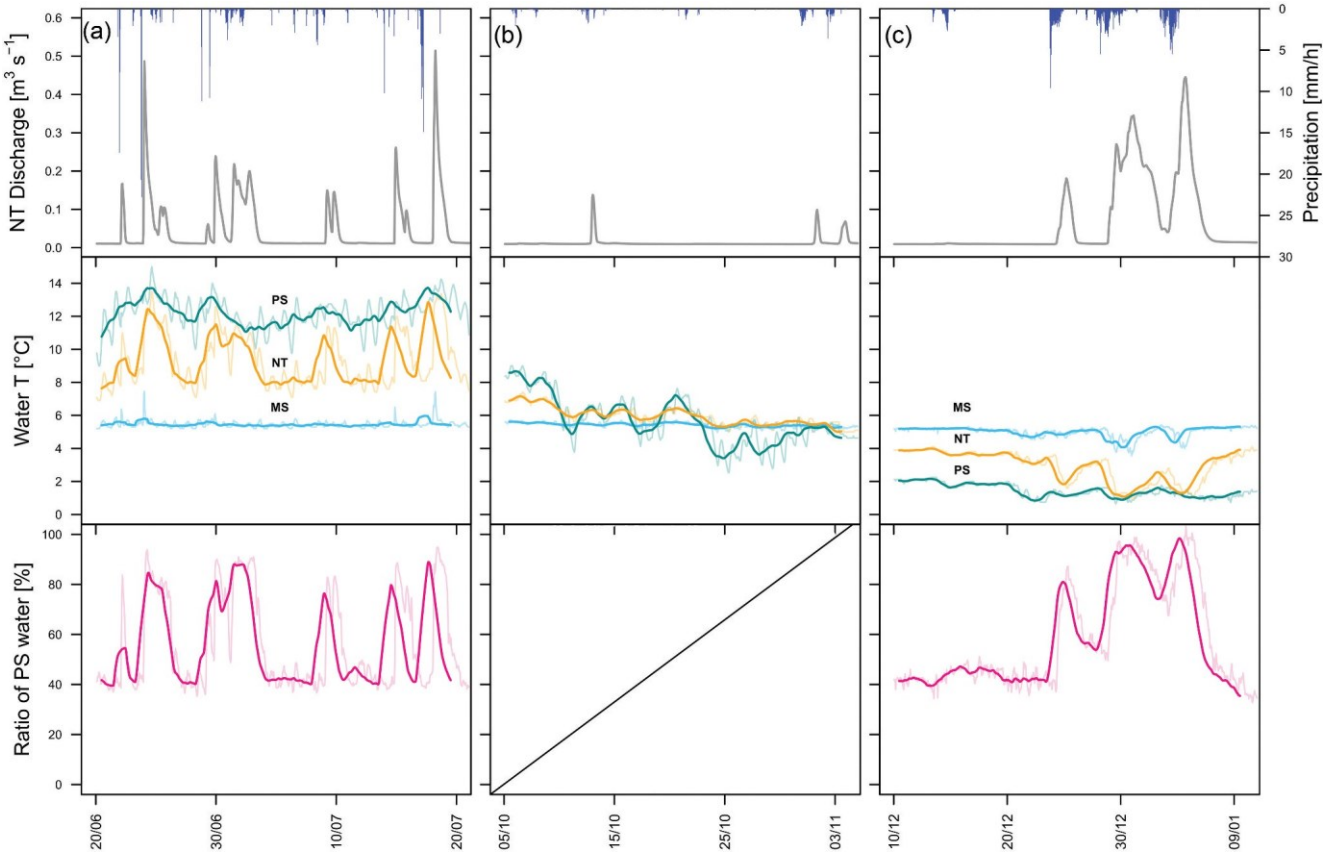

Figure 2. Water temperature of the stream (NT) and two mixing model components (PS - peat bog stream, MS - mineral hillslope stream), and the resulting ratio of peat bog hillslope water in the NT stream discharge (%PS). Example periods in: (a) the warm season, (b) the transition between the cold and warm seasons, (c) the cold season. The ratio of PS water was not calculated for the transition period (b) as the mixing model components were not distinguishable from one another. The thin light-coloured line of water temperature and %PS shows hourly variations; the solid bold line represents a 24-h rolling mean.

3.2 Contribution of the peat bog to the stream

The two-component mixing model approach based on the water temperature yielded credible results: the range of the % PS values showed consistent patterns during the observed baseflow and event periods.

Although the water temperature dataset is available at a high temporal resolution for the whole observation period, there are limitations to when the mixing model approach can yield meaningful results. Five cases of PS, MS, and NT stream water temperature interrelationships were distinguished (Fig. 2):

(a) Baseflow – warm season ($T_{MS} < T_{NT} < T_{PS}$);
(b) Baseflow – cold season ($T_{MS} > T_{NT} > T_{PS}$);
(c) Event – warm season (cause: rainfall; T_{NT} increases towards T_{PS});
(d) Event – cold season (cause: snow melting; T_{NT} decreases towards T_{PS});
(e) Intersection of water temperatures (transition between the warm and cold seasons).

The first three cases (a–c) were suitable for employing the mixing model and thus determining the contribution of peat bog hillslope water to the total runoff. The latter two cases (d and e) were not suitable, as the individual components could not be satisfactorily separated.

3.2.1 Baseflow periods

To analyse the contribution of the peat bog hillslope during baseflow, we further divided the observation period into warm and cold periods. The warm periods are 5 June - 10 October 2020 (127 days) and 6 June - 9 October 2021 (125 days), and the cold periods are 20 November 2020 - 20 April 2021 (151 days) and 20 November 2021 - 6 April 2022 (137 days). The cold periods are slightly longer, which is due to the climatic conditions of the region, especially cold springs and later termination of snow melting. The average length of the baseflow period during a warm season is 137 h (5.7 days); during a cold season, the average duration is 288 h (12 days). This indicates a larger number of events interrupting the baseflow during the warm season (rainfall) relative to the cold season (rain-on-snow events and air temperature-induced snow melting).

The mean contribution of the peat bog hillslope to the NT stream during baseflow was approximately 40.2% (±13.6%). However, the %PS varies significantly between the warm and cold periods. The difference between the two datasets (with a non-normal distribution) was confirmed with the Kruskal-Wallis test ($p < .05$). The average contribution of PS water to the NT stream was 48.9% (±9.4%) during the warm baseflow periods and 33.4% (±8.1%) during the cold baseflow periods (Fig. 3). These values differ by only 1–3% when employing the different inclinations (4°–10°) and window sizes (3–12 h). During the warm season, the %PS value fluctuated between 40% and 60%, showing a daily fluctuation amplitude of <10%.

During the cold season, a daily fluctuation amplitude of <10% was also observed, with the %PS values mostly ranging from 20% to 45%. The mean baseflow flow rate was generally very similar between the warm period (0.0102 ± 0.0005 m^3 s^{-1}) and the cold period (0.0107 ± 0.0009 m^3 s^{-1}). The stable NT stream flow rate and the different %PS values suggest that the mineral slope stream flow rate is higher during the cold season. We address this issue more thoroughly in the Discussion section.

3.2.2 Rainfall-runoff events

Over the observation period of June 2020 to May 2022, we selected a total of 13 rainfall–runoff events (Table 1) that fulfilled the set of conditions described in Section 2.3.1. The trend of %PS was similar during all the observed events: %PS showed an almost immediate response to the rising flow rate, peaked a short time after the maximum flow rate, and then exhibited a slow decline towards pre-event values (~40%). The average delay of the peak hourly precipitation total value and the peak flow rate at the NT stream was 2.7 h. The lag time between the peak NT stream flow rate and the peak %PS value was ~3 h. The peat bog contribution ranged from its baseflow value to 80–90% (83.4% on average, with a range of 63.5–96.1%), and the total duration of the events ranged from 24 to 131 h. The total runoff volume of each individual event ranged from 1990 to 30 163 m^3. PS water accounted for 50.7–85.6% of the total runoff during rainfall–runoff events, with an average of 72.8%. The major factors controlling the peat bog outflow volume were the amount of rainfall and the duration of rainfall events.

Figure 4 shows two types of selected events – namely, a single-peak hydrograph (Fig. 4(a)) and a double-peak hydrograph (Fig. 4(b)) – and the contribution of peat bog hillslope water during such events. The counterclockwise loop of the normalized plots indicates that the return of the %PS value to pre-event values took longer than the return of the NT stream flow rate to baseflow levels. The antecedent soil moisture conditions (Table 1) and rainfall intensity determined the magnitude of the stream response to rainfall. This was clearly demonstrated in the case of medium precipitation totals, which could cause a higher streamflow response if the soil moisture was high at the time of rainfall. Additionally, if there was little rain during the week preceding an event and the soil moisture was low, the response to similar rainfall totals was significantly lower. Normalized flow rate–%PS plots for all events can be found in the Supplementary material of this paper.

3.3 Hydrological simulation of the water balance

3.3.1 Hydrological model efficiency

The model efficiency in terms of the total runoff was 0.69 during the calibration period and 0.61 during the validation period. These values occur at the boundary between good and satisfactory simulations, according to Moriasi *et al.* (2007). The corresponding RMSE values equalled 2.7 and 4.2 mm d^{-1}, respectively. The total simulated runoff volume accounted for 102.1% of the observed runoff volume, indicating the model ability to estimate the total water balance. The most obvious differences between the observed and simulated discharge values could be found during the snowmelt periods in both years (March–April) or were restricted to a few simulated minor peak discharge values (< 10 mm d^{-1}) not observed by the measuring gauge. Moreover, two out of the six major peak discharge values (> 25 mm d^{-1}) were underestimated by the model by ~30% (Fig. 5(a)). The snow water equivalent was estimated with a calculated RMSE value of 33 mm (25% of the average value), a Nash-Sutcliffe coefficient value of 0.64, and a Pearson correlation coefficient value of 0.98.

Soil water storage was estimated with RMSE values of 14.1 mm during the calibration period and 16.7 mm during the validation period. These values correspond to 1.9% and 2.2%, respectively, of the volumetric water content (VWC). The most prominent deviations from the observed values were found during the cold period, when the model occasionally

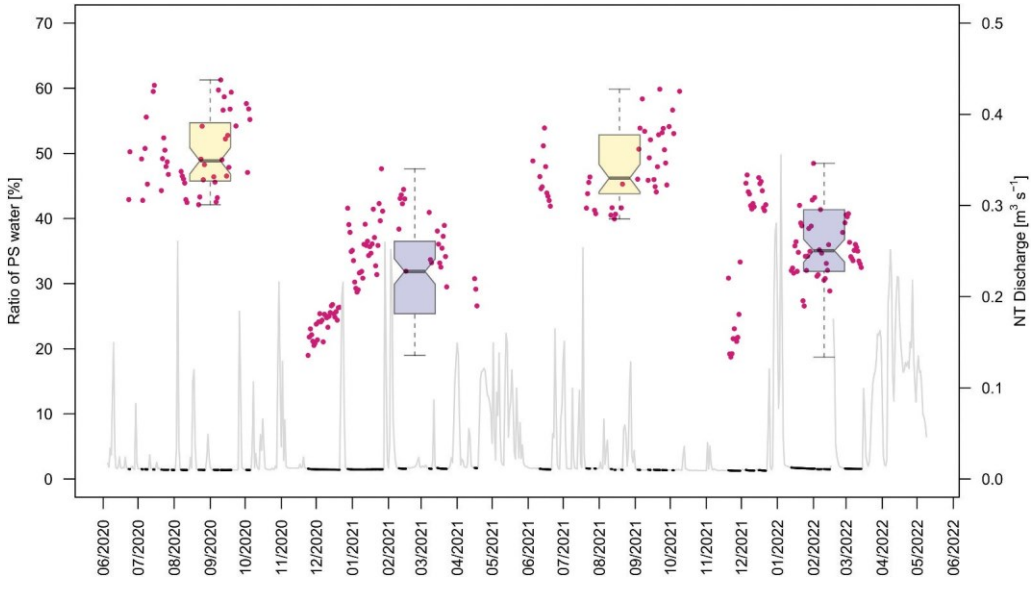

Figure 3. Mean daily ratio of the peat bog stream (PS) water to the total discharge of the northern tributary (NT) stream during baseflow in the warm and cold seasons. Mean daily ratio of the PS water is marked with dots; its seasonal statistics are represented by box plots. Baseflow periods are marked with a black line at the discharge line plot.

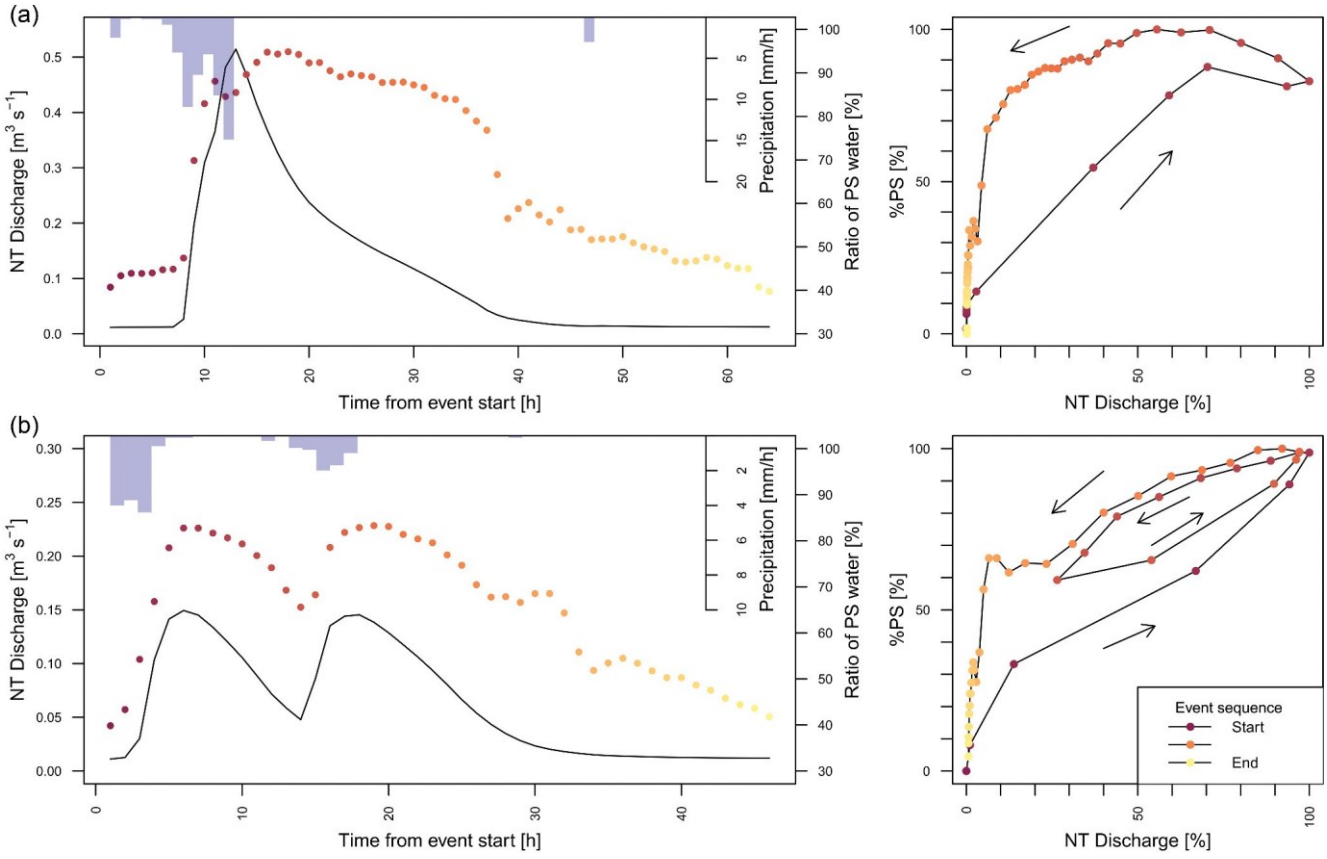

Figure 4. Example of two rainfall-runoff events recorded at the northern tributary (NT) stream in summer 2021 and the contribution of peat bog stream to the runoff (%PS) (hourly data, marked with dots). Plots with normalized values of the NT stream discharge and the ratio of peat bog hillslope water are shown on the right. (a) A single-peaked hydrograph of the 17 July 2021 event; (b) a double-peaked hydrograph of the 8 July 2021 event.

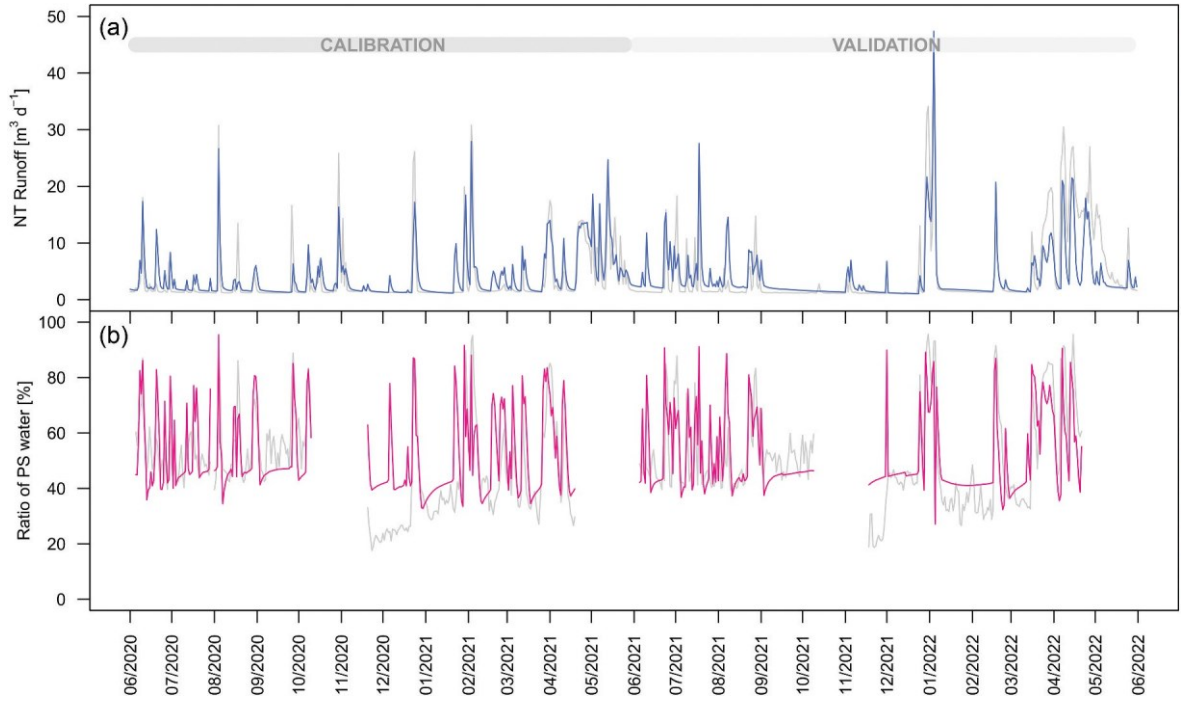

Figure 5. Comparison of the observed (light grey) and simulated values of: (a) the northern tributary stream (NT) daily runoff (blue) and (b) the peat bog stream contribution to the runoff (%PS) (pink) in June 2020 - May 2022. The extent of the calibration and validation periods is marked at the top.

underestimated soil water storage by ~40 mm/5–6% of the VWC. The warm period was simulated very efficiently, with an underestimation by only up to ~20 mm of the highest soil water storage (2.8% of the VWC). The saturation in the peat bog, represented by the groundwater level depth, was estimated with an RMSE of 10.9 mm (5.3% of the average value) during the calibration period. During the validation period, sensor malfunction unfortunately limited the data usage. All the presented error statistics agree with the model efficiency results presented by Vlček *et al.* (2021) using the same model with different calibration periods, from 2014 to 2019.

The peat bog contribution to the total runoff was simulated with an RMSE of 14.1% during the calibration period and 13.4% during the validation period. The average ratio of peat bog water in the NT stream discharge was, based on stream water temperature analysis, 53.2% during the warm period and 46% during the cold period. The average simulated %PS values were 52.2% over the warm period and 50.7% over the cold period. A comparison of the simulated and measured values of %PS is shown in Fig. 5(b). The model generally overestimated %PS at the beginning of each cold season and efficiently estimated the warm-season dynamics of both hillslopes.

3.3.2 Water balance estimation

The newly established model that accounts for stream water temperature analysis enabled better estimation of the catchment water balance in terms of runoff partitioning and estimation of the total actual evapotranspiration (AET). Our previous study (Vlček *et al.* 2021) focused on quantifying the water balance based only on knowledge of the total runoff, as the PS water contribution was a modelled variable. Here, we present results that are limited by knowledge of the water temperature-based ratio of PS water in the total NT stream runoff; therefore, the water balance can now be more efficiently divided between the two adjacent hillslopes.

The catchment water balance is summarized in Table 2, showing significant differences in the AET and total runoff rates between the two domains. The peat bog hillslope exhibited a significantly lower AET rate, reaching 68% and 70% (in 2020 and 2021, respectively) of the mineral hillslope evapotranspiration. This directly led to higher levels of runoff from the peat bog by 18% and 11% in 2020 and 2021, respectively. The runoff coefficients were higher by 12.2% (2020) and 8.0% (2021) on the peat bog. Moreover, the majority of the runoff from the PS (79% in 2020 and 75% in 2021) originated from subsurface stormflow of preferential flow, suggesting a notable hydrograph. In contrast, runoff from the mineral hillslope was mainly formed (55% in 2020 and 61% in 2021) by water that percolated into deeper layers (which was also confirmed by the seasonally stable stream water temperatures).

4 Discussion

Water temperature has scarcely been used as a tracer over the last few decades, as the measurement techniques based on stable isotopes of water have advanced. Despite the undeniable assets of water isotope tracing, we believe that the water temperature can be employed in small-scale catchment experiments involving distinct water sources in terms of the water temperature. The reliability of the method was confirmed by comparing the results with the analysis results for stable water isotopes, e.g. in Pomije *et al.* (2022). Zajíček *et al.* (2011, 2016) verified that this method could also be very useful in agricultural environments. However, due to its nonconservative trait, water temperature should be used as a tracer with caution. Due to our detailed knowledge of the study site and given our previous studies (Vlček *et al.* 2017, 2021), we are confident that the water temperature sensor installation locations were correctly selected to achieve the desired outcome.

Water from both hillslopes mixes in the concave lower part of the valley, which is mostly formed by a lagg–peaty saturated area with spruce trees, with both the water quality and quantity influenced by both hillslopes (Tetzlaff *et al.* 2014, Langlois *et al.* 2015, Scheliga *et al.* 2019). In our case, springs of MS and PS are both situated higher on the slope above the lagg. Although peat bog springs are generally closely linked to the water table and are prone to drying when the water table drops, the selected peat bog spring has remained stable since the first reconnaissance activities in 2012. From this location, water flows in shallow channels through the lagg directly into the NT stream, not mixing within the lagg. Therefore, the hydrological connectivity of this peat bog spring and stream is not reduced even at low water table, which is often the case elsewhere, as described by Dick *et al.* (2018).

The two components used for the mixing model have been labelled “water from the mineral slope” and “water from the peat bog.” This simplistic distinction represents two major groups of runoff processes: percolation (slow flow) and surface/near-surface (fast) flow. Both of these processes occur on both hillslopes; however, one always dominates over the other. While surface flow has not been observed on the mineral hillslope during our field trips at the site and is considered minor, the real contribution at deep positions in the peat bog is difficult to estimate. McKenzie *et al.* (2007) measured the soil

Table 2. Modelled water balance of the northern tributary catchment and its two parts: peat bog hillslope and mineral hillslope.

	2020		2021	
	Peat bog	Mineral h.	Peat bog	Mineral h.
Precipitation	1927		1933	
PET	575		602	
AET	387	572	412	592
Q_s	1189	573	1150	533
Q_p	326	706	381	843
Q_{total}	1515	1279	1531	1376

Q_s – stormflow or fast preferential (macropore) flow; Q_p – percolation or slow flow; Q_{total} – total runoff from each hillslope; PET – potential evapotranspiration; AET – actual evapotranspiration. All variables are in mm.

temperature of a peat bog at a depth of 4 m, which varied between 4 and 6°C throughout the year. As the thermal conductivity of peat is lower than that of mineral soil or water (Mustamo *et al.* 2019), we could assume that the temperature at this depth in the bog might also remain similarly stable in our case. This would suggest that the waters from the mineral hillslope and peat bog catotelm are indistinguishable temperature-wise. In addition, especially during baseflow, the contribution of the peat bog could be even higher than estimated.

Water from the peat bog increases the NT stream discharge fluctuation because fast flow dominates runoff formation here, and thus, the water temperature in peat is significantly influenced by the trend of the air temperature. Moreover, streams from an area with sparse vegetation are more greatly affected by weather conditions (mainly the air temperature) than those from densely forested areas (Brown *et al.* 2010). Water flows through macropores, which mainly occur in the acrotelm and a thin upper layer of the catotelm. This thin surface soil layer, to a depth of ~30 cm, is prone to heat accumulation on warm days, and low temperatures persist after cold days (Kettridge and Baird 2007). Therefore, it is not possible to distinguish rain and near-surface pre-event water from the peat bog.

The box plots for D = 1 cm, D = 30 cm, and D = 70 cm in Fig. 6 show the amplitude of the peat temperature fluctuation during the warm and cold parts of the year. During the warm season, the daily temperature fluctuation is observed only to a depth of ~20 cm, while the mean peat temperatures at depths of 1 and 30 cm are similar. The mean PS temperature is more closely correlated with the peat temperature at a depth of 70 cm below the surface, which might be considered the upper layer of the catotelm. In peatlands, the acrotelm is generally more permeable than the catotelm, and the catotelm permeability further decreases with depth. During the warm season, the water table often reaches the catchment, and therefore, the highest connectivity might occur at a depth of 30 cm and below. During the cold season, the PS water temperature is similar to the peat temperature at a depth of 30 cm. As the catchment is covered with snow from November until May, the weather extremes are attenuated. Moreover, the surface layer of peat (~5 cm) freezes, and the groundwater level then fluctuates below this frozen layer (Kettridge and Baird 2007). The resulting high hydrological connectivity of the acrotelm facilitates water transfer to the peat bog spring.

The determination of the periods to be omitted, i.e. when the water temperature of the two sources was too similar and the mixing model could not be satisfactorily employed, was slightly problematic. In the case of the hydrological model, the performance of the model could be improved if we extended the omitted autumn period further into the cold season. We set the beginning of the cold season to a point where the distinction between the PS and MS water temperatures is clear and stable. However, during the first week or two into the cold season, the %PS value stays relatively low (approximately 20%). The hydrological model simulated the PS contribution during this period rather poorly, as it retained minimum values of approximately 40% throughout the whole validation period. This occurs because models, due to their inherent parameter stationary conceptualization, cannot generally adapt to changes in runoff generation mechanisms on both seasonal (Lan *et al.* 2020) and inter-annual bases (Wallner and Haberlandt 2015). This was obviously the case for the peat bog, which demonstrated significant differences between the warm and cold season behaviours. Although the delineation of the omitted periods impacts the baseflow statistics of the two

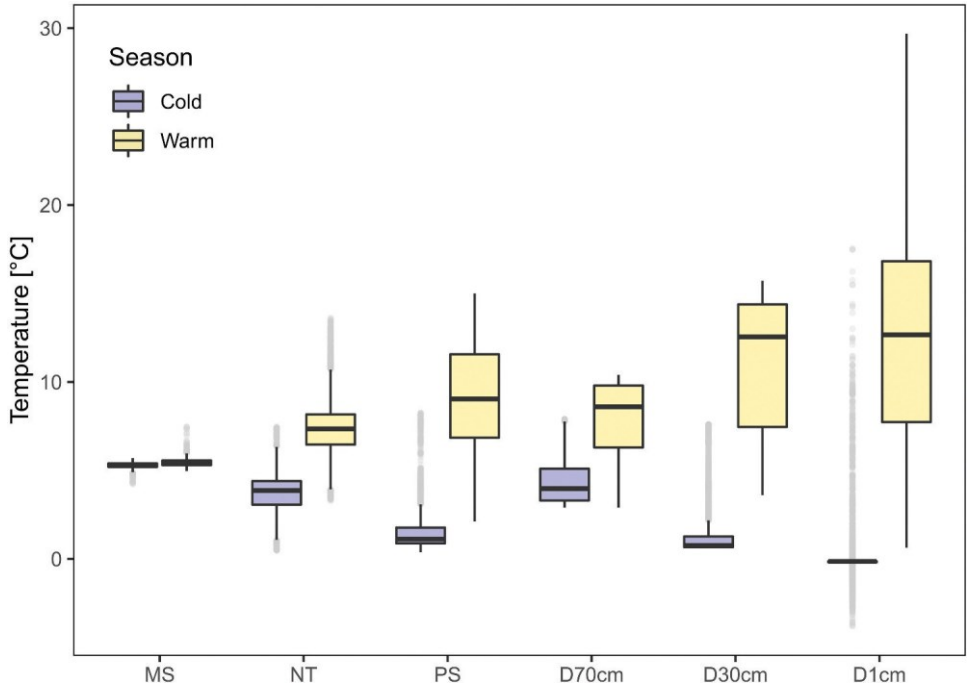

Figure 6. Annual temperature amplitudes of water sources at the northern tributary catchment. Temperature values are given for three positions (depths) within peat (D1cm, D30cm, D70cm), along with the water temperatures of mineral hillslope stream (MS), peat bog stream (PS), and northern tributary stream (NT) for the period August 2020 - July 2021. Outliers are marked with grey dots.

seasons, shifting the start of the cold season would not affect the overall results – the mean %PS value for the cold season would still be significantly lower than that for the warm season.

In addition to the PS contribution, the most profound drawbacks of the model results lie in the period of snow accumulation and melting. This part of the simulation causes a deterioration in the model error statistics for the entire season. We examined the two most common snowmelt modelling approaches (radiation balance and degree-day), and we used the degree-day model, as it is generally more efficient. The obtained average Nash-Sutcliffe coefficient value occurs within the range presented by Jeníček and Ledvinka (2020), who used the same model for various catchments in a wider region, and it agrees with the results of Vlček *et al.* (2021), where different periods and the same catchment were analysed. Nevertheless, as this model is based on the average daily air temperature, temperatures below zero at night often outweighed snowmelt-producing temperatures above zero during the day. In these cases, the modelling approach did not capture the real situation and did not produce a runoff event. This flaw could be overcome by utilizing an hourly time scale. Nevertheless, as the model is intended for the assessment of the impact of climate change on hydrological regimes, the currently available datasets only provide future climate scenarios at daily time scales (Michel *et al.* 2021). In terms of discharge, the overall model performance corresponds to the efficiency values presented by Jeníček *et al.* (2018) and Jeníček and Ledvinka (2020) for Switzerland and Czechia, respectively.

The contribution of peat bog water to the NT stream showed a constant daily fluctuation (~10%), especially during baseflow. Such a daily regime could be the effect of evapotranspiration; however, we did not record the changes in the stream discharge or in the water level in spring. These slight changes in the peat bog water ratio are probably caused by the daily regime of the air temperature and radiation. This suggests that MS water probably gains a slight temperature fluctuation pattern on its way to the confluence and/or PS water exhibits a higher fluctuation than recorded by the sensor. In either case, our goal of determining the mean %PS value during baseflow over a long period was not compromised by this technicality.

One of the findings concerning the peat bog water contribution is its distinct seasonality – the mean baseflow %PS value during the cold season is approximately 33%, while during the warm season, the mean value reaches almost 50%. As discussed above, a certain part of this difference could be attributed to the delimitation of cold and warm seasons (i.e. the extent of the autumn/spring omitted period). However, this difference cannot be explained by only this aspect. As the mean NT stream discharge during baseflow is practically the same between the two seasons, a lower contribution of the peat bog suggests a higher contribution of water from the mineral hillslope. From a hydrogeological perspective, seasonal fluctuations in the spring yield are common. Some of the factors driving such fluctuations include the geological structure of the area, temporal distributions of precipitation and snow cover, seasonality of evapotranspiration and groundwater recharge (Price 1996, Exner-Kittridge *et al.* 2016, Żelazny *et al.* 2018). In the case of the NT stream catchment, the significantly lower cold-season PET value of the mineral hillslope could lead to a higher hydraulic head and thus discharge in spring. The seasonal difference in %PS could partly be affected by the baseflow selection. However, when comparing the results obtained using the various baseflow selection parameters (hydrograph inclination limits of 4°–10° and window sizes of 3–12 h), the difference between the warm and cold seasons was still notable.

5 Conclusions

The study focused on the determination of the contribution of a peat bog to the total outflow of the catchment formed by two distinct units: peat bog and mineral hillslopes. The stream water temperature was used as a tracer because it can provide continuous data not limited to sampling campaigns. Although the use of stable water isotopes is currently an accepted method for separating runoff components, the water temperature could also serve similar purposes under certain conditions.

The peat bog contribution significantly differed during baseflow periods and runoff events. During baseflow periods, the mean peat bog contribution ranged from 33.4% in the cold part of the year to 48.9% in the warm part. This indicates the importance of the peat bog even during rainless periods, especially in the warm part of the year. The contribution of peatlands could actually be even higher, as deeper positions of catotelm may exhibit year-round temperatures very similar to those recorded on the mineral hillslope. A different behaviour was observed during runoff events when the peat bog dominated the mineral hillslope. In terms of runoff peaks, nearly all water in the stream originated from the peat bog (83.4%). The peat bog accounted for 73% of the total runoff volume on average during all inspected events. When comparing the simulated hydrological balance of the two parts of the catchment, the results showed a markedly higher AET rate on the mineral hillslope (~600 mm per year), which indicates a higher total runoff from the peat bog (~1500 mm per year). The modelled lower AET value of peatlands (~400 mm per year) indicates that peaty areas lose less water via evapotranspiration than mineral soils with landcover. The hydrological significance of peatlands is, however, substantial as it feeds streams during both wet and dry periods.

The results of this study, obtained from detailed description of the peat bog water balance relative to the forested mineral hillslope and the adjusted hydrological model, enable more reliable modelling assessment of the reaction of peatlands to climate change. This is especially relevant in the situation when more frequent drought periods interrupted with more intense rainfall are expected to occur. Based on the obtained peat bog behaviour, further studies of peatland hydrology could greatly benefit from detailed research and knowledge of the vertical pressure head dynamics and limitations of the evapotranspiration rate in peatlands.

Acknowledgements

We thank Jitka Toušková for help with calculation of evapotranspiration, Julius Česák for technical support with the installation of measuring devices, and NP Šumava for a permit to conduct the research on its land. This work was supported by the Czech Grant Agency (GA22-12837S), Praemium Academiae of the Czech Academy of Sciences, the institutional support of the Czech Academy of Sciences (RVO: 67985874), and the research programme Strategy AV21 Water for life.

Disclosure statement

No potential conflict of interest was reported by the author(s).

Funding

This work was supported by the Akademie Věd České Republiky [RVO: 67985874]; and the Grantová Agentura České Republiky [GA22-12837S].

ORCID

Kristyna Falatkova http://orcid.org/0000-0001-8679-2157
Václav Šípek http://orcid.org/0000-0002-8079-0270
Lukáš Vlček http://orcid.org/0000-0002-6906-6054
Jiří Kocum http://orcid.org/0009-0001-1833-4741
Martin Pivokonský http://orcid.org/0000-0003-2067-2632

References

Acreman, M. and Holden, J., 2013. How wetlands affect floods. *Wetlands*, 33 (5), 773–786. doi:10.1007/s13157-013-0473-2.

Ahmad, S., *et al.*, 2020. Long-term rewetting of degraded peatlands restores hydrological buffer function. *Science of the Total Environment*, 749, 141571. doi:10.1016/j.scitotenv.2020.141571

Anderson, M.P., 2005. Heat as a ground water tracer. *Groundwater*, 43 (6), 951–968. doi:10.1111/j.1745-6584.2005.00052.x.

Bacon, K.L., *et al.*, 2017. Questioning ten common assumptions about peatlands. *Mires and Peat*, 19, 1–23.

Ballard, C.E., McIntyre, N., and Wheater, H.S., 2012. Effects of peatland drainage management on peak flows. *Hydrology and Earth System Sciences*, 16 (7), 2299–2310. doi:10.5194/hess-16-2299-2012.

Bechtold, M. *et al.*, 2019. PEAT-CLSM: a specific treatment of peatland hydrology in the NASA catchment land surface Model. *Journal of Advances in Modeling Earth Systems*, 11, 2130–2162. doi:10.1029/2018MS001574

Beck, H., *et al.*, 2018. Present and future Köppen-Geiger climate classification maps at 1-km resolution. *Scientific Data*, 5 (1), 1–12. doi:10.1038/sdata.2018.214.

Bergström, S., 1992. *The HBV model: its structure and applications*. Sweden: Swedish Meteorological and Hydrological Institute (SMHI), Norrköping.

Bescansa, P., *et al.*, 2006. Soil water retention as affected by tillage and residue management in semiarid Spain. *Soil and Tillage Research*, 87 (1), 19–27. doi:10.1016/j.still.2005.02.028.

Bhaskar, A.S., Harvey, J.W., and Henry, E.J., 2012. Resolving hyporheic and groundwater components of streambed water flux using heat as a tracer. *Water Resources Research*, 48 (8). doi:10.1029/2011WR011784.

Bianchin, M., Smith, L., and Beckie, R., 2010. Quantifying hyporheic exchange in a tidal river using temperature time series. *Water Resources Research*, 46 (7), W07507. doi:10.1029/2009WR008365.

Birkinshaw, S.J. and Webb, B., 2010. Flow pathways in the Slapton Wood catchment using temperature as a tracer. *Journal of Hydrology*, 383 (3–4), 269–279. doi:10.1016/j.jhydrol.2009.12.042.

Bragg, O.M., 2002. Hydrology of peat-forming wetlands in Scotland. *Science of the Total Environment*, 294 (1–3), 111–129. doi:10.1016/S0048-9697(02)00059-1.

Brown, L.E., *et al.*, 2010. A comparison of stream water temperature regimes from open and afforested moorland, Yorkshire Dales, northern England. *Hydrological Processes*, 24 (22), 3206–3218. doi:10.1002/hyp.7746.

Brown, L.E. and Hannah, D.M., 2007. Alpine stream temperature response to storm events. *Journal of Hydrometeorology*, 8 (4), 952–967. doi:10.1175/JHM597.1.

Burt, T.P., Heathwaite, A.L., and Labadz, J.C., 1990. Runoff production in peat-covered catchments. *In:* M.G. Anderson and T.P. Burt, eds. *Process Studies in Hillslope Hydrology*. Chichester, UK: John Wiley & Sons, 463–500.

Clymo, R.S., 2004. Hydraulic conductivity of peat at Ellergower Moss, Scotland. *Hydrological Processes*, 18 (2), 261–274. doi:10.1002/hyp.1374.

Dick, J.J., Tetzlaff, D., and Soulsby, C., 2018. Role of riparian wetlands and hydrological connectivity in the dynamics of stream thermal regimes. *Hydrology Research*, 49 (3), 634–647. doi:10.2166/nh.2017.066.

Erwin, K.L., 2009. Wetlands and global climate change: the role of wetland restoration in a changing world. *Wetlands Ecology and Management*, 17 (1), 71–84. doi:10.1007/s11273-008-9119-1.

Exner-Kittridge, M., *et al.*, 2016. The seasonal dynamics of the stream sources and input flow paths of water and nitrogen of an Austrian headwater agricultural catchment. *Science of the Total Environment*, 542, 935–945. doi:10.1016/j.scitotenv.2015.10.151

Gao, J., Holden, J., and Kirkby, M., 2016. The impact of land-cover change on flood peaks in peatland basins. *Water Resources Research*, 52 (5), 3477–3492. doi:10.1002/2015WR017667.

Gat, J.R. and Gonfiantini, R., 1981. *Stable isotope hydrology deuterium and oxygen-18 in the water cycle*. A monograph prepared under the aegis of the IAEA/UNESCO working group on nuclear techniques in hydrology of the international hydrological programme. IAEA, Vienna.

Genthon, P., *et al.*, 2005. Temperature as a marker for karstic waters hydrodynamics. Inferences from 1 year recording at La Peyrére cave (Ariège, France). *Journal of Hydrology*, 311 (1–4), 157–171. doi:10.1016/j.jhydrol.2005.01.015.

Gosling, S.N. and Arnell, N.W., 2016. A global assessment of the impact of climate change on water scarcity. *Climatic Change*, 134 (3), 371–385. doi:10.1007/s10584-013-0853-x.

Gracz, M.B., *et al.*, 2015. Analyzing peatland discharge to streams in an Alaskan watershed: an integration of end-member mixing analysis and a water balance approach. *Journal of Hydrology*, 530, 667–676. doi:10.1016/j.jhydrol.2015.09.072

Grayson, R., Holden, J., and Rose, R., 2010. Long-term change in storm hydrographs in response to peatland vegetation change. *Journal of Hydrology*, 389 (3–4), 336–343. doi:10.1016/j.jhydrol.2010.06.012.

Holden, J., 2006. Peatland hydrology. *Developments in Earth Surface Processes*, 9, 319–346.

Holden, J., *et al.*, 2008. Overland flow velocity and roughness properties in peatlands. *Water Resources Research*, 44 (6). doi:10.1029/2007WR006052.

Holden, J., *et al.*, 2011. Water table dynamics in undisturbed, drained and restored blanket peat. *Journal of Hydrology*, 402 (1–2), 103–114. doi:10.1016/j.jhydrol.2011.03.010.

Holden, J., *et al.*, 2015. Impact of prescribed burning on blanket peat hydrology. *Water Resources Research*, 51 (8), 6472–6484. doi:10.1002/2014WR016782.

Holden, J. and Burt, T.P., 2003a. Hydrological studies on blanket peat: the significance of the acrotelm-catotelm model. *Journal of Ecology*, 91 (1), 86–102. doi:10.1046/j.1365-2745.2003.00748.x.

Holden, J. and Burt, T.P., 2003b. Runoff production in blanket peat covered catchments. *Water Resources Research*, 39 (7). doi:10.1029/2002WR001956.

Iglesias, A., *et al.*, 2007. Challenges to manage the risk of water scarcity and climate change in the Mediterranean. *Water Resources Management*, 21 (5), 775–788. doi:10.1007/s11269-006-9111-6.

Ingram, H.A.P., 1978. Soil layers in mires: function and terminology. *Journal of Soil Science*, 29 (2), 224–227. doi:10.1111/j.1365-2389.1978.tb02053.x.

Ingram, H.A.P., 1983. Hydrology. *In*: A.J.P. Gore, ed. *Ecosystems of the World 4A*. Mires: Swamp, Bog, Fen and Moor. Elsevier, Oxford, 67–158.

James, E.R., *et al*., 2000. The use of temperature and the isotopes of O, H, C, and noble gases to determine the pattern and spatial extent of groundwater flow. *Journal of Hydrology*, 237 (1–2), 100–112. doi:10.1016/S0022-1694(00)00303-6.

Jeníček, M. and Ledvinka, O., 2020. Importance of snowmelt contribution to seasonalrunoff and summer low flows in Czechia. *Hydrology and Earth System Sciences*, 24 (7), 3475–3491. doi:10.5194/hess-24-3475-2020.

Jeníček, M., Seibert, J., and Staudinger, M., 2018. Modeling of future changes in seasonal snowpack and impacts on summer low flows in alpine catchments. *Water Resources Research*, 54 (1), 538–556. doi:10.1002/2017WR021648.

Jones, J.A.A., 1997. Pipeflow contributing areas and runoff response. *Hydrological Processes*, 11 (1), 35–41. doi:10.1002/(SICI)1099-1085(199701)11:1<35::AID-HYP401>3.0.CO;2-B.

Kettridge, N. and Baird, A., 2007. In situ measurements of the thermal properties of a northern peatland: implications for peatland temperature models. *Journal of Geophysical Research*, 112 (F2), F02019. doi:10.1029/2006JF000655.

Keys, W.S. and Brown, R.F., 1987. The use of temperature logs to trace the movement of injected water. *Ground Water*, 16 (1), 32–48. doi:10.1111/j.1745-6584.1978.tb03201.x.

Kimmel, K. and Mander, Ü., 2010. Ecosystem services of peatlands: implications for restoration. *Progress in Physical Geography*, 34 (4), 491–514. doi:10.1177/0309133310365595.

Klaus, J. and McDonnell, J.J., 2013. Hydrograph separation using stable isotopes: review and evaluation. *Journal of Hydrology*, 505, 47–64. doi:10.1016/j.jhydrol.2013.09.006

Lan, T., *et al*., 2020. Dynamics of hydrological-model parameters: mechanisms, problems and solutions. *Hydrology and Earth System Sciences*, 24 (3), 1347–1366. doi:10.5194/hess-24-1347-2020.

Langlois, M.N., Price, J.S., and Rochefort, L., 2015. Landscape analysis of nutrient-enriched margins (lagg) in ombrotrophic peatlands. *Science of the Total Environment*, 505, 573–586. doi:10.1016/j.scitotenv.2014.10.007

Lüthi, M.P., 2019. Stream gauge calibration of a cave stream using water temperature variability as a tracer. *Water Resources Research*, 55 (7), 5738–5750. doi:10.1029/2018WR023762.

Mancosu, N., *et al*., 2015. Water scarcity and future challenges for food production. *Water*, 7 (3), 975–992. doi:10.3390/w7030975.

McKenzie, J.M., *et al*., 2007. Heat transport in the Red Lake Bog, Glacial Lake Agassiz Peatlands. *Hydrological Processes*, 21 (3), 369–378. doi:10.1002/hyp.6239.

Mekonnen, M.M. and Hoekstra, A.Y., 2016. Four billion people facing severe water scarcity. *Science Advances*, 2 (2), e1500323. doi:10.1126/sciadv.1500323.

Meriö, L.J., *et al*., 2019. Snow to precipitation ratio controls catchment storage and summer flows in boreal headwater catchments. *Water Resources Research*, 55 (5), 4096–4109. doi:10.1029/2018WR023031.

Michel, A., *et al*., 2021. Climate change scenarios at hourly time-step over Switzerland from an enhanced temporal downscaling approach. *International Journal of Climatology*, 41 (9), 3503–3522. doi:10.1002/joc.7032.

Mitsch, W.J., 2005. Applying science to conservation and restoration of the world's wetlands. *Water Science & Technology*, 51 (8), 13–26. doi:10.2166/wst.2005.0215.

Monteith, J.L., 1965. Evaporation and the environment. The state and movement of water in living organisms. *In: Proceedings of 19th Symposium of the Society of Experimental Biology*. Cambridge: Cambridge University Press, 205–234.

Moriasi, D.N., *et al*., 2007. Model evaluation guidelines for systematic quantification of accuracy in watershed simulations. *Transactions of the Asabe*, 50 (3), 885–900. doi:10.13031/2013.23153.

Mustamo, P., *et al*., 2019. Thermal conductivity of unfrozen and partially frozen managed peat soils. *Soil and Tillage Research*, 191, 245–255. doi:10.1016/j.still.2019.02.017

Padrón, R.S., *et al*., 2020. Observed changes in dry-season water availability attributed to human-induced climate change. *Nature Geoscience*, 13 (7), 477–481. doi:10.1038/s41561-020-0594-1.

Pomije, T., *et al*., 2022. Drainage runoff separation of new and old water based on precipitation, air, water, and soil temperature compared to stable isotopes 18O and 2H. *Water*, 14 (15), 2349. doi:10.3390/w14152349.

Price, M., 1996. *Introducing groundwater*. London: Chapman and Hall, 278.

Price, J.S., Heathwaite, A.L., and Baird, A.J., 2003. Hydrological processes in abandoned and restored peatlands: an overview of management approaches. *Wetlands Ecology and Management*, 11 (1), 65–83. doi:10.1023/A:1022046409485.

Quinton, W.L., Hayashi, M., and Carey, S.K., 2008. Peat hydraulic conductivity in cold regions and its relation to pore size and geometry. *Hydrological Processes: An International Journal*, 22 (15), 2829–2837. doi:10.1002/hyp.7027.

R Core Team, 2021. R: *a language and environment for statistical computing*. Vienna, Austria: R Foundation for Statistical Computing. https://www.R-project.org/.

Rezanezhad, F., *et al*., 2010. Influence of pore size and geometry on peat unsaturated hydraulic conductivity computed from 3D computed tomography image analysis. *Hydrological Processes*, 24 (21), 2983–2994. doi:10.1002/hyp.7709.

Rezanezhad, F., *et al*., 2016. Structure of peat soils and implications for water storage, flow and solute transport: a review update for geochemists. *Chemical Geology*, 429, 75–84. doi:10.1016/j.chemgeo.2016.03.010

Rezanezhad, F., Price, J.S., and Craig, J.R., 2012. The effects of dual porosity on transport and retardation in peat: a laboratory experiment. *Canadian Journal of Soil Science*, 92 (5), 723–732. doi:10.4141/cjss2011-050.

Roudier, P., Ducharne, A., and Feyen, L., 2014. Climate change impacts on runoff in West Africa: a review. *Hydrology and Earth System Sciences*, 18 (7), 2789–2801. doi:10.5194/hess-18-2789-2014.

Šanda, M., *et al*., 2014. Run-off formation in a humid, temperate headwater catchment using a combined hydrological, hydrochemical and isotopic approach (Jizera Mountains, Czech Republic). *Hydrological Processes*, 28 (8), 3217–3229. doi:10.1002/hyp.9847.

Scheliga, B., *et al*., 2019. Assessing runoff generation in riparian wetlands: monitoring groundwater–surface water dynamics at the micro-catchment scale. *Environmental Monitoring and Assessment*, 191 (2), 1–25. doi:10.1007/s10661-019-7237-2.

Scherrer, S. and Naef, F., 2003. A decision scheme to indicate dominant hydrological flow processes on temperate grassland. *Hydrological Processes*, 17 (2), 391–401. doi:10.1002/hyp.1131.

Scholz, M., 2007. Ecological effects of water retention in the River Rhine Valley: a review assisting future retention basin classification. *International Journal of Environmental Studies*, 64 (2), 171–187. doi:10.1080/00207230601125200.

Seibert, J. and Vis, M., 2012. Teaching hydrological modeling with a user-friendly catchment-runoff-model software package. *Hydrology and Earth System Sciences*, 16 (9), 3315–3325. doi:10.5194/hess-16-3315-2012.

Shanley, J.B. and Peters, N.E., 1988. Preliminary observations of streamflow generation during storms in a forested Piedmont watershed using temperature as a tracer. *Journal of Contaminant Hydrology*, 3 (2–4), 349–365. doi:10.1016/0169-7722(88)90040-X.

Soulsby, C., *et al*., 2006. Runoff processes, stream water residence times and controlling landscape characteristics in a mesoscale catchment: an initial evaluation. *Journal of Hydrology*, 325 (1–4), 197–221. doi:10.1016/j.jhydrol.2005.10.024.

Starostová, M., 2012. Měření srážek totalizátory na Šumavě (Precipitation measurement with rain gauges at the Bohemian Forest). *Meteorologické zprávy*, 65, 180–183. (In Czech).

Staudinger, M., *et al*., 2017. Catchment water storage variation with elevation. *Hydrological Processes*, 31 (11), 2000–2015. doi:10.1002/hyp.11158.

Tetzlaff, D., *et al*., 2014. Storage dynamics in hydropedological units control hillslope connectivity, runoff generation, and the evolution of catchment transit time distributions. *Water Resources Research*, 50 (2), 969–985. doi:10.1002/2013WR014147.

van Vliet, M.T., *et al*., 2013. Global river discharge and water temperature under climate change. *Global Environmental Change*, 23 (2), 450–464. doi:10.1016/j.gloenvcha.2012.11.002.

Verhoeven, J.T., 2014. Wetlands in Europe: perspectives for restoration of a lost paradise. *Ecological Engineering*, 66, 6–9. doi:10.1016/j.ecoleng.2013.03.006

Vlček, L., Falátková, K., and Schneider, P., 2017. Identification of runoff formation with two dyes in a mid-latitude mountain headwater. *Hydrology and Earth System Sciences*, 21 (6), 3025–3040. doi:10.5194/hess-21-3025-2017.

Vlček, L., *et al*., 2021. Runoff formation in a catchment with Peat bog and Podzol hillslopes. *Journal of Hydrology*, 593, 125633. doi:10.1016/j.jhydrol.2020.125633

Wallner, M. and Haberlandt, U., 2015. Non-stationary hydrological model parameters: a Framework based on SOM-B. *Hydrological Processes*, 29 (14), 3145–3161. doi:10.1002/hyp.10430.

Wheeler, T. and Von Braun, J., 2013. Climate change impacts on global food security. *Science*, 341 (6145), 508–513. doi:10.1126/science.1239402.

Whitehead, P.G., *et al*., 2009. A review of the potential impacts of climate change on surface water quality. *Hydrological Sciences Journal*, 54 (1), 101–123. doi:10.1623/hysj.54.1.101.

Whitfield, P.H. *et al*., 2006. Restoring the natural hydrology of Burns Bog, Delta, British Columbia–the key to the bog's ecological recovery. Water under Pressure. Vancouver: Proceedings of the CWRA Conference, 58–70.

Wong, L.S., Hashim, R., and Ali, F.H., 2009. A review on hydraulic conductivity and compressibility of peat. *Journal of Applied Sciences*, 9 (18), 3207–3218. doi:10.3923/jas.2009.3207.3218.

Yang, F., *et al*., 2014. Organic matter controls of soil water retention in an alpine grassland and its significance for hydrological processes. *Journal of Hydrology*, 519, 3086–3093. doi:10.1016/j.jhydrol.2014.10.054

Zajíček, A., *et al*., 2011. Drainage water temperature as a basis for verifying drainage runoff composition on slopes. *Hydrological Processes*, 25 (20), 3204–3215. doi:10.1002/hyp.8039.

Zajíček, A., Pomije, T., and Kvítek, T., 2016. Event water detection in tile drainage runoff using stable isotopes and a water temperature in small agricultural catchment in Bohemian-Moravian Highlands, Czech Republic. *Environmental Earth Sciences*, 75 (9), 1–13. doi:10.1007/s12665-016-5561-1.

Żelazny, M., *et al*., 2018. Water temperature fluctuation patterns in surface waters of the Tatra Mts., Poland. *Journal of Hydrology*, 564, 824–835. doi:10.1016/j.jhydrol.2018.07.051

7.3 Stable isotope-based analysis of seasonal runoff dynamics in a mountain peat bog

The study *Tracing Water Sources in a Mountain Catchment Using Stable Isotopes: Insights from Peat and Mineral Soils* (Vlček et al., submitted) builds upon the findings of Falátková et al. (2024) by extending the investigation to include additional sampling sites within the Rokytka experimental catchment. In this follow-up study, stable hydrogen and oxygen isotopes were used to trace water sources and flow paths, encompassing peatland and mineral springs as well as downstream runoff.

This study highlights the role of mountain peat bogs in catchment hydrology by analyzing the stable isotope composition of water sources within a peaty catchment. Our results from the Rokytka catchment reveal that peat bogs have distinct hydrological impacts compared to mineral soils, such as Podzols. The results indicate that peat bog soil water is predominantly influenced by summer precipitation, which plays a vital role in maintaining groundwater levels and preventing peat desiccation. In contrast, mineral soils gradually absorb snowmelt, contributing to the recharge of deeper aquifers and sustaining baseflow from local springs. Due to peaty soils near-surface water flow paths, peat bogs respond rapidly to rainfall, significantly shortening residence times. This quick transmission of rainwater through surface and near-surface flows is particularly evident in high groundwater levels. The findings underscore the significance of soil type and seasonal precipitation in shaping catchment-scale hydrological dynamics.

Manuscript review stage

The manuscript was submitted to Journal of Hydrology on 12 August 2025.

Tracing Water Sources in a Mountain Catchment Using Stable Isotopes: Insights from Peat and Mineral Soils

Lukáš Vlček [1,2 *], Kristýna Falatková[1], Jiří Kocum [1,2], Ondřej Ledvinka [2,3], Ye Su[2], Martin Pivokonský [1], Václav Šípek[1]

* corresponding author: vlcek@ih.cas.cz

1) Institute of Hydrodynamics of the Czech Academy of Sciences, Pod Paťankou 30/5, 160 00 Prague, Czechia
2) Faculty of Science, Charles University, Albertov 6, 128 00 Prague, Czechia
3) Czech Hydrometeorological Institute, Na Šabatce 2050/17, 143 06 Praha, Czechia

Abstract

This study uses stable water isotopes to investigate the hydrological role of mountain peat bogs and adjacent mineral soils in runoff formation. The main objectives were to determine the contributions of dominant water sources to catchment outflow, to examine seasonal runoff dynamics, and to assess the influence of dry and wet periods on runoff formation.

The findings reveal that peat bogs significantly contribute to rapid runoff during intense rainfall, while groundwater from mineral soils is the dominant source during dry periods. In winter, when snow cover prevails, mineral soils accumulate water that is gradually released during snowmelt, helping to stabilize catchment runoff. In summer, peat bogs contribute to higher runoff variability due to their ability to rapidly convey rainwater through the acrotelm.

Isotopic analysis further indicated that water originating from peat bogs contains a higher proportion of summer precipitation and exhibits increased evaporation signals, as shown by shifts in isotope ratios

with elevation and vegetation cover. In contrast, springs from mineral soils show a more stable isotopic composition, contributing to runoff primarily through deep percolation that recharges soil/bedrock storage in winter and is released during summer months.

This study provides new insights into the hydrological connectivity between peat bogs and adjacent soil units, highlights distinct runoff generation regimes based on soil type and seasonal conditions, and underscores the importance of peat bogs in ensuring stable runoff patterns in mountainous catchments with diverse soil compositions.

1. Introduction

To understand runoff formation in a catchment, it is essential to examine the water regime of local soils. Since landscapes typically contain multiple soil types with varying coverage, each soil unit needs individual evaluation to clearly understand each system's effects on water storage and chemistry (McDonnell et al., 2007; Robinson et al., 2013, or Uhlenbrook et al., 2008). However, this approach is often impractical in real−world applications. Therefore, experimental catchments with relatively homogeneous physical−geographical characteristics are usually selected for hydrological studies, even though complete homogeneity is rarely achievable (Kirchner, 2016).

In the headwaters of the Czech mountains, typical of lower temperate mountain regions, two main soil types dominate: peaty soils (Histosols) and mineral soils (mainly Podzols). The hydrological connectivity of such soil types plays a significant role in water transport to streams (Kleine et al., 2021) due to their distinct hydraulic properties and hydrological behavior (Scherrer & Naef, 2003; Boorman et al., 1995). Besides mineral soils, peaty soils often form parts of mountain catchments, where runoff formation predetermines the water regime in the lower parts of a stream (Tetzlaff et al., 2014; Vlček et al., 2017).

Peatlands form a specific environment that impacts many sites of the catchment or surrounding landscape (Waddington et al., 2015). Peat hydrological processes, such as water storage or runoff formation, can be significantly different from those of other soils in the catchment (Šanda et al., 2014;

Tetzlaff et al., 2014; Vlček et al., 2021). However, these different soil units (or hillslopes) influence each other depending on several factors, such as position in the terrain or bedrock (Langlois et al., 2015; Bourgault et al., 2019).

Peaty soils, such as Histosols, tend to affect runoff by amplifying significant discharge fluctuations, exhibit low baseflow during dry periods, and have sharp peak flows after rainfall (Baird, 1997; Bragg, 2002; Conway & Millar, 1960; Evans et al., 1999; Holden et al., 2001; Holden & Burt, 2003; McDonald, 1973). While this behavior has been well−documented, most studies focus only on peat areas, with limited research comparing the hydrological behavior of peat soils. Histosols typically form in areas where excess water prevents organic matter decomposition. These include valley bottoms, spring areas at hillslopes, or regions with heavy rainfall and slow drainage, which receive water from groundwater, stream water, precipitation, or a mix of these sources (Dick et al., 2018; Hrachowitz et al., 2009; Lessels et al., 2016; Scheliga et al., 2019; Šanda et al., 2014, 2018; Tetzlaff et al., 2007). In some cases, this phenomenon combines with saturated bedrock beneath the soil, impacting vertical water flow, which can also be the case of ombrotrophic peat bogs (Koit et al., 2021). Most of the water sources then mix in the riparian zone, mainly covered by peat, which forms a hydrological unit for water transport and storage (Seibert et al., 2009; Von Freyberg et al., 2014).

Stable isotopes of water (δ^2H, $\delta^{18}O$) represent a widely applied tool for tracing water origin (Dansgaard, 1964), describing the dominant hydrological processes, or estimating water storage within most studied temperate zone catchments (Tetzlaff et al., 2015). This approach has been used in several studies of catchments (Geris et al., 2015, 2017), evapotranspiration (Gibson et al., 2008; Kool et al., 2014; Sprenger et al., 2017a, 2017b, 2018), groundwater recharge or water bodies (Carrer et al., 2016; Isokangas et al., 2017), or travel time (Ala−aho et al., 2017).

In this study, we investigate water flows at two distinct hillslopes formed by contrasting soil types − an ombrotrophic raised peat bog hillslope and a mineral soil hillslope. This unique setup allows for a natural comparison, facilitating a clearer understanding of peat bogs' impact on catchment hydrology.

The main objectives of this study are:

1. To analyze the contributions of primary water sources to catchment outflow.
2. To identify the roles of summer and winter precipitation in hydrological processes.
3. To evaluate differences in runoff formation during wet and dry periods

Understanding how seasonal precipitation interacts with different soil types is critical for predicting runoff patterns, particularly in regions experiencing shifts in climate. Seasonal water residence time plays a key role in shaping these hydrological responses, and studying these dynamics is increasingly important as many areas face changing precipitation regimes and rising air temperatures, which may alter the timing and magnitude of runoff.

2. Study area

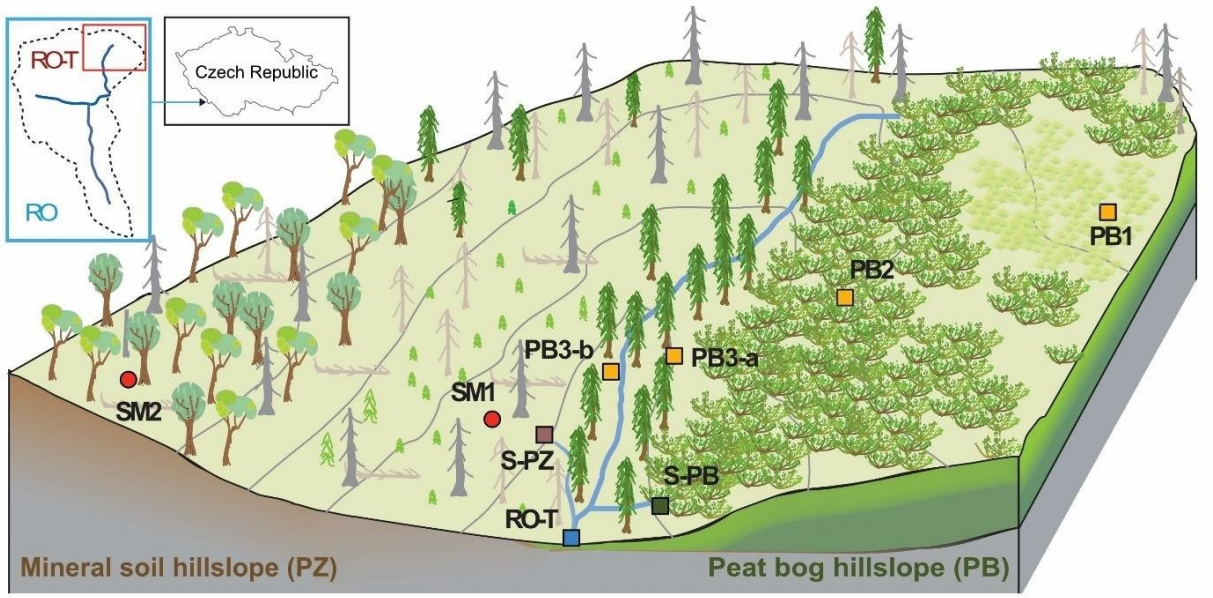

Figure 1. A sketch of the study area at the Rokytka tributary (RO–T) catchment with the individual sampling sources. Soil water in spruce (SM1) and beech stand (SM2); stream water (RO–T); springs at the mineral soil hillslope (S–PZ) and the peat bog (S–PB); groundwater at the peat bog (PB1 – upper part, PB2 – middle part, PB3–a – lower part at the left and PB3−b at the right bank of the stream).

The experimental catchment is located in the upper headwaters of the Vydra River in the central Bohemian Forest, Czech Republic (49.0188039N 13.4162831E; Fig. 1). This region's climate is influenced by both oceanic and continental patterns, resulting in high variability and a relatively even distribution of precipitation, similar to subarctic climates within the Dfc climate zone (Köppen classification) (Tolasz et al., 2007). According to the records from a nearby meteorological station (at a distance of 15 km) at a similar altitude, the annual precipitation averages 1695 mm (1981–2010) (Starostová, 2012), with an average daily temperature of 4.8 °C. The catchment hydrology balance is typically affected by snow cover from December to April (Jeníček et al., 2021).

The Rokytka catchment (RO) spans 3.8 km², with approximately 30 % of its area covered by peat and other hydromorphic soils (Fig. 1; upper left). Within this catchment, a smaller tributary catchment, RO–

T, was selected to study hydrological processes in detail. RO−T covers 0.65 km², with peatlands comprising over 60 % of its area. It is divided into two primary east−west hillslopes, each with unique vegetation and soil characteristics.

The RO–T catchment's soil cover is relatively homogeneous within each hillslope, with distinct soil profiles between the two sides. The mineral soil Podzol hillslope (PZ) predominantly consists of entic Podzol, characterized by a shallow organic top layer (<5 cm) and consistent soil texture down to a depth of 1 meter. Some small sections contain haplic Podzol, which is challenging to differentiate without excavation. No clear boundary was identified between the mineral soil and the underlying bedrock (weathered Gneiss or Granite) using electrical resistivity tomography (ERT) measurements, and no persistent groundwater level was observed up to a depth of 15 m (Vlček et al., 2017; see supplementary Fig. S1).

The eastern pead bog hillslope (PB) is formed by a raised homogenous bog with Histosol as the primary soil type, varying in depth from 0.5 meters at the lower section to approximately 6 meters at the top. This well−developed peat bog significantly influences the hydrology and provides a contrasting soil environment to the PZ hillslope.

The vegetation cover can distinguish both hillslopes of the small RO−T catchment as vegetation relates closely to soils (Fig. 1). The PZ hillslope is covered by beech stands at the upper hillslope zone; "dead" spruce stands (*Picea abies* L., Karst.) with healthy seedlings cover the lower hillslope zone and the addition of fir (*Abies alba* Mill.) and beech (*Fagus sylvatica* L.). Due to the bark beetle calamity outbreak, most spruce stands are deceased. The forest is slowly recovering with new spruce seedlings. The eastern PZ hillslope is created by a well−developed raised ombrogenous peat bog with three vegetation subsections. The upper subsection of the bog is covered mainly by cotton−grass (*Eriophorum L.*) or moss (*Sphagnum L.*) around many small lakes. The middle subsection has the lowest water table fluctuation, and the vegetation cover consists of pine (*Pinus mugo*), blueberry, and moss. The lowest subsection occupies the bottom of the valley and is covered by a waterlogged spruce forest with blueberry and moss.

3. Methods

3.1.1 Automatic measurements

Several sites have hydro−meteorological measurements and water sampling in the studied catchment. Meteorological measurements necessary for this study were composed of air temperature and relative humidity (RV12/RK5, Fiedler Comp., CZE), which were measured directly in the RO catchment. The global radiation (Kipp & Zonen CMP3, NL), precipitation, and wind speed (Fiedler Comp., CZE) data were available from the Modrava meteorological station, located 5.7 km from the catchment divide. All the above parameters were measured at 10−minute intervals from 11/2013 to 10/2020 (Fig. 2). A rainfall gauge was also installed directly in the Rokytka catchment. However, this gauge is not heated during the winter, so it serves only as a control measurement. Winter precipitation from Modrava was also compared with data from a snow pillow installed at the RO, which helped us interpret the contribution of winter precipitation to runoff.

The soil water regime was measured at the PZ hillslope at two sites (upper and lower part) at two depths (20 and 60 cm) by soil tensiometers (T8, UMS Comp, GER). Their position was selected based on previous soil and vegetation cover surveys. At the Peat bog hillslope (PB), five sites for groundwater level measurements and water sampling were selected (see Fig. 1) – upper PB1 in the non−forest vegetation, PB2 in the middle of the PB hillslope, and two in the waterlogged spruce forest (PB3−a, PB3−b). These sites contain groundwater−level automatic probes (TSH22, Hydro Logger H40, Fiedler Comp., CZE) installed to a depth of 70 cm and tubes for groundwater sampling. Stream outflow was calculated from the water level measured at the outlet of the catchment RO−T using a water level probe (TSH22, Hydro Logger H40, Fiedler Comp., CZE).

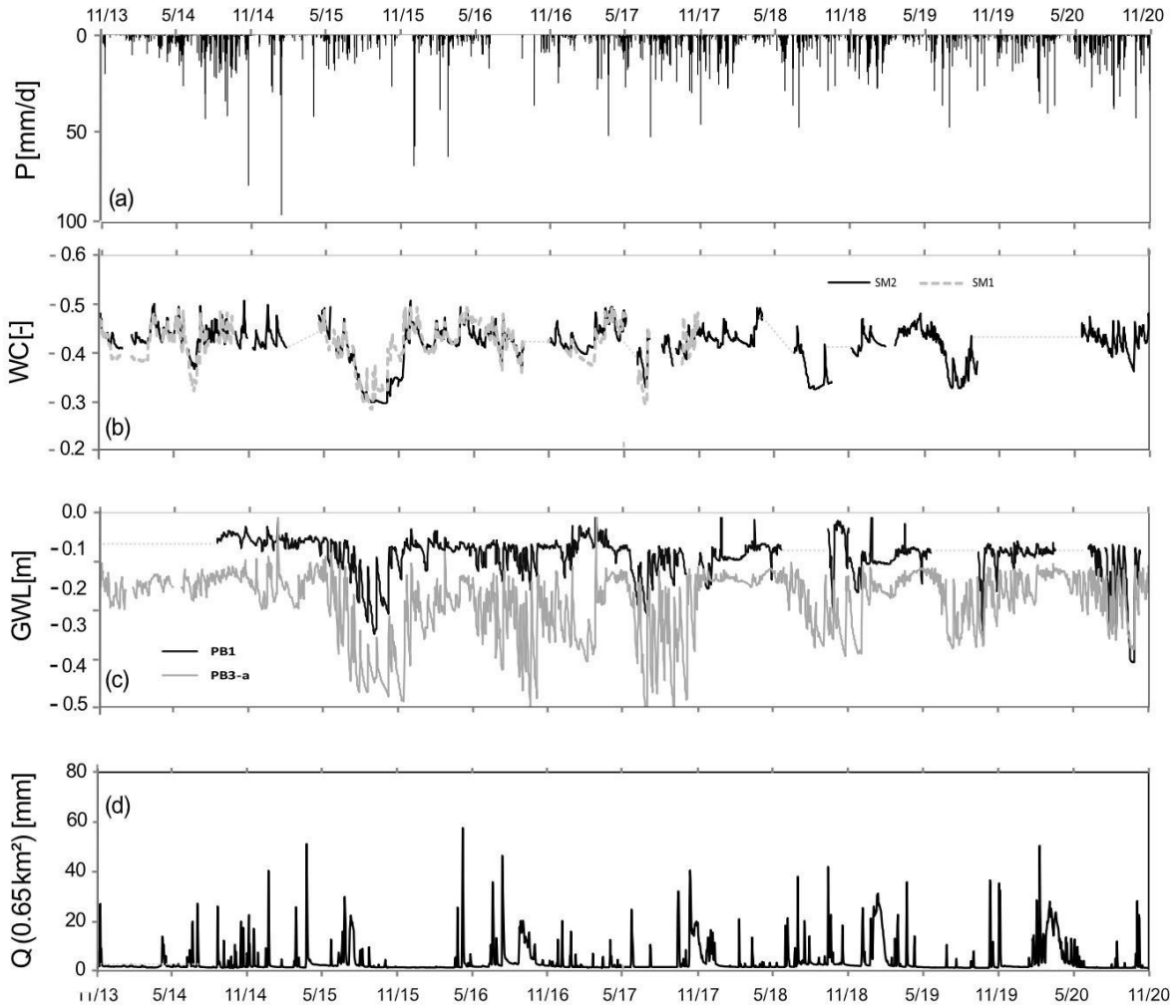

Figure 2. Meteorological and discharge input data from hydrological years 2014–2020 at the Rokytka tributary catchment (RO−T); a) precipitation (P); b) mean soil water content at two locations of the mineral PZ hillslope (SM1, SM2); c) mean groundwater level at peat bog PB hillslope; d) specific discharge at the outflow from the RO−T catchment.

3.2 Water sampling

Sampling campaigns to collect water from various sources, including precipitation, seasonally occurring snow, soil, groundwater, springs, and streams, were conducted once or twice a month during the warm season (May−October) and up to four times during the cold season (November−April). Precipitation was collected using a rain sampler that prevented evaporation (Palmex, HR) at RO–T and

Modrava. Snow water was sampled during campaigns from snow profiles near the soil water source SM1 (Fig. 1).

Soil water at the PZ hillslope was sampled manually by suction cups—1900 Soil Water Samplers (Soil Moisture Equipment Corp.) installed to a depth of 60 cm and set to a suction pressure of −60 kPa. One was installed at a lower−lying spruce stand (SM1), and the other at a higher beech stand (SM2). Drilling deep boreholes to reach groundwater was not possible on this hillslope. However, several tubes were installed at the PB hillslope to allow groundwater sampling (Tab. 1). At PB1 and PB2, sampling tubes were installed at two depths: a) one at 0.5 m (PB1) and 1 m (PB2), a tube perforated along its entire length to get water from Acrotelm (upper part of soil Histosol); b) one at 2 m (PB1−2, PB2−2), a tube perforated at a depth −of 1.5–2 m for water sampling from Catotelm (lower part of soil Histosol). The peat depth at PB1 reaches 5 m, and at PB2, it is approximately 4 m. Sites PB3−a and PB3−b contain only one tube for sampling perforated along its length of ~ 0.8 m (= peat depth at this site).

Only two stable springs were found at the RO−T catchment – one at the mineral soil PZ hillslope (PZ spring), the other at the PB hillslope (PB spring) near a former drainage channel. The water samples were collected, and the water level was measured manually during campaigns at both springs. The stream water at the RO−T outflow was sampled by an automatic sampler (ISCO 6712, Teledyne Isco, Inc., USA) during rainfall events at 1.5−hour intervals and also manually during sampling campaigns.

Well name	Position within the hillslope	Wetland type	Peat depth [m]	Well depth [m]	Well perforation depth [m]	Dominant vegetation
PB1–0.5	upper	peat bog	3.5–4	0.5	0–0.5	cotton grass, moss
PB1–2	upper	peat bog	3.5–4	2	1.5–2	cotton grass, moss
PB2–1	middle	peat bog	3.5–4	1	0–1	pine
PB2–2	middle	peat bog	3.5–4	2	1.5–2	pine
PB3–a	lower	lagg	0.5–1	0.8	0–0.8	spruce
PB3–b	lower	lagg	0.5–1	0.8	0–0.8	spruce

Tab. 1. Description of wells and their surrounding

3.3 Sample analysis and data processing

The stable isotope analyses (δ^2H and $\delta^{18}O$) were performed using a laser spectrometer (Picarro L2140−i, USA) at the Institute of Hydrodynamics, CAS, Prague, CZ. Standard mode (precision of ± 0.03‰ and ± 0.15‰ for δ18O and δ2H, respectively) was used with six injections per sample, with the first three injections discarded. The isotope ratios are reported in per mil (‰) relative to Vienna Standard Mean Ocean Water (VSMOW) (δ^2H or $\delta^{18}O = (R_{sample}/R_{standard}-1) \times 1000‰$, where R_{sample} is the isotope ratio of the sample and $R_{standard}$ is the known reference value (i.e., VSMOW) (Craig, 1961). Together with this, deuterium excess (d−excess) was calculated to understand the climate pattern in the rainwater and its possible influence on sampled sources within the catchment (Pfahl and Sodemann, 2014).

Furthermore, the line−condition excess (lc−excess; Landwehr and Coplen, 2006) was calculated (Eq. 1) to identify the evaporation effect at chosen sampling sites.

$$lc - excess = \delta^2H - a \cdot \delta^{18}O - b \quad (1)$$

Where a and b are the coefficients of the local meteoric water line (LMWL) from individual experimental plots.

To characterize whether the extracted soil water originated from winter or summer precipitation, we calculated the seasonal origin index (SOI; Eq. 2; Allen et al., 2019) for individual seasons to provide a more detailed representation of gradual changes in water origin resulting from mixing with newly infiltrating water.

$$SOI = \begin{cases} \dfrac{\delta_x - \delta_{annP}}{\delta_{summerP} - \delta_{annP}}, if\ \delta_x > \delta_{annP} \\ \dfrac{\delta_x - \delta_{annP}}{\delta_{annP} - \delta_{winterP}}, if\ \delta_x < \delta_{annP} \end{cases} \quad (2)$$

Where δ_x are the $\delta^{18}O$ isotopic values of soil water, and $\delta_{winterP}$, $\delta_{summerP}$, and δ_{annP} are the $\delta^{18}O$ isotopic values of typical winter, typical summer, and volume−weighted annual precipitation. The SOI

ranges from −1 to 1, where values close to −1 represent water predominantly derived from winter precipitation, and values approaching 1 reflect a dominant contribution from summer precipitation.

Seasonal trends in δ^2H values in precipitation and other water sources were modeled using an iteratively reweighted least squares (IRLS) regression method with moving time windows to determine the amplitude and phase of individual isotopic signals. Before sine−wave fitting, a detrending correction was applied following Xia et al. (2024) to account for linear trends in isotopic composition potentially induced by climate change. This step was necessary to prevent biased estimates of the seasonal amplitudes, especially given the seven−year duration of the dataset, during which such trends may become evident. The isotopic increase at each sampling date was calculated using the following equation:

(3)

$$\Delta\delta^2H = \Delta T \times Sen's\ slope$$
$$\delta^2H_c = \delta^2H - \Delta\delta^2H$$

where December 31, 2013, was set as the initial time (T_o), and ΔT represents the time elapsed since T_o. The resulting $\Delta\delta^2H$ values were then adjusted by subtracting the observed δ^2H values, yielding the corrected δ^2H_c (Eq. 3). A sinusoidal function was subsequently fitted to the full time series of δ^2H_c using the IRLS method with a moving time window (1−year time windows with ~ 4−week timespets), providing corrected seasonal amplitudes for precipitation and other water sources (Eq. 4).

$$\delta^2H = mean(\delta^2H_c) + A * sin\left[\left(\frac{2\pi t}{b}\right) + c\right] \quad (4)$$

where mean(δ^2H_c) (‰ V−SMOW) represents the average δ^2H_c value, A is the seasonal amplitude, b is the period of the seasonal cycle (with a 1−year period equivalent to 2π), t (in months) denotes time, and c (in radians) indicates the phase shift.

The obtained amplitudes were then used to estimate the mean residence times (MRT) of individual

water sources, following the approach of Soulsby et al. (2000) (Eq. 5).

$$T = \omega^{-1}\left[\left(\frac{A2}{A1}\right)^{-2} - 1\right]^{0.5} \quad (5)$$

where *A1* is the amplitude of the initial water (precipitation), *A2* is the amplitude of the resulting water (streamflow, groundwater, etc.), and ω is the radial frequency of annual fluctuations (2π).

To find out how the proportion of rain versus snow changed at selected sampled sites over months or years, first, the isotope means and standard deviations for both sources (rain and snow) were computed. After investigating isospace plots, we proceeded with building stable isotope mixing models (Parnell et al., 2010, 2013) that included covariates using the R package 'cosimmr' (Gowan and Parnell, 2024), employing the fixed−form variational Bayes function to fit the model. The covariates of interest were months (seasonality) and years. Both covariates were converted to factor (categorical) variables. To obtain information about all the levels of factor variables, models without the intercept parameter were specifically constructed.

In terms of a comparison between warm and cold seasons, the data set is affected by an uneven distribution of sampling campaigns (Supplementary Fig. S2). Where data from growing seasons prevail. For detailed analysis, each year was divided into two seasons. The first season (January−June) is more affected by winter precipitation, especially when the snowpack continuously lasts from December to April, and snowmelt, with annual high outflows at the end of April or the beginning of May. The second season (July−December) is more affected by summer precipitation, or rather summer droughts, which often continue into autumn.

4. Results

4.1 Variability of δ^2H and $\delta^{18}O$ ratios within sampled sources

The δ^2H precipitation values vary the most across all sampling sites (Fig. 3, upper left). Modrava village lies at a slightly lower altitude than the studied catchment (920 m a.s.l. vs. 1100 m a.s.l.), so the precipitation values show slight continental patterns. The local meteoric water line (LMWL; see Fig. 3, upper right) is defined as $\delta^2H = 7.35 \times \delta^{18}O + 3.75$.

The isotopic composition of groundwater sampled at a PB hillslope varied according to the position of a borehole and its depth. The lower its position on the slope, the closer the annual mean δ^2H to that of precipitation. The visible increase in the heavier isotope ratio up the slope indicates a possible evaporation influence at sites less covered by vegetation. The δ^2H $\delta^{18}O$ dual plot (Fig. 3 – upper right) supports this as the samples from the upper peat bog (PB1) are positioned at the local evaporation line (LEL; $\delta^2H = 6.9 \times \delta^{18}O - 1.51$), thus shifting from the LMWL. The δ^2H ratios at all shallow groundwater wells fluctuate more than at deeper wells (PB1–2 and PB2–2). The latter are probably less affected by climate conditions. On the other hand, groundwater samples in the lagg covered by spruce stands (concave part of the valley; PB3−a,b) were affected by the position of shallow tubes perforated within the whole depth, visible in relatively high δ^2H variability. Therefore, PB3 contains three sources of water: rain, water from the upper part of the bog, and groundwater from the underlying sediment (ca 0.8−1.2 m below the surface).

The soil water δ^2H ratio correlates with annual precipitation variation (Figure 3, upper left), as the suction lysimeters were used preferentially during periods of high soil saturation, often following rainfall events. The two springs at opposing hillslopes show differences in isotopic patterns (Fig. 3, upper left). The one located at the PZ hillslope, PZ spring, is stable in terms of discharge and isotopic composition. The annual isotopic mean δ^2H ranged between −69.4 and −73.8‰. Such a narrow range suggests a very good mixing of percolated water from summer and winter precipitation. The mean δ^2H value (−71.1‰), however, is slightly higher compared to the mean estimated from the sine curve fitting (−69.5‰), as shown in chapter 4.3.

In contrast, the PB spring (PB hillslope) δ^2H ratio varies according to weather conditions and peat bog saturation. However, it contains less water from the upper surface part of the peat bog (PB1−0.5). In Figure 3 (lower left), the Deuterium excess (d−excess) indicates that the spring at the PB hillslope contains more summer precipitation than the PZ spring.

The stream isotopic ratio varies according to the discharge. Stream RO–T is supplied during baseflow mainly by water with an isotopic ratio similar to that of the PZ spring, indicating that it is older water from the subsoil (Fig. 3; upper left). During rainfall, the stream contains more water from the peat bog or precipitation.

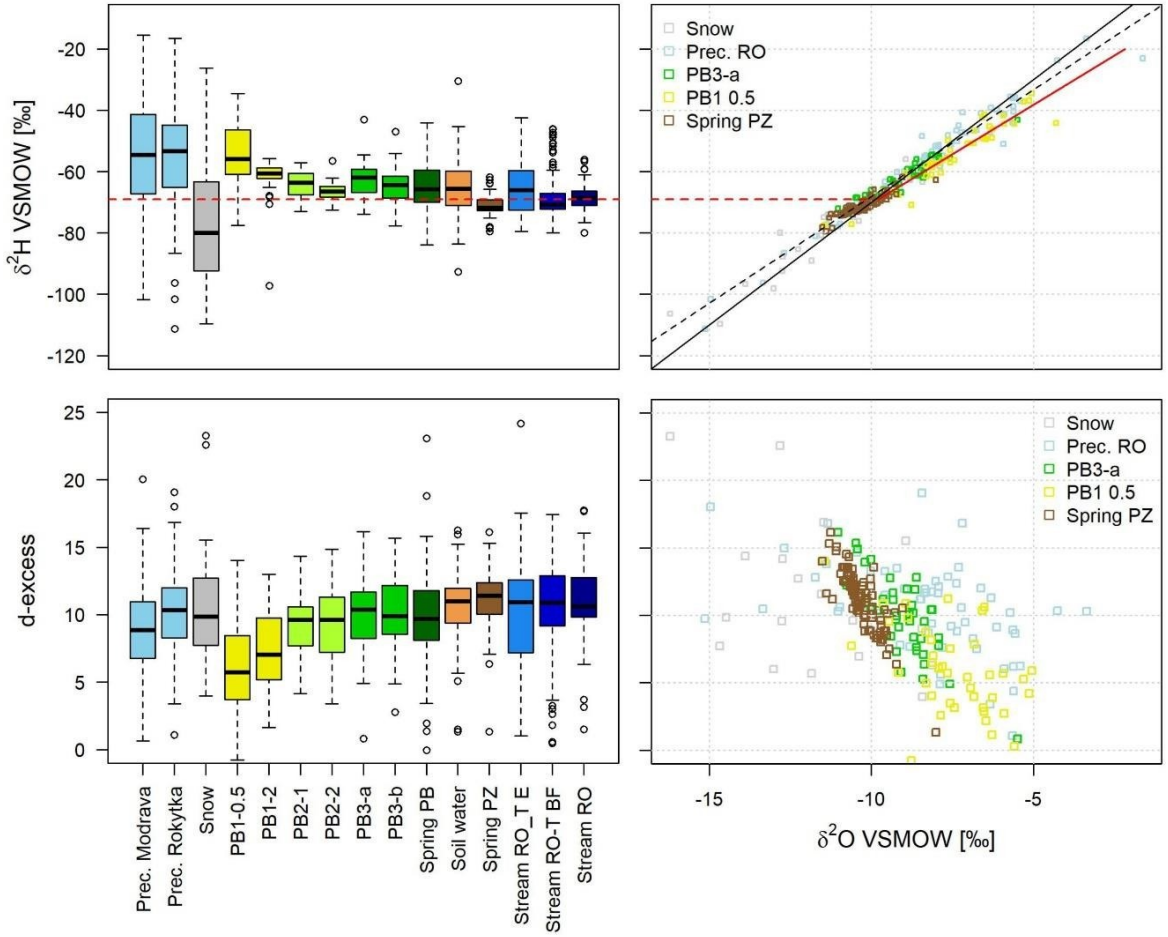

Figure 3. Distribution of δ^2H and $\delta^{18}O$ from all sampling sources. Upper left: δ^2H distribution; Upper right: δ^2H $\delta^{18}O$ dual plot with LMWL (local meteoric water line; dashed black), GMWL (global meteoric water line, solid black), LEL for PB1–0.5 (local evaporation line; solid red) and mean δ^2H precipitation Rokytka from TTD (dotted red line; δ^2H= −72.02); Lower left: Deuterium excess (d−excess) distribution;

Lower right: d−excess and $\delta^{18}O$ plot; Prec. – precipitation; well names: PB1–0.5 = PB1 – position at the peat bog (Fig. 1), 0.5 – well depth [m]; Stream water E – event, BF – baseflow.

4.2 Seasonal pattern in the precipitation in the observed sources

Figure 3 indicates that baseflow samples from the stream and PZ spring contain higher d−excess values, which indicates a higher proportion of winter precipitation. On the other hand, the δ^2H values of summer precipitation increase with upslope at the PB hillslope, with the maximum at the upper open part of PB1. As you go down the slope, the wells contain more water from winter precipitation.

On the other hand, there is no visible difference between the first and second halves of a year (Supplementary Fig. S3). Additionally, SOI does not indicate any significant effect of seasonality (Supplementary Fig. S4). A slight difference is visible in comparison between the first and the second halves of the year (Fig. 4). Throughout the year, PZ spring contains more cold−season precipitation compared to spring PB. Even though all peat bog sampled sites show significant supply from warm−season precipitation, there is no clear decrease from the top of the bog (PB1) towards lower sites (PB3) as visible in Fig. 3. Especially PB2−1 in the period July−December, the SOI is near zero, meaning seasonal contribution while surrounding sits (PB1–0.5, PB1–2 or PB2–2) according to the assumption, they contain more warm−season precipitation.

PB3 wells (a and b), which lie in the lagg, contain more warm−season precipitation during the second half of the year than the upper well PB2, probably caused by mixing of water from two different hillslopes. Spring PB lies more above the lagg, therefore fed by water from the surroundings of PB1 and PB2.

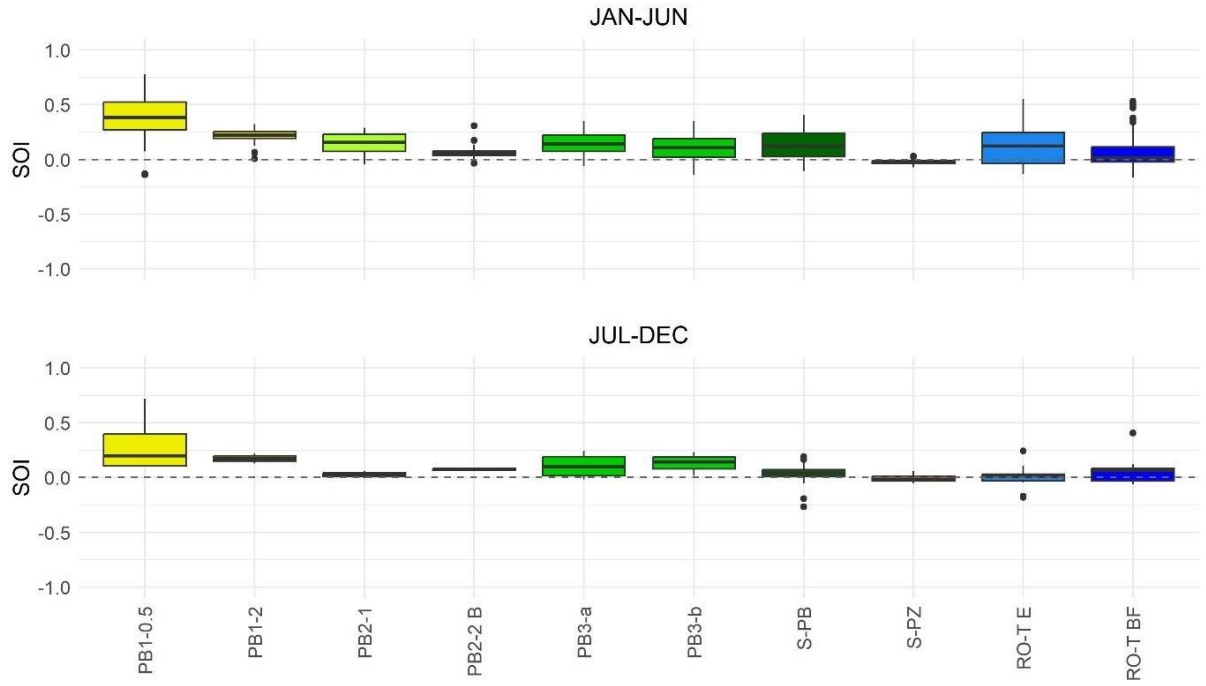

Figure 4. Seasonal origin index (SOI). All sampling sources were divided into two charts according to the first (upper chart) and the second half (lower chart) of a year from the period 2014–2020.

SOI also indicates differences between shallow(0.5/1m) and deep (2m) wells at PB1 and PB2 (Fig. 4). As the near surface water fractionates by evaporation (Fig. 1), its isotopical footprint is visible in lc–excess (Fig. 5). Evaporation effect on peat water in the first half of the year decrease according to density of vegetation and to position on the PB hillslope.

In the second half of the year, fractionated water from PB1–0.5 percolated deeper, while water from the shallow well was replenished with new rainwater. This pattern is more pronounced at well PB2, where well PB2–1 is likely to be more supplied by rainwater in autumn. Surprisingly, RO–T BF samples during the second half of the year contained more fractionated water compared to RO–T E, likely due to flow delay caused by percolation.

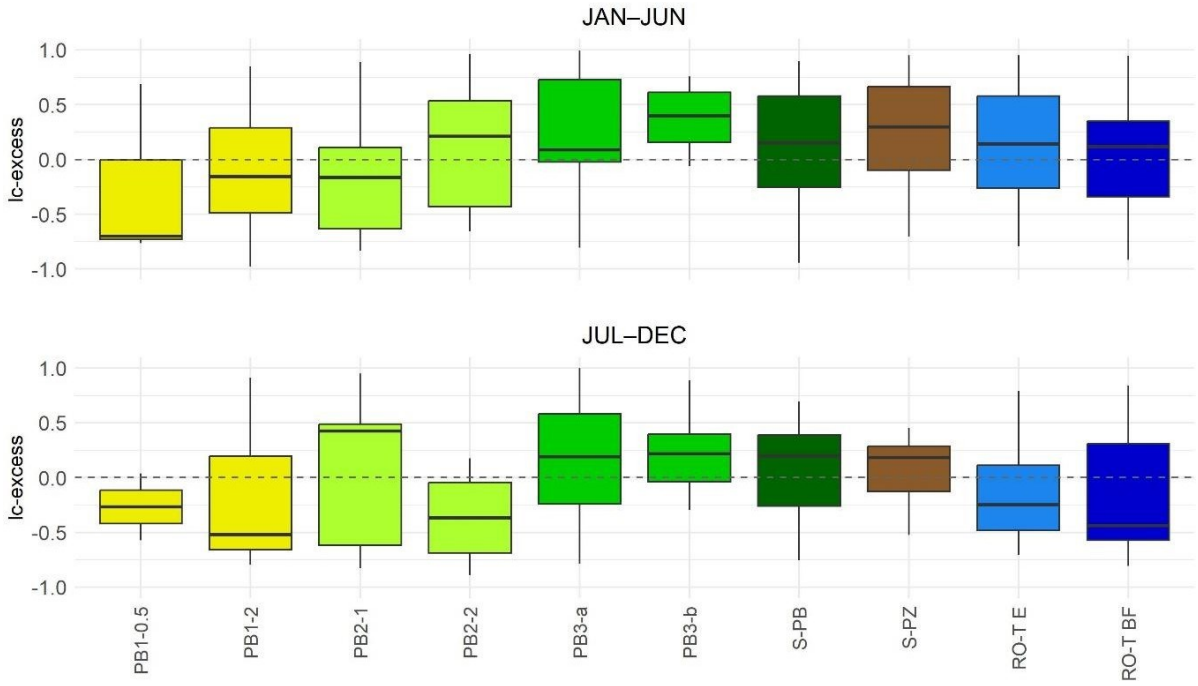

Figure 5. Line−condition excess (lc−excess) for all sampling sources divided into two charts according to the first (upper chart) and second (lower chart) half of a year from the period 2014–2020.

PB and PZ springs contribute to runoff formation according to catchment saturation (Fig. 3). The contribution of rainwater depends on its proportion in spring water (Fig. 6). The rain proportion in PB spring dominates during the warm part of the year (May−October), with its maximum in June/July (~ 80 %), which are usually rain−rich months. During the cold part of the year, especially from February to April, the proportion of rainwater drops to a minimum in March (approximately 30%) as water from solid precipitation becomes more dominant.

PZ spring water analysis reveals a different pattern of rainwater proportion throughout the year. Contrary to the PB spring, it contains the highest snow−water proportion during the late period of the warm season (August/September). Overall, the ratio of rainwater in the PZ spring is relatively stable, with monthly averages ranging from 27% in August to 48% in December. The rain contribution to the PZ spring, therefore, seems delayed.

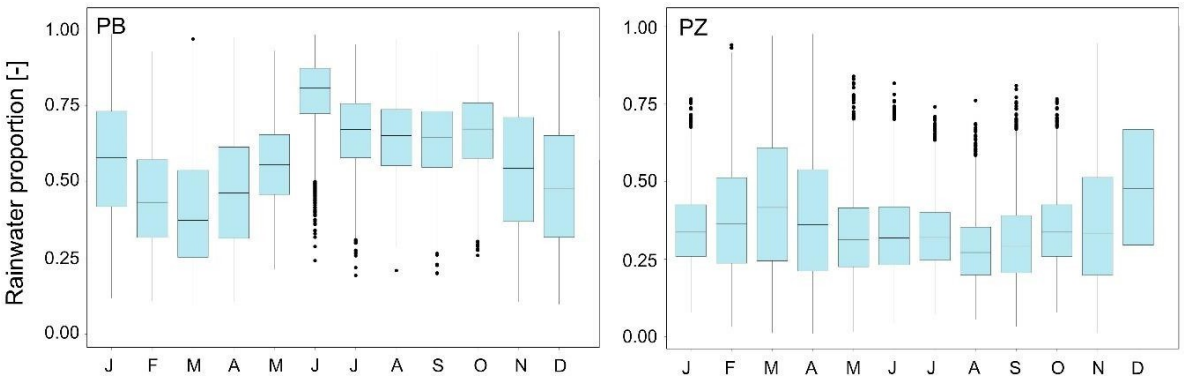

Figure 6. Mean rainwater (liquid water) proportion in peat bog (PB) and mineral hillslope (PZ) springs in individual months.

4.3 Mean residence times estimates

Travel times reflect different hillslope properties (mainly soil). While water from the PB hillslope more closely matches the isotopic pattern of precipitation, which means that summer precipitation affects the general water balance in a similar period. On the other hand, the summer precipitation pattern occurs in PZ spring during winter (Fig. 7); for example, low summer precipitation may decrease mineral soil spring outflows during winter. These types of springs also contribute to the outflow according to weather conditions and catchment saturation. During a rainfall event, more water comes from the PB hillslope, while the PZ hillslope dominates during base flow. The MRT of water in the PZ spring, which has been identified as the oldest source, was calculated to be approximately 3.6 years. This suggests that infiltrated water percolates through the soil and bedrock.

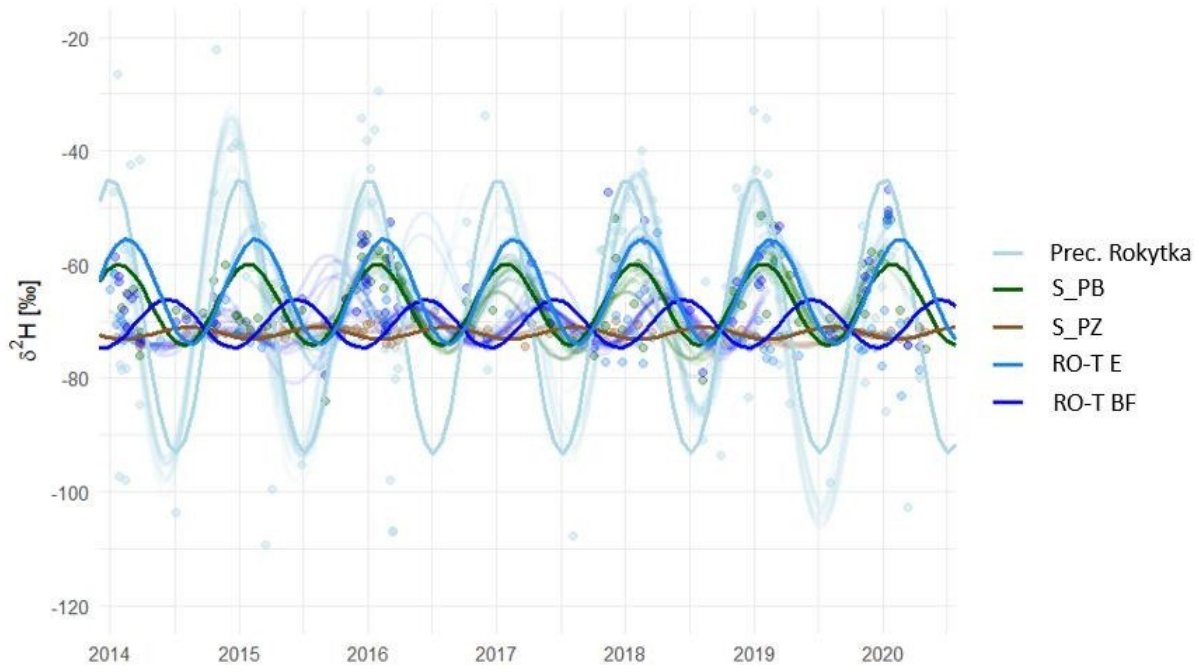

Figure 7. Fitted sine curves of δ^2H time series in measured precipitation and selected surface water sampling sites from 2014 to 2020. All sinusoids derived using a moving time window are shown in light colors; their average is displayed in dark colors. Individual measurements are represented by dots matching the color of their corresponding fitted curve.

All water wells at the peat bog (PB) reflect a sine−wave precipitation pattern (Fig. 8). Shallow water wells are more under the influence of climate (rain, evaporation) than deep wells, and together with the similar soil type, the same dominant flow was expected. However, wells contain water with different water ages (Table 1). While the MRT of shallow well PB1−0.5 was estimated to be 0.2 years, and shallow PB2−1 was 0.78 years, in upper deep well PB1−2, the water was more than one year younger than in the deep well PB2–2 (Tab. 2). This probably indicates a difference in lateral flow velocities between acrotelm and catotalm on the way down the slope from PB1 through PB2 into the stream.

Well installed in lagg (PB3–a,b) contains water with a similar age (0.4−0.5 years), thus younger than most sampling sites within the catchment. Also, contrary to expectations, the PB3–b is not affected by the PZ hillslope.

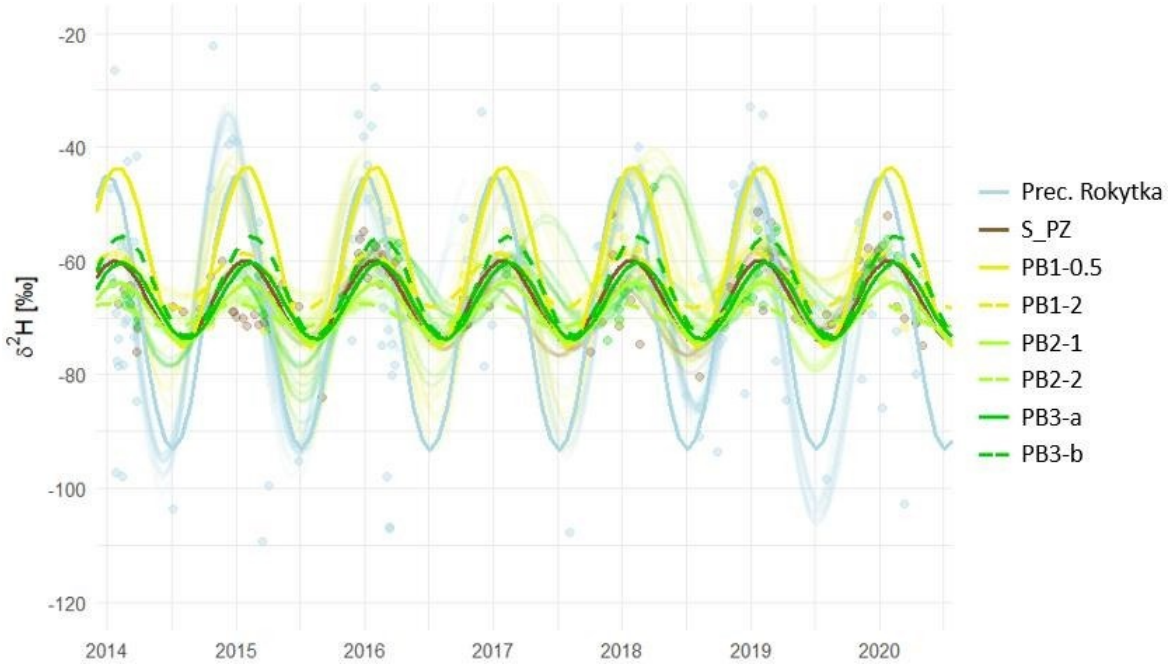

Figure 8. Fitted sine curves of δ^2H time series in measured precipitation and selected groundwater sampling sites from 2014 to 2020. All sin curves derived using a moving time window are shown in light colors; their average is displayed in dark colors. Individual measurements are represented by dots matching the color of their corresponding fitted curve.

	Prec. RO	PB1-0.5	PB1-2	PB2-1	PB2_2	PB3-a	PB3-b	S_PB	S_PZ	RP_E	RP_B
Amplitude	24.2	15.19	4.84	5.24	2.09	6.69	8.8	7.19	1.06	9.23	4.26
Phase	1.5	1.04	1.24	0.95	1.54	0.81	0.8	1.11	2.23	0.74	1.27
Mean δ^2H	−69.05	−59.27	−63.44	−69.02	−69.64	−67.02	−64.4	−67.07	−72.02	−64.73	−70,37
MRT (year)		0.2	0.78	0.72	1.84	0.55	0.41	0.51	3.63	0.39	0,89

Table 2. Estimated mean residence times (MRT) and parameters of fitted sine curves for individual sampling sources; Prec. RO – precipitation.

4.4 Wet and dry year comparison

The data was selected from the dry year 2015 (349 mm y^{-1}) and the wet year 2020 (1331 mm y^{-1}). SOI analysis did not identify any significant differences, except for a wide range of values in PB1–0.5 (Supplementary Fig. S5). This well sometimes dries up during drought; hence, the sampled mobile water from the well reflects the precipitation isotopic composition. The wet season, as expected, contains more summer water from precipitation.

More interesting results are visible in Figure 9 using lc−excess. During a dry year, the upper peat bog shallow well (PB1–0.5) contains less fractionated water than deep PB1−2. The shallow well usually dries during summer, hence the samples are represented rather by fresh rainwater. This water mix appears in the wells down the slope where the evaporation effect is relatively small, even at sites with young water (PB3). Water in the upper deep well PB1−2 is affected by evaporation, which indicates percolation from the soil subsurface. This fractionated water also appears in the stream during rainfall events (RO–T E), but with no significant impact on water in wells PB2 and PB3.

In a wet year, the sequence of evaporation effect decreases down the PB hillslope is visible. Water from shallow PB1–0.5 is fractionated more during the wet than during the dry season. The mobile groundwater is probably closer to the evaporation front near the surface. Then, PB2–1 contains less fractionated water during the wet year than PB2–2. This might be due to lateral flow (or pipe flow) from the upper part of the peat bog. PB2–1 may be unaffected by this flow or more likely washed out from the old, partly evaporated water.

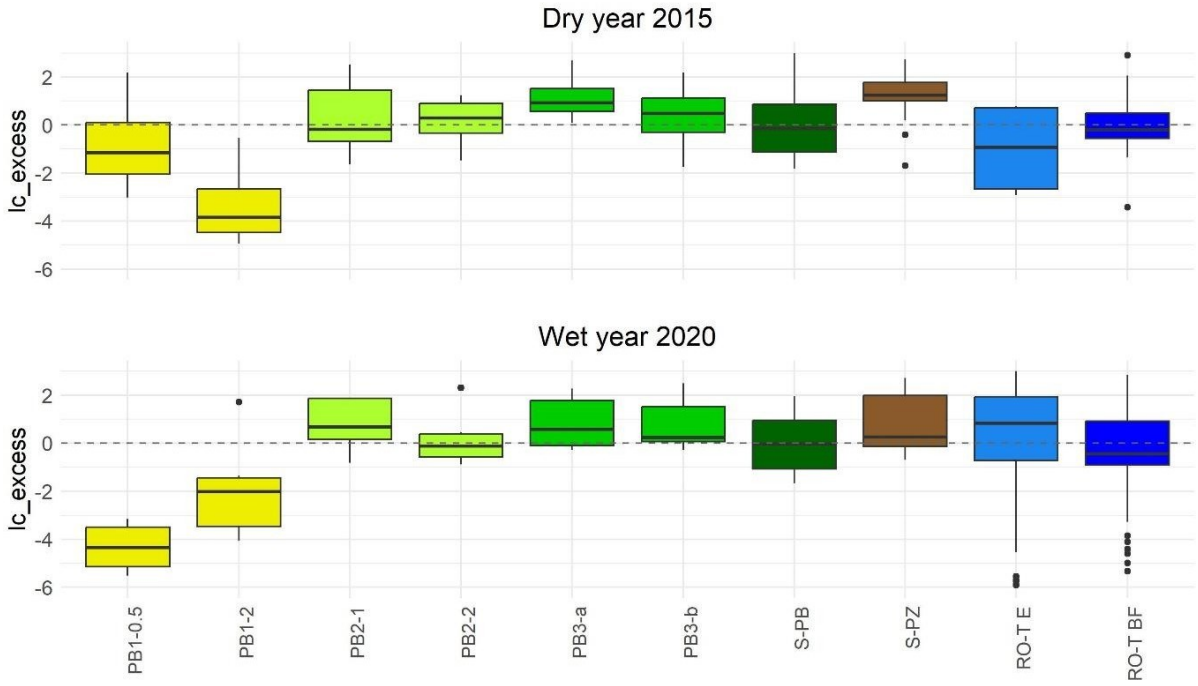

Figure 9. Lc−excess from all sampling sources during the growing season from the dry year 2015 (349 mm y^{-1}; upper Fig.) and a wet year (> 814 mm y^{-1}; lower Fig.).

5. Discussion

5.1 Water mixing process and seasonal pattern in water sources

The evaluation of water mixing from multiple sub−catchments commonly relies on the assumption of homogeneity among contributing water sources, which might be biased (Kirchner, 2016). Even so, we assume that the studied hillslopes' different soil hydrological properties allow us to consider two soil units in water mixing during runoff formation from the catchment. All water samples analyzed in this study are classified as mobile water sensu McDonnell (2014), as the transition between mobile and immobile water is documented mainly by soil suction in the pF curve (Sprenger et al., 2018), and we sampled freely flowing water. The hydrological behavior of the PZ hillslope is reflected in the PZ spring, which exhibits a stable outflow, thus mobile water contributions. On the PB hillslope, within the permanently saturated zone with low saturated hydraulic conductivity, we assume that water belongs predominantly to the mobile fraction. Due to this reduced permeability and extended residence times, any immobile water present is expected to have a similar isotopic composition to the mobile fraction, besides spaces for preferential flows active during rain events. In the upper peat layers with periodic drying (mainly acrotelm), on the contrary, the interaction between mobile and immobile water appears to be limited due to the high permeability. In this near−surface zone, the isotopic composition of mobile water is rather influenced by recent precipitation inputs and evaporative processes.

Peaty soils increase runoff fluctuation due to the low permeability of the Catotelm (Evans et al., 1999; Holden & Burt, 2003). Therefore, travel times during rainfall events are relatively short (minutes to hours), and most event water flows directly to the stream through the Acrotelm. In contrast, during droughts, water percolates through the peat profile for several days or more (Vlček et al., 2021). In this study, the MRT at most wells was estimated to be several months. From this result, winter precipitation prevails during the growing season; however, the SOI, statistical analysis of rainwater contribution, or d−excess instead indicate that summer rainwater is the dominant source in wells. We can therefore assume a minimal water mixing process within the peat bog, which is also supported by young water

in the upper shallow well PB1–0.5, almost 2 years MRT in PB2–2, and significant isotopical variability in PB spring.

The peat bog is wholly saturated with water during winter when snowpack occurs. Snow melts continuously and flows directly into the stream, except for a small amount that can percolate to the Catotelm (approximately 1 cm per day). The same infiltrating process occurs during periods of high groundwater levels and prolonged rainfalls in the summer.

During drought, the deep wells contain seasonally mixed water. In contrast, shallow wells affected by Acrotelm are more prone to water depletion and replenishment of older water with younger water due to a fast biomat flow. Most of the sampling sites do not vary in terms of the SOI or the isotopic ratio δ^2H; thus, the isotopic signal can be attenuated (Muhic et al., 2022). However, a significant pattern is observed in the lc−excess within the peat bog wells. More water affected by evaporation occurs in the deep wells. This is probably because of several reasons: 1) pre−event water from the more porous Acrotelm is washed out with every rainfall event; 2) it is assumed that the evaporation front occurs in the catotelm during droughts; hence, more fractionated water arises in deeper soil; 3) low soil water mixing between mobile and immobile water. The flushing effect is amplified at the middle part of the peat bog (PB2−1), where a shallow well is affected by the biomat flow (Sidle et al., 2007).

Lagg can be influenced by water from mineral soils above, stream water, or groundwater (Seibert et al., 2009; Von Freyberg et al., 2014). PB3 wells situated in the lagg contain, against expectation, less water from the mineral PZ hillslope. Both groundwater wells (PB3−a,b) have similar stable isotopic composition and significantly differ from the water from the PZ spring. It appears that the gravel beneath the approximately 1 m deep peat drains all groundwater from the mineral PZ hillslope directly to the stream. Moreover, rainwater has a more pronounced effect than water flowing from another upper part of the peat bog. Therefore, this peaty area in a narrow lagg forms an independent unit rather than a space for water mixing.

In the PZ hillslope, winter precipitation percolates deeply, while warm−season precipitation is stored in shallow layers and used by shallow−rooting plants (Allen et al., 2019). Our analysis indicates that the

spring PZ is supplied mainly by water from the cold part of the year, when snowpack occurs, and confirms other results (Vlček et al., 2017) that slow infiltration and percolation are dominant PZ hillslope hydrological processes. This also explains why snow cover or winter precipitation, in general, affects spring (Lamacova et al., 2024) or summer low flows (Jeníček et al., 2021; Šípek et al., 2021).

The MRT of the PZ spring was estimated to be 3.6 years, which appears to be a significant delay compared to the relatively short length of the PZ hillslope (~0.6 km). However, the weathered bedrock provides a sufficient volume for water storage. The MRT of spring PB is noticeably short (several days/months) depending on antecedent wetness (van Meerveld et al., 2019).

5.2 The dominant water flow in the catchment - shrnutí

In general, the most important factor of hillslope runoff formation is catchment saturation (mainly groundwater level in hydromorphic soils) in terms of connectivity (van Meerveld et al., 2019) or preferential flows through the soil systems – mineral soil and peat (Šanda et al., 2014; Tetzlaff et al., 2014). The analyzed runoff process at the PZ hillslope in the Rokytka catchment is identical to that in the abovementioned studies – the dominant matrix flow or deep percolation (Fig. 10). During heavy rainfall, the biomat flow or near−subsurface flow is recognizable.

When the groundwater level is near the surface, most water from precipitation or snowmelt flows through Acrotelm as a biomat flow, surface flow, or pipe flow (Vlček et al., 2017). These rapid flows are also active mainly during stormflow (Sprenger et al., 2016). From this study, the main water flux during dry summer is lateral deep subsurface flow in the catotelm supported by hydrological estimation (Vlček et al., 2021), where deep percolation is more prominent at the PZ hillslope. However, Falátková et al. (2024) pointed out from the analysis of water temperature that there is non−negligible deep percolated water at the PB hillslope that supplies local streams during dry periods. This water can percolate through the whole peat bog into the sediments below, revealed by geophysical investigation (ERT). Such a several−meter−deep aquifer in the concave part of a valley can influence the above−developed peatland hydrologically (Klove et al., 2011; Šanda et al., 2014; Koit et al., 2021).

Therefore, we also assume a stable flow from this aquifer (supplied from both hillslopes) to the stream (Fig. 11; dashed arrows). The measurements at our site also indicate an impact of the aquifer on groundwater level in the wells at depths of 0.5 m and 2 m by mitigating the groundwater dropping due to drying. Such a peat−aquifer interaction was also described in other studies (Goodbrand et al., 2019; Levy et al., 2014; Blumstock et al., 2015; Isokangas et al., 2017).

5.3 Sampling interval

The time step of sampling affects the final results of tracer analysis. It is recommended to sample in shorter intervals than two weeks (Stockinger et al., 2016). It was impossible to manage such a sampling period in this locality. In particular, winter conditions limited accessibility, resulting in sparse data coverage during this period. The stable spring PZ is assumed to reflect the mean annual isotopic signal of precipitation δ^2H = −71.7 ± 2.5‰. However, we are aware that this spring is affected by the seasonality of our sampling. Thus, we estimated the mean annual isotopic ratio from the fitted sine wave of the PZ spring (δ^2H = −69.5‰). Therefore, sampled water from the PZ spring contains more winter precipitation. Most of the samples were taken during the warm season because this area is unavailable during winter. However, the local peat bogs are frozen during winter, and the groundwater level is stable until spring, when all the snow melts (Vlček et al., 2021). The sparse sampling interval in winter influenced mainly the snow data. The snow was sampled from the snowpack, sometimes several days after the precipitation event. Thus, the snowpack was slightly enriched by heavy isotopes due to fractionation.

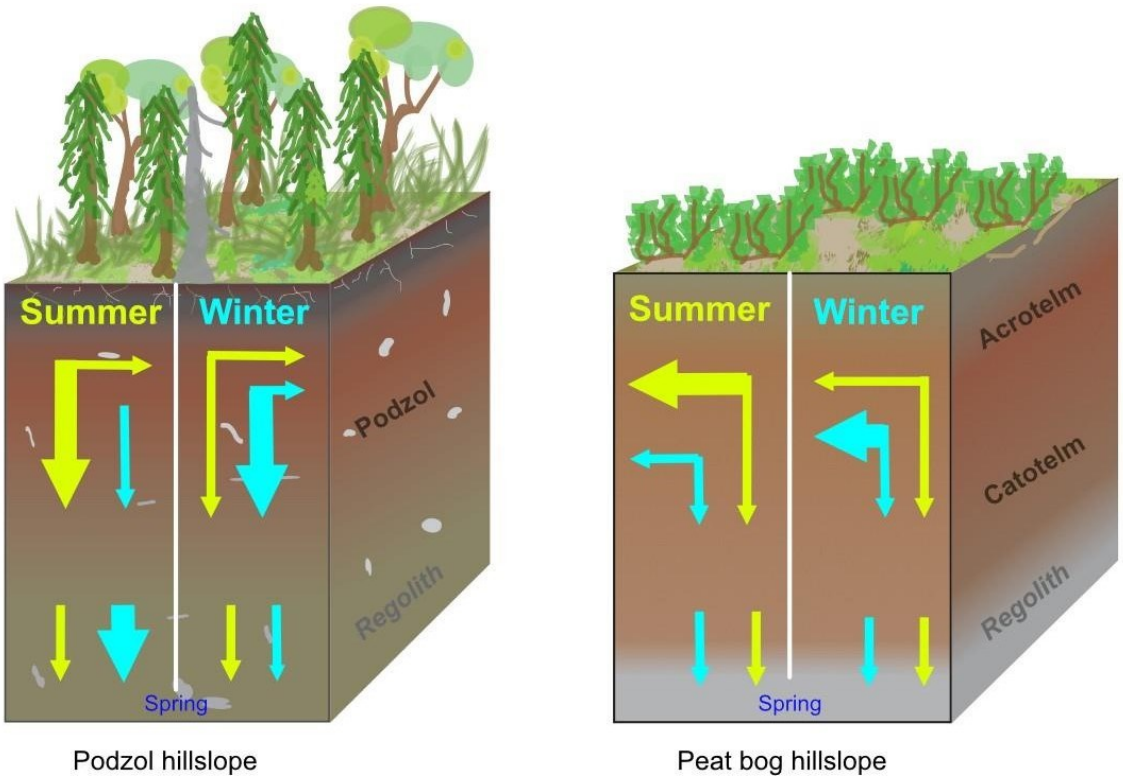

Figure 10. The scheme of estimated dominant water flows during summer and winter, containing summer (green) or winter precipitation (blue arrows) during summer or winter; the arrow thickness represents the estimation of importance in the runoff formation (low/high).

6. Conclusion

This study highlights the role of mountain peat bogs in catchment hydrology by analyzing the stable isotope composition of water sources within a peaty catchment. Our results from the Rokytka catchment reveal that peat bogs have distinct hydrological impacts compared to mineral soils, such as Podzols. The results show that peat bogs and mineral soils play different roles in seasonal hydrological dynamics. Due to their near−surface water flow paths, peat bogs respond rapidly to rainfall, significantly shortening residence times. This quick transmission of rainwater through surface and near−surface flows is particularly evident in high groundwater levels. Conversely, mineral soils exhibit higher mobile water storage, allowing for deeper percolation and slower integration into baseflow.

Peatbogs are dependent on summer rainfalls to mitigate the impact of droughts. Therefore, the amount of snow and the duration of snow cover have only a minor effect on water balance. Much more important is the frequency of summer precipitation, which prevents the groundwater level from dropping and peat drying. Mineral soils, on the other hand, tend to slowly infiltrate water from melted snow, which then supplies deep aquifers and local springs. Summer precipitation, however, increases the discharge fluctuation of the stream, which is more noticeable in peat than in podzol. Therefore, climate change affects both soil systems – mineral soil hillslopes dry more due to the loss of snow cover, and peat bogs due to more frequent and more prolonged summer droughts.

These findings highlight the contribution of seasonal precipitation across dominant soil types, underscoring the importance of water residence time in predicting seasonal runoff patterns. Understanding these dynamics in peat and mineral soil catchments is essential for regions facing changing precipitation or air temperature patterns.

Acknowledgments

We thank Julius Česák for technical support with the installation of measuring devices and NP Šumava for a permit to conduct the research on its land. This work was supported by the Czech Grant Agency (GA22–12837S), Premium Academiae of the Czech Academy of Sciences, and the institutional support of the Czech Academy of Sciences (RVO: 67985874).

References

Ala−aho P, Tetzlaff D, McNamara JP, Laudon H, Soulsby C. 2017. Using isotopes to constrain water flux and age estimates in snow−influenced catchments using the STARR (Spatially distributed Tracer−Aided Rainfall−Runoff) model. Hydrology and Earth System Sciences 21: 5089–5110. https://doi.org/10.5194/hess−21−5089−2017

Allen ST, Kirchner JW, Braun S, Siegwolf RTW, Goldsmith GR. 2019. Seasonal origins of soil water used by trees. Hydrology and Earth System Sciences 23: 1199–1210. https://doi.org/10.5194/hess−23−1199−2019

Baird AJ. 1997. Field estimation of macropore functioning and surface hydraulic conductivity in a fen peat. Hydrological Processes 11: 287–295. https://doi.org/10.1002/(SICI) 1099−1085(19970315)11:3<287::AID−HYP443>3.0.CO;2−L

Blumstock M, Tetzlaff D, Malcolm IA, Nuetzmann G, Soulsby C. 2015. Baseflow dynamics: Multi−tracer surveys to assess variable groundwater contributions to montane streams under low flows. Journal of Hydrology 527: 1021−1033. https://doi.org/10.1016/j.jhydrol.2015.05.019

Bourgault M, Larocque M, Garneau M. 2019. How do hydrogeological setting and meteorological conditions influence water table depth and fluctuations in ombrotrophic peatlands? Journal of Hydrology: 4: 100032. https://doi.org/10.1016/j.hydroa.2019.100032

Boorman DB, Hollis JM, Lilly A. 1995. Hydrology of soil types: a hydrologically−based classification of the soils of the United Kingdom. Institute of Hydrology report no. 126

Bragg OM. 2002. Hydrology of peat−forming wetlands in Scotland. Science of the Total Environment 294 (1–3): 111–129. https://doi.org/10.1016/S0048−9697(02)00059−1

Carrer GE, Rousseau AN, Jutras S, Fossey M. 2016. Assessment of the impact of pools on the water isotopic signature of a boreal patterned peatland. Hydrological Processes 30: 1292–1307. https://doi.org/10.1002/hyp.10715

Conway VM, Millar A. 1960. The hydrology of some small peat−covered catchments in the northern Pennines. Journal of the Institution of Water Engineers 14: 415–424

Craig, H. 1961. Standard for reporting concentrations of deuterium and oxygen−18 in natural waters, Science, 133, 1833–1834, https://doi.org/10.1126/science.133.3467.1833

Dansgaard, W. (1964), Stable isotopes in precipitation. Tellus, 16: 436−468. https://doi.org/10.1111/j.2153−3490.1964.tb00181.x

Dick JJ, Tetzlaff D, Soulsby C. 2018. Role of riparian wetlands and hydrological connectivity in the dynamics of stream thermal regimes. Hydrology Research 49 (3): 634–647. doi: https://doi.org/10.2166/nh.2017.066

Evans MG, Burt TP, Holden J, Adamson JK. 1999. Runoff generation and water table fluctuations in blanket peat: evidence from UK data spanning the dry summer of 1995. Journal of Hydrology 221 (3–4): 141–160. https://doi.org/10.1016/S0022−1694(99) 00085−2

Falátkova K, Šípek V, Vlček L, Kocum J, Pivokonský M. 2024. Hydrological balance and runoff from a montane peat bog traced by water temperature. Hydrological Sciences Journal 69(4): 393–406. https://doi.org/10.1080/02626667.2024.2320392

Geris J, Tetzlaff D, McDonnell J, Soulsby C. 2015. The relative role of soil type and tree cover on water storage and transmission in northern headwater catchments. Hydrological Processes 29: 1844–1860. https://doi.org/10.1002/hyp.10289

Geris J, Tetzlaff D, McDonnell JJ, Soulsby C. 2017. Spatial and temporal patterns of soil water storage and vegetation water use in humid northern catchments. Science of the Total Environment 595: 486–493. https://doi.org/10.1016/j.scitotenv.2017.03.275

Gibson JJ, Birks SJ, Edwards TWD. 2008. Global prediction of _A and _2H−_18O evaporation slopes for lakes and soil water accounting for seasonality. Global Biogeochemical Cycles 22: GB2031. https://doi.org/10.1029/2007GB002997

Goodbrand A, Westbrook CJ, van der Kamp G. 2019. Hydrological functions of a peatland in a Boreal Plains catchment. Hydrological Processes 33: 562–574. https://doi.org/10.1002/hyp.13343

Gowan E, Parnell A. 2024. Cosimmr: Fast Fitting of Stable Isotope Mixing Models with Covariates. R package version 1.0.12. Available at: https://CRAN.R−project.org/package=cosimmr

Holden J, Burt TP, Cox NJ. 2001. Macroporosity and infiltration in blanket peat: The implicaions of tension disc infiltrometer measurements. Hydrological Processes 15: 289–303. https://doi.org/10.1002/hyp.93

Holden J, Burt TP. 2003. Hydrological studies on blanket peat: The significance of the acrotelm–catotelm model. Journal of Ecology 91 (1): 86–102. https://doi.org/10.1046/j.1365–2745.2003.00748.x

Hrachowitz M, Soulsby C, Tetzlaff D, Dawson JJC, Dunn SM, Malcolm IA. 2009. Using long–term data sets to understand transit times in contrasting headwater catchments. Journal of Hydrology 367 (3–4): 237–248. https://doi.org/10.1016/j.jhydrol.2009.01.001

Isokangas E, Rossi PM, Ronkanen AK, Marttila H, Rozanski K, Kløve B. 2017. Quantifying spatial groundwater dependence in peatlands through a distributed isotope mass balance approach. Water Resources Research 53: 2524–2541. https://doi.org/10.1002/2016WR019661

Jenicek M, Hnilica J, Nedelcev O, Sipek V. 2021. Future changes in snowpack will impact seasonal runoff and low flows in Czechia. Journal of Hydrology: Regional Studies 37: 100899. https://doi.org/10.1016/j.ejrh.2021.100899

Kleine L, Tetzlaff D, Smith A, Goldhammer T, Soulsby C. 2021. Using isotopes to understand landscape–scale connectivity in a groundwater–dominated, lowland catchment under drought conditions. Hydrological Processes 35: e14197. https://doi.org/10.1002/hyp.14197

Kløve B, Allan A, Bertrand G, Druzynska E, Ertürk A, Goldscheider N, Henry S, Karakaya N, Karjalainen TP, Koundouri P, Kupfersberger H, Kvœrner J, Lundberg A, Muotka T, Preda E, Pulido–Velazquez M, Schipper P. 2011. Groundwater dependent ecosystems. Part II. Ecosystem services and management in Europe under risk of climate change and land use intensification, Environmental Science & Policy 14 (7): 782–793. https://doi.org/10.1016/j.envsci.2011.04.005

Kirchner JW. 2016. Aggregation in environmental systems – Part 2: Catchment mean transit times and young water fractions under hydrologic nonstationarity. Hydrology and Earth System Sciences 20: 299–328. https://doi.org/10.5194/hess–20–299–2016

Koit O, Tarros S, Pärn J, Küttim M, Abreldaal P, Sisask K, Vainu M, Terasmaa J, Retike I, Polikarpus M. 2021. Contribution of local factors to the status of a groundwater dependent terrestrial ecosystem in

the transboundary Gauja−Koiva River basin, North−Eastern Europe. Journal of Hydrology 600: 126656. https://doi.org/10.1016/j.jhydrol.2021.126656

Kool D, Agam N, Lazarovitch N, Heitman J, Sauer T, Ben−Gal A. 2014. A review of approaches for evapotranspiration partitioning. Agricultural and Forest Meteorology 184: 56–70. https://doi.org/10.1016/j.agrformet.2013.09.003

Lamacova A, Ledvinka O, Bohdalkova L, Oulehle F, Kreisinger J, Vlnas R. 2024. Response of spring yield dynamics to climate change across altitude gradient and varied hydrogeological conditions. Science of The Total Environment 921: 171082. https://doi.org/10.1016/j.scitotenv.2024.171082

Landwehr JM, and Coplen TB. 2006. Line−condition excess: A new method for characterizing stable hydrogen and oxygen isotope ratios in hydrologic systems, Isotopes in Environmental Studies, Edition: 1, IAEA, ISBN: 92−0−111305−X

Langlois MN, Price JS, Rochefort L. 2015. Landscape analysis of nutrient−enriched margins (lagg) in ombrotrophic peatlands. Science of the Total Environment 505: 573−586. https://doi.org/10.1016/j.scitotenv.2014.10.007

Lessels JS, Tetzlaff D, Birkel C, Goodbrand J, Soulsby C. 2016. Water sources and mixing in riparian wetlands revealed by tracers and geospatial analysis. Water Resources Research 52: 456–470. https://doi.org/10.1002/2015WR017519

Levy ZF, Siegel DI, Dasgupta SS, Glaser PH, Welker JM. 2014. Stable isotopes of water show deep seasonal recharge in northern bogs and fens. Hydrological Processes 28: 4938−4952. https://doi.org/10.1002/hyp.9983

McDonald A. 1973. Some views on the effects of peat drainage. Scottish Forestry 27, 315–327

McDonnell JJ, Sivapalan MM, Vache K, Dunn S, Grant G, Haggerty R, Hinz C, Hooper R, Kirchner J, Roderick ML, Selker J, Weiler M. 2007. Moving beyond heterogeneity and process complexity: a new vision for watershed hydrology. Water Resources Research 43: W07301. https://doi.org/10.1029/2006WR005467

McDonnell, J.J. 2014, The two water worlds hypothesis: ecohydrological separation of water between streams and trees?. WIREs Water, 1: 323−329. https://doi.org/10.1002/wat2.1027

Muhic, F., Ala−Aho, P., Noor, K., Welker, J. M., Klöve, B., & Marttila, H. (2023). Flushing or mixing? Stable water isotopes reveal differences in arctic forest and peatland soil water seasonality. Hydrological Processes, 37(1), e14811. https://doi.org/10.1002/hyp.14811

Parnell AC, Inger R, Bearhop S, Jackson AL. 2010. Source partitioning using stable isotopes: coping with too much variation. PLoS ONE 5 (3): e9672, DOI: 10.1371/journal.pone.0009672

Parnell AC, Phillips DL, Bearhop S, Semmens BX, Ward EJ, Moore JW, Jackson AL, Grey J, Kelly DJ, Inger R. 2013. Bayesian stable isotope mixing models. Environmetrics 24 (6): 387–399 DOI: 10.1002/env.2221

Pfahl S, Sodemann H. 2014. What controls deuterium excess in global precipitation? Climate of the Past 10: 771–781. https://doi.org/10.5194/cp−10−771−2014

Robinson M, Rodda JC, Sutcliffe JV. 2013. Long−term environmental monitoring in the UK: origins and achievements of the Plynlimon catchment study. Transactions of the Institute of British Geographers 38 (3): 451–463. https://doi.org/10.1111/j.1475−5661.2012

Šanda M, Vitvar T, Jankovec J. 2018. Seasonal Subsurface Water Contributions to Baseflow in the Mountainous Uhlířská Catchment (Czech Republic). Journal of Hydrology and Hydromechanics 67: 41–48. https://doi.org/10.2478/johh−2018−0018

Šanda M, Vitvar T, Kulasová A, Jankovec J, Císlerová M. 2014. Run−off formation in a humid, temperate headwater catchment using a combined hydrological, hydrochemical, and isotopic approach (Jizera Mountains, Czech Republic). Hydrological Processes 28 (8): 3217–3229. https://doi.org/10.1002/hyp.9847

Scheliga B, Tetzlaff D, Nuetzmann G. et al. 2019. Assessing runoff generation in riparian wetlands: monitoring groundwater–surface water dynamics at the micro−catchment scale. Environmental Monitoring and Assessment 191: 116. https://doi.org/10.1007/s10661−019−7237−2

Scherrer S, Naef F. 2003. A decision scheme to indicate dominant hydrological flow processes on temperate grassland. Hydrological Processes 17: 391–401. https://doi.org/10.1002/hyp.1131

Seibert J, Grabs T, Köhler S, Laudon H, Winterdahl M, Bishop K. 2009. Linking soil− and stream−water chemistry based on a riparian flow−concentration integration model. Hydrology and Earth System Sciences 13: 2287–2297. https://doi.org/10.5194/hess−13− 2287−2009

Sidle, R. C., Hirano, T., Gomi, T., and Terajima, T. 2007. Hortonian overland flow from Japanese forest plantations – an aberration, the real thing, or something in between?, Hydrol. Process., 21, 3237–3247, https://doi.org/10.1002/hyp.6876

Šípek V, Jenicek M, Hnilica J, Zelíková N. 2021. Catchment Storage and its Influence on Summer Low Flows in Central European Mountainous Catchments. Water Resources Management 35: 2829–2843. https://doi.org/10.1007/s11269−021−02871−x

Soulsby C, Malcolm R, Helliwell R, Ferrier RC, Jenkins A. 2000. Isotope hydrology of the Allt a'Mharcaidh catchment, Cairngorms, Scotland, implications for hydrologic pathways and residence times. Hydrological Processes 14: 747–762. https://doi.org/10.1002/(SICI)1099−1085(200003)14:4<747::AID−HYP970>3.0.CO;2−0

Sprenger M, Tetzlaff D, Tunaley C, Dick J, Soulsby C. 2017a. Evaporation fractionation in a peatland drainage network affects stream water isotope composition. Water Resources Research 53: 851–866. https://doi.org/10.1002/2016WR019258

Sprenger M, Tetzlaff D, Soulsby C. 2017b. Soil water stable isotopes reveal evaporation dynamics at the soil–plant–atmosphere interface of the critical zone. Hydrology and Earth System Sciences 21: 3839–3858. https://doi.org/10.5194/hess−21−3839−2017

Sprenger, M., Tetzlaff, D., Buttle, J., Laudon, H., Leistert, H., Mitchell, C.P.J., Snelgrove, J., Weiler, M., Soulsby, C. 2018. Measuring and Modeling Stable Isotopes of Mobile and Bulk Soil Water. Vadose Zone Journal, 17: 1−18 170149. https://doi.org/10.2136/vzj2017.08.0149

Starostová M. 2012. Měření srážek totalizátory na Šumavě. Meteorologické zprávy 65: 180–183 (in Czech)

Stockinger MP, Bogena HR, Lücke A, Diekkrüger B, Cornelissen T, Vereecken H. 2016. Tracer sampling frequency influences estimates of young water fraction and streamwater transit time distribution. Journal of Hydrology 541: 952−964. https://doi.org/10.1016/j.jhydrol.2016.08.007

Tetzlaff D, Soulsby C, Bacon PJ, Youngson AF, Gibbins C, Malcolm IA. 2007. Connectivity between landscapes and riverscapes—a unifying theme in integrating hydrology and ecology in catchment science? Hydrological Processes 21: 1385−1389. https://doi.org/10.1002/hyp.6701

Tetzlaff D, Birkel C, Dick J, Geris J, Soulsby C. 2014. Storage dynamics in hydropedological units control hillslope connectivity, runoff generation, and the evolution of catchment transit time distributions. Water Resources Research 50: 969– 985. https://doi.org/10.1002/2013WR014147

Tetzlaff D, Buttle J, Carey SK, McGuire K, Laudon H, Soulsby C. 2015. Tracer−based assessment of flow paths, storage and runoff generation in northern catchments: a review. Hydrological Processes 29(16): 3475−3490. https://doi.org/10.1002/hyp.10412

Tolasz R. et al. 2007. Atlas podnebí Česka. ČHMU a ÚP Olomouc. Praha. 256 s. (in Czech only)

Uhlenbrook S, Didszun J, Wenninger J. 2008. Source areas and mixing of runoff components at the hillslope scale – a multi−technical approach. Hydrological Sciences Journal 53 (4): 741–753. https://doi.org/10.1623/hysj. 53.4.741

Van Meerveld HJI, Kirchner JW, Vis MJP, Assendelft RS, Seibert J. 2019. Expansion and contraction of the flowing stream network alter hillslope flowpath lengths and the shape of the travel time distribution. Hydrology and Earth System Sciences 23: 4825–4834. https://doi.org/10.5194/hess−23−4825−2019

Vlček L, Falátková K, Schneider P. 2017. Identification of runoff formation with two dyes in a mid−latitude mountain headwater. Hydrology and Earth System Sciences 21: 3025–3040. https://doi.org/10.5194/hess−21−3025−2017

Vlček L, Šípek V, Kofroňová J, Kocum J, Doležal T, Janský B. 2021. Runoff formation in a catchment with Peat bog and Podzol hillslopes. Journal of Hydrology 593: 125633. https://doi.org/10.1016/j.jhydrol.2020.125633

Von Freyberg J, Radny D, Gall HE, Schirmer M. 2014. Implications of hydrologic connectivity between hillslopes and riparian zones on streamflow composition. Journal of Contaminant Hydrology 169: 62–74. https://doi.org/10.1016/j.jconhyd.2014.07.005

Waddington JM., Morris PJ, Kettridge N, Granath G, Thompson DK, Moore PA. 2015. Hydrological feedbacks in northern peatlands. Ecohydrology 8: 113–127. https://doi.org/10.1002/eco.1493

Xia C., Zuecco G., Marchina C., Penna D., Borga M. 2024. Effects of Short−Term Climate Variations on Young Water Fraction in a Small Pre−Alpine Catchment. Water Resources Research 60: e2023WR036245. https://doi.org/10.1029/2023WR036245

Supplements

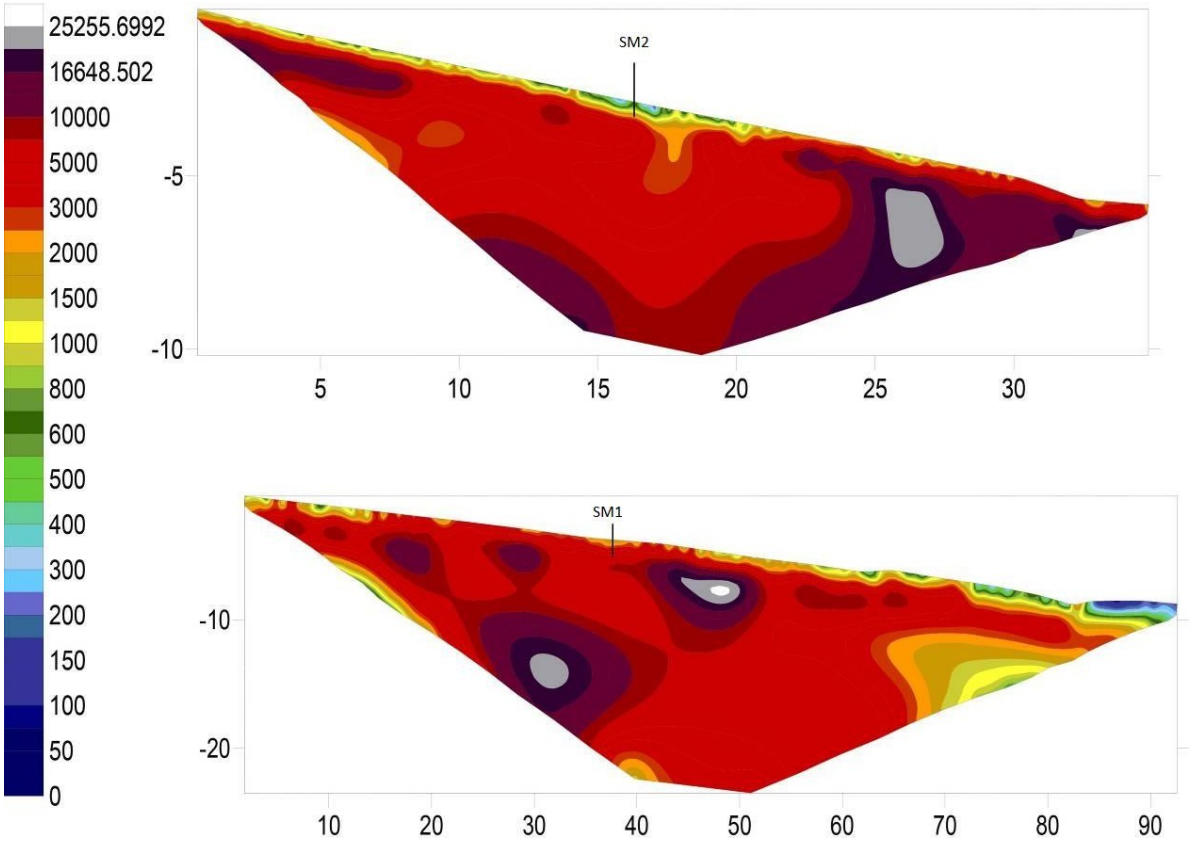

Figure S1. ERT (Electrical resistivity tomography) profile at PZ hillslope at the location of SM1 and SM2; Scale [m].

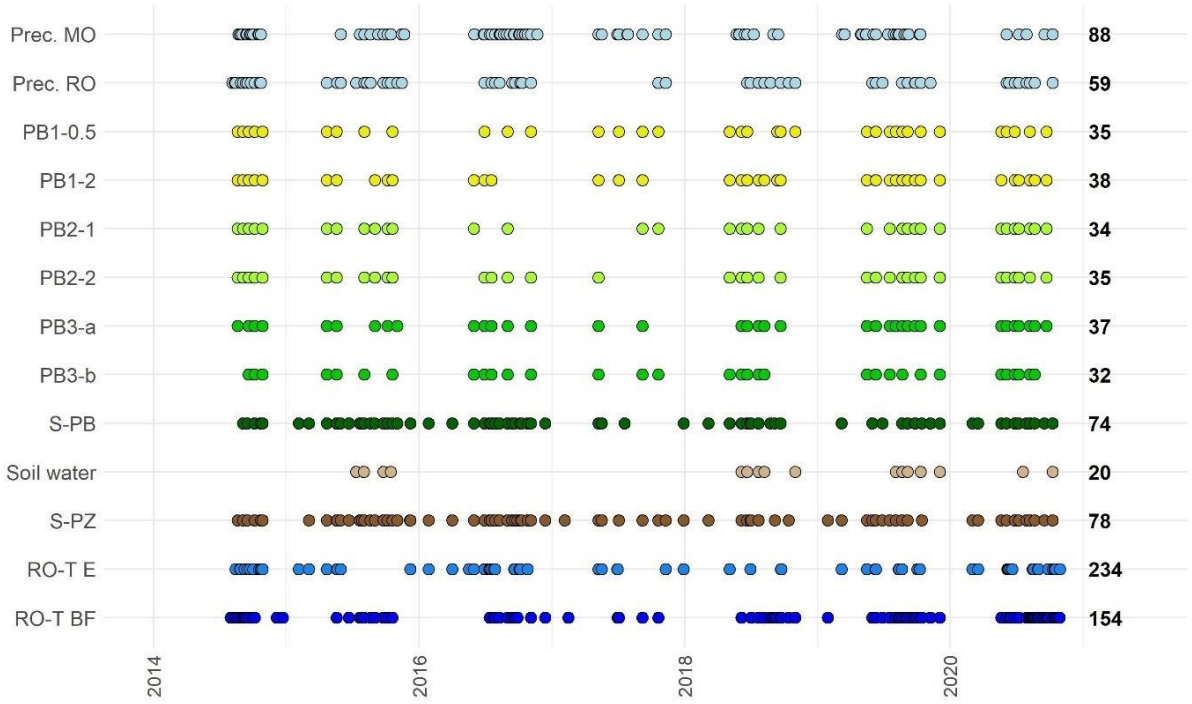

Figure S2. Scheme of sampling period with total amount of samples from each source (black number) during the whole period (2014–2020).

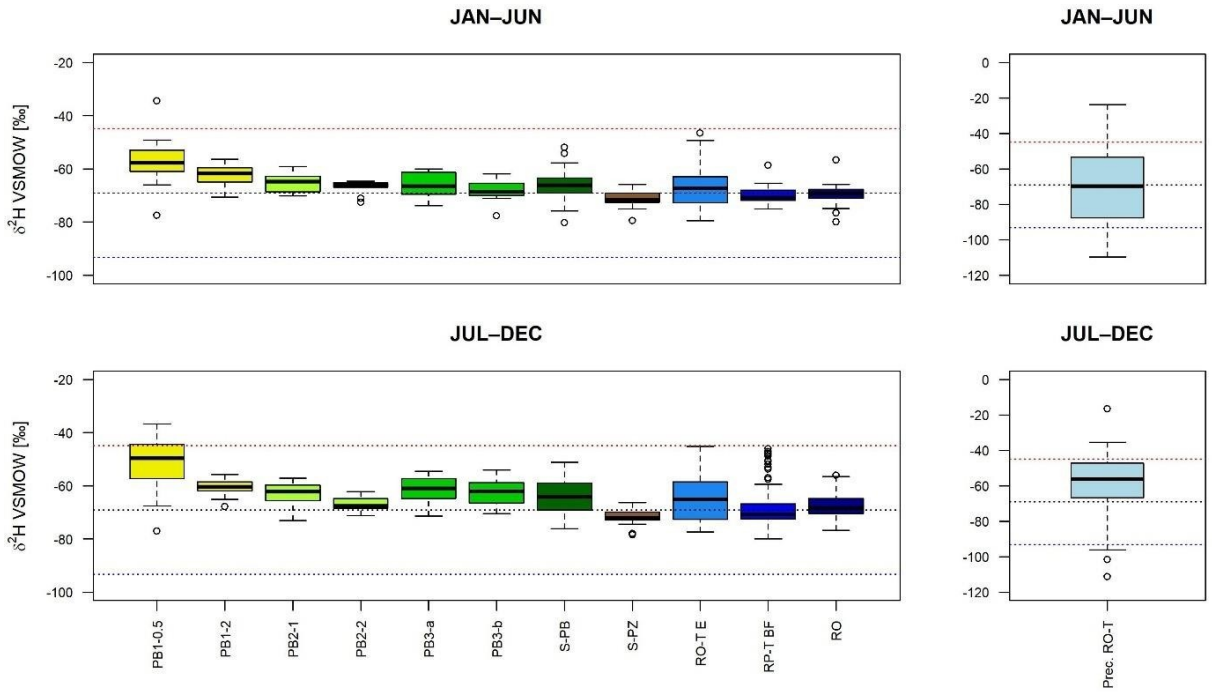

Figure S3. Distribution of δ^2H from all sampling sources divided into two charts according to the first (upper chart) and second (lower chart) half of the year from the period 2014–2020. Dotted lines represent parameters estimated from Sine wave curves: red – upper part of the amplitude (summer values); blue – lower part of the amplitude (winter values), and its mean (gray).

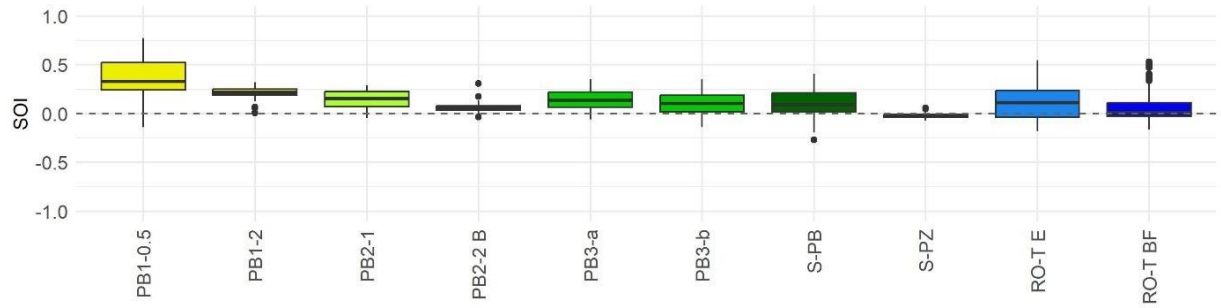

Figure S4. Seasonal origin index (SOI) from the period 2014–2020.

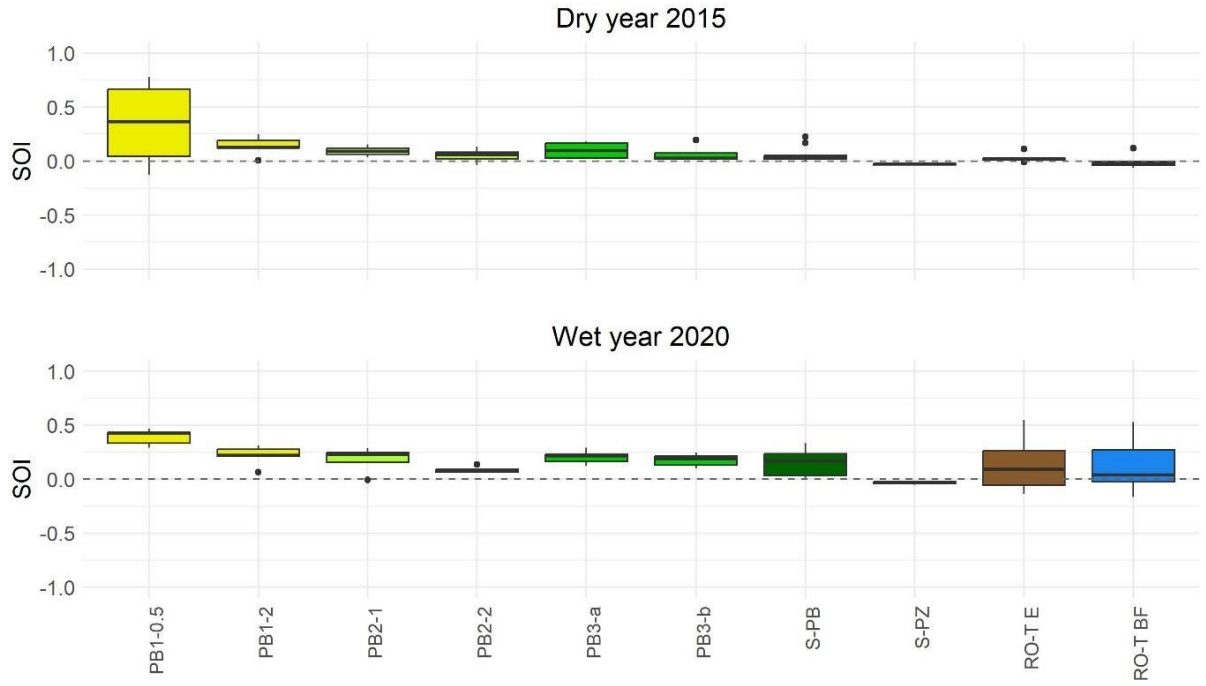

Figure S5. Seasonal origin index for all sampling sources during the growing season from the dry year 2015 (349 mm y^{-1}; upper) and a wet year (> 814 mm y^{-1}; lower).

7.4 A new laboratory approach to extract soil water

The study *Technical note: A new laboratory approach to extract soil water for stable isotope analysis from large soil samples* (Kocum et al., 2025) aimed to develop a more accurate and user-friendly method for soil water extraction, eliminating the need for chemicals or vacuum systems. The proposed technique allows also high-precision extraction of tightly bound soil water. This is important in cases where some soil types, such as clay soils, can store a small but necessary volume of water for plants during dry periods.

Laboratory experiments conducted on various soil types and simulated moisture levels demonstrated that the new method achieves high extraction efficiency with minimal isotopic bias. In comparison with the widely used cryogenic vacuum extraction, the new approach produced comparable or, in some cases, superior results, with isotopic accuracy exceeding that of alternative methods by up to an order of magnitude.

Hydrol. Earth Syst. Sci., 29, 2863–2880, 2025
https://doi.org/10.5194/hess-29-2863-2025

Hydrology and Earth System Sciences
Open Access
EGU

Technical note: A new laboratory approach to extract soil water for stable isotope analysis from large soil samples

Jiri Kocum[1,2], Jan Haidl[1], Ondrej Gebousky[1], Kristyna Falatkova[1], Vaclav Sipek[1], Martin Sanda[3], Natalie Orlowski[4], and Lukas Vlcek[1]

[1]Institute of Hydrodynamics of the Czech Academy of Sciences, Prague, 160 00, Czech Republic
[2]Department of Physical Geography and Geoecology, Faculty of Science, Charles University, Prague, 128 00, Czech Republic
[3]Department of Landscape Water Conservation, Faculty of Civil Engineering,
Czech Technical University, Prague, 166 29, Czech Republic
[4]Chair of Forest Sites and Hydrology, Institute of Soil Science and Site Ecology,
Technical University Dresden, 01737 Tharandt, Germany

Correspondence: Jiri Kocum (kocum@ih.cas.cz)

Received: 19 July 2024 – Discussion started: 22 August 2024
Revised: 21 March 2025 – Accepted: 9 April 2025 – Published: 8 July 2025

Abstract. A correct soil water extraction represents an initial step in stable water isotope analysis. With this aim, we present a new soil water extraction method based on the principle of complete evaporation and condensation of the soil water in a closed circuit. The proposed device has four extraction slots and can be used up to two times a day. Owing to its simple design, there is no need for any chemicals, gases, or high-pressure or high-temperature regimes. The experimental tests proved that the extraction itself does not cause any major isotope fractionation effects leading to erroneous results. Extraction of pure-water samples shifts the isotope composition by 0.04 ± 0.06 ‰ and 0.06 ± 0.35 ‰ for $\delta^{18}O$ and $\delta^{2}H$, respectively. Soil water extraction tests were conducted for five distinct soil types (loamy sand, sandy loam, sandy clay, silt loam, and clay) using 40–150 g of pre-oven-dried soil, which was subsequently rehydrated to 10 % and 20 % water content. The shift in the isotopic composition of these tests ranged between −0.04 ‰ and 0.07 ‰ for $\delta^{18}O$ and 0.4 ‰ and 1.3 ‰ for $\delta^{2}H$, with the standard deviations of ± (0.08–0.25) ‰ and ± (0.34–0.58) ‰ for $\delta^{18}O$ and $\delta^{2}H$, respectively. The results exhibit high accuracy, which makes this method suitable for high-precision studies where unambiguous determination of the water origin is required.

1 Introduction

Measurements of soil water isotopic composition (^{2}H and ^{18}O) provide a description of soil water movement and mixing processes in the vadose zone (Stumpp et al., 2018). In some cases, different trends in soil water sample characterization without the application of an exact isotopic composition method (tracer experiments to prove interconnection) give sufficient information about sample dissimilarity. However, for characterizing the transport processes and residence times, accurate evaluation of the sample origin, soil water dynamic modelling, or inter-laboratory comparison, the exact values of the isotopic composition are indispensable. This justifies the emphasis placed on correct soil water extraction. Unlike liquid-water samples of precipitation, snow cover, stream water, or groundwater, where the isotopic compositions are easily accessible, the extraction of matrix-bound or tightly bound soil water is challenging from the viewpoint of exact determination of isotopic composition. It has been shown that the storage and sample preparation for extraction, the soil texture, and the soil water content, as well as the organic matter and carbonate content, strongly influence the final results (West et al., 2006; Wassenaar et al., 2008; Koeniger et al., 2011; Meißner et al., 2014; Hendry et al., 2015; Orlowski et al., 2016a; Newberry et al., 2017). Parallelly, the specifics of the extraction methods, e.g. the different pore spaces that may or may not be extracted via the different

approaches (Orlowski et al., 2019; Kübert et al., 2020), and the modifications of the procedures themselves (Orlowski et., 2018) can affect the isotope results.

There are several classes of different extraction methods; some of them were compared in Zhu et al. (2014), Sprenger et al. (2015), and Orlowski et al. (2016b, 2018). In brief, there are methods using the following:

a. various chemical compounds or elements like toluene for azeotropic distillation (Revesz and Woods, 1990; Thorburn et al., 1993), dichloromethane for accelerated solvent extraction techniques (Zhu et al., 2014), and/or zinc or uranium for micro-distillation (Kendall and Coplen, 1985; Brumsack et al., 1992);

b. microwave water extraction (Munksgaard et al., 2014);

c. force in terms of mechanical squeezing (Wershaw et al., 1966; White et al., 1985; Böttcher et al., 1997) or centrifugation (Mubarak and Olsen, 1976; Batley and Giles, 1979; Barrow and Whelan, 1980; Peters and Yakir, 2008);

d. equilibration methods such as in situ equilibration (Garvelmann et al., 2012; Rothfuss et al., 2013, 2015; Volkmann and Weiler, 2014; Gaj et al., 2016), CO_2 and H_2 equilibration (Jusserand, 1980; Scrimgeour, 1995; Hsieh et al., 1998; McConville et al., 1999; Koehler et al., 2000; Kelln et al., 2001), and the direct liquid–vapour equilibrium laser spectroscopy (DVE-LS) method (Wassenaar et al., 2008; Hendry et al., 2015);

e. cryogenic vacuum extraction (CVE) (Dalton, 1988; West et al., 2006; Koeniger et al., 2011; Goebel and Lascano, 2012; Orlowski et al., 2013, 2016a; Gaj et al., 2017), the modified CVE–He-purging method (Ignatev et al., 2013), and the automatic cryogenic vacuum distillation (ACVD) system LI-2100 (Lica United Technology Limited Inc.).

In addition, many laboratories use various modifications of these methods (Walker et al., 1994; Munksgaard et al., 2014; Orlowski et al., 2018). A more detailed description of the above-stated methods is presented in Sprenger et al. (2015) and Ceperley et al. (2024).

At present, DVE-LS and CVE are the most commonly used methods for soil water extraction. Both methods provide very accurate results but only under specific conditions. For the DVE-LS method, the different equilibration times, low water content, and selection of bags play a crucial role (Hendry et al., 2015; Gralher et al., 2016). It has also been shown that soil samples with a high content of fine particles – and, thus, high soil tension – can cause isotope fractionation in closed systems (Gaj and McDonell, 2019). For the CVE method, the major challenge is the treatment of soils containing clay minerals. Such soils require an application of higher temperatures (up to 300 °C). However, this results in the release of water by oxidation of organics and dihydroxylation of hydroxide-containing minerals such as goethite (Gaj et al., 2017) and, in such a way, affects the experimental results. Moreover, the soil sample size acceptable for this method is rather low, usually between 10 to 20 g, allowing for the extraction of only grams of the soil water. Another disadvantage of the CVE method consists of the incomparable outputs among different laboratories due to the CVE setup modifications and different workflows (Orlowski et al., 2018). Laboratories' differences in terms of their setups are as follows: the extraction containers (form, size, volume, and material), the heating module and its working temperature (heating tapes or lamps, water baths or hot plates), the type of fittings and connections (glass, stainless steel), and the vacuum-producing units. In addition, different temperatures, pressures, extraction times, and sample sizes are applied by different laboratories. However, if a certain setup of all these parameters for the given situation is chosen, very accurate results can be achieved for certain soil types and water contents. Nevertheless, each of these two methods exhibits apparent inconveniences:

- in the case of the DVE-LS method, significant time consumption (a requirement of the permanent presence of an operator);
- in the case of the CVE method, an application of technically complicated methods (work with liquid nitrogen, low pressures, and high temperatures in an open laboratory apparatus).

In this study, we present a new extraction method – circulating-air soil water extraction (CASWE). It is a relatively simple, inexpensive method that can handle soil samples of different sizes, moisture contents, and textures. It is based on the simple principle of complete evaporation and condensation in a closed circuit and does not require an application of hazardous substances (acids, toluene, liquid nitrogen) and/or high temperatures and pressures. In the following we (1) introduce a new extraction principle, (2) present the results of soil extraction efficiency testing, and (3) compare the results with other state-of-the-art approaches. The advantage of the proposed method over the others is its accuracy, even with clay samples, known for causing inaccurate results for other extraction methods (Ceperley et al., 2024). The biggest advantages of this extraction method are as follows:

a. the high accuracy of the results,

b. the simple design and low cost of the apparatus setup,

c. the low operating costs,

d. the time reduction in operating the device, and

e. the ability to process large soil samples and thus obtain large and representative quantities of soil water.

2 Methodology

2.1 Principle of extraction

The CASWE method is based on the principle of complete evaporation and subsequent condensation of soil water in a closed circuit using air as the circulating medium. The soil sample is heated inside the evaporation chamber to 105 °C, and the evaporated soil water is carried by air circulation to a cooling unit, where the water vapour condenses, and finally, the liquid water is collected. Dried cool air is then circulated back into the evaporation chamber. The process continues until no air moisture condensation is visible.

The extraction temperature was chosen based on the standard Czech methodology for soil drying (ISO 11 465, 1998), which is consistent with standard methodologies used in the UK (BSI 1377: 105 ± 5 °C) and the US (ASTM D2216: 110 ± 5 °C). Values exceeding 100 °C have to be chosen as pore water remains in the soil when temperatures below 100 °C are used (O'Kelly, 2004, 2005). The water vapour is then condensed using tap water at a temperature of 8 °C. The usage of tap water for cooling is motivated by the following reasons:

a. its availability;

b. the temperature of the cooling water is close to the ambient-air dew temperature (preventing the appearance of ambient-air condensation on the cooling loops and, hence, possible sample contamination);

c. the prevention of frost formation inside the apparatus, which otherwise increases the risk of blocking the inlet pipes, damaging the glass parts, and causing difficulty in extracted-sample handling (prior to the sample handling, frost on the cooler and collecting vessel walls has to be melted);

d. with respect to the vapour pressure at the extraction temperature (105 °C, 121 kPa), there is no apparent difference in terms of the extraction rates or residual soil moisture at the point of equilibrium with the cooling circuit operated at 8 °C (1 kPa) or −10 °C (0.3 kPa).

2.2 Description of the apparatus

The newly designed apparatus (Fig. 1a) is composed of three main system units – heating, cooling, and air circulation (Fig. 2). The apparatus has four separate circuits for simultaneous water extraction from four different soil samples.

The heating system comprises a standard kitchen oven (model VT 332 CX; MORA MORAVIA, s.r.o., Czechia) housing four evaporation chambers made of stainless steel boxes equipped with airtight insulation. Each box has two openings, one for a dry-air inlet and the other for a moist-air outlet. The soil sample inside the box is placed on a stainless steel wire mesh bed providing good contact between the sample and the air, which enhances the water evaporation rate (Fig. 1b). The dry air is led to the evaporation chamber through a silicone rubber tube coiled inside the oven; its length (~ 2 m) is sufficient to preheat the air to be close to the oven temperature (Fig. 1c). The hot and moist air from the evaporation chamber is led through the insulated silicone tube to the cooling system; the length of the outlet tubes is as short as possible to minimize the heat losses and to prevent undesired water condensation. To monitor the extraction process, a temperature sensor is installed inside each box close to the air outlet.

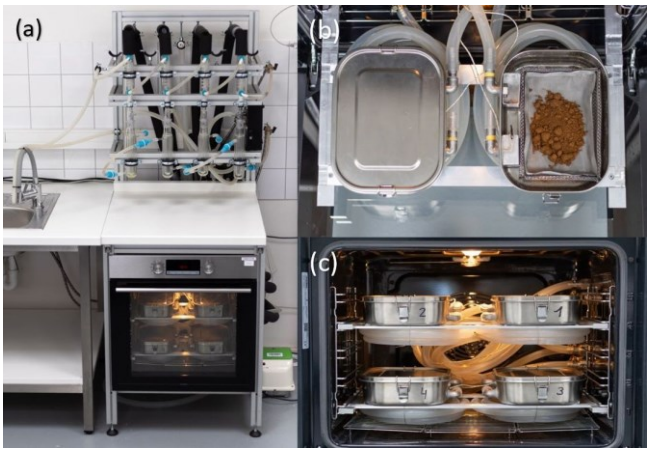

Figure 1. (a) Photo of the proposed CASWE apparatus. (b) Details of the heating chamber with wire mesh bed and aluminium fabric bedding. (c) Internal arrangement of heating chambers and coiled supply hoses.

The cooling system consists of three glass components – a spiral cooler, a custom-made connecting part, and a jacketed collecting vessel (Fig. 3). Two separate cooling-water circuits are used for the spiral coolers and for the collecting vessels (Fig. 2).

The cooled and dried air from the cooling system is fed back to the evaporation chamber by means of the air circulation system, comprised of two regulated high-speed fans per circuit, ensuring the air flow rate of ~ 10 L min^{-1}. The temperature sensors and fan speed in each circuit are monitored by the control unit running on the Arduino platform. The apparatus is complemented by an air diaphragm pump that can be connected to any circuit to flush the circuit with fresh dry air to remove possible residual moisture in the apparatus prior to extraction, thus achieving more accurate results. The tests presented in this work were carried out without the use of this pump. However, for the extraction of soil water with significantly different isotopic compositions, the execution of an initial purge between extractions would be appropriate.

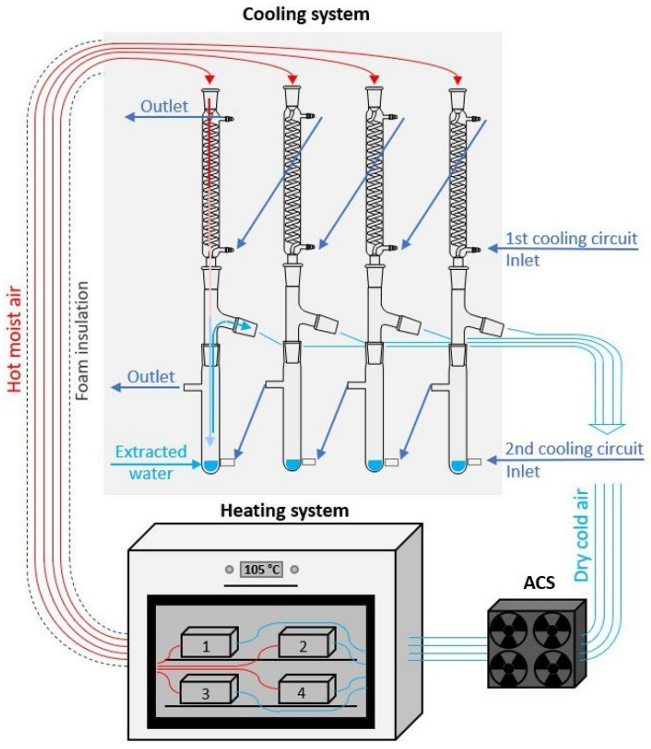

Figure 2. A simplified diagram of the three main components of the CASWE apparatus (heating, cooling, and air circulation systems (ACSs)). The apparatus consists of four separate drying circuits and two cooling circuits.

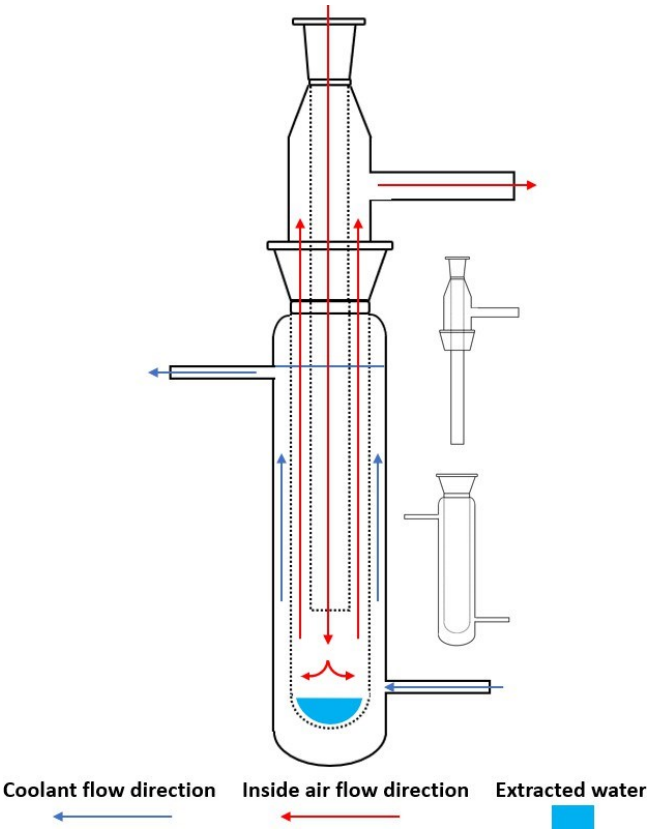

Figure 3. Lower part of the cooling system – custom-made connecting part and jacketed collecting vessel. The arrows indicate the flow direction within the assembly. Thumbnails show individual parts before assembly.

2.3 Extraction procedure

Soil samples are inserted on the wire bed of the evaporation chambers. A target temperature of 105 °C is reached within approximately 15 min. This initiates the first intensive part of the drying process, during which both cooling circuits operate, with most of the water being extracted. The upper cooling circuit (Fig. 2) is disconnected once the spiral cooler starts to dry out. The extraction continues with the bottom cooling circuit only. During this time, residual moisture in the apparatus is collected in the cooled collection vessel.

The extraction is complete when there are no visible signs of condensation anywhere other than in the collection vessel. To check the completeness of the extraction, the recovery ratio was calculated for each extraction by comparing the weights of the added and extracted waters. For complete checking of the functionality of the apparatus, some soil samples were weighed after pre-oven-drying and after extraction. Depending on the sample type, water content, and size, the extraction time intervals ranged from 3 to 6 h per sample. Between each extraction, the circuit is disassembled to retrieve the extracted water from the collection vessel and to exchange soil samples. Thorough mixing of the sample before pouring from the collection vessel and catching of all of the droplets from the walls to ensure the homogeneity of the sample are needed. The collection vessel must then be dried to avoid contamination during further extraction.

2.4 Functional tests

In total, six functional tests were performed. All of the tests were aimed at recovering the same amount of water that was used with no changes in its isotopic composition. The first test served to provide a verification of the principle of extraction and to check the waterproofing and airtightness of the apparatus. The remaining five tests verified the accuracy of the extraction with soil samples via spike experiments. In these experiments, disturbed-soil samples were pre-oven-dried (105 °C for 24 h), spiked in the evaporation chamber with a specific amount of labelled water, mixed, and then left to equilibrate for 2 h. Five sets of spike experiments with different soil textures were performed as soil texture plays a crucial role during soil water extraction (Orlowski et al., 2016a). In each spike experiment, identical samples were rewetted repeatedly (with the exception of artificially prepared sandy clay, which is described below) to reveal any shift in the isotopic composition of the extracted water and, thus, to eliminate any possible influence of the residual water from the

sample due to incomplete drying prior to extraction. This follows a procedure described in Gaj et al. (2017).

Six consequent tests (Table 1) were carried out in the following way:

- *First test.* Water of known isotopic composition and quantity (15 mL) was poured into the heating chambers.
- *Second test.* Disturbed-soil samples (65 g each) with a texture of loamy sand were spiked with 15 mL of water of known isotopic composition. The soil samples were reused and re-hydrated thrice.
- *Third test.* The procedure was the same as in the second test but using sandy loam soil samples.
- *Fourth test.* Samples weighted at 40 g were prepared in the laboratory by mixing sand (60 %) with clay (40 %) and spiking with 10 mL of known isotopic composition. A lower sample size and water amount were used to reduce the corresponding extraction time. In this case, a new sample was prepared for each extraction run due to concerns of possible sealing of the sample after extraction, which would make it difficult to re-hydrate.
- *Fifth and sixth tests.* These tests were used to verify the functionality of the method with a lower water content (10 %). For the fifth test, disturbed-soil samples (150 g each) with a texture of silt loam were spiked with 15 mL of water of known isotopic composition. Since we did not observe any significant sealing in the previous test, the soil samples were reused and re-hydrated twice. The same procedure was used for the sixth test, only with a different soil texture (clay), with the samples being reused and re-hydrated thrice.

For each test, we employed labelled water that differed slightly in terms of the stable isotope composition (Table 2), analysed at the Institute of Hydrodynamics (Czech Academy of Sciences) with the L2140-i isotope analyser (Picarro Inc., US). The standard mode (precision of ± 0.03 ‰ and ± 0.15 ‰ for $\delta^{18}O$ and $\delta^{2}H$, respectively) was used, with six injections per sample and with the first three injections being discarded. The isotope ratios are reported in per mil (‰) relative to Vienna Standard Mean Ocean Water (VSMOW) ($\delta^{2}H$ or $\delta^{18}O = (R_{sample}/R_{standard} - 1) \times 1000$ ‰, where R_{sample} is the isotope ratio of the sample, and $R_{standard}$ is the known reference value (i.e. VSMOW, Craig, 1961). The target accuracy of the method is given by the limit of ± 0.2 ‰ for $\delta^{18}O$ and ± 2 ‰ for $\delta^{2}H$, which is considered to be reasonable for hydrologic studies (Wassenaar et al., 2012; Orlowski et al., 2016b). The terms "shift" and "bias" were used for an evaluation of the results, where shift means a difference compared to the labelled water, and bias indicates the standard deviation of the data. Please note that these terms are often replaced by the terms accuracy (shift) and precision (bias) in some studies (Revesz and Woods, 1990; Koeniger et al., 2011; Ignatev et al., 2013; Zhu et al., 2014; Sprenger et al., 2015; Gaj et al., 2017).

3 Results

3.1 Waterproof and airtightness test

To test the extraction method and the water- and air-tightness of the apparatus (first test), 15 mL of water of known isotopic composition was used. Extraction of this water amount took, on average, 5 h. The resulting recovery ratio after the extraction process averaged 99.7 % of the volume of the used labelled water. The remaining water fractions were given by the sum of the thin residual layer of moisture left on the walls inside the collection vessel during the transfer of the samples into the vials, the residual moisture inside the apparatus, and possible diffusion through the silicon tubing. The stable isotope composition of the labelled water used for this test was −9.61 ± 0.01 ‰ for $\delta^{18}O$ and −66.34 ± 0.05 ‰ for $\delta^{2}H$ ($N = 4$) (Table 2, Fig. 4). The total average of the mean stable isotope composition of extracted water ($N = 13$) was shifted by −0.04 ‰ (bias ± 0.06 ‰) and 0.06 ‰ (bias ± 0.35 ‰) for $\delta^{18}O$ and $\delta^{2}H$, respectively.

3.2 Spike experiments

The other five tests – the spike experiments – verifying the functionality of the extraction took, on average, 3 h for the loamy sand, 4 h for the sandy loam, 5 h for the sandy clay and silt loam, and 6 h for the clay samples. The resulting recovery rate after the extraction process attained, on average, 99.3 % of the used labelled water volume (Table 2). The remaining water fractions were given, analogously to before, by the sum of the thin residual layer of moisture left on the walls inside the collection vessel during the transfer of the samples into the vials, the residual moisture inside the apparatus, and the possible diffusion through the silicon tubing. The sixth test represented the only exception (clay soil from the Halaba area, central Ethiopia), where the recovery rate often exceeded 100 %. Since a similar phenomenon was not observed with the other samples and because the apparatus was tested for possible leakage (which was not found), we hypothesize that this error is due to the extreme chemical composition of the selected samples (potential release of crystalline water from the soil itself) or insufficient pre-oven-drying (despite being applied for 72 h).

In the second test (loamy sand), the stable isotope composition of labelled water was −49.22 ± 0.01 ‰ for $\delta^{18}O$ and −64.56 ± 0.04 ‰ for $\delta^{2}H$ ($N = 3$). The average obtained isotopic composition was depleted by 0.03 ± 0.08 ‰ in $\delta^{18}O$ and enriched by 0.4 ± 0.34 ‰ in $\delta^{2}H$ ($N = 11$) (Table 2, Fig. 4). As in the first test, the $\delta^{18}O$ values were slightly depleted but almost matched the labelled water. However, the $\delta^{2}H$ values were relatively enriched (Fig. 4; Table A2 in the Appendix).

Table 1. Sample properties to verify the apparatus functionality.

Test	Sample (g)	Water (mL)	Soil (g)	w (%)	ϑ (%)	Soil texture	% sand	% silt	% clay
First	15	15	–	–	–	–	–	–	–
Second	80	15	65	23	18.75	Loamy sand	85.5	5.5	9
Third	80	15	65	23	18.75	Sandy loam	56.5	34.8	8.7
Fourth	50	10	40	25	20	Sandy clay	60	–	40
Fifth	165	15	150	10	9	Silt loam	16	60	24
Sixth	165	15	150	10	9	Clay	28	28	44

w is gravimetric water content, and ϑ is volumetric water content.

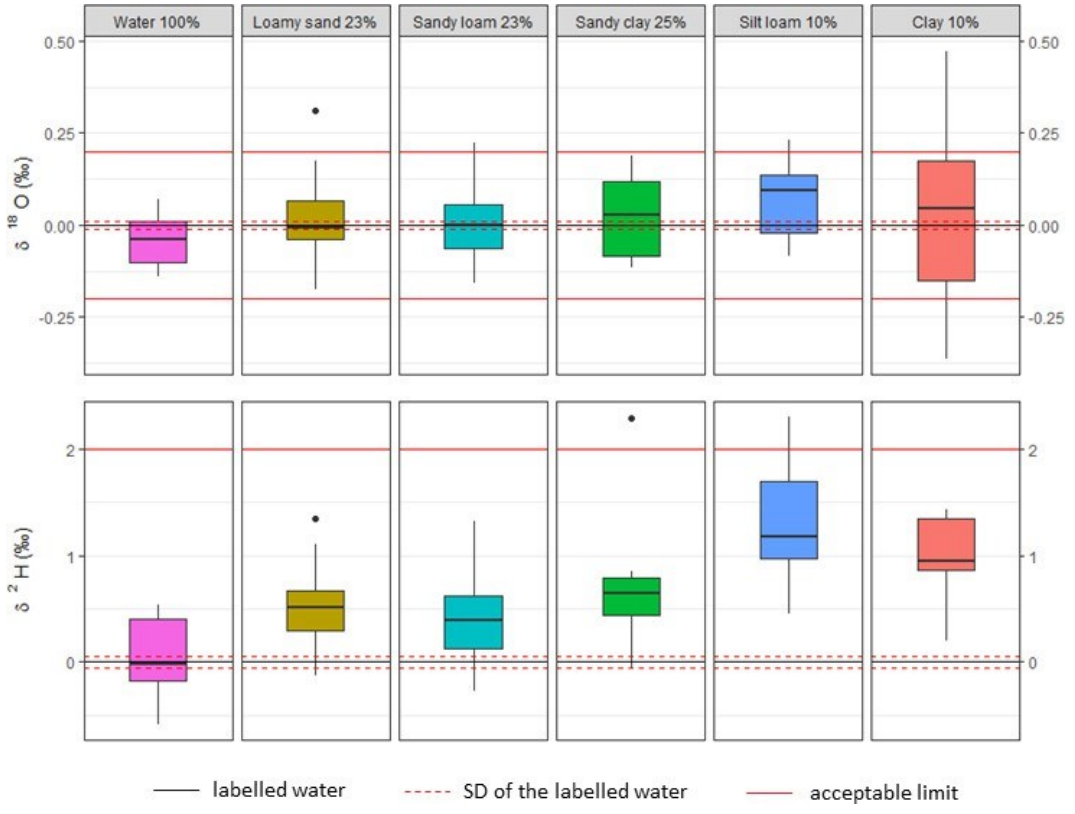

Figure 4. Relative deviation of the isotopic ratio of extracted water compared to the labelled water and its standard deviation. For better clarity, all results are recalculated as if the used labelled water had a VSMOW composition. The acceptable limits are represented by the errors of ± 0.2 ‰ for δ^{18}O and ± 2 ‰ for δ^{2}H, which is considered to be reasonable for hydrologic studies (Wassenaar et al., 2012; Orlowski et al., 2016b).

In the third test (sandy loam), the stable isotope composition of the labelled water was -9.37 ± 0.01 ‰ for δ^{18}O and -64.70 ± 0.05 ‰ for δ^{2}H (N=3). The mean isotope composition of the extracted water was enriched for both isotopes but with no statistical significance for δ^{18}O (Table A2). The average shift and bias attained 0.03 ± 0.13 ‰ for δ^{18}O and 0.51 ± 0.5 ‰ for δ^{2}H ($N = 15$). Compared to the second test, the variance of the values increased.

In the fourth test (sandy clay), the stable isotope composition of the labelled water was -9.54 ± 0.01 ‰ for δ^{18}O and -75.92 ± 0.05 ‰ for δ^{2}H ($N = 3$). The mean isotope composition of the extracted water was enriched for both isotopes but with no statistical significance for δ^{18}O. The values of δ^{18}O increased by 0.03 ± 0.11 ‰, and those of δ^{2}H increased by 0.68 ± 0.58 ‰ ($N = 11$).

In the fifth test (silt loam), the stable isotope composition of the labelled water attained -9.35 ± 0.02 ‰ for δ^{18}O and -66.06 ± 0.05 ‰ for δ^{2}H ($N = 3$). The mean isotope composition of the extracted water was enriched for both isotopes but with no statistical significance for δ^{18}O. The values of

Table 2. Summary of the individual test results.

Test	Type	N	δ^{18}O (‰)	SD (‰)	δ^{2}H (‰)	SD (‰)	Sample type	Extraction time (h)	Recovery rate (%)
First	L	4	−9.61	± 0.01	−66.34	± 0.05	Water	5	99.7
	E	13	−9.65	± 0.06	−66.28	± 0.35			
Second	L	3	−9.22	± 0.01	−64.56	± 0.04	Loamy sand	3	99.5
	E	11	−9.25	± 0.08	−64.16	± 0.34			
Third	L	3	−9.37	± 0.01	−64.70	± 0.05	Sandy loam	4	99.2
	E	15	−9.34	± 0.13	−64.19	± 0.50			
Fourth	L	3	−9.54	± 0.01	−75.92	± 0.05	Sandy clay	5	99.3
	E	11	−9.51	± 0.11	−75.24	± 0.58			
Fifth	L	3	−9.35	± 0.02	−66.06	± 0.05	Silt loam	6	99.1
	E	8	−9.27	± 0.11	−64.75	± 0.55			
Sixth	L	3	−9.35	± 0.02	−66.06	± 0.05	Clay	6	99.9
	E	12	−9.34	± 0.25	−65.11	± 0.39			

L and E indicate the labelled and extracted water used in the test, respectively. N stands for the number of samples. The isotope ratios (δ^{18}O, δ^{2}H) and their standard deviations (SD) are reported in per mil (‰) relative to the Vienna Standard Mean Ocean Water (VSMOW). The extraction times quoted are average times valid for the disturbed-soil samples and may vary with other samples depending on the sample size, texture, and water content. The recovery ratio was calculated as the weight of extracted water divided by the weight of the added labelled water, multiplied by 100.

δ^{18}O increased by 0.07 ± 0.11 ‰, and those of δ^{2}H increased by 1.31 ± 0.55 ‰ ($N = 8$).

In the sixth test (clay), the same labelled water was used as in the fifth test. The mean isotope composition of the extracted water was enriched for both isotopes but with no statistical significance for δ^{18}O. The values were shifted by 0.01 ± 0.25 ‰ for δ^{18}O and by 0.96 ± 0.39 ‰ for δ^{2}H ($N = 12$).

The Kolmogorov–Smirnov test at a 5 % significance level was performed for all sets of the results to determine the normality of the data. The measured data for all six tests exhibited a normal distribution. Furthermore, one sample t test was performed at a 5 % significance level to determine whether the extracted values were significantly different from the standard used in the given test. For the first set of the results (extraction test with water only), the average of the data is not statistically different from the standard used. In the remaining extraction tests, using soil, the mean is always statistically identical to the standard used only in the case of δ^{18}O. In the case of δ^{2}H values, the null hypothesis was always rejected. Furthermore, the data variance of δ^{2}H increases with a higher number of fine particles in the soil (silt, clay). The statistical test results are summarized in Table A2.

Since the normality test, which is a prerequisite for the t test, may not be valid for such small data sets, we also performed the bootstrap analysis, which does not require this assumption. This analysis calculates the 95 % confidence interval in which the true value is located (Fig. A1). The results of this analysis were consistent with the results of the t test.

4 Discussion

4.1 Residual moisture in the apparatus

The apparatus is designed to handle an entire standard soil core (100 cm^3). The sample size is limited only by the volume of the heating chamber (roughly 400 cm^3 of usable space) and the size of the collection vessel (~ 25 mL). An advantage of extracting a bigger soil sample over extracting the smaller ones (e.g. < 10 g) is a much better representation of the sample properties. The larger amount of obtained extracted water with the proposed extraction apparatus lowers the potential inaccuracy which accompanies lower sampling amounts in other extraction methods. Additionally, it offers the advantage of being able to run the same extracted water sample using both the isotope ratio mass spectrometry (IRMS) and the isotope ratio infrared spectroscopy (IRIS) machines. However, not all water ends up in the collection vessel. Based on the estimated gas volume of 4 L, the ideal gas law, and the equilibrium conditions at 8 °C, the amount of water left in the circuit is approximately 50 mg. Furthermore, humidity gains and losses can occur during the extraction procedure because of the silicon hoses' permeability. The estimates of humidity losses for the extraction time not exceeding 24 h are less than 0.5 % of the total sample mass, regardless of the extracted water amount. The estimates are based on the water–silicone solubility and permeability (Barrie and Machin, 1969), supposing 50 % relative humidity in the room outside the extractor and 8 °C cooling water. Under these conditions, the absolute air humidity inside the extractor is higher (during the proceeding extraction) or equal to the ambient-air humidity, allowing for minor sample losses

(< 0.5 %) via vapour permeation when the extraction proceeds and no losses once the sample is almost or completely dry. The hoses can also absorb water vapour from the air. The water absorbed in the silicone hoses is released back into the circuit when heated (by calculation, estimated to be approximately 50 µg). Although silicone hoses may not seem ideal for this purpose, the choice of construction materials was a compromise between handling and operating the extractor and material resistance or neutrality with respect to the extracted water. Despite the potential sample gains or losses, these amounts are still marginal compared to the amount of extracted water and so do not exhibit a major effect on the results (as demonstrated).

Most of these error sources can be suppressed by using larger sample sizes. For even more accurate results, it might help to choose a different construction material (PTFE, stainless steel), to seal the apparatus entirely during idle time, to pre-dry the empty apparatus, or to purge the apparatus with dry air or nitrogen (as inert gas). However, the extraction procedure would be more complicated, and the nuances that this would resolve are negligible in comparison to other factors (e.g. the amount of clay in the sample and the accuracy of measurements of the stable isotope composition itself) which will affect the final composition more significantly.

Thorough mixing of the sample before pouring from the collection vessel and catching all droplets from the walls to ensure the homogeneity of the sample is necessary. Because of that, the water adheres to the walls of the collecting vessel, whereby the residual amount always remains there while the sample is poured into the vials. This adhered water contributes significantly to the incomplete recovery rate and often covers the majority of this error. Since the sample was mixed (homogenized) during the collection of all residual droplets on the walls of the collection vessel, we assume that the residual film in the glass will not affect the isotopic composition of the sample but, rather, will only affect the recovery ratio.

With respect to the Rayleigh distillation principle (Dansgaard, 1964; Araguás-Araguás et al., 1995), the observed shift of extracted soil water towards enriched values of the heavier isotopes also points to imperfect collection of extracted water. The slight enrichment indicates incomplete water condensation and the presence of lighter isotopes (as quantified above) inside the apparatus, as also evidenced by the high but incomplete recovery rate. Complete evaporation of the soil water is confirmed by comparison of the soil sample weights (the weight after extraction for selected samples was equal to or slightly lower than the sample weight after pre-oven-drying).

As discussed earlier, two factors, outlined below, can notably influence the composition of the collected water and, thus, the reliability of the proposed method: insufficient tightness of the whole circuit (joints, etc.) and permeability of the pipes made of silicon. The absence of the former factor is checked by the recovery rate being close to 100 %. The latter factor – possible sample contamination with ambient moisture comprising substantially lighter isotopic compositions (~ -13 ‰ and -125 ‰ for $\delta^{18}O$ and $\delta^{2}H$, respectively) – is almost completely suppressed as the experimental results exhibit only negligible changes in the labelled water isotopic composition. Moreover, the observed shift in the water composition (enrichment by heavier isotopes) indicates marginal sample fractionation instead of its contamination by ambient moisture.

4.2 Extraction time

For many methods, extraction time often plays a significant role in the resulting isotopic composition of the sample (Revesz and Woods, 1990; West et al., 2006; Zhu et al., 2014; Hendry et al., 2015; Orlowski et al., 2018; Orlowski and Breuer, 2020). In this case, no significant differences were observed between ending the extraction at the time when the circuit is visibly dry and prolonging the extraction by an hour or more because the same dry, cold air is still flowing when the extraction is completed. Once the extraction is complete, the apparatus reaches an equilibrium state in which the amount and composition of the water sample are fixed. The proposed method is one of the slower ones compared to other extraction methods. The extraction time using the CVE method varies from 15 min (Orlowski et al., 2018) to 6 h (Mora and Jahren, 2003). However, it should be added that, for the CVE method, sample sizes of 10–20 g are used, and only a few millilitres of water is extracted (Table 3), whereas, in the presented method, extraction of the sample size attained up to 150 g and extracted liquid-water amounts of up to 15 mL. The extraction time is therefore longer and varies between 3 to 6 h depending on the soil texture (the larger porosity of the sample reduces the extraction time significantly), water content, and sample size. The presence of pores in the soil and, thus, the larger surface area for evaporation also constitute the reason why the extraction time of some soil samples was shorter than the extraction of water alone (first test). The soils are dried on a manufactured bed to allow air to reach the soil sample from all sides. Contrarily, the water sample was placed in a small stainless steel bowl, enabling air–water interaction only on the surface (upper side). By making this surface larger for the soil, the extraction is faster. Also, the soil itself exhibits a higher thermal conductivity than air.

In the case of low soil moisture, a larger soil sample should be used (to extract at least 7–10 mL of water), resulting in a longer extraction time. The extraction times quoted above are average times valid for the samples used in this study and may vary with other samples (especially undisturbed samples or samples with different water contents).

In large-scale studies, higher sample throughput is an important factor. For these purposes, apparatuses with higher throughput that can handle 30 or more samples in an 8 h working day are used (Goebel and Lascano, 2012; Orlowski

Table 3. Comparison of the reported results of selected soil water extraction methods in different studies.

Method	Study	Sample type	Average $\delta^{18}O$ shift ± SD (‰)	Average $\delta^{2}H$ shift ± SD (‰)	N	T (min)	Spiked water (mL)
Extraction with accelerated solvent	Zhu et al. (2014)	Unknown soil	0.36 ± 0.37	3.6 ± 0.89	1*	30	1
Azeotropic distillation	Revesz and Woods (1990)	Sandy soil	0.35–0.77 ± 0.2	2–3.2 ± 2	1*	25	3
Ultrasonic centrifugation	Zhu et al. (2014)	Unknown soil	0.49 ± –	1 ± –	10	40	1
Centrifugation	Leaney et al. (1993)	Clayey soil	0–3 ± –	–	–	–	–
Direct equilibrium	Scrimgeour (1995)	Unknown soil	−1.5 to −0.11 ± 0.4	– ± 2	1	16	–
Direct equilibrium	McConville et al. (1999)	Sandy soil	0.1 ± 0.12	–	1	15	–
Direct equilibrium	Wassenaar et al. (2008)	Clay-rich soil	1 ± 0.02	2 ± 0.5	1	5	–
ACVD	Yang et al. (2023)	Clay loam	−0.16 ± 0.14	−2.6 ± 1.3	14	240	1.2
CVE	Koeniger et al. (2011)	Sandy soil	– ± 0.4	– ± 3	12	15	0.5
CVE	Newberry et al. (2017)	Sandy soil	−0.59 ± –	–	6	90	3
CVE	Orlowski et al. (2018)	Water	0.1 ± 0.1	−0.8 ± 0.4	24	90	2
He purging	Ignatev et al. (2013)	Clay and silt	0.03 ± 0.08	0.7 ± 0.7	12	180	1.5
CASWE (proposed method)	First test	Water	−0.04 ± 0.06	0.06 ± 0.35	4	300	15
	Second test	Loamy sand	−0.03 ± 0.08	0.40 ± 0.34	4	180	15
	Third test	Sandy loam	0.03 ± 0.13	0.51 ± 0.50	4	240	15
	Fourth test	Sandy clay	0.03 ± 0.11	0.68 ± 0.58	4	300	10
	Fifth test	Silt loam	0.07 ± 0.11	1.31 ± 0.55	4	360	15
	Sixth test	Clay	0.01 ± 0.25	0.96 ± 0.39	4	360	15

The values represent the average shift from the labelled water used ± the standard deviation. ACVD stands for automatic cryogenic vacuum distillation, CVE stands for cryogenic vacuum extraction, and CASWE stands for circulating-air soil water extraction method. CVE results from the study by Orlowski et al. (2018) show only the best results achieved in the comparison of CVEs conducted in that study. Average $\delta^{18}O$ and $\delta^{2}H$ shifts represent the deviation from the mean of the used labelled waters. SD stands for standard deviation (bias). T is the extraction time for N samples that can be processed simultaneously. The number of samples marked with * may vary depending on the size of the apparatus. The last column gives the amount of labelled water used.

et al., 2013; Yang et al, 2023). The proposed apparatus currently has only four circuits; hence, four soil samples can be processed simultaneously. Depending on the soil type and water content, a maximum of two runs per day can be processed. Reduction of the sample size could increase the throughput, resulting in a reduction of the extraction time, but this could be projected to lead to higher inaccuracy in the results.

4.3 Comparison of soil water extraction approaches

In order to compare the proposed method of soil water extraction with other approaches, we gathered the results presented in other references. The results proved (Table 3 and Fig. 5) that the presented method is able to fit safely within an acceptable range of accuracy (± 0.2 ‰ for $\delta^{18}O$ and ± 2 for $\delta^{2}H$ ‰; Wassenaar et al., 2012), which is, for other methods, rather problematic even if different soil types are used. For example, with a clay-rich soil sample, the DVE-LS method (Wassenaar et al., 2008) achieves low standard deviations (± 0.02 ‰ and ± 0.5 ‰ for $\delta^{18}O$ and $\delta^{2}H$, respectively), but the shift in the data is at (+2 ‰ for $\delta^{2}H$) or beyond (+1 ‰ for $\delta^{18}O$) the limit of acceptability. McConville et al. (1999) obtained very accurate results with the direct-equilibrium method (0.1 ± 0.12 ‰ for $\delta^{18}O$), but only a sandy soil was studied. A comparison with the most commonly used method, CVE, is difficult due to the huge dispersion of values presented by different laboratories (Orlowski et al., 2016b, 2018). In this study, we used the reported values of Yang et al. (2023), Newberry et al. (2017), and Koeniger et al. (2011) as a reference. The reported shifts in the data were between −0.16 ‰ to −0.59 ‰ and −2.6 ‰ to 2 ‰ for $\delta^{18}O$ and $\delta^{2}H$, respectively, and the deviation was in the range of ± 0.14 ‰ to 0.4 ‰ and ± 1.3 ‰ to 3 ‰ for $\delta^{18}O$ and $\delta^{2}H$, respectively, where the most problematic samples exhibited a high content of clay particles. Based on the tests we have carried out so far, it seems that, in some cases, the obtained shifts are up to 1 order of magnitude lower than the shifts in the above studies. The reported values are depleted in both isotopes, which contradicts the values reported in this study (where, in particular, the $\delta^{2}H$ values are rather enriched). Orlowski et al. (2016b) showed that, in the case of extraction from sandy samples, the water extracted by means of the

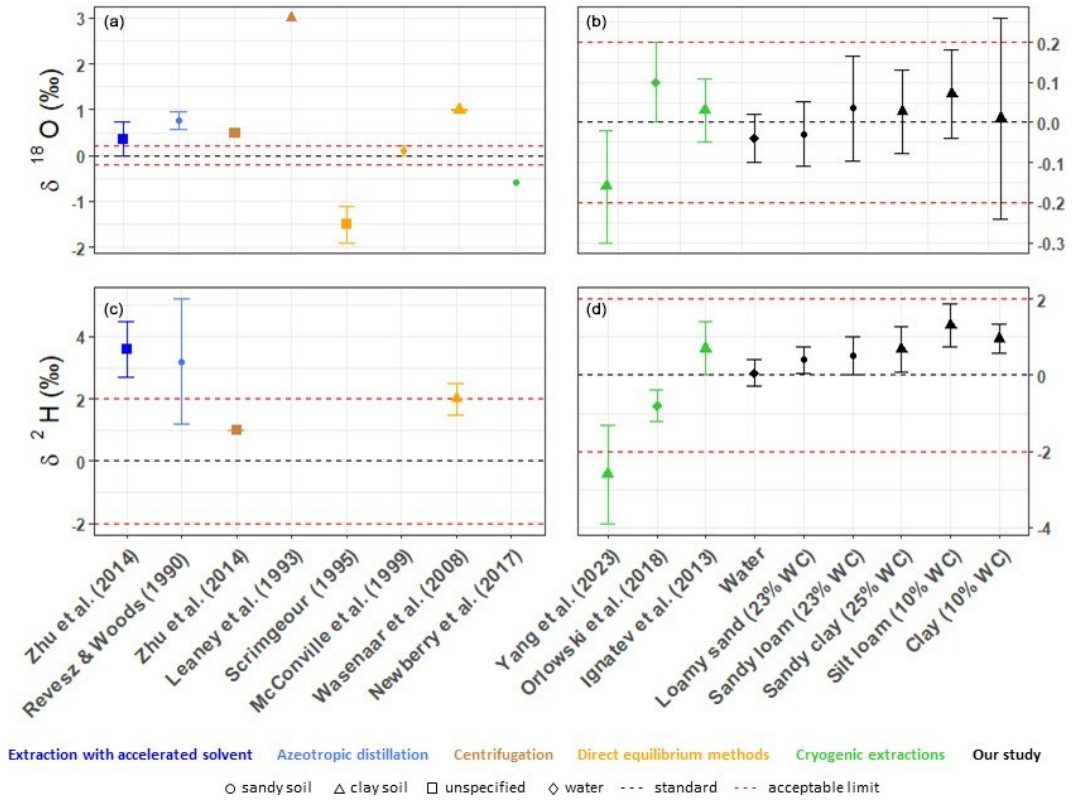

Figure 5. A graphical comparison of the presented results with other methods (a, b for $\delta^{18}O$; c, d for $\delta^{2}H$). Different markings indicate different sample types. The acceptable limits are represented by the errors of ± 0.2 ‰ for $\delta^{18}O$ and ± 2 ‰ for $\delta^{2}H$, which are considered to be reasonable for hydrologic studies (Wassenaar et al., 2012; Orlowski et al., 2016b). The right side of the oxygen graph (b) with more accurate methods has a zoomed-in *y* axis.

CVE method is almost identical to the applied label water. However, as the proportion of clay particles in the sample increases, the accuracy decreases significantly, and the difference compared to the labelled water for clay samples is more than 1.5 ‰ and 12 ‰ for $\delta^{18}O$ and $\delta^{2}H$, respectively. In this study, with an increasing amount of clay in the sample, only a gradual shift in isotopic composition is visible. For both isotopes, there is a higher enrichment of heavy isotopes in the sample, and the dispersion of the values increases. Only the $\delta^{2}H$ is statistically different from the labelled water used (Table A2, Fig. A1).

Many laboratories have considerable problems with the extraction of water itself (Orlowski et al., 2018). The best-reported results of extracted water in the interlaboratory study by Orlowski et al. (2018) were 0.1 ± 0.1 ‰ for $\delta^{18}O$ and −0.8 ± 0.4 ‰ for $\delta^{2}H$, which, again, differed by almost 1 order of magnitude from the results presented in this study. Only 2 out of 16 laboratories in the CVE interlaboratory comparison study presented comparable results. This indicates that the problem with accuracy is not caused by the method itself (CVE can give very accurate results) but is rather connected with the possibility of how to arrange the settings of the apparatus. Minor differences may occur due to the measurement of the isotopic composition itself depending on the instrument and method used (Penna et al., 2010, 2012).

The method providing comparable results with this study is a modification of the CVE method presented by Ignatev et al. (2013), which uses He as carrier gas instead of water vapour diffusion only. In both cases, mass transfer coupled with gas flow (air in the presented study and He in Ignatev et al.'s case) was shown to be more efficient compared to diffusive mass transfer (Ishimaru et al., 1992), and, hence, more accurate results can be achieved. The reported values by Ignatev et al. (2013) are 0.03 ± 0.08 ‰ and 0.7 ± 0.7 ‰ for $\delta^{18}O$ and $\delta^{2}H$, respectively. In comparison with the proposed method, there is a higher shift in $\delta^{18}O$ values but a lower shift in $\delta^{2}H$ values in the He-purging method. However, it should be noted that these differences of hundredths ($\delta^{18}O$) to units of tenths ($\delta^{2}H$) are mostly within the measurement inaccuracy of an isotope analyser.

In our opinion, another step possibly affecting the CVE results (that is not present in the proposed procedure) is the actual vacuum formation in the CVE apparatus. Although the soil sample is inserted into the apparatus frozen in the pre-

vailing majority of cases, there is no guarantee that evaporation or sublimation does not occur at very low pressures.

4.4 Limitations of the proposed method and future development

The main advantage of the CASWE method consists in its ability to extract water from relatively large (hundreds of grams) soil samples, which reduces the effect of soil heterogeneity and sample handling on the measured isotopic composition. On the other hand, such a sample size brings about some less favourable effects. In the field, the commonly used narrow soil probes may be insufficient to collect the required amount of soil, which may necessitate the excavation of a larger pit to obtain a sample. This makes the process more complex and time-consuming, and extra care must be taken to prevent isotopic fractionation of the collected samples. Moreover, the larger amount of soil causes a longer extraction time. In this manner, the complications with handling large soil samples restrict the CASWE method utilization.

For broader use, it would be necessary to change the apparatus design in order to simultaneously enable parallel treatment of more samples and to reduce the extraction time. The latter could be achieved by increasing the air flow circulation rate and reducing the premature condensation inside the pipeline by, for example, improved insulation or additional heating of the tubes. The apparatus could be adapted for medium-scale studies by choosing a different source of heating and by inserting additional evaporation chambers.

5 Conclusions

A new method for soil water extraction – circulating-air soil water extraction (CASWE) – is presented, and a new apparatus is developed for its purposes. The method works on the principle of complete evaporation and condensation in a closed circuit. The soil water was successfully extracted from dried and rehydrated soil samples of different textures (loamy sand, sandy loam, sandy clay, silt loam, and clay). Depending on the soil texture, the average shift from the labelled water used ranged between -0.04 ‰ and 0.07 ‰ for $\delta^{18}O$ and between 0.4 ‰ and 1.3 ‰ for $\delta^{2}H$, with the bias ranging from $\pm$ 0.08 ‰ to 0.25 ‰ and $\pm$ 0.34 ‰ to 0.58 ‰ for $\delta^{18}O$ and $\delta^{2}H$, respectively. The differences between the extracted and used labelled water were often within the measurement error of the used isotope analyser. From the tests we have executed so far, we obtained results with lower shift than what is reported using other soil water extraction and/or equilibration methods, such as the CVE and DVE-LS methods, and with up to an order of magnitude lower shift compared to other methods (extraction with accelerated solvent, centrifugation, azeotropic distillation). This is achieved through the ability to process large soil samples, thereby reducing the effect of soil heterogeneity on the isotopic composition of extracted water and suppressing the inaccuracies accompanying the extraction process. However, the developed apparatus currently has a low throughput, with a maximum of eight samples per day, due to, besides its small capacity, the long extraction times. As a result, its use for fast processing of large sample quantities is limited. It is designed specifically for small-scale high-precision studies where unambiguous determination of the water origin is required. Also, it can be applied as a supplementary method for studies requiring high throughput, serving as a reference for the calibration of less accurate extraction methods. We believe that further development, leading to an increased throughput, could also enable the application of this method in medium-scale studies and could contribute to a deeper understanding of processes in the vadose zone.

Appendix A

This Appendix contains two additional tables and one figure. Table A1 shows all of the measured data from all of the functional tests. Table A2 presents the statistical results (test of variance, Kolmogorov–Smirnov test, and t test). Figure A1 depicts the results of the bootstrap analysis.

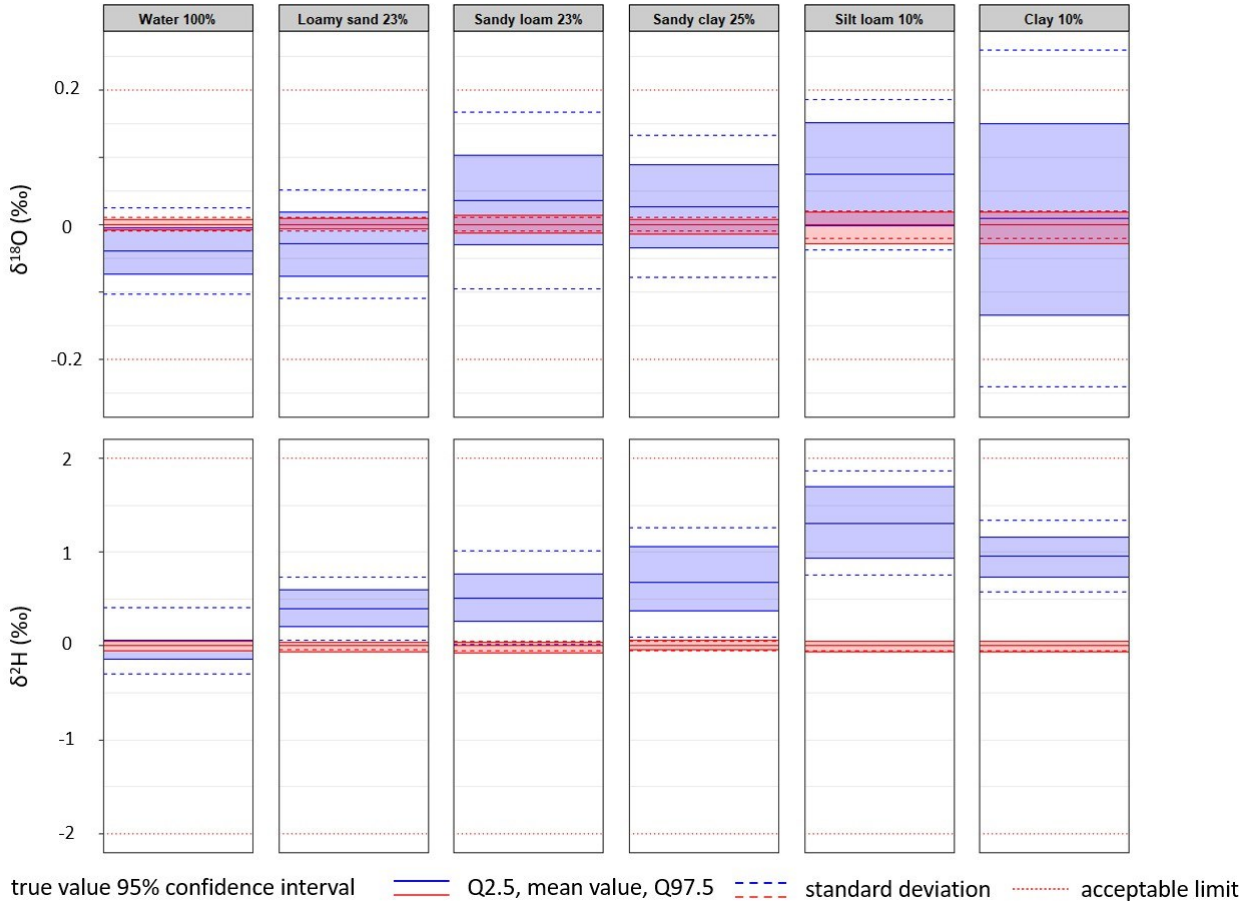

Figure A1. The results of the bootstrap analysis. The blue colour represents the extracted values, and the red colour represents the standards used in these tests.

Table A1. Summary of the measured data.

Sample no.	First test (water)				Second test (loamy sand)				Third test (sandy loam)			
	Extracted water		Labelled water		Extracted water		Labelled water		Extracted water		Labelled water	
	$\delta^{18}O$	$\delta^{2}H$	$\delta^{18}O$	$\delta^{2}H$	$\delta^{18}O$	$\delta^{2}H$	$\delta^{18}O$	$\delta^{2}H$	$\delta^{18}O$	$\delta^{2}H$	$\delta^{18}O$	$\delta^{2}H$
1	−9.74	−66.10	−9.60	−66.25	−9.30	−64.26	−9.23	−64.62	−9.06	−63.36	−9.36	−64.66
2	−9.68	−66.49	−9.60	−66.38	−9.36	−64.25	−9.22	−64.52	−9.20	−63.74	−9.37	−64.67
3	−9.65	−66.93	−9.62	−66.33	−9.26	−64.16	−9.21	−64.54	−9.15	−63.53	−9.38	−64.77
4	−9.73	−66.71	−9.61	−66.39	−9.40	−64.68			−9.44	−64.44		
5	−9.59	−66.36			−9.22	−64.47			−9.35	−64.08		
6	−9.60	−66.52			−9.26	−64.62			−9.47	−64.29		
7	−9.71	−66.41			−9.23	−63.89			−9.34	−63.38		
8	−9.57	−65.83			−9.15	−63.92			−9.28	−64.31		
9	−9.59	−65.92			−9.10	−63.46			−9.43	−64.70		
10	−9.54	−65.94			−9.22	−64.04			−9.21	−64.01		
11	−9.71	−66.04			−9.25	−64.04			−9.50	−64.97		
12	−9.64	−65.81							−9.37	−64.58		
13	−9.64	−66.09							−9.53	−64.97		
14									−9.31	−64.12		
15									−9.41	−64.32		
Average	−9.65	−66.28	−9.61	−66.34	−9.25	−64.16	−9.22	−64.56	−9.34	−64.19	−9.37	−64.70
SD	0.06	0.35	0.01	0.05	0.08	0.34	0.01	0.04	0.13	0.50	0.01	0.05

Sample no.	Fourth test (sandy clay)				Fifth test (silt loam)				Sixth test (clay)			
	Extracted water		Labelled water		Extracted water		Labelled water		Extracted water		Labelled water	
	$\delta^{18}O$	$\delta^{2}H$	$\delta^{18}O$	$\delta^{2}H$	$\delta^{18}O$	$\delta^{2}H$	$\delta^{18}O$	$\delta^{2}H$	$\delta^{18}O$	$\delta^{2}H$	$\delta^{18}O$	$\delta^{2}H$
1	−9.64	−75.42	−9.53	−75.85	−9.43	−64.22	−9.34	−66.12	−9.17	−65.28	−9.34	−66.12
2	−9.64	−75.98	−9.53	−75.95	−9.25	−63.77	−9.33	−66.02	−9.11	−65.18	−9.33	−66.02
3	−9.49	−73.63	−9.53	−75.96	−9.12	−64.41	−9.38	−66.05	−8.88	−65.16	−9.38	−66.05
4	−9.65	−75.55			−9.13	−64.78			−9.31	−65.86		
5	−9.45	−75.27			−9.24	−64.98			−9.30	−64.64		
6	−9.39	−75.28			−9.25	−65.17			−9.70	−65.76		
7	−9.62	−75.20			−9.36	−65.06			−9.43	−64.72		
8	−9.52	−75.89			−9.41	−65.62			−9.17	−64.65		
9	−9.39	−75.31							−9.71	−65.11		
10	−9.35	−75.07							−9.37	−65.12		
11	−9.51	−75.07							−9.70	−65.09		
12									−9.23	−64.70		
13												
14												
15												
Average	−9.51	−75.24	−9.54	−75.92	−9.27	−64.75	−9.35	−66.06	−9.34	−65.11	−9.35	−66.06
SD	0.11	0.58	0.01	0.05	0.11	0.55	0.02	0.05	0.25	0.39	0.02	0.05

Table A2. Statistical test results.

Test		Variance	KS p values	H_0	T-test p values	H_0
First	$\delta^{18}O$	0.004	0.870	True	0.052	True
	$\delta^{2}H$	0.134	0.837	True	0.553	True
Second	$\delta^{18}O$	0.007	0.766	True	0.284	True
	$\delta^{2}H$	0.126	0.976	True	0.004	False
Third	$\delta^{18}O$	0.018	0.985	True	0.337	True
	$\delta^{2}H$	0.270	0.983	True	0.002	False
Fourth	$\delta^{18}O$	0.012	0.786	True	0.440	True
	$\delta^{2}H$	0.375	0.228	True	0.004	False
Fifth	$\delta^{18}O$	0.014	0.933	True	0.121	True
	$\delta^{2}H$	0.349	0.978	True	4×10^{-4}	False
Sixth	$\delta^{18}O$	0.068	0.850	True	0.909	True
	$\delta^{2}H$	0.162	0.761	True	4×10^{-6}	False

KS H_0: the data set has a normal distribution. T-test H_0: the sample mean is equal to the reference value. True denotes an acceptance of the null hypothesis, and false denotes a rejection of it. The values were rounded to three valid decimal figures, respecting the uncertainty of the experimental errors.

Appendix B

Table B1. List of used components.

Component	Type	Supplier	Reference (last access: 1 July 2025)	Quantity	Price (EUR)
Oven	VT 332 CX	MORA MORAVIA, s.r.o	https://www.alza.cz/mora-vt-332-cx-d6977919.htm?o=1	1	219
Stainless steel bowl	1400 mL	GoEco	https://www.dedra.cz/sk/da30751-dozivotni-celonerezova-doza	4	96
Spiral cooler	Dimroth 14/23	VERKON, s.r.o.	https://www.verkon.cz/chladic-spiralovy-dle-dimrotha/?keyword=dimrotha	4	549
Customized glass	Fig. 3	Institute of Chemical Technology in Prague		8	239
Fan	PF40281B1-000U-A99	SUNON	https://www.gme.cz/v/1500620/sunon-pf40281b1-000u-a99-dc-ventilator	8	132
Control unit and accessories	Arduino	Arduino	https://store.arduino.cc/?gad_=1&gclid=CjwKCAjwkJm0BhBxEiwAwT1AXIKf44cTbvuNm3HGYdzOgppb_OPpGEhaKcywffRo7OP_m2G709MI9RoCE-EQAvD_BwE	–	80
Aluminium profile	40 × 40 – 104 040	ALUTEC KK, s.r.o.	https://katalog.aluteckk.cz/produkt/profil-40x40-104040/	13 m	449
Silicon tube	R973851; R098081	P-LAB	https://www.p-lab.cz/hadicka-silikonova-silnostenna?search=hadice	25 m	510
Glass elbow	14/23	VERKON, s.r.o.	https://www.verkon.cz/koleno-s-nz/?keyword=koleno	4	45
Temperature sensors	(TP-01) K	HOTAIR	https://www.hotair.cz/detail/merici-pristroje/teplomery-a-sondy/	4	40
Technical stainless steel fabric	2/0.56/1000 mm	Euro Sitex, s.r.o.	https://eshop.eurositex.cz/produkt/281/technicka-tkanina-nerezova-2-0-56-1000-mm/	1	52
	0.05/0.035/1000 mm	Euro Sitex, s.r.o.	https://eshop.eurositex.cz/produkt/257/technicka-tkanina-nerezova-0-05-0-035-1000-mm/	1	73
Hose couplings	R034351	P-LAB	https://www.p-lab.cz/spojka-hadicova-system-keck?v=R035451_V_7406	15	96
	R034351			10	84
3D printing material	PETG	Prusa Research a.s.	https://www.prusa3d.com/cs/produkt/prusament-petg-jet-black-2kg/	4 kg	95
Rubber hose insulation	KAIFLEX EF	HORNBACH BAUMARKT CS, s.r.o.	https://www.hornbach.cz/p/potrubni-izolace-kaiflex-ef-tube-ef-o-22-mm-sirka-vrstvy-13-mm-delka-1-m/5852909/	8	12
Other components	Fittings; hose holders, reducers; bolts and nuts	–	–	–	239
				Total	3010

Code availability. The code is available from the corresponding author upon request.

Data availability. The data from this study are fully available in Table A1.

Author contributions. Concept: JH, OG. Methodology: JK, JH, OG. Software: JH, OG. Investigation: JK. Validation: JK, KF, VS, MS, LV. Visualization: JK. Writing (original draft preparation): JK, KF. Writing (review and editing): JK, JH, OG, KF, VS, MS, NO, LV. Supervision: LV.

Competing interests. At least one of the (co-)authors is a member of the editorial board of *Hydrology and Earth System Sciences*. The peer-review process was guided by an independent editor, and the authors also have no other competing interests to declare.

Disclaimer. Publisher's note: Copernicus Publications remains neutral with regard to jurisdictional claims made in the text, published maps, institutional affiliations, or any other geographical representation in this paper. While Copernicus Publications makes every effort to include appropriate place names, the final responsibility lies with the authors.

Acknowledgements. The authors warmly thank Petr Filip at the Institute of Hydrodynamics of the Czech Academy of Sciences for his help in the final revision of the paper. We are also grateful to three anonymous reviewers for their useful comments on an earlier version of the paper.

Financial support. This work was supported by the Czech Academy of Sciences (grant no. RVO 67985874), the research programme Strategy AV21 Water for Life, the Czech Science Foundation (grant no. GA CR 22-12837S); the Faculty of Science of Charles University in Prague (grant no. SVV 244-2606941), and the German Federal Environmental Foundation (DBU).

Review statement. This paper was edited by Genevieve Ali and reviewed by three anonymous referees.

References

Araguás-Araguás, L., Rozanski, K., Gonfiantini, R., and Louvat, D.: Isotope effects accompanying vacuum extraction of soil water for stable isotope analyses, J. Hydrol., 168, 159–171, https://doi.org/10.1016/0022-1694(94)02636-P, 1995.

Barrow, N. J. and Whelan, B. R.: A study of a method for displacing soil solution by centrifuging with an immiscible liquid, J. Environ. Qual., 9, 315–319, https://doi.org/10.2134/jeq1980.00472425000900020031x, 1980.

Batley, G. and Giles, M.: Solvent displacement of sediment interstitial waters before trace metal analysis, Water Res., 13, 879–886, https://doi.org/10.1016/0043-1354(79)90223-9, 1979.

Barrie, J. A. and Machin. D.: The sorption and diffusion of water in silicone rubbers: Part I. Unfilled rubbers, J. Macromol. Sci. B, 3, 645–672, https://doi.org/10.1080/00222346908217112, 1969.

Böttcher, G., Brumsack, H.-J., Heinrichs, H., and Pohlmann, M.: A new high-pressure squeezing technique for pore fluid extraction from terrestrial soils, Water Air Soil Pollut., 94, 289–296, https://doi.org/10.1007/BF02406064, 1997.

Brumsack, H., Zuleger, E., Gohn, E., and Murray, R.: Stable and radiogenic isotopes in pore waters from leg 127, Japan Sea, in: Proceedings of the Ocean Drilling Program, edite by: Pisciotto, K., Ingle, J., von Breymann, M., and Barron, J., Sci. Res., 127/128, 635–650, https://doi.org/10.2973/odp.proc.sr.127128-1.165.1992, 1992.

Ceperley, N., Gimeno, T. E., Jacobs, S. R., Beyer, M., Dubbert, M., Fischer, B., Geris, J., Holko, L., Kübert, A., Le Gall, S., Lehmann, M. M., Llorens, P., Millar, C., Penna, D., Prieto, I., Radolinski, J., Scandellari, F., Stockinger, M., Stumpp, C., Tetzlaff, D., van Meerveld, I., Werner, C., Yildiz, O., Zuecco, G., Barbeta, A., Orlowski, N., and Rothfuss, Y.: Toward a common methodological framework for the sampling, extraction, and isotopic analysis of water in the Critical Zone to study vegetation water use, WIREs Water, 11, e1727, https://doi.org/10.1002/wat2.1727, 2024.

Craig, H.: Standard for reporting concentrations of deuterium and oxygen-18 in natural waters, Science, 133, 1833–1834, https://doi.org/10.1126/science.133.3467.1833, 1961.

Dansgaard, W.: Stable isotopes in precipitation, Tellus, 16, 436–468, https://doi.org/10.1111/j.2153-3490.1964.tb00181.x, 1964.

Dalton, F. N.: Plant root water extraction studies using stable isotopes, Plant Soil, 111, 217–221, https://doi.org/10.1007/BF02139942, 1988.

Gaj, M. and McDonell, J. J.: Possible soil tension controls on the isotopic equilibrium fractionation factor for evaporation from soil, Hydrol. Process., 33, 1629–1634, https://doi.org/10.1002/hyp.13418, 2019.

Gaj, M., Beyer, M., Koeniger, P., Wanke, H., Hamutoko, J., and Himmelsbach, T.: In situ unsaturated zone water stable isotope (^{2}H and ^{18}O) measurements in semi-arid environments: a soil water balance, Hydrol. Earth Syst. Sci., 20, 715–731, https://doi.org/10.5194/hess-20-715-2016, 2016.

Gaj, M., Kaufhold, S., and McDonnell, J. J.: Potential limitation of cryogenic vacuum extractions and spiked experiments, Rapid Commun. Mass Sp., 31, 821–823, https://doi.org/10.1002/rcm.7850, 2017.

Garvelmann, J., Külls, C., and Weiler, M.: A porewater-based stable isotope approach for the investigation of subsurface hydrological processes, Hydrol. Earth Syst. Sci., 16, 631–640, https://doi.org/10.5194/hess-16-631-2012, 2012.

Goebel, T. S. and Lascano, R. J.: System for high throughput water extraction from soil material for stable isotope analysis of water, Journal of Analytical Sciences, Method. Instrum., 2, 203–207, https://doi.org/10.4236/jasmi.2012.24031, 2012.

Gralher, B., Herbstritt, B., Weiler, M., Wassenaar, L. I., and Stumpp, C.: Correcting Laser-Based Stable Isotope Reading Biased by

Carrier Gas Changes, Environ. Sci. Technol., 50, 7047–7081, https://doi.org/10.1021/acs.est.6b01124, 2016.

Hendry, M. J., Schmeling, E., Wassenaar, L. I., Barbour, S. L., and Pratt, D.: Determining the stable isotope composition of pore water from saturated and unsaturated zone core: improvements to the direct vapour equilibration laser spectrometry method, Hydrol. Earth Syst. Sci., 19, 4427–4440, https://doi.org/10.5194/hess-19-4427-2015, 2015.

Hsieh, J. C. C., Savin, S. M., Kelly, E. F., and Chadwick, O. A.: Measurement of soil-water $\delta^{18}O$ values by direct equilibration with CO_2, Geoderma, 82, 255–268, https://doi.org/10.1016/S0016-7061(97)00104-3, 1998.

Ignatev, A., Velivetckaia, T., Sugimoto, A., and Ueta, A.: A soil water distillation technique using He-purging for stable isotope analysis, J. Hydrol., 498, 265–273, https://doi.org/10.1016/j.jhydrol.2013.06.032, 2013.

Ishimaru, H., Itoh, K., Ishigaki, T., and Furutate, M.: Fast pump-down aluminum ultrahigh vacuum system, J. Vacuum Sci. Technol., 10, 547–552, https://doi.org/10.1116/1.578186, 1992.

Jusserand, C.: Pore water extraction from sediment and soil: Oxygen-18 abundances comparisons between different techniques. First results, Catena, 7, 87–96, https://doi.org/10.1016/S0341-8162(80)80006-3, 1980.

Kelln, C. J., Wassenaar, L. I., and Hendry, M. J.: Stable Isotopes ($\delta^{18}O$, $\delta^{2}H$) of Pore Waters in Clay-Rich Aquitards: A Comparison and Evaluation of Measurement Techniques, Ground Water Monit. R., 21, 108–116, https://doi.org/10.1111/j.1745-6592.2001.tb00306.x, 2001.

Kendall, C. and Coplen, T. B.: Multi-sample conversion of water to hydrogen by zinc for stable isotope determination, Anal. Chem., 57, 1437–1440, https://doi.org/10.1021/ac00284a058, 1985.

Koehler, G., Wassenaar, L. I., and Hendry, M. J.: An Automated Technique for Measuring δD and $\delta^{18}O$ Values of Porewater by Direct CO_2 and H_2 Equilibration, Anal. Chem., 72, 5659–5664, https://doi.org/10.1021/ac000498n, 2000.

Koeniger, P., Marshall, J. D., Link, T., and Mulch, A.: An inexpensive, fast, and reliable method for vacuum extraction of soil and plant water for stable isotope analyses by mass spectrometry, Rapid Commun. Mass Sp., 25, 3041–3048, https://doi.org/10.1002/rcm.5198, 2011.

Kübert, A., Paulus, S., Dahlmann, A., Werner, C., Rothfuss, Y., Orlowski, N., and Dubbert, M.: Water stable isotopes in ecohydrological field research: comparison between in situ and destructive monitoring methods to determine soil water isotopic signatures, Plant Sci., 11, 387, https://doi.org/10.3389/fpls.2020.00387, 2020.

Leaney, F. W., Smettem, K. R. J., and Chittleborough, D. J.: Estimating the contribution of preferential flow to subsurface runoff from a hillslope using deuterium and chloride, J. Hydrol., 147, 83–103, https://doi.org/10.1016/0022-1694(93)90076-L, 1993.

McConville, C., Kalin, R. M., and Flood, D.: Direct equilibration of soil water for $\delta^{18}O$ analysis and its application to tracer studies, Rapid Commun. Mass Sp., 13, 1339–1345, https://doi.org/10.1002/(SICI)1097-0231(19990715)13:13<1339::AID-RCM559>3.0.CO;2-N, 1999.

Meißner, M., Köhler, M., Schwendenmann, L., Hölscher, D., and Dyckmans, J.: Soil water uptake by trees using water stable isotopes ($\delta^{2}H$ and $\delta^{18}O$) – a method test regarding soil moisture, texture and carbonate, Plant Soil, 376, 327–335, https://doi.org/10.1007/s11104-013-1970-z, 2014.

Mora, G. and Jahren, A. H.: Isotopic evidence for the role of plant development on transpiration in deciduous forests of southern United States, Global Biogeochem. Cy., 17, 13-1–13-7, https://doi.org/10.1029/2002GB001981, 2003.

Mubarak, A. and Olsen, R.: Immiscible displacement of soil solution by centrifugation, Soil Sci. Soc. Am. J., 40, 329–331, 1976.

Munksgaard, N. C., Cheesman, A. W., Wurster, C. M., Cernusak, L. A., and Bird, M. I.: Microwave extraction–isotope ratio infrared spectroscopy (ME-IRIS): a novel technique for rapid extraction and in-line analysis of $\delta^{18}O$ and $\delta^{2}H$ values of water in plants, soils and insects, Rapid Commun. Mass Sp., 28, 2151–2161, https://doi.org/10.1002/rcm.7005, 2014.

Newberry, S. L., Prechsl, U. E., Pace, M., and Kahmen, A.: Tightly bound soil water introduces isotopic memory effects on mobile and extractable soil water pools, Isot. Environ. Healt. S., 52, 368–381, https://doi.org/10.1080/10256016.2017.1302446, 2017.

O'Kelly, B. C.: Accurate Determination of Moisture Content of Organic Soils Using the Oven Drying Method, Dry. Technol., 22, 1767–1776, https://doi.org/10.1081/DRT-200025642, 2004.

O'Kelly, B. C.: Oven-Drying Characteristics of Soil of Different Origins, Dry. Technol., 23, 1141–1149, https://doi.org/10.1081/DRT-200059149, 2005.

Orlowski, N. and Breuer, L.: Sampling soil water along pF curve for $\delta^{2}H$ and $\delta^{18}O$ analysis, Hydrol. Process., 34, 4959–4972, https://doi.org/10.1002/hyp.13916, 2020.

Orlowski, N., Frede, H.-G., Brüggemann, N., and Breuer, L.: Validation and application of a cryogenic vacuum extraction system for soil and plant water extraction for isotope analysis, J. Sensors Sensor Syst., 2, 179–193, https://doi.org/10.5194/jsss-2-179-2013, 2013.

Orlowski, N., Breuer, L., and McDonell, J. J.: Critical issues with cryogenic extraction of soil water for stable isotope analysis, Ecohydrology, 9, 3–10, https://doi.org/10.1002/eco.1722, 2016a.

Orlowski, N., Pratt, D. L., and McDonell, J. J.: Intercomparison of soil pore water extraction methods for stable isotope analysis, Hydrol. Process., 30, 3433–3449, https://doi.org/10.1002/hyp.10870, 2016b.

Orlowski, N., Breuer, L., Angeli, N., Boeckx, P., Brumbt, C., Cook, C. S., Dubbert, M., Dyckmans, J., Gallagher, B., Gralher, B., Herbstritt, B., Hervé-Fernández, P., Hissler, C., Koeniger, P., Legout, A., Macdonald, C. J., Oyarzún, C., Redelstein, R., Seidler, C., Siegwolf, R., Stumpp, C., Thomsen, S., Weiler, M., Werner, C., and McDonnell, J. J.: Inter-laboratory comparison of cryogenic water extraction systems for stable isotope analysis of soil water, Hydrol. Earth Syst. Sci., 22, 3619–3637, https://doi.org/10.5194/hess-22-3619-2018, 2018.

Orlowski, N., Pratt, D. L., and McDonnell, J. J.: Intercomparison of soil pore water extraction methods for stable isotope analysis and interpretation of hillslope runoff sources, Hydrol. Process., 33, 2939–2954, https://doi.org/10.1002/hyp.13539, 2019.

Penna, D., Stenni, B., Šanda, M., Wrede, S., Bogaard, T. A., Gobbi, A., Borga, M., Fischer, B. M. C., Bonazza, M., and Chárová, Z.: On the reproducibility and repeatability of laser absorption spectroscopy measurements for $\delta^{2}H$ and $\delta^{18}O$ isotopic analysis, Hydrol. Earth Syst. Sci., 14, 1551–1566, https://doi.org/10.5194/hess-14-1551-2010, 2010.

Penna, D., Stenni, B., Šanda, M., Wrede, S., Bogaard, T. A., Michelini, M., Fischer, B. M. C., Gobbi, A., Mantese, N., Zuecco, G., Borga, M., Bonazza, M., Sobotková, M., C̆ejková, B., and Wassenaar, L. I.: Technical Note: Evaluation of between-sample memory effects in the analysis of δ^2H and δ^{18}O of water samples measured by laser spectroscopes, Hydrol. Earth Syst. Sci., 16, 3925–3933, https://doi.org/10.5194/hess-16-3925-2012, 2012.

Peters, L. I. and Yakir, D.: A direct and rapid leaf water extraction method for isotopic analysis, Rapid Commun. Mass Sp., 22(18), 2929–2936, https://doi.org/10.1002/rcm.3692, 2008.

Revesz, K. and Woods, P. H.: A method to extract soil water for stable isotope analysis, J. Hydrol., 115, 397–406, https://doi.org/10.1016/0022-1694(90)90217-L, 1990.

Rothfuss, Y., Vereecken, H., and Brüggemann, N.: Monitoring water stable isotopic composition in soils using gas-permeable tubing and infrared laser absorption spectroscopy, Water Resour. Res., 49, 1–9, https://doi.org/10.1002/wrcr.20311, 2013.

Rothfuss, Y., Merz, S., Vanderborght, J., Hermes, N., Weuthen, A., Pohlmeier, A., Vereecken, H., and Brüggemann, N.: Long-term and high-frequency non-destructive monitoring of water stable isotope profiles in an evaporating soil column, Hydrol. Earth Syst. Sci., 19, 4067–4080, https://doi.org/10.5194/hess-19-4067-2015, 2015.

Scrimgeour, C. M.: Measurement of plant and soil water isotope composition by direct equilibration methods, J. Hydrol., 172, 261–274, https://doi.org/10.1016/0022-1694(95)02716-3, 1995.

Sprenger, M., Herbstritt, B., and Weiler, M.: Established methods and new opportunities for pore water stable isotope analysis, Hydrol. Process., 29, 5174–5192, https://doi.org/10.1002/hyp.10643, 2015.

Stumpp, C., Brüggemann, N., and Wingate, L.: Stable Isotope Approaches in Vadose Zone Research, Vadose Zone J., 17, 1–7, https://doi.org/10.2136/vzj2018.05.0096, 2018.

Thorburn, P. J., Walker, G. R., and Brunel, J.-P.: Extraction of water from Eucalyptus trees for analysis of deuterium and oxygen-18: laboratory and field techniques, Plant Cell Environ., 16, 269–277, https://doi.org/10.1111/j.1365-3040.1993.tb00869.x, 1993.

Volkmann, T. H. M. and Weiler, M.: Continual in situ monitoring of pore water stable isotopes in the subsurface, Hydrol. Earth Syst. Sci., 18, 1819–1833, https://doi.org/10.5194/hess-18-1819-2014, 2014.

Walker, G. R., Woods, P. H., and Allison, G. B.: Interlaboratory comparison of methods to determine the stable isotope composition of soil water, Chem. Geol., 111, 297–306, https://doi.org/10.1016/0009-2541(94)90096-5, 1994.

Wassenaar, L. I., Hendry, M. J., Chostner, V. L., and Lis, G. P.: High Resolution Pore Water δ^2H and δ^{18}O Measurements by $H_2O_{(liquid)}$-$H_2O_{(vapor)}$ Equilibration Laser Spectroscopy, Environ. Sci. Technol., 42, 9262–9267, https://doi.org/10.1021/es802065s, 2008.

Wassenaar, L. I., Ahmad, M., Aggarwal, P., van Duren, M., Pöltenstein, L., Araguas, L., and Kurttas, T.: Worldwide proficiency test for routine analysis of δ^2H and δ^{18}O in water by isotope-ratio mass spectrometry and laser absorption spectroscopy, Rapid Commun. Mass Sp., 26, 1641–1648, https://doi.org/10.1002/rcm.6270, 2012.

Wershaw, R. L., Friedman, I., Heller, S. J., and Frank, P. A.: Hydrogen isotopic fractionation of water passing through trees, in: Advances in Organic Geochemistry: Proceedings of the Third International Congress, edited by: Hobson, F. and Speers, M., Pergamon Press Ltd., Elsevier, New York, USA, 55–67, https://doi.org/10.1016/B978-0-08-012758-3.50007-4, 1966.

West, A. G., Patrickson, S. J., and Ehleringer, J. R.: Water extraction times for plant and soil materials used in stable isotope analysis, Rapid Commun. Mass Sp., 20, 1317–1321, https://doi.org/10.1002/rcm.2456, 2006.

White, J. W. C., Cook, E. R., Lawrence, J. R., and Wallace, S. B.: The D/H ratios of sap in trees: Implications for water sources and tree ring D/H ratios, Geochim. Cosmochim. Ac., 49, 237–246, https://doi.org/10.1016/0016-7037(85)90207-8, 1985.

Yang, B., Dossa, G. G. O., Hu, Y. H., Liu, L. L., Meng, X. J., Du, Y. Y., Li, J. Y., Zhu, X. A., Zhang, Y. J., Singh, A. K., Yuan, X., Wu, J. E., Zakari, S., Liu, W. J., and Song, L.: Uncorrected soil water isotopes through cryogenic vacuum distillation may lead to a false estimation on plant water source, Method. Ecol. Evol., 6, 1443–1456, https://doi.org/10.1111/2041-210X.14107, 2023.

Zhu, Q.-Z., Sun, Q., Su, Z.-G., Xie, M.-M., Song, J.-Y., Shan, Y.-B., Wang, N., and Chu, G.-Q.: A Soil Water Extraction Method with Accelerated Solvent Extraction Technique for Stable Isotope Analysis, Chinese J. Anal. Chem., 42, 1270–1275, https://doi.org/10.1016/S1872-2040(14)60766-0, 2014.

7.5 Pan-European dataset of soil and stem xylem water isotopes

The expertise acquired in isotope analysis during the doctoral research, along with collaborative networks established through the WATSON COST Action project, contributed to involvement in creating of the first pan-European systematic dataset of soil and stem xylem water isotopes. The resulting study, *Soil and stem xylem water isotope data from two pan-European sampling campaigns* (Lehmann et al., under review), provides stable isotope data of soil and xylem water for two widespread European tree species: Norway spruce (*Picea abies* L.) and European beech (*Fagus sylvatica* L.).

Samples were collected from 39 sites across 18 European countries. The Czech Republic is represented by two locations: the Uhlířská experimental catchment in the Jizera Mountains (Department of Landscape Water Conservation, Faculty of Civil Engineering, Czech Technical University in Prague) and the Liz experimental catchment. Notably, the Liz site was one of only three locations able to provide data from both habitat types—spruce and beech forest stands.

The dataset is openly accessible and offers a valuable resource for a wide range of ecohydrological applications. These include identifying the factors controlling tree water uptake depth and seasonal water sources, calibrating and constraining isotope-enabled ecohydrological models, developing isoscape models, and investigating species-, soil-, or climate-dependent biases in cryogenic water extraction methods.

Manuscript review stage

The manuscript was submitted to Earth System Science Data on 13 September 2024 and is currently, as of August 2025, undergoing minor revisions following the first round of peer review. Acceptance is anticipated in the coming months.

https://doi.org/10.5194/essd-2024-409
Preprint. Discussion started: 17 October 2024

Open Access Earth System Science Data Discussions

Soil and stem xylem water isotope data from two pan-European sampling campaigns

Marco M. Lehmann[1,*], Josie Geris[2], Ilja van Meerveld[3], Daniele Penna[4], Youri Rothfuss[5], Matteo Verdone[4], Pertti Ala-Aho[6], Matyas Arvai[7], Alise Babre[8], Philippe Balandier[9], Fabian Bernhard[1], Lukrecija Butorac[10], Simon D. Carrière[11], Natalie C. Ceperley[12], Zuosinan Chen[6], Alicia Correa[13], Haoyu Diao[14], David Dubbert[15], Maren Dubbert[15], Fabio Ercoli[16], Marius G. Floriancic[17], Teresa E. Gimeno[18], Damien Gounelle[19], Frank Hagedorn[1], Christophe Hissler[20], Frédéric Huneau[21], Alberto Iraheta[22], Tamara Jakovljević[23], Nerantzis Kazakis[24], Zoltan Kern[25], Karl Knaebel[26], Johannes Kobler[27], Jiri Kocum[28], Charlotte Koeber[15], Gerbrand Koren[29], Angelika Kübert[30], Dawid Kupka[31], Samuel le Gall[5], Aleksi Lehtonen[32], Thomas Leydier[21], Philippe Malagoli[9], Francesca Sofia Manca di Villahermosa[4], Chiara Marchina[33], Núria Martínez-Carreras[20], Nicolas Martin-StPaul[19], Hannu Marttila[6], Aline Meyer Oliveira[3], Gael Monvoisin[34], Natalie Orlowski[35], Kadi Palmik-Das[16], Aurel Persoiu[36], Andrei Popa[37], Egor Prikaziuk[38], Cécile Quantin[34], Katja T. Rinne-Garmston[39], Clara Rohde[15], Martin Sanda[40], Matthias Saurer[14], Daniel Schulz[5], Michael P. Stockinger[26], Christine Stumpp[26], Jean-Stéphane Vénisse[9], Lukas Vlcek[28], Stylianos Voudouris[41], Björn Weeser[13], Mark Wilkinson[42], Giulia Zuecco[33], Katrin Meusburger[1]

[*]*Correspondence to*: Marco M. Lehmann (marco.lehmann@wsl.ch)

[1]Forest Soils and Biogeochemistry, Swiss Federal Institute for Forest, Snow and Landscape Research WSL, Birmensdorf, Switzerland

[2]School of Geosciences, University of Aberdeen, Aberdeen, United Kingdom

[3]Department of Geography, University of Zurich, Zurich, Switzerland

[4]Department of Agriculture, Food, Environment and Forestry (DAGRI), University of Florence, Florence/Firenze, Italy

[5]Institute of Biogeosciences, Agrosphere (IBG-3), Forschungszentrum Jülich GmbH, Jülich, Germany

[6]Water, Energy and Environmental Engineering Research Unit, University of Oulu, Oulu, Finland

[7]Institute for Soil Sciences, HUN-REN Centre for Agricultural Research, Budapest, Hungary

[8]Faculty of Science and Technology, University of Latvia, Riga, Latvia

[9]Université Clermont Auvergne, INRAE, UMR PIAF, Clermont-Ferrand, France

[10]Department of Forestry, Institute for Adriatic Crops and Karst Reclamation, Split, Croatia

[11]UMR METIS, Sorbonne Université, UPMC, CNRS, EPHE, Paris, France

[12]Hydrology Group, Institute of Geography & Oeschger Centre for Climate Change Research, University of Bern, Bern, Switzerland

[13]Centre for International Development and Environmental Research (ZEU), Justus Liebig University Giessen, Germany

[14]Forest Dynamics, Swiss Federal Institute for Forest, Snow and Landscape Research WSL, Birmensdorf, Switzerland

https://doi.org/10.5194/essd-2024-409
Preprint. Discussion started: 17 October 2024

Open Access Earth System Science Data Discussions

[15]Isotope Biogeochemistry and Gas Fluxes, Leibniz Centre for Agricultural Landscape Research (ZALF), Müncheberg, Germany

[16]Chair of Hydrobiology and Fisheries, Institute of Agricultural and Environmental Sciences, Estonian University of Life Sciences, Tartu, Estonia

[17]Department of Civil, Environmental and Geomatic Engineering, ETH Zürich, Zürich, Switzerland

[18]CREAF, Bellaterra, Spain

[19]URFM, INRAE, Domaine Saint Paul, Site Agroparc, Avignon, France

[20]Catchment and Ecohydrology group, Environmental Sensing and Modelling unit, Luxembourg Institute of Science and Technology, Belvaux, Luxembourg

[21]CNRS UMR 6134 SPE, Université de Corse, Corte, France

[22]Institute for Geoecology, TU Braunschweig, Braunschweig, Germany

[23]Division for Forest Ecology, Croatian Forest Research Institute, Jastrebarsko, Croatia

[24]Laboratory of Hydrogeology, Department of Geology, University of Patras, Faculty of Natural Sciences, Rion, Patras, Greece

[25]Institute for Geological and Geochemical Research, HUN-REN Research Centre for Astronomy and Earth Sciences, Budapest, Hungary

[26]Department of Water, Atmosphere and Environment, Institute of Soil Physics and Rural Water Management, University of Natural Resources and Life Sciences, Vienna, Austria

[27]Ecosystem Research & Environmental Information Management, Environment Agency Austria, Vienna, Austria

[28]Institute of Hydrodynamics, Czech Academy of Sciences, Prague, Czech Republic

[29]Copernicus Institute of Sustainable Development, Utrecht University, Utrecht, Netherlands

[30]Institute for Atmospheric and Earth System Research / Physics, University of Helsinki, Helsinki, Finland

[31]Department of Forest Ecology and Silviculture, Faculty of Forestry, University of Agriculture in Kraków, Poland

[32]Natural Resources Institute Finland (Luke), Helsinki, Finland

[33]Department of Land, Environment, Agriculture and Forestry, University of Padova, Legnaro, Italy

[34]Université Paris-Saclay, UMR8148 GEOPS, Orsay, France

[35]Chair of Forest Sites and Hydrology, Institute of Soil Science and Site Ecology, TU Dresden, Tharandt, Germany

[36]Emil Racovita Institute of Speleology, Romanian Academy, Cluj-Napoca, Romania and Stable Isotope Laboratory, Stefan cel Mare University, Suceava, Romania

[37]National Institute for Research and Development in Forestry "Marin Dracea", Bucharest, Romania

[38]Faculty of Geo-Information Science and Earth Observation (ITC), University of Twente, Enschede, Netherlands

[39]Stable Isotope Laboratory of Luke (SILL), Natural Resources Institute Finland (Luke), Finland

[40]Department of Landscape Water Conservation, Faculty of Civil Engineering, Czech Technical University, Prague, Czech Republic

[41]Earth Sciences and Environmental Technologies Division, IFP Energies Nouvelles, Rueil-Malmaison, France

[42]Environmental and Biochemical Sciences, James Hutton Institute, Aberdeen, United Kingdom

https://doi.org/10.5194/essd-2024-409
Preprint. Discussion started: 17 October 2024

Open Access Earth System Science Data Discussions

Abstract. Stable isotope ratios of hydrogen (δ2H) and oxygen (δ18O) are crucial for studying ecohydrological dynamics in forests. However, most studies are confined to single sites, resulting in a lack of large-scale isotope data for understanding tree water uptake. Here, we provide a first systematic isotope dataset of soil and stem xylem water collected during two pan-European sampling campaigns at 40 beech (Fagus sylvatica), spruce (Picea abies), or mixed beech-spruce forest sites in spring and summer 2023 (Lehmann et al., 2024). The dataset is complemented by additional site-, soil-, and tree-specific metadata. The samples and metadata were collected by different researchers across Europe following a standardized protocol. Soil samples were taken at up to 5 depths (ranging from 0 to 90 cm) and stem xylem samples from three beech and/or spruce trees per site. All samples were sent to a single laboratory, where all analytical work was conducted. Water was extracted using cryogenic vacuum distillation and analyzed with an isotope laser spectrometer. Additionally, a subset of the samples was analyzed with an isotope ratio mass spectrometer. Data quality checks revealed a high mean total extraction efficiency, mean absolute water amount (> 1 mL), as well as high analytical accuracy and precision. The water isotopic signature of soil and stem xylem water varied as a function of the geographic origin and changed from spring to summer across all sites. While δ^2H and $\delta^{18}O$ values were strongly correlated, the soil water data plotted closer to the Global Meteoric Water Line (GMWL) than the stem xylem water. Specifically, the δ^2H values of the stem xylem were more enriched than those of the soil water, leading to a systematic deviation from the GMWL. Isotopic enrichment of the stem xylem water was larger for spruce than for beech trees at mixed forest sites. This dataset is particularly useful for large-scale studies on plant water use, ecohydrological model testing, and isotope mapping across Europe.

Keywords: Critical Zone Science, Europe, Forest, Hydrology, Hydrogen Isotopes, Oxygen Isotopes, Root Water Uptake, Soil Water Recharge, Water Stable Isotopes, Water Sources.

1 Introduction

Understanding how tree water uptake from soils varies with species, site characteristics, time, and across climate zones is essential to assess forest resilience to climate change; particularly the response of forests to the increasing frequency and intensity of droughts (Lindner et al., 2010; Spinoni et al., 2014; Büntgen et al., 2021). Despite some uncertainties, the stable isotope ratios of hydrogen (δ^2H) and oxygen ($\delta^{18}O$) in water extracted from soil and plants allow for the determination of the sources of water that are used by plants and to quantify the relative contribution of different water sources to plant water use (Rothfuss and Javaux, 2017; Beyer and Penna, 2021). Determination of water uptake patterns based on isotope data assumes that roots do not discriminate against the heavier hydrogen and oxygen stable isotopes during water uptake (Poca et al., 2019). Additionally, it is assumed that: (i) the sampling design captures the spatiotemporal variability of the isotopic composition of soil water sources, (ii) the water extracted from the plant xylem is a mixture of the different water sources taken up from the soil profile without isotopic alteration (e.g., due to stem evaporation or leaf transpiration, see Ellsworth and Sternberg (2015), and (iii) soil and xylem samples are collected, transported, stored, and extracted in a manner that avoids isotope fractionation (Ceperley et al., 2024). Although these assumptions are not always met, the method described here—

https://doi.org/10.5194/essd-2024-409
Preprint. Discussion started: 17 October 2024

whether used independently or in combination with others—can effectively test our understanding of the mechanisms driving plant responses to both short- and long-term droughts. It is also now affordable enough for practical applications beyond the field of isotope ecohydrology (Penna et al., 2018). Isotope-based analyses in forest ecosystems have, for example, been used to determine the changes in root water uptake depths of trees in response to drought (Brinkmann et al., 2018; Gessler et al., 2022), whether trees use summer or winter precipitation (Allen et al., 2019; Floriancic et al., 2024a), soil water, groundwater, or streamwater (Bowling et al., 2017; Engel et al., 2022), or to assess competitive or complementary water use strategies (Penna et al., 2020; Kinzinger et al., 2024). However, systematic datasets at large scales, i.e., spanning continents or multiple countries, are lacking. This hampers our understanding of how water uptake strategies for the same tree species vary across space and time (Beyer and Penna, 2021; Orlowski et al., 2023; Dubbert and Werner, 2019; Bachofen et al., 2024).

There are established networks for the observation of isotopes in freshwater systems, such as precipitation by the International Atomic Energy Agency (IAEA) Global Network of Isotopes in Precipitation (GNIP), which currently contains data for 300 active sites in 93 countries (Terzer-Wassmuth et al., 2023). The Global Network of Isotopes in Rivers (GNIR) contains data from 750 sites in 35 countries (Halder et al., 2015). Both networks have proven to provide valuable input data for modeling of the local to regional climate or surface-atmosphere water interactions with process-based (e.g., CLM, Wong et al. (2017), ISOLSM Cai et al. (2015), ECHAM5-JSBACH Haese et al. (2013)) or statistical models (e.g., Isoscapes (Bowen, 2010; Terzer et al., 2013; Allen et al., 2018; Koeniger et al., 2022), and time series analyses (Nelson et al., 2021; Erdélyi et al., 2023; Reckerth et al., 2017). They have furthermore helped to assess water flow pathways and the fraction of young water in streamflow (Von Freyberg et al., 2018; Floriancic et al., 2024b). The Moisture Isotopes in Biosphere and Atmosphere (MIBA) network, initiated by the IAEA in 2003-2004, is, to our knowledge, the only international network to survey the isotopic composition of water across different ecosystem compartments (i.e., soil, plant stems and leaves, soil, and atmospheric vapor). However, despite the global distribution of sites at the time of the establishment and a local application in Australia (Twining et al., 2006), the network is currently inactive.

Building on the idea of the MIBA and the proven usefulness of national large-scale sampling campaigns to determine regional differences in tree water uptake (Allen et al., 2019), the COST Action "WATer isotopeS in the critical zONe: from groundwater recharge to plant transpiration WATSON" (CA19120) organized two sampling campaigns across Europe in 2023. The effort took advantage of the European network of researchers to establish a unique systematic water isotope dataset and corresponding metadata. More specifically, the goal of the sampling campaigns was to obtain soil and stem xylem water isotope data of two tree species, namely beech (*Fagus sylvatica* L.) and spruce (*Picea abies* (L.) H. Karst) across a large climate gradient for the spring (25th May to 16th June) and summer (17th August to 18th September) of 2023. The two time points were selected to compare tree water uptake patterns under different soil moisture conditions (e.g., lower soil moisture in summer). The two species were selected because of their wide geographical distribution across Europe (Figure 1) and their important ecological and economical relevance, as well the expected differences in water uptake depth (Allen et al. 2019; Brinkmann et al. 2018; Goldsmith et al. 2019) with beech having a deeper rooting system than spruce.

During the European sampling campaigns, a total of 381 soil and 311 stem xylem samples were taken from 40 sites across 18 countries, following a standardized protocol. The water of these samples was cryogenically extracted and isotopically analyzed in a single laboratory. The simultaneous collection of soil and stem xylem

https://doi.org/10.5194/essd-2024-409
Preprint. Discussion started: 17 October 2024

samples across all European sites, combined with a centralized processing of the samples, ensures the uniqueness of this dataset. Using one laboratory prevents inconsistencies that might arise from varying sample handling and analysis methods, which can influence isotopic offsets (Orlowski et al., 2016; Orlowski et al., 2018). The isotope dataset is accompanied by site-, soil-, and tree-specific metadata at each location. Together, the metadata and isotope data provide a strong foundation for research on tree water use, model testing, and isotope mapping. This manuscript outlines the sample collection process, cryogenic water extraction, and isotope analysis, and details the dataset organization and metadata. Finally, we give an overview of the data and discuss potential applications. The full dataset is freely available (Lehmann et al., 2024).

2 Material and Methods

2.1 Organization of the WATSON pan-European sampling campaigns

During the initial phase (spring 2023), the members of the WATSON community (~200 members at that time) were contacted to assess their interest in participating in a coordinated sampling campaign. Based on the large interest, a core team was formed. The core team asked researchers from a similar region to form one team to keep the laboratory and analytical work manageable, while still obtaining samples from a broad geographic region. The core team wrote detailed instructions to ensure systematic sampling. The instructions provided detailed standardized protocols for collecting soil and stem xylem samples, including specifications for sampling depths, core dimensions and numbers, and the maximum number of samples. The protocols also covered short-term sample storage and shipment to the Swiss Federal Institute for Forest, Snow, and Landscape Research in Birmensdorf, Switzerland (WSL Birmensdorf), where all cryogenic water extractions and isotopic analyses were performed. In addition, participants were given instructions on how to take pictures for canopy cover analysis and the list of required metadata (e.g., geographical parameters, soil properties, tree diameter and height). The instructions were emailed to all interested contributors prior to the first sampling campaign in spring 2023 (Section S1). For the second campaign in summer 2023, the sampling protocol was slightly updated for clarity (i.e., weather conditions at sampling day, bark removal during stem xylem sampling, labelling of exetainers, taking photos) and emailed to all interested contributors again (Section S2). In addition, we held an online meeting between the two sampling campaigns to provide feedback to the participants, clarify any field issues, and answer questions.

2.2 Description of the sampling sites

Samples were taken from 40 different mono-specific and mixed forest sites with beech trees (*Fagus sylvatica*; 14 sites), spruce trees (*Picea abies;* 13 sites), or both tree species (13 sites) in 18 European countries (Figure 1; Table 1): 36 sites were sampled in the spring and 39 sites in the summer. For 35 of the 40 sites, samples were collected during both campaigns. In three of the sampling sites, separate beech (LIZ1, GLS1, WEI1) and spruce (LIZ2, GLS2, WEI2) stands were found close to each other (i.e. the sampling sites share the same geographic coordinates). Although there was a good cover of sites across central Europe for both species, most north-eastern sites were sampled for spruce only, while the spread of sampled beech trees extended more to south-western Europe. The sampling sites correspond to the natural and naturalised ranges of the tree species across Europe (Figure 1) and cover a range of temperate (Köppen-Geiger Cfa, Cfb, Csb) and cold (Köppen-Geiger Dfb, Dfc) climates. The

https://doi.org/10.5194/essd-2024-409
Preprint. Discussion started: 17 October 2024

sampling sites also differed in elevation (14 to 1870 m a.s.l.; Table 1). The sampling sites were evenly distributed across different slopes (i.e., flat, gentle, and steep). Most sites were located on Cambisols or Leptosols; with just one Histosol (i.e., peat at the site ROT in Finland). The maximum existing soil depth varied between 0.3 m and > 1 m and for half of the sites, the maximum soil depth was > 0.6 m. Canopy cover was determined for 30 of the 40 sampling sites from non-hemispherical photographs taken with a phone camera, as described in Section S3. Most of the pictures were taken during the spring campaign, however, for some sites, pictures were taken during the summer campaign or both campaigns. For the sites for which canopy cover could be determined, it was generally higher for the beech trees than the spruce trees (Table 1).

Table 1: Summary statistics for sampling campaigns across 40 European beech and spruce study sites, including 13 sites with both species. *Köppen-Geiger classification based on Beck et al. (2023).

		Beech	Spruce
Number of sites		27	26
Number of sites sampled during both campaigns		24	23
Elevation [m a.s.l.]	Min	63	14
	Mean	756	648
	Max	1541	1870
Climate* (Köppen-Geiger classification) [number of sites]	Cfa	1	0
	Cfb	10	6
	Csb	1	0
	Dfb	14	14
	Dfc	1	6
Tree height [m]	Min	7	4
	Mean	22	23
	Max	44	39
Diameter at breast height [cm]	Min	11	8
	Mean	39	36
	Max	87	65
Canopy cover (%)	Min	58	54
	Mean	88	80
	Max	100	94

https://doi.org/10.5194/essd-2024-409
Preprint. Discussion started: 17 October 2024

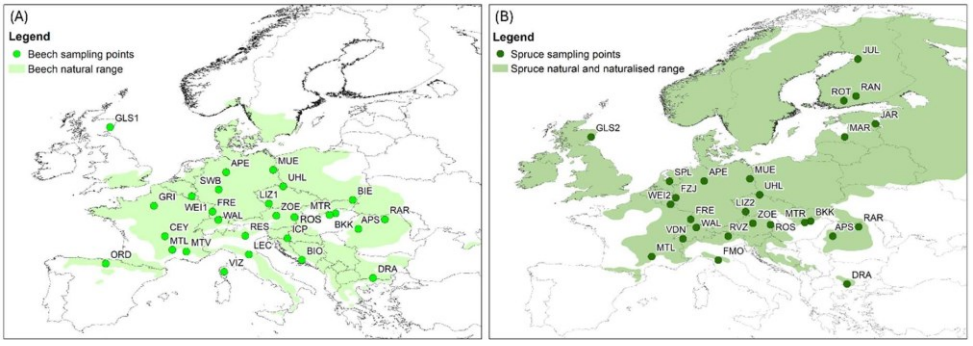

Figure 1. Maps showing the sampling sites (circles) for beech (A) and spruce (B) trees and their natural and naturalised ranges across Europe (shaded areas; data from Caudullo et al. (2017)).

2.3 Sampling, transport, and storage of stem xylem and soil samples

At each sampling site, three beech (*Fagus sylvatica*) and/or three spruce (*Picea abies*) trees were selected based on their representativeness for the stand. The selected spruce and beech trees ranged in size but were similar in mean height (22-23 m) and diameter at breast height (36-39 cm, Table 1). Stem xylem samples were taken from each selected tree at breast height using a 0.5 cm increment borer. Each sample (one per selected tree) consisted of two to three ~5 cm long stem sapwood samples. Most samples consisted of fully intact wood cores; but 9.8% of all stem xylem samples were non-intact stem xylem samples. The outer and inner bark of the wood cores were removed from the cores, yet, bark residue was observed in 40% of all stem xylem samples after cryogenic water extraction. The same three trees were sampled during both campaigns at each site, except at the beech site GRI, where different trees were sampled in spring and summer, and at the beech site MTV, where six samples were taken. This resulted in a total of 311 stem xylem samples.

In addition to the stem xylem samples, soil samples were taken at each site for each sampling campaign with a manual soil auger. The samples were typically taken from one soil core at three to five depths spanning 10 cm intervals (0-10, 10-20, 20-30, 50-60, and 80-90 cm below the surface), but occasionally also for other depths. The number of soil samples and the depth of the deepest soil sample depended on the maximum existing soil depth at the sampling site. The soil samples were taken from a location close to the selected trees. The litter was removed before taking the 0-10 cm soil sample. For some sites and sampling campaigns, soil samples from an additional two to four soil cores were taken. For a few sites with both species (i.e., DRA, FRE, UHL, ZOE), soil cores were separately taken for beech, spruce, and both species. This resulted in a total of 381 soil samples.

Stem xylem and soil samples were transferred into 12 mL gas-tight glass vials (“Exetainers”, Labco, Lampeter, UK). For the soil samples, exetainers were filled with 50-80% of their volume with soil. Some soil and stem xylem samples (13% of all 692 samples) were stored in other types of gas-tight plastic or glass vials. Most samples were taken midday on dry and sunny days. Samples were handled as fast as possible to avoid evaporative fractionation. Back in the laboratory, all samples were stored in a refrigerator to avoid moisture loss to evaporation and subsequent isotope fractionation until transportation. All samples were then shipped without cooling and arrived

https://doi.org/10.5194/essd-2024-409
Preprint. Discussion started: 17 October 2024

within four weeks of the final day of each sampling campaign at the laboratory at WSL Birmensdorf in Switzerland, where they were kept at -20°C until cryogenic water extraction.

2.4 Cryogenic vacuum water extraction

Water was extracted from all 692 samples at WSL Birmensdorf using a cryogenic vacuum distillation method as described in Diao et al. (2022). In brief, the exetainers with the samples were taken from the freezer and fitted with polypropylene fiber filters (Nozzle protection filter, Socorex Isba SA, Ecublens, Switzerland) to prevent particles from being drawn into the extraction line. Samples originally stored in other types of vials were transferred to exetainers that fit the cryogenic vacuum distillation system. Samples were then heated to 80°C in a water bath, while the extraction line was kept under a vacuum of < 5 Pa (BS2212, Brook Crompton Ltd, Doncaster, UK). The extracted water was trapped in U-shaped glass tubes, constantly kept in liquid nitrogen. After a minimum of 2 hours, the water extraction was stopped and atmospheric pressure was established in the extraction line by passing dry nitrogen gas through it. Then, the U-tubes were removed, the ends of the tubes were closed with rubber plugs and the water samples were thawed at room temperature. Depending on the extracted water amount, the water was pipetted to 350 µL or 2 mL glass vials (Infochroma AG, Goldau, Switzerland) and kept frozen at -20°C until isotope analysis. A few samples that appeared turbid after extraction were filtered with 0.45 µm nylon syringe filters (Infochroma AG).

We determined the sample weight before water extraction ("fw"), after water extraction ("dw1"), and after drying at 105°C for 24 hours (dw2) to estimate the absolute water amount ("awa"), the total extraction efficiency ("tef"), and the gravimetric water content (gwc) for each sample (for equations, see Table 3). The sample weights (i.e., "fw", "dw1", "dw2") were corrected for the weight of the exetainer ("exe_weight", Table 3). The latter was based on the mean weight of approximately thirty exetainers for 10 different types ("exe_type", Table 3; i.e., different combinations of glass vials, cap with a rubber seal, and label), which averaged around 13.0 g and varied by a maximum of 0.3 g. Across all soil and stem xylem samples (Figure 2A), "awa" averaged around 1.4 mL, and was well above the critical thresholds for extracted water volume in the vast majority of samples (Diao et al., 2022). The average value for "tef" was 100.6%, and was for most samples (N = 543) within the optimal range of 98-102% (Ceperley et al., 2024). The "gwc" varied between soil samples and stem xylem samples of beech and spruce, averaging around 40.9%, 61.3%, and 83.9%, respectively (Figure 2C). Note that variations in "awa", "tef", and "gwc", and "tef" values > 100%, may partly be due to uncertainties arising from the estimation of the exetainer weight ("exe_weight"; Table 3), reflecting an average value rather than the actual weight of each exetainer.

https://doi.org/10.5194/essd-2024-409
Preprint. Discussion started: 17 October 2024

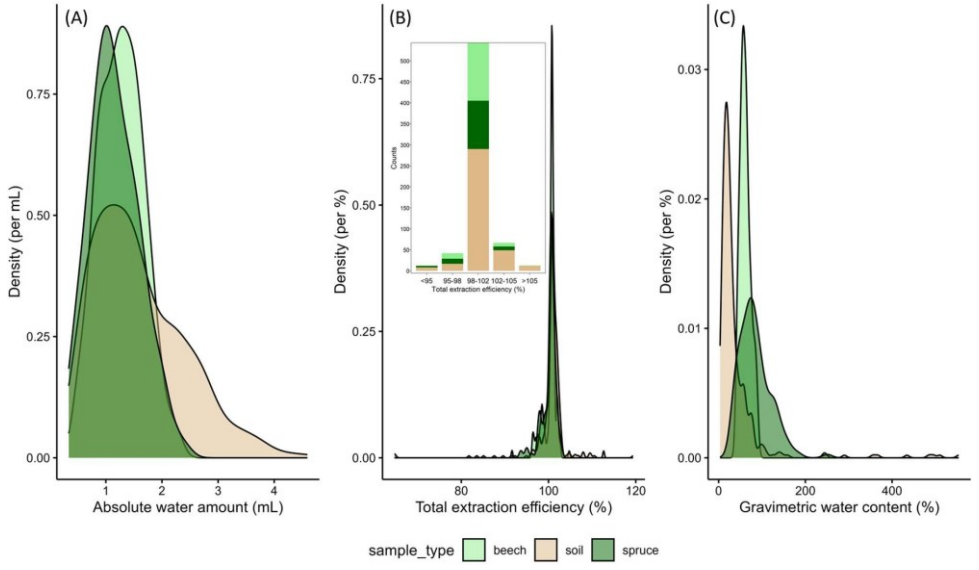

Figure 2: Density plots for (A) the extracted absolute water amounts, (B) the total extraction efficiency (tef), and (C) the gravimetric water content (gwc) for stem xylem (beech and spruce) and soil samples for all samples analysed (i.e., all sites and sampling campaigns). The insert in figure (C) shows the sample count for different types of samples across five different tef classifications.

2.5 Isotope analysis with laser spectrometer and IRMS

The stable isotope ratios of hydrogen (δ^2H) and oxygen ($\delta^{18}O$) of the cryogenically extracted water were measured at WSL Birmensdorf using a cavity ring-down spectrometer (L2140i, Picarro Inc., Santa Clara, USA) connected to a micro-combustion module (MCM) to eliminate sample artefacts caused by co-extracted organic compounds (Martín-Gómez et al., 2015). Each sample was injected eight times and the average of the final five injections was taken to minimize memory effects (Penna et al., 2012). Samples were calibrated with four reference isotope standards spanning from -10.5‰ to -120.2‰ for δ^2H and from -3.0‰ to -16.1‰ for $\delta^{18}O$ (LGR; Envitec NV, Lessines, Belgium) and normalized to the international Vienna Standard Mean Ocean Water (VSMOW-2) scale. The maximum deviation (i.e., accuracy) of an interspersed in-house laboratory standard (analysed every ~25 samples, $\delta^{18}O$: -9.6‰, δ^2H: -84.9‰) from the expected value was ≤ 0.2‰ for $\delta^{18}O$ and ≤ 0.5‰ for δ^2H. The standard deviation (SD) of the repeated measurements of the laboratory standards (i.e., precision) was ≤ 0.1‰ for $\delta^{18}O$ and ≤ 0.6‰ for δ^2H.

To check for spectral interferences with plant-produced volatile organic compounds during the isotope analysis with laser spectrometer, a subset of 83 samples were also analyzed using a thermal combustion/elemental analyzer (TC/EA) coupled to a DeltaPlus XP isotope ratio mass spectrometer (IRMS, Finnigan MAT, Bremen, Germany), with a typical precision of 1.0‰ for δ^2H and 0.2‰ for $\delta^{18}O$. This subset was representative for both sampling campaigns, sample types (stem xylem vs. soil), tree species, geographic locations, and range of isotopic values. The IRMS data were highly correlated with the data of the laser spectrometer (Figures 3A, 3B). Most of the data

https://doi.org/10.5194/essd-2024-409
Preprint. Discussion started: 17 October 2024

were within the range of ± 1 SD and showed a positive offset for both elements (Figure 3C). The δ^2H and $\delta^{18}O$ offset between the two types of analysis had mean values around 0.7‰ and 0.3‰ across all samples (Figure 3C), respectively. These mean offsets represent the average of the differences between the two methods, accounting for both positive and negative values. The SD of these offsets were 1.4‰ for δ^2H and 0.5‰ for $\delta^{18}O$, indicating the variability around the mean offsets, not zero. Paired t-tests across the samples of the subset show that the δ^2H and $\delta^{18}O$ differences between the two analytical methods were significantly ($P < 0.05$) larger for spruce (mean = 0.7‰ and 1.1‰) than for beech (mean = 0.4‰ and 0.7‰) and soils of all depth (only significant for δ^2H; mean = 0.6‰).

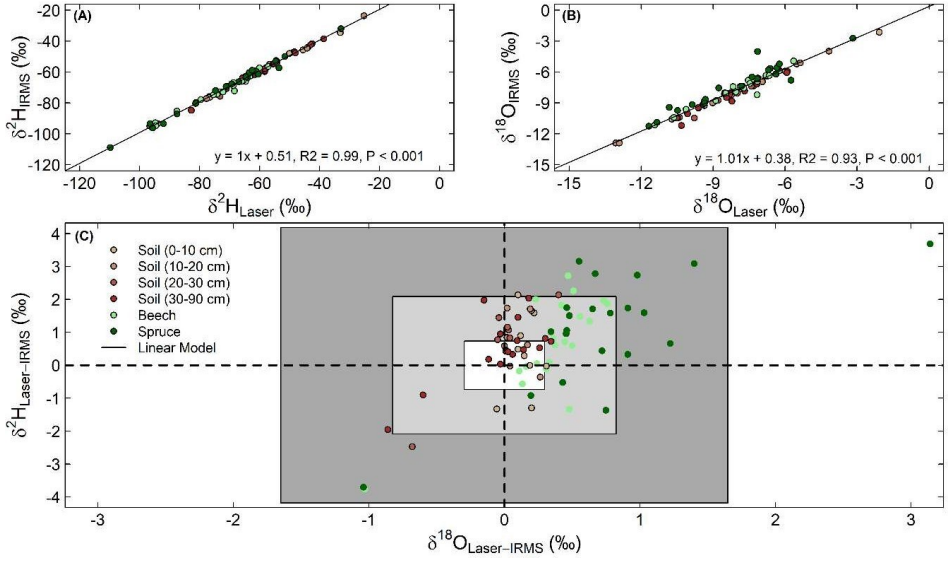

Figure 3: Linear relationships between hydrogen (A; δ^2H) and oxygen (B; $\delta^{18}O$) isotopic composition for the water samples analyzed using a laser spectrometer (Laser) and an isotope ratio mass spectrometer (IRMS). Panel (C) displays a biplot of the differences in the $\delta^{18}O$ and δ^2H values for the two instruments. The small white box in the middle of C represents the mean isotopic difference, while the light grey and dark grey boxes denote ± one and two standard deviations for the isotopic difference, respectively.

2.6 Description of the dataset

The dataset consists of three comma-separated files and one zip file with photos of the canopy at the sampling sites. The first datafile ("WATSON_Metadata.csv") contains all the metadata about the sampling sites including site-, soil- and tree-specific information (Table 2), the second file ("WATSON_Isotopedata.csv") contains the information about sample weights, cryogenic water extraction and the actual hydrogen and oxygen isotope data (Table 3), and the third file ("WATSON_Canopydata.csv") contains the information on the canopy cover (Table 4). The photos on which the canopy cover data are based are stored in the "WATSON_Canopy_Pictures.zip" file. All files can be linked by the "site_id", which is a three-letter identifier of the sampling sites.

Table 2: Description of the columns in the "WATSON_Metadata.csv" file containing all the meta-information about the sampling sites [and units].

https://doi.org/10.5194/essd-2024-409
Preprint. Discussion started: 17 October 2024

Column name	Description
site_id	A three-letter identifier of the sampling site. Note that for the three sites (LIZ, GLS, WEI), an additional number was added indicating the species: "1" refers to beech and "2" to spruce.
site_name	Full site and country name
country_id	A two-letter country code, as defined in ISO 3166-1
latitude	Latitude in decimal degree rounded to three decimals, WGS84 coordinate system
longitude	Longitude in decimal degree rounded to three decimals, WGS84 coordinate system
elevation	Elevation of the sample site [m above sea level]
slope_type	Descriptor of the slope: "flat", "gentle" or "steep"
spruce_site	Descriptor highlighting whether spruce trees were sampled at the site ("yes") or not ("no").
beech_site	Descriptor highlighting whether beech trees were sampled at the site ("yes") or not ("no").
stand_type	Descriptor highlighting whether the stand is a mixed species stand ("mixed") or a monoculture stand ("mono"). Note that "mixed" refers to stands with various species, not limited only spruce and beech.
understory	Descriptor highlighting the presence of understory vegetation ("yes") or not ("no").
soil_type	Soil type according to the FAO classification
soil_texture	Soil texture based on either measurement of the sand, silt and clay content or hand tests in the field (see Section S1, S2).
soil_depth_max	Maximum soil depth [m], for soils deeper than 1 m, > 1 is used.
sampling_doy_spring	Day of the year of sample collection for the spring sampling campaign
sampling_doy_summer	Day of the year of sample collection for the summer sampling campaign
sampling_daytime_spring	Time of the day of sample collection (local time) for the spring sampling campaign. When a start and end time were given, the middle point is recorded.
sampling_daytime_summer	Time of the day of sample collection (local time) for the summer sampling campaign. When a start and end time were given, the middle point is recorded.
height_spruce1	(Estimated) Height of spruce tree 1 [m]
height_spruce2	(Estimated) Height of spruce tree 2 [m]

https://doi.org/10.5194/essd-2024-409
Preprint. Discussion started: 17 October 2024

height_spruce3	(Estimated) Height of spruce tree 3 [m]
height_beech1	(Estimated) Height of beech tree 1 [m]
height_beech2	(Estimated) Height of beech tree 2 [m]
height_beech3	(Estimated) Height of beech tree 3 [m]
dbh_spruce1	Diameter at breast height (DBH) of spruce tree 1 [cm]
dbh_spruce2	Diameter at breast height (DBH) of spruce tree 2 [cm]
dbh_spruce3	Diameter at breast height (DBH) of spruce tree 3 [cm]
dbh_beech1	Diameter at breast height (DBH) of beech tree 1 [cm]
dbh_beech2	Diameter at breast height (DBH) of beech tree 2 [cm]
dbh_beech3	Diameter at breast height (DBH) of beech tree 3 [cm]
koppen	Three letter Köppen-Geiger climate code extracted from Beck et al. (2023).
canopy_cover_picture	Descriptor highlighting whether pictures of the canopy cover (see Table 4) are available in the WATSON_canopy_photos.zip file ("yes") or not ("no").
canopy_cover	Mean canopy cover (C) for the sampling site, reflecting the average value for all photos for a sampling site (varying *n* per sampling site). Calculation of C as described in Section S3.
gap_fraction	Average gap fraction. One minus the average canopy cover, 1-C
network	Comment field, indicating to which monitoring network the site belongs
website_link	URL of a website describing the sampling site
paper_1	DOI of paper 1 describing the sampling site
paper_2	DOI of paper 2 describing the sampling site
paper_3	DOI of paper 3 describing the sampling site

Table 3: Description of the columns in the "WATSON_Isotopedata.csv" file containing all the isotope data and additional information about the extraction [and units].

Column name	Description
site_id	A three-letter identifier of the sampling site. Note that for the three sites (LIZ, GLS, WEI), an additional number was added indicating the species: "1" refers to beech and "2" to spruce.
country_id	A two-letter country code, as defined in ISO 3166-1

https://doi.org/10.5194/essd-2024-409
Preprint. Discussion started: 17 October 2024

sampling_date	Date that the sample was collected in yymmdd format
sampling_campaign	Descriptor indicating whether the sample was collected during the “spring” or “summer” sampling campaign.
sample_type	Descriptor indicating whether the sample was a “beech”, “spruce” or “soil” sample
replicate	Number to indicate the tree from which the sample was taken (varying between 1 to 3, and occasionally between 4 to 6) or the replicate of the soil sample (typically only 1, but occasionall varying between 1 and 4).
spruce	Descriptor indicating if the sample was a vegetation sample from a spruce tree or if the soil was taken from a site that has spruce trees (“yes”), otherwise left blank
beech	Descriptor indicating if the sample was a vegetation sample from a beech tree or if the soil was taken from a site that has beech trees (“yes”), otherwise left blank
both	Descriptor indicating if the soil sample was taken from a site that has both beech and spruce trees (“yes”), otherwise left blank
species	Descriptor of the vegetation: “beech” and “spruce” for beech and spruce sites, respectively, or “both” if the soil samples were taken at a site where there are beech and spruce trees
soil_depth	Depth of the soil sample. Numbers ranging between 10 and 90, indicating the maximum depth of an interval, e.g. 10 for 0-10 cm, 20 for 10-20 cm, and 75 for 65-75 cm. For the vegetation samples, the field is left blank.
sample_id	A sample identifier used for all laboratory analyses
bark	“yes” when the sample included (remaining) pieces of bark, otherwise "no”
original_vial	The vial type in which the sample was received: exetainer that fit the cryogenic extraction line (“exetainer”) or other types of gas-tight glass and plastic vials (“others”)
extractionist	ID for the person responsible for cryogenic water extraction (A to D). Note that person D was only responsible for a very small subset.
cvd_slot_id	Slot ID of the cryogenic water extraction line at which a sample was placed during the extraction
exe_type	Numbers (1 to 10) indicate the type of exetainers (i.e., various combinations of glass vials, caps with rubber seals, and labels)
exe_weight	The mean weight of an empty exetainer of the exe_type, including glass vials, caps with rubber seals, and labels [mg]
fw	The fresh (field) weight of the sample [mg]

https://doi.org/10.5194/essd-2024-409
Preprint. Discussion started: 17 October 2024

dw1	The dry weight of the sample after cryogenic extraction [mg]
dw2	The dry weight of the sample after cryogenic extraction and oven drying at 105°C for 24 h [mg]
awa	Absolute water amount extracted from the sample during cryogenic extraction [mL], calculated as: awa=(fw-dw1)/1000
gwc	The gravimetric water content of the sample [%], calculated as: gwc = (fw-dw1)/dw1)*100)
tef	Total extraction efficiency [%], calculated as: tef = ((fw-dw1)/(fw-dw2))*100)
d18O	The $\delta^{18}O$ value (relative to VSMOW-2) as determined by the laser spectrometer [‰]
d2H	The $\delta^{2}H$ value (relative to VSMOW-2) as determined by the laser spectrometer [‰]
d18O_irms	The $\delta^{18}O$ value (relative to VSMOW-2) as determined by the isotope ratio mass spectrometer [‰]
d2H_irms	The $\delta^{2}H$ value (relative to VSMOW-2) as determined by the isotope ratio mass spectrometer [‰]

Table 4: Description of the columns in the "WATSON_Canopydata.csv" file describing the canopy cover for the sampling sites for which canopy pictures were available.

Column name	Description
site_id	A three-letter identifier of the sampling site. Note that for the three sites (LIZ, GLS, WEI), an additional number was added indicating the species: "1" refers to beech and "2" to spruce.
country_id	A two-letter country code, as defined in ISO 3166-1
species	Descriptor iinndicating the species for which the pictures were taken, either "beech" or "spruce" or "canopy" if the picture represents a picture of a mixed site or the overall canopy of the sampling site.
photo	Name of the file of the photo as given in the WATSON_canopy_photos.zip file. The general structure of each file name is: country_site_date_speciesm_xxx.JPG, where "country" indicates the country_id, "site" indicates the site_id, "date" the date that the picture was taken in yymmdd format, "species" the tree species (beech or spruce), "m" the tree number, and "xxx" refers to additional information, such as the distance from the tree in meters (1, 3, 5) or the direction in which the picture was taken (N, E,

https://doi.org/10.5194/essd-2024-409
Preprint. Discussion started: 17 October 2024

	S, W). Where "canopy" is used for the "species", the picture shows the overall canopy of the forest site.
gap_fraction	One minus the canopy cover, 1-C
canopy_cover	The canopy cover (C), calculated as described in Section S3 [-]

305

306 **3 Results and discussion**

307 **3.1 Isotopic variation for the spring and summer sampling campaigns**

308 The isotopic composition of the soil and the stem xylem water samples varied spatially (Figure 4). The samples
309 were more depleted in heavy isotopes at sites located further north and inland. Multiple linear regression analyses
310 showed that latitude, longitude, and elevation were all important variables explaining the observed spatial variation
311 in the isotopic composition of soil and stem xylem water (Table 5). Among the three geographic variables,
312 longitude and latitude explained most of the variance for seven of the eight cases shown in Table 5. Since the total
313 variance explained by latitude, longitude, and elevation was relatively low in most cases (R^2 = 0.17 to 0.6), other
314 factors likely contributed to the variation in the isotopic composition of the samples. In combination with the
315 gravimetric water content of the soil (e.g., "gwc"; Table 3), gridded climate data, and precipitation isotope data
316 (Nelson et al., 2021), the data could be useful for new soil and stem xylem water isoscape models or function as
317 additional data in hydrological studies.

https://doi.org/10.5194/essd-2024-409
Preprint. Discussion started: 17 October 2024

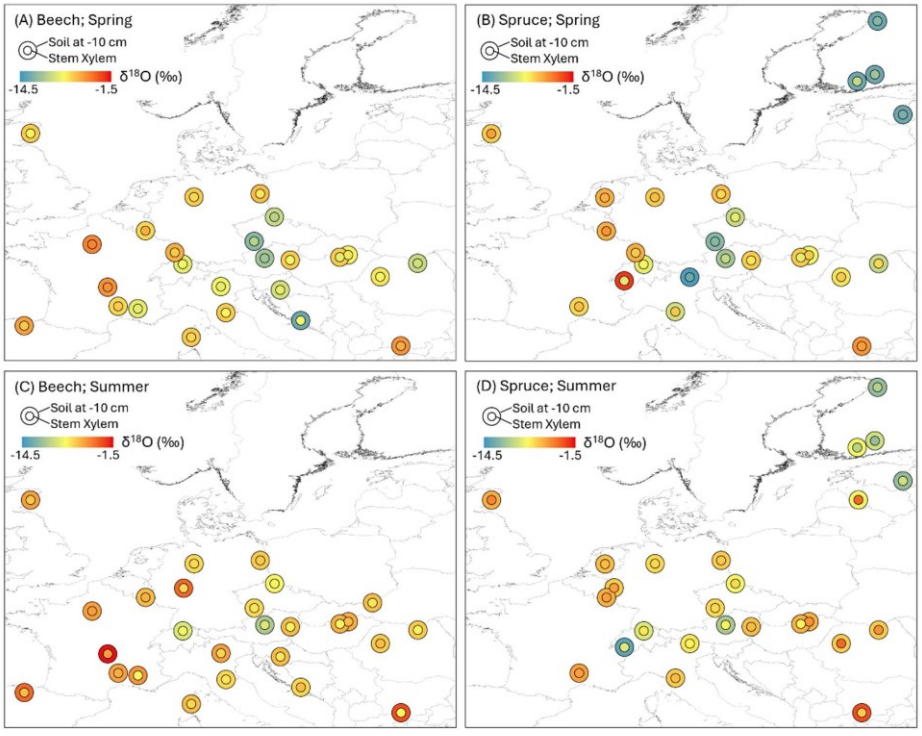

Figure 4: Map showing the $\delta^{18}O$ values for stem xylem water (inner circle) and soil water at 0-10 cm (outer circle) for the spring (A,B) and summer (C,D) sampling campaigns. Results for beech trees are reported on the left and spruce trees on the right. For some sites, the isotopic composition of the stem xylem samples was similar to that of the shallow soil (0-10 cm depth) (both circles have the same color); for others, the differences were large (i.e., the color of the inner and outer circle differs) indicating water uptake from a different (e.g. deeper) water source.

Table 5: Percentage of variance in $\delta^{18}O$ values explained by latitude, longitude, and elevation, as determined by multiple linear regression analyses. Values in bold indicate the highest relative contribution of a geographical parameter to the total variance for each sample type for each campaign (Spring/Summer). R^2 reflects the total variance explained by latitude, longitude, and elevation. All linear models were statistically significant ($P < 0.001$).

Campaign	Sample	R^2	Longitude (%)	Latitude (%)	Elevation (%)
Spring	Stem xylem (spruce)	0.48	25	50	25
	Stem xylem (beech)	0.34	29	33	38
	Soil (0-10 cm)	0.35	50	38	12
	Soil (30-90 cm)	0.60	35	46	19
Summer	Stem xylem (spruce)	0.32	13	66	21
	Stem xylem (beech)	0.17	56	13	31

https://doi.org/10.5194/essd-2024-409
Preprint. Discussion started: 17 October 2024

	Soil (0-10 cm)	0.29	19	64	17
	Soil (30-90 cm)	0.38	72	23	5

The isotopic composition of the soil and stem xylem water samples also varied between the two sampling campaigns (Figures 4 and 5). For instance, $\delta^{18}O$ values were higher (i.e., less negative) in summer compared to those of the spring for the different soil depths and the two tree species (unpaired t-test, $P < 0.05$), except for soils in the depth range of 30-90 cm for which there was no significant difference between spring and summer (unpaired t-test, $P > 0.05$; Figure 5). For the $\delta^{18}O$ values of stem xylem water, the median seasonal difference (summer-spring), averaged per site, was 0.8‰ across all spruce sites (ranging from -1.4 to 4.8‰) and 0.6 ‰ across all beech sites (ranging from -1.9 to 2.9‰). In comparison, the average median seasonal $\delta^{18}O$ difference was larger and/or showed higher a variability for soil water, e.g., 1.3‰ at 0-10 cm depth (ranging from -10.8 to 6.1‰) and 0.6 ‰ at 30-90 cm depth (ranging from -3.3 to 9.6‰). In spring, the $\delta^{18}O$ values of deep soils (30-90 cm) were only lower (i.e., more negative) compared to those of the shallower soils (0-10 cm), while in summer, $\delta^{18}O$ values of deep soils were lower compared to all other soil depths above 30 cm (unpaired t-test, $P < 0.05$). Similar seasonal differences for stem xylem and soil water were observed for the $\delta^{2}H$ values (Figure 5). The data may, therefore, be used to investigate the infiltration of precipitation and snowmelt into the soil, but also evaporative enrichment of the shallow soil water, or to test models that simulate these processes.

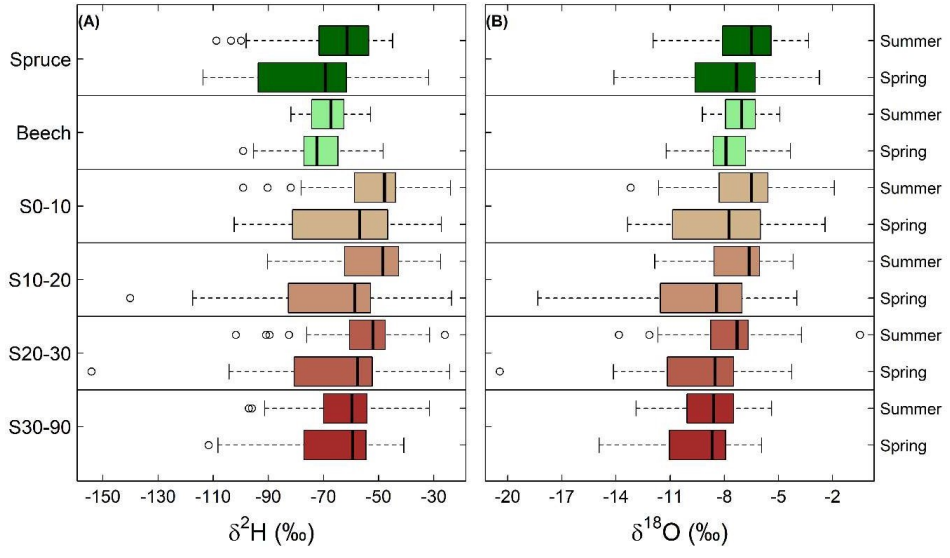

Figure 5: Boxplots for (A) hydrogen and (B) the oxygen isotopic composition ($\delta^{2}H$, $\delta^{18}O$) of stem xylem water of both tree species (beech and spruce) and soil water at different depths for the spring and summer campaigns. Soil depths are shown for 0-10 cm (S0-10), 10-20 cm (S10-20), 20-30 cm(S20-30) and 30-90 cm (S30-90). The vertical line within the box indicates the median (50th percentile). The box represents the interquartile range (IQR),

https://doi.org/10.5194/essd-2024-409
Preprint. Discussion started: 17 October 2024

spanning from the 25th percentile to the 75th percentile. The whiskers extend to the furthest data points within 1.5 times the IQR from the quartiles. Symbols outside the whiskers represent outliers.

Further, we found that the isotopic composition of the stem xylem water plotted in the range of soil water at the site level ("overlap"), though not consistently across all sites (Figure 6). The mean $\delta^{18}O$ values overlapped for more beech sites (68% in spring, 84% in summer) than for spruce sites (41 in spring, 48% in summer). The number of sites for which the $\delta^{18}O$ values of the soil and stem xylem water overlapped was also larger for the summer than for the spring sampling campaign. In contrast, the overlap in mean $\delta^{2}H$ values was higher for spruce sites (58% in spring, 68% in summer) than beech sites (28% in spring, 23% summer). A lack of overlap may indicate that the trees used water from other sources, such as recent precipitation events, water stored in organic surface layers, deeper, unsampled soil layers or groundwater. Another explanation might be related to cryogenic water extraction artefacts (see section on "Cryogenic water extraction biases").

The soil and stem xylem data could be used to test models that simulate plant-soil-water dynamics (Klein et al., 2014; Brinkmann et al., 2018; Knighton et al., 2020) and to test how this depends on site-, soil-, and tree-specific information (Table 3). When the data are combined with isotope data of precipitation, such as those from the GNIP network (e.g.,Terzer-Wassmuth et al., 2023), or models, such as Piso.AI (Nelson et al., 2021), the data can also be used to study the seasonal origins of tree water uptake, as well as the spatial and temporal patterns associated with it (Allen et al., 2019; Floriancic et al., 2024a). For sites without overlap, the application of mixing models, such as IsoSource (Phillips and Gregg, 2003) or MixSIAR (Stock et al., 2018), might be limited. However, alternative mixing models with incomplete end-members could be tested (Kirchner, 2023).

For sites with both species, the isotopic data for the stem xylem water of the two species appear to be different (Figure 6). The median difference between species across all sites for the mean $\delta^{2}H$ and $\delta^{18}O$ values (spruce-beech), averaged per site, was 4.1‰ and 0.7‰ in spring and 10.1‰ and 1.1‰ in summer, respectively. Thus, the stem xylem water in spruce tended to be isotopically enriched compared to ones in beech, which is consistent with the generally shallower root system of spruce compared to beech. The data can therefore be used to study species-specific differences in root water uptake depth across Europe.

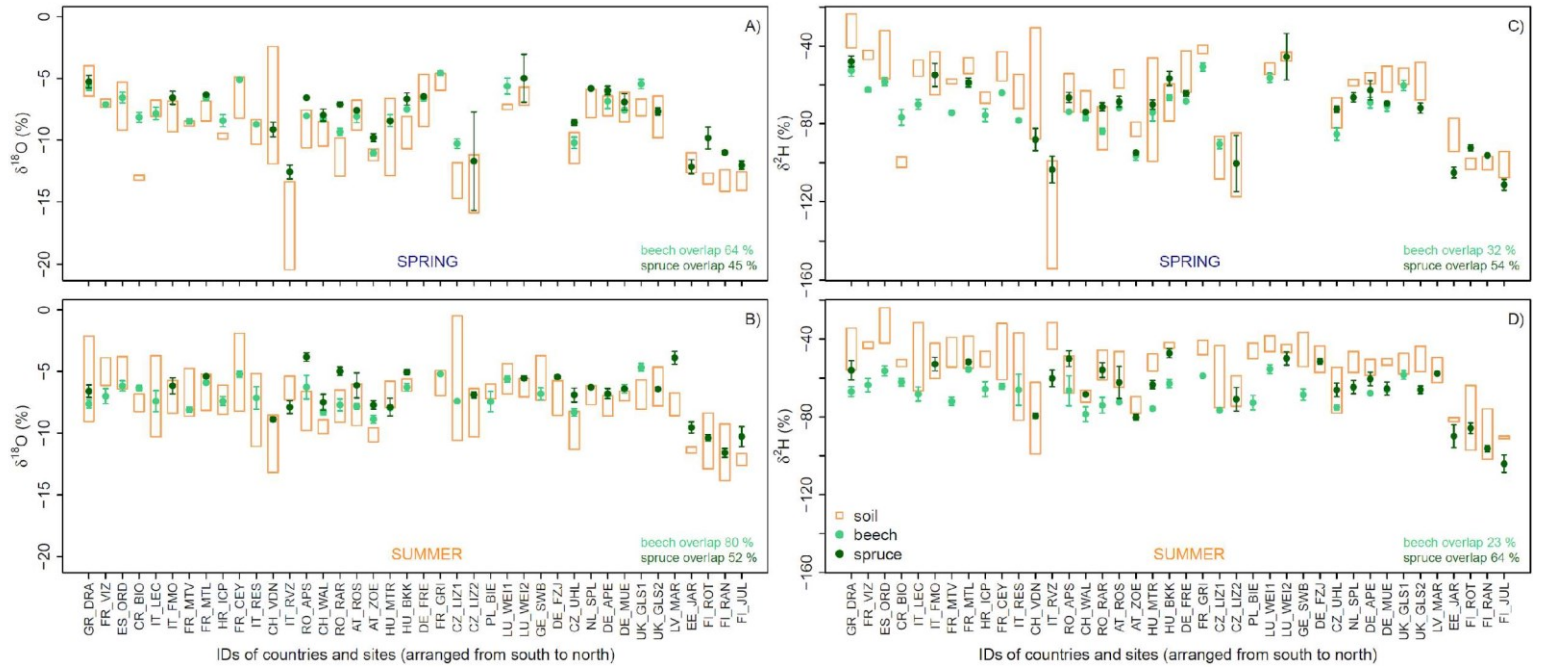

Figure 6: Overlap between the isotopic composition of soil and stem xylem water for spring (A, C) and summer (B, D) campaign. Oxygen ($\delta^{18}O$) and hydrogen ($\delta^{2}H$) isotope data are shown in the left and right panels, respectively. Orange bars indicate the minimum to maximum range of soil water isotope values. Mean values and standard errors are shown for the isotopic composition of stem xylem water.

https://doi.org/10.5194/essd-2024-409
Preprint. Discussion started: 17 October 2024

Open Access Earth System Science Data Discussions

3.2 Cryogenic water extraction biases

The dual isotope plots show that the isotope ratios of the soil were closer to the GMWL than those of stem xylem water for both species (Figure 7). However, particularly in summer, the isotope ratios of the shallower soils at some locations also deviated from the GMWL. This may indicate that the water in the shallow soil was affected by evaporation and that the trees used this enriched water. While evaporation might be responsible for some of the offset between the soil and stem xylem samples, there was no evaporative enrichment for most soil samples. Nevertheless, it should be considered that soil organic matter can bias the isotopic composition of the extracted water (Ceperley et al., 2024; Orlowski et al., 2016), as well as the presence of volatile organic compounds that may interfere isotopic analysis with laser spectrometers (Martín-Gómez et al., 2015). The latter, however, should be reduced by the use of the micro-combution modul in our study. Furthermore, given the relatively small isotopic differences between the laser and IRMS measurements (Figure 3), the overall large δ^2H deviation from the GMWL for the stem xylem samples is more likely caused by methodological issues related to the cryogenic vacuum distillation method (Chen et al., 2020; Diao et al., 2022; Barbeta et al., 2022). According to these studies, biases might be related to stem water content, differences in the isotopic composition of the xylem water and water in plant cells, exchange of H-atoms between organic material and water or water vapour, and isotope fractionation related to evaporation and sublimation during the extraction procedure.

To address these issues, we performed further quality checks for the cryogenic extraction (Figure 8). Although there was a significant difference in the total extraction efficiency for the samples handled by the three main lab technicians (one-way ANOVA, $P < 0.001$; Figure 8A), the efficiency did not depend on the cryogenic vacuum distillation slot (Figure 8B) and showed no systematic effect on the δ^2H and $\delta^{18}O$ values (Figure 8C). The presence of bark residue in the samples did not significantly affect the isotope signals (unpaired t-test, $P > 0.05$), although the slopes of the dual isotope plots tended to be different ($P = 0.06$, Figure 8D). Comparing the δ^2H and $\delta^{18}O$ values between samples stored in exetainers and other vials (Table 3, “original_vial”) revealed no visual or statistical differences either, suggesting that sampling, transport, and transfer of samples from other vials to exetainers before cryogenic water extraction in the laboratory did not notably affect the isotope results. The data of this study can be used to further explore the cryogenic water extraction biases with the additionally provided site-, soil- and tree-specific information (Zhao et al., 2024; Sobota et al., 2024). Alternatively, they can be used to support other studies on methodological issues related to cryogenic water extraction.

https://doi.org/10.5194/essd-2024-409
Preprint. Discussion started: 17 October 2024

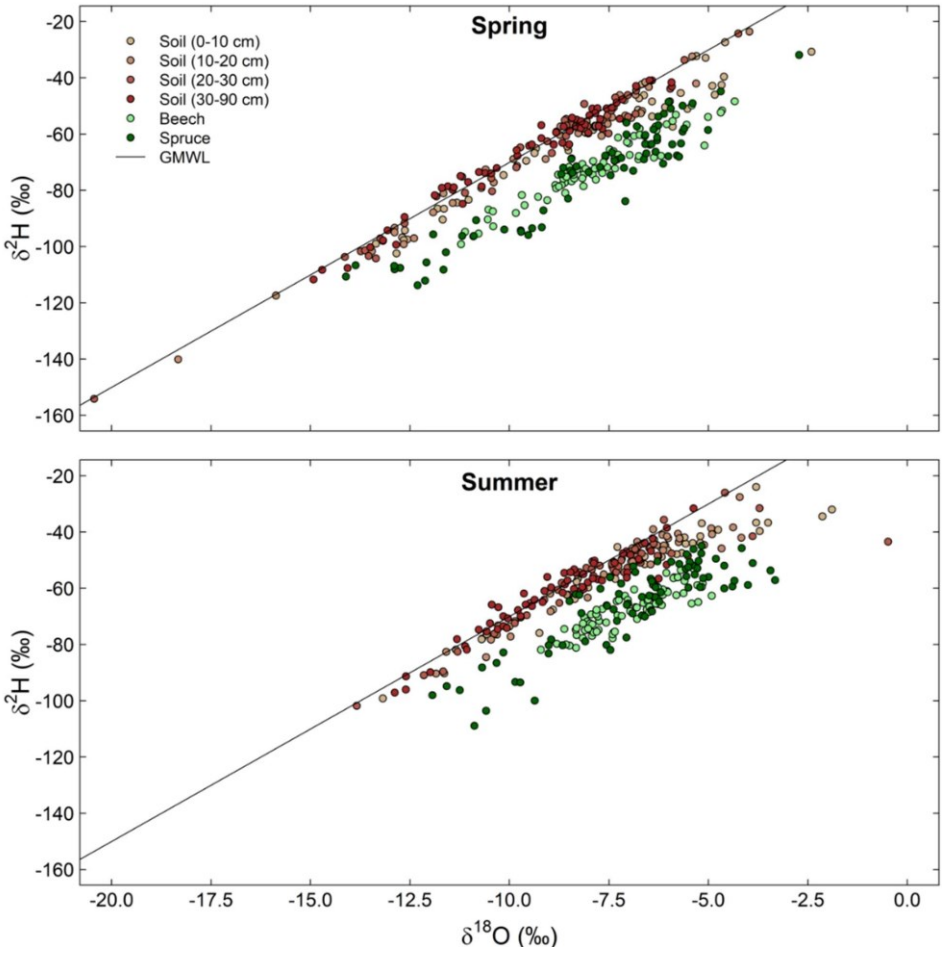

Figure 7: Dual isotope plots of oxygen and hydrogen isotope ratios (δ^2H, $\delta^{18}O$) for all soil and stem xylem water samples for the spring (top panel) and the summer (bottom panel) campaigns. Isotope values for soil samples are color coded according to soil depth. GMWL = Global Meteoric Water Line: $\delta^2H = 8\ \delta^{18}O + 10$.

https://doi.org/10.5194/essd-2024-409
Preprint. Discussion started: 17 October 2024

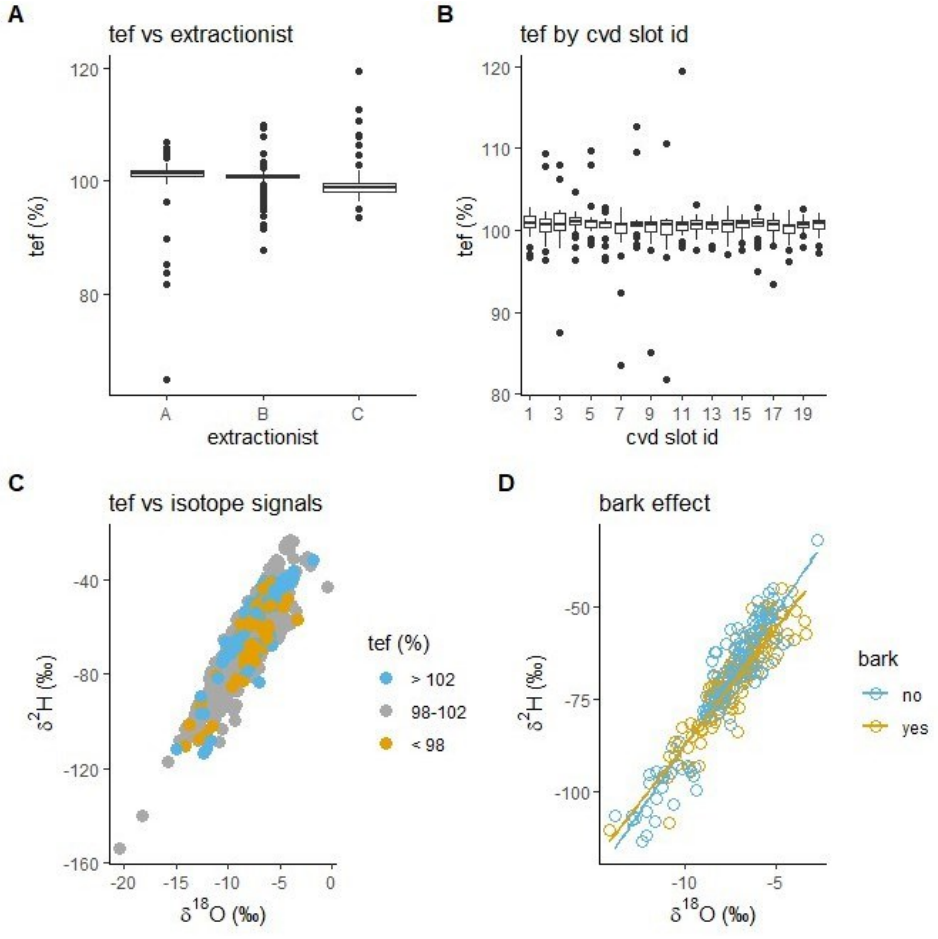

411

412 **Figure 8**: Total extraction efficiency (tef, %) quality checks: (A) tef values categorized by extractionist (Person
413 A, B, or C) and (B) by cryogenic vacuum distillation slot IDs. Correlation between oxygen ($\delta^{18}O$) and hydrogen
414 ($\delta^{2}H$) isotope values for (C) all samples colored by different tef categories and for (D) stem xylem samples with
415 ("yes") and without presence of bark ("no"), including fitted trend lines.

416 **4 Concluding remarks**

417 We present a large pan-European dataset of soil and stem xylem water isotopes of two common tree species
418 collected during spring and summer 2023. Since our observations are standardized according recently published
419 sampling and extraction procedures (Ceperley et al., 2024; Scandellari et al., 2024), this data can serve as a baseline
420 for future ecohydrological studies. This dataset is freely available and represents a valuable resource for different
421 research topics. These may include identifying the factors that affect tree water uptake depth and the seasonal
422 sources of water used by trees, calibrating and constraining isotope-aided ecohydrological models, incorporating

https://doi.org/10.5194/essd-2024-409
Preprint. Discussion started: 17 October 2024

the data into isoscape models, or studying how biases caused by cryogenic water extraction vary by species, soil type, or climate.

Statistics

For all statistical analyses we used R version 4.3.1 (R Core Team, 2023). For our multiple linear regression analyses, we applied a cube root transformation to the data to address non-normality. We then utilized the R package "relaimpo" (Grömping, 2006) to assess the relative importance of the geographical parameters in our model. If data is presented for soil at a depth of 30-90 cm, it represents all available data points for soil depths greater than 30 cm, without any additional modifications of the data.

Funding

This study was financially supported by the COST Action: "Water isotopes in the critical zone: from groundwater recharge to plant transpiration - WATSON" CA19120 (www.cost.eu). The extraction of the water and isotope analyses were financially supported by the Swiss National Science Foundation ("TreeWater", No. 205492; "InsightForest", No. 213367) and by WSL ("Innovative project Oxygen17"). Alicia Correa was supported by the German Academic Exchange Service (DAAD) from funds of Federal Ministry for Economic Cooperation (BMZ), SDGnexus Network (No. 57526248). Aurel Persoiu and Andrei Popa were supported by UEFISCDI Romania (No. PN-III-P2-2.1-PED-2019-4102 & No. PN-III-P4-ID-PCE-2020-2723). Maren Dubbert acknowledges the funding by the Deutsche Forschungsgemeinschaft (No. 501530203) and by the Leibniz collaborative excellent grant (No. K444/2022), supporting Alberto Iraheta, Charlotte Koeber, and Clara Rohde. Katja Rinne was funded by the Academy of Finland (No. 343059). Research part at University of Oulu was supported by Research Council of Finland (No. 347348 and No. 356043), and Marie Skłodowska-Curie Postdoctoral Fellowship (No. 101111527).

Acknowledgements

The pan-European sampling campaign and the data collection initiative was developed during a workshop of the COST Action: "WATSON" CA19120 (http://www.cost.eu/; https://watson-cost.eu/) held in March 2023 in Dubrovnik, Croatia. We thank Timon Dufner, Sophia Ezhold, Noemi Kammerlander, Alligin Gazhoul, Jan Ziegler, Jonathan Frei, Roger Köchli, David Schweizer, Manuela Oettli for the laboratory assistance, as well as Enara Aldai, Wisam Almohamed, Hatice Türk, Patricia Vieira Pompeu, Fernanda Gianasi, Konstantinos Voudouris, Ionel Popa, Martine Helfer, Anna Meier, Ladina Gaudy, Laura Kinzinger, Dominik Gerber, Simon Bürki, Dominik Dubach, Paavo Ojanen, Ellinoora Ekman, Christiaan van der Tol, and Joni Koivula for their help with site selection, and/or sample- or metadata collection.

Data availability

All data is freely available under the agreement "Creative Commons Zero - No Rights Reserved (CC0 1.0)" in the data repository EnviDat: Lehmann, M. M., Geris, J., van Meerveld, I., Penna, D., Rothfuss, Y., Verdone, M., Ala-Aho, P., Arvai, M., Babre, A., Balandier, P., Bernhard, F., Butorac, L., Carrière, S. D., Ceperley, N. C., Chen, Z., Correa, A., Diao, H., Dubbert, D., Dubbert, M., Ercoli, F., Floriancic, M. G., Gimeno, T. E., Gounelle, D.,

https://doi.org/10.5194/essd-2024-409
Preprint. Discussion started: 17 October 2024

Hagedorn, F., Hissler, C., Huneau, F., Alberto, I., Jakovljević, T., Kazakis, N., Kern, Z., Knaebel, K., Kobler, J., Kocum, J., Koeber, C., Koren, G., Kübert, A., Kupka, D., le Gall, S., Lehtonen, A., Leydier, T., Malagoli, P., Manca di Villahermosa, F. S., Marchina, C., Martínez-Carreras, N., Martin-StPaul, N., Marttila, H., Meyer Oliveira, A., Monvoisin, G., Orlowski, N., Palmik-Das, K., Persoiu, A., Popa, A., Prikaziuk, E., Quantin, C., Rinne-Garmston, K. T., Rohde, C., Sanda, M., Saurer, M., Schulz, D., Stockinger, M. P., Stumpp, C., Vénisse, J.-S., Vlcek, L., Voudouris, S., Weeser, B., Wilkinson, M., Zuecco, G., and Meusburger, K.: Soil and stem xylem water isotope data from two pan-European sampling campaigns [dataset], https://www.doi.org/10.16904/envidat.542, 2024.

Competing interests

The authors declare that they have no conflict of interest.

Author contribution (CRediT)

The WATSON sampling campaign core organization and writing team consisted of Marco M. Lehmann (MML), Josie Geris (JG), Ilja van Meerveld (IvM), Daniele Penna (DP), Youri Rothfuss (YR) and Katrin Meusburger (KM). Conceptualization: MML, JG, IvM, DP, YR, KM; Data curation: MML, MV; Formal Analysis: MML, JG, IvM, DP, YR, MV, KM; Funding acquisition: MML, JG, IvM, DP, YR, KM; Investigation: MML, JG, IvM, DP, YR, KM; Methodology: MML, JG, IvM, DP, YR, KM; Project administration: MML, JG, IvM, DP, YR, KM; Resources: MML, KM; Validation: MML, JG, IvM, DP, YR, KM; Visualization: MML, JG, IvM, DP, YR, KM; Writing – original draft: MML, JG, IvM, DP, YR, KM; Writing – review & editing: all.

References

Allen, S. T., Kirchner, J. W., and Goldsmith, G. R.: Predicting spatial patterns in precipitation isotope (δ^2H and $\delta^{18}O$) seasonality using sinusoidal isoscapes, Geophysical Research Letters, 45, 4859-4868, 10.1029/2018GL077458, 2018.

Allen, S. T., Kirchner, J. W., Braun, S., Siegwolf, R. T. W., and Goldsmith, G. R.: Seasonal origins of soil water used by trees, Hydrol Earth Syst Sc, 23, 1199-1210, 10.5194/hess-23-1199-2019, 2019.

Bachofen, C., Tumber-Dávila, S. J., Mackay, D. S., McDowell, N. G., Carminati, A., Klein, T., Stocker, B. D., Mencuccini, M., and Grossiord, C.: Tree water uptake patterns across the globe, New Phytol, 242, 1891-1910, https://doi.org/10.1111/nph.19762, 2024.

Barbeta, A., Burlett, R., Martín-Gómez, P., Fréjaville, B., Devert, N., Wingate, L., Domec, J. C., and Ogée, J.: Evidence for distinct isotopic compositions of sap and tissue water in tree stems: consequences for plant water source identification, New Phytol, 233, 1121-1132, 10.1111/nph.17857, 2022.

Beck, H. E., Mcvicar, T. R., Vergopolan, N., Berg, A., Lutsko, N. J., Dufour, A., Zeng, Z. Z., Jiang, X., van Dijk, A. I. J. M., and Miralles, D. G.: High-resolution (1 km) Köppen-Geiger maps for 1901-2099 based on constrained CMIP6 projections, Sci Data, 10, 10.1038/s41597-023-02549-6, 2023.

Beyer, M. and Penna, D.: On the spatio-temporal under-representation of isotopic data in ecohydrological studies, Front Water, 3, 10.3389/frwa.2021.643013, 2021.

Bowen, G. J.: Isoscapes: Spatial Pattern in Isotopic Biogeochemistry, Annual Review of Earth and Planetary Sciences, Vol 38, 38, 161-187, 10.1146/annurev-earth-040809-152429, 2010.

Bowling, D. R., Schulze, E. S., and Hall, S. J.: Revisiting streamside trees that do not use stream water: can the two water worlds hypothesis and snowpack isotopic effects explain a missing water source?, Ecohydrology, 10, e1771, https://doi.org/10.1002/eco.1771, 2017.

https://doi.org/10.5194/essd-2024-409
Preprint. Discussion started: 17 October 2024

Brinkmann, N., Seeger, S., Weiler, M., Buchmann, N., Eugster, W., and Kahmen, A.: Employing stable isotopes to determine the residence times of soil water and the temporal origin of water taken up by *Fagus sylvatica* and *Picea abies* in a temperate forest, New Phytol, 219, 1300-1313, 10.1111/nph.15255, 2018.

Büntgen, U., Urban, O., Krusic, P. J., Rybníček, M., Kolář, T., Kyncl, T., Ač, A., Koňasová, E., Čáslavský, J., Esper, J., Wagner, S., Saurer, M., Tegel, W., Dobrovolný, P., Cherubini, P., Reinig, F., and Trnka, M.: Recent European drought extremes beyond Common Era background variability, Nat Geosci, 14, 190–196, 10.1038/s41561-021-00698-0, 2021.

Cai, M. Y., Wang, L. X., Parkes, S. D., Strauss, J., McCabe, M. F., Evans, J. P., and Griffiths, A. D.: Stable water isotope and surface heat flux simulation using ISOLSM: Evaluation against *in-situ* measurements, J Hydrol, 523, 67-78, 10.1016/j.jhydrol.2015.01.019, 2015.

Caudullo, G., Welk, E., and San-Miguel-Ayanz, J.: Chorological maps for the main European woody species, Data in Brief, 12, 662-666, https://doi.org/10.1016/j.dib.2017.05.007, 2017.

Ceperley, N., Gimeno, T. E., Jacobs, S. R., Beyer, M., Dubbert, M., Fischer, B., Geris, J., Holko, L., Kuebert, A., Le Gall, S., Lehmann, M. M., Llorens, P., Millar, C., Penna, D., Prieto, I., Radolinski, J., Scandellari, F., Stockinger, M., Stumpp, C., Tetzlaff, D., van Meerveld, I., Werner, C., Yildiz, O., Zuecco, G., Barbeta, A., Orlowski, N., and Rothfuss, Y.: Toward a common methodological framework for the sampling, extraction, and isotopic analysis of water in the Critical Zone to study vegetation water use, Wires Water, 11, 10.1002/wat2.1727, 2024.

Chen, Y. L., Helliker, B. R., Tang, X. H., Li, F., Zhou, Y. P., and Song, X.: Stem water cryogenic extraction biases estimation in deuterium isotope composition of plant source water, P Natl Acad Sci USA, 117, 33345-33350, 10.1073/pnas.2014422117, 2020.

Diao, H., Schuler, P., Goldsmith, G. R., Siegwolf, R. T. W., Saurer, M., and Lehmann, M. M.: Technical note: On uncertainties in plant water isotopic composition following extraction by cryogenic vacuum distillation, Hydrol Earth Syst Sc, 26, 5835-5847, 10.5194/hess-26-5835-2022, 2022.

Dubbert, M. and Werner, C.: Water fluxes mediated by vegetation: emerging isotopic insights at the soil and atmosphere interfaces, New Phytol, 221, 1754-1763, 10.1111/nph.15547, 2019.

Ellsworth, P. Z. and Sternberg, L. S. L.: Seasonal water use by deciduous and evergreen woody species in a scrub community is based on water availability and root distribution, Ecohydrology, 8, 538-551, 10.1002/eco.1523, 2015.

Engel, M., Frentress, J., Penna, D., Andreoli, A., van Meerveld, I., Zerbe, S., Tagliavini, M., and Comiti, F.: How do geomorphic characteristics affect the source of tree water uptake in restored river floodplains?, Ecohydrology, 15, e2443, https://doi.org/10.1002/eco.2443, 2022.

Erdélyi, D., Kern, Z., Nyitrai, T., and Hatvani, I. G.: Predicting the spatial distribution of stable isotopes in precipitation using amachine learning approach: a comparative assessment of random forest variants, Gem Int J Geomathema, 14, 10.1007/s13137-023-00224-x, 2023.

Floriancic, M. G., Allen, S. T., and Kirchner, J. W.: Isotopic evidence for seasonal water sources in tree xylem and forest soils, Ecohydrology, 10.1002/eco.2641, 2024a.

Floriancic, M. G., Stockinger, M. P., Kirchner, J. W., and Stumpp, C.: Monthly new water fractions and their relationships with climate and catchment properties across Alpine rivers, Hydrol Earth Syst Sc, 28, 3675-3694, 10.5194/hess-28-3675-2024, 2024b.

Gessler, A., Bachli, L., Freund, E. R., Treydte, K., Schaub, M., Haeni, M., Weiler, M., Seeger, S., Marshall, J., Hug, C., Zweifel, R., Hagedorn, F., Rigling, A., Saurer, M., and Meusburger, K.: Drought reduces water uptake in beech from the drying topsoil, but no compensatory uptake occurs from deeper soil layers, New Phytol, 233, 194-206, 10.1111/nph.17767, 2022.

Grömping, U.: Relative Importance for Linear Regression in R: The Package relaimpo, Journal of Statistical Software, 17, 1-27, 2006.

Haese, B., Werner, M., and Lohmann, G.: Stable water isotopes in the coupled atmosphere-land surface model ECHAM5-JSBACH, Geosci Model Dev, 6, 1463-1480, 10.5194/gmd-6-1463-2013, 2013.

Halder, J., Terzer, S., Wassenaar, L. I., Araguás-Araguás, L. J., and Aggarwal, P. K.: The Global Network of Isotopes in Rivers (GNIR): integration of water isotopes in watershed observation and riverine research, Hydrol Earth Syst Sc, 19, 3419-3431, 10.5194/hess-19-3419-2015, 2015.

https://doi.org/10.5194/essd-2024-409
Preprint. Discussion started: 17 October 2024

548 Kinzinger, L., Mach, J., Haberstroh, S., Schindler, Z., Frey, J., Dubbert, M., Seeger, S., Seifert, T., Weiler, M.,
549 Orlowski, N., Werner, C., and Meinzer, F.: Interaction between beech and spruce trees in temperate forests affects
550 water use, root water uptake pattern and canopy structure, Tree Physiology, 44, 10.1093/treephys/tpad144, 2024.

551 Kirchner, J. W.: Mixing models with multiple, overlapping, or incomplete end-members, quantified using time
552 series of a single tracer, Geophysical Research Letters, 50, 10.1029/2023GL104147, 2023.

553 Klein, T., Rotenberg, E., Cohen-Hilaleh, E., Raz-Yaseef, N., Tatarinov, F., Preisler, Y., Ogée, J., Cohen, S., and
554 Yakir, D.: Quantifying transpirable soil water and its relations to tree water use dynamics in a water- limited pine
555 forest, Ecohydrology, 7, 409-419, 10.1002/eco.1360, 2014.

556 Knighton, J., Kuppel, S., Smith, A., Soulsby, C., Sprenger, M., and Tetzlaff, D.: Using isotopes to incorporate tree
557 water storage and mixing dynamics into a distributed ecohydrologic modelling framework, Ecohydrology, 13,
558 10.1002/eco.2201, 2020.

559 Koeniger, P., Stumpp, C., and Schmidt, A.: Stable isotope patterns of German rivers with aspects on scales,
560 continuity and network status, Isotopes in Environmental and Health Studies, 58, 363-379,
561 10.1080/10256016.2022.2127702, 2022.

562 Lehmann, M. M., Geris, J., van Meerveld, I., Penna, D., Rothfuss, Y., Verdone, M., Ala-Aho, P., Arvai, M., Babre,
563 A., Balandier, P., Bernhard, F., Butorac, L., Carrière, S. D., Ceperley, N. C., Chen, Z., Correa, A., Diao, H.,
564 Dubbert, D., Dubbert, M., Ercoli, F., Floriancic, M. G., Gimeno, T. E., Gounelle, D., Hagedorn, F., Hissler, C.,
565 Huneau, F., Alberto, I., Jakovljević, T., Kazakis, N., Kern, Z., Knaebel, K., Kobler, J., Kocum, J., Koeber, C.,
566 Koren, G., Kübert, A., Kupka, D., le Gall, S., Lehtonen, A., Leydier, T., Malagoli, P., Manca di Villahermosa, F.
567 S., Marchina, C., Martínez-Carreras, N., Martin-StPaul, N., Marttila, H., Meyer Oliveira, A., Monvoisin, G.,
568 Orlowski, N., Palmik-Das, K., Persoiu, A., Popa, A., Prikaziuk, E., Quantin, C., Rinne-Garmston, K. T., Rohde,
569 C., Sanda, M., Saurer, M., Schulz, D., Stockinger, M. P., Stumpp, C., Vénisse, J.-S., Vlcek, L., Voudouris, S.,
570 Weeser, B., Wilkinson, M., Zuecco, G., and Meusburger, K.: Soil and stem xylem water isotope data from two
571 pan-European sampling campaigns [dataset], https://www.doi.org/10.16904/envidat.542, 2024.

572 Lindner, M., Maroschek, M., Netherer, S., Kremer, A., Barbati, A., Garcia-Gonzalo, J., Seidl, R., Delzon, S.,
573 Corona, P., Kolström, M., Lexer, M. J., and Marchetti, M.: Climate change impacts, adaptive capacity, and
574 vulnerability of European forest ecosystems, Forest Ecology and Management, 259, 698-709,
575 10.1016/j.foreco.2009.09.023, 2010.

576 Martín-Gómez, P., Barbeta, A., Voltas, J., Peñuelas, J., Dennis, K., Palacio, S., Dawson, T. E., and Ferrio, J. P.:
577 Isotope-ratio infrared spectroscopy: a reliable tool for the investigation of plant-water sources?, New Phytol, 207,
578 914-927, 10.1111/nph.13376, 2015.

579 Nelson, D. B., Basler, D., and Kahmen, A.: Precipitation isotope time series predictions from machine learning
580 applied in Europe, P Natl Acad Sci USA, 118, e2024107118, 10.1073/pnas.2024107118, 2021.

581 Orlowski, N., Breuer, L., and McDonnell, J. J.: Critical issues with cryogenic extraction of soil water for stable
582 isotope analysis, Ecohydrology, 9, 1-5, https://doi.org/10.1002/eco.1722, 2016.

583 Orlowski, N., Rinderer, M., Dubbert, M., Ceperley, N., Hrachowitz, M., Gessler, A., Rothfuss, Y., Sprenger, M.,
584 Heidbüchel, I., Kübert, A., Beyer, M., Zuecco, G., and McCarter, C.: Challenges in studying water fluxes within
585 the soil-plant-atmosphere continuum: A tracer-based perspective on pathways to progress, Sci Total Environ, 881,
586 10.1016/j.scitotenv.2023.163510, 2023.

587 Orlowski, N., Breuer, L., Angeli, N., Boeckx, P., Brumbt, C., Cook, C. S., Dubbert, M., Dyckmans, J., Gallagher,
588 B., Gralher, B., Herbstritt, B., Herve-Fernandez, P., Hissler, C., Koeniger, P., Legout, A., Macdonald, C. J.,
589 Oyarzun, C., Redelstein, R., Seidler, C., Siegwolf, R., Stumpp, C., Thomsen, S., Weiler, M., Werner, C., and
590 McDonnell, J. J.: Inter-laboratory comparison of cryogenic water extraction systems for stable isotope analysis of
591 soil water, Hydrol Earth Syst Sc, 22, 3619-3637, 10.5194/hess-22-3619-2018, 2018.

592 Penna, D., Geris, J., Hopp, L., and Scandellari, F.: Water sources for root water uptake: Using stable isotopes of
593 hydrogen and oxygen as a research tool in agricultural and agroforestry systems, Agr Ecosyst Environ, 291,
594 10.1016/j.agee.2019.106790, 2020.

595 Penna, D., Stenni, B., Sanda, M., Wrede, S., Bogaard, T. A., Michelini, M., Fischer, B. M. C., Gobbi, A., Mantese,
596 N., Zuecco, G., Borga, M., Bonazza, M., Sobotková, M., Cejková, B., and Wassenaar, L. I.: Technical Note:
597 Evaluation of between-sample memory effects in the analysis of δ^2H and $\delta^{18}O$ of water samples measured by laser
598 spectroscopes, Hydrol Earth Syst Sc, 16, 3925-3933, 10.5194/hess-16-3925-2012, 2012.

https://doi.org/10.5194/essd-2024-409
Preprint. Discussion started: 17 October 2024

599 Penna, D., Hopp, L., Scandellari, F., Allen, S. T., Benettin, P., Beyer, M., Geris, J., Klaus, J., Marshall, J. D.,
600 Schwendenmann, L., Volkmann, T. H. M., von Freyberg, J., Amin, A., Ceperley, N., Engel, M., Frentress, J.,
601 Giambastiani, Y., McDonnell, J. J., Zuecco, G., Llorens, P., Siegwolf, R. T. W., Dawson, T. E., and Kirchner, J.
602 W.: Ideas and perspectives: Tracing terrestrial ecosystem water fluxes using hydrogen and oxygen stable isotopes
603 - challenges and opportunities from an interdisciplinary perspective, Biogeosciences, 15, 6399-6415, 10.5194/bg-
604 15-6399-2018, 2018.

605 Phillips, D. L. and Gregg, J. W.: Source partitioning using stable isotopes: coping with too many sources,
606 Oecologia, 136, 261-269, 10.1007/s00442-003-1218-3, 2003.

607 Poca, M., Coomans, O., Urcelay, C., Zeballos, S. R., Bodé, S., and Boeckx, P.: Isotope fractionation during root
608 water uptake by is enhanced by arbuscular mycorrhizas, Plant Soil, 441, 485-497, 10.1007/s11104-019-04139-1,
609 2019.

610 R Core Team: R: A language and environment for statistical computing., R foundation for statistical computing,
611 Vienna, Austria, https://www.r-project.org/, 2023.

612 Reckerth, A., Stichler, W., Schmidt, A., and Stumpp, C.: Long-term data set analysis of stable isotopic composition
613 in German rivers, J Hydrol, 552, 718-731, 10.1016/j.jhydrol.2017.07.022, 2017.

614 Rothfuss, Y. and Javaux, M.: Reviews and syntheses: Isotopic approaches to quantify root water uptake: a review
615 and comparison of methods, Biogeosciences, 14, 2199-2224, 10.5194/bg-14-2199-2017, 2017.

616 Scandellari, F., Attou, T., Barbeta, A., Bernhard, F., D'Amato, C., Dimitrova-Petrova, K., Donaldson, A.,
617 Durodola, O., Ferraris, S., Floriancic, M. G., Fontenla-Razzetto, G., Gerchow, M., Han, Q., Khalil, I., Kirchner, J.
618 W., Kühnhammer, K., Liu, Q., Llorens, P., Magh, R. K., Marshall, J., Meusburger, K., Oliveira, A. M., Muñoz-
619 Villers, L., Pires, S. S., Todini-Zicavo, D., van Meerveld, I., Voigt, C., Wirsig, L., Beyer, M., Geris, J., Hopp, L.,
620 Penna, D., and Sprenger, M.: Using stable isotopes to inform water resource management in forested and
621 agricultural ecosystems, J Environ Manage, 365, 10.1016/j.jenvman.2024.121381, 2024.

622 Sobota, M., Li, K. V., Hren, M., and Knighton, J.: Evidence for variations in cryogenic extraction deuterium biases
623 of plant xylem water across foundational northeastern US trees, Hydrol Process, 38, 10.1002/hyp.15079, 2024.

624 Spinoni, J., Naumann, G., Carrao, H., Barbosa, P., and Vogt, J.: World drought frequency, duration, and severity
625 for 1951-2010, Int J Climatol, 34, 2792-2804, 10.1002/joc.3875, 2014.

626 Stock, B. C., Jackson, A. L., Ward, E. J., Parnell, A. C., Phillips, D. L., and Semmens, B. X.: Analyzing mixing
627 systems using a new generation of Bayesian tracer mixing models, Peerj, 6, 10.7717/peerj.5096, 2018.

628 Terzer-Wassmuth, S., Araguás-Araguás, L. J., Wassenaar, L. I., and Stumpp, C.: Global and local meteoric water
629 lines for $\delta^{17}O/\delta^{18}O$ and the spatiotemporal distribution of $\Delta'^{17}O$ in Earth's precipitation, Sci Rep-Uk, 13,
630 10.1038/s41598-023-45920-8, 2023.

631 Terzer, S., Wassenaar, L. I., Araguás-Araguás, L. J., and Aggarwal, P. K.: Global isoscapes for $\delta^{18}O$ and $\delta^{2}H$ in
632 precipitation: improved prediction using regionalized climatic regression models, Hydrol Earth Syst Sc, 17, 4713-
633 4728, 10.5194/hess-17-4713-2013, 2013.

634 Twining, J., Stone, D., Tadros, C., Henderson-Sellers, A., and Williams, A.: Moisture Isotopes in the Biosphere
635 and Atmosphere (MIBA) in Australia: A priori estimates and preliminary observations of stable water isotopes in
636 soil, plant and vapour for the Tumbarumba Field Campaign, Global Planet Change, 51, 59-72,
637 10.1016/j.gloplacha.2005.12.005, 2006.

638 von Freyberg, J., Allen, S. T., Seeger, S., Weiler, M., and Kirchner, J. W.: Sensitivity of young water fractions to
639 hydro-climatic forcing and landscape properties across 22 Swiss catchments, Hydrol Earth Syst Sc, 22, 3841-3861,
640 10.5194/hess-22-3841-2018, 2018.

641 Wong, T. E., Nusbaumer, J., and Noone, D. C.: Evaluation of modeled land-atmosphere exchanges with a
642 comprehensive water isotope fractionation scheme in version 4 of the Community Land Model, J Adv Model Earth
643 Sy, 9, 978-1001, 10.1002/2016ms000842, 2017.

644 Zhao, L. J., Liu, X. H., Wang, N. L., Barbeta, A., Zhang, Y., Cernusak, L. A., and Wang, L. X.: The determining
645 factors of hydrogen isotope offsets between plants and their source waters, New Phytol, 241, 2009-2024,
646 10.1111/nph.19492, 2024.

647

Supplementary

S1: Protocol for the spring sampling campaign

WATSON Sampling Instructions – Spring 2023 campaign

Before you go out:

- Where relevant, please make sure that you've **liaised with the appropriate colleagues of your team**. We prefer well established sites with existing data above new sites.
- Make sure that you have **permission** to access the site and take samples.
- **Collect and check metadata:** Please add as much metadata as possible using the following google doc: XXX
- Make sure that you have the necessary **equipment** (wood corer, exetainers, labelling tape and marker, soil auger or shovel, as well as a measurement tape to measure the DBH of the tree or depth of the soil sample), GPS (or map), tools for estimating tree height, as well as spirit or bubble level and mobile phone. 12 ml exetainers are supplied by Labco: XXX
- If you cannot organise all the equipment such as a 0.5 cm wood corer or exetainers in your country or from colleagues nearby, send asap a "**NEED EQUIPMENT**" email to X and Y.

During sampling in the field:

Make sure that your hands are dry during sampling and that you do this as quickly as possible to avoid evaporation from the stem and soil samples.

Tree stem sapwood samples: Take two to three stem sapwood samples of ~5 cm with a 0.5 cm wood corer from 3 spruce (*Picea abies*) trees and/or 3 beech (*Fagus sylvatica*) trees at breast height (i.e. we expect three vials (one for each tree) with two to three 5cm cores inside each). A minimum of two cores (more the better) are needed to get enough water for isotope analysis and to avoid isotope fractionations related to cryogenic extraction. The trees should be site-representative trees with a diameter at breast height (DBH) of at least 10 cm. Remove the bark of the tree cores with a knife but make sure to include the tissue of the outer tree rings!

Soil samples: Take a maximum of 5 soil samples at 0-10, 10-20, 20-30, 50-60, 80-90 cm at a location between the 3 (or 6) trees that you sampled. Litter should be removed for the soil sample at 0-10cm. Fill the exetainers for 50-80% with soil. In the case of a maximum soil depth of 30 cm, simply take 3 samples as indicated above. In the case of a maximum soil depth of 50 cm, take an additional 10 cm sample between 30 to 50 cm and note the exact depth (4 sample in total). In the case of maximum soil depth of 80 cm, take an additional 10 cm sample between 60 to 80 cm and note the exact depth (5 samples in total).

Close the sample vial: Please make sure the exetainer caps are tightly screwed on the vials. Hand tight is just fine but check that the rubber sealing in the cap is not overly bend. Seal the cap additionally with parafilm (or if you don't have parafilm use tape). Remember, evaporation is the enemy!

Label the sample: Please make sure that your samples are clearly labelled. The label should include country (2-letter), site code (3-letter), sampling date (yymmdd), soil/tree species, and depth/number (e.g. CH_WSL_230525_Soil_20-30, or CH_WSL_230525_Beech_1). Double-check with metadata.

Take photos: For all pictures, please use your mobile phone. Please use the back and not the front camera (the latter typically provides photos at lower resolution compared to the one on the back)! Take a (1) representative landscape photo of each site, (2) representative photos of each tree, as well as (3) representative photos of the canopy. The latter will be analysed by us for obtaining the crown gap fraction as a rough estimate of tree vitality on your site (description below). And of course, take pictures of yourself .

Label and upload photos: Please make sure that your photos are clearly labelled for landscape (e.g. CH_WSL_230525_Beech_Landscape), trees (CH_WSL_230525 _Beech1), canopy (CH_WSL_230525_Beech_Lab or CH_WSL_230525_Beech_1m_N) and yourself (CH_WSL_230525_Beech_Fun1). Upload your photos on google drive: XXX

After sampling:

- Store all samples in a fridge (~4°C). Don't freeze them!
- Send your vials as soon as possible to the following address: XXX.

Please **pack them nicely** in a box with some bubble wrap and double check that the labels are readable. Add a paper copy of the **import licence (attached to email)**.

- Send an email to X and Y to confirm that you have sent the samples. Double-check again the metadata and tick the box for "sent".

Instructions for taking canopy photos

In the office/lab:

We need to know the field of view of your mobile phone camera. Put your phone horizontally with the back camera upward at 1 meter distance from a ruler and take a photo. Use a smartphone app or a physical bubble level to achieve a prober level. Make sure that meter divisions are clearly visible in photo.

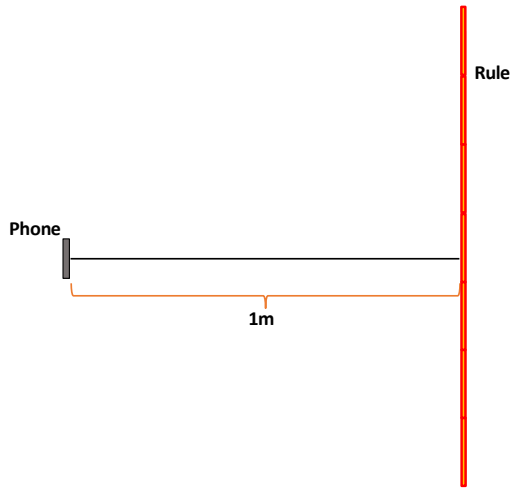

In the field:

Put your phone horizontally with the back camera upward underneath a representative tree of each site and species, approximately above 1 m from the soil surface. Use a smartphone app or a physical bubble level to achieve a prober level. Take photos at 1- and 5-meters distance to the stem. Repeat this procedure for 3 opposite directions (North, South, East or West). In total a **minimum of 6 photos** are needed (i.e., 2 photos per direction). To improve the estimate, additional photos at 3-, 7- or 9-meters distance to the stem or at the fourth direction are highly welcome.

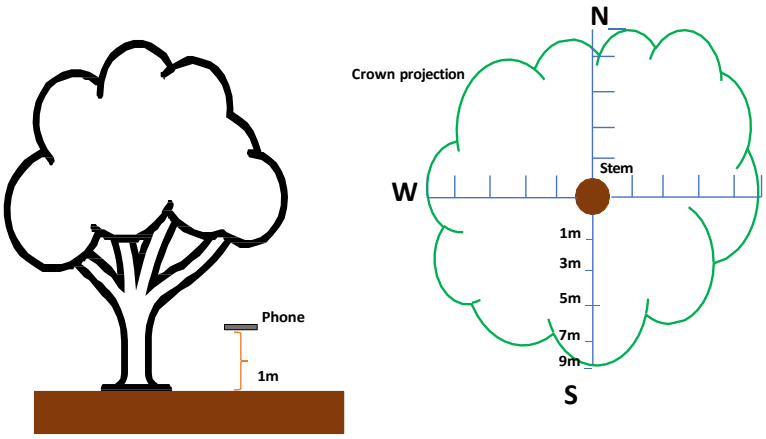

Recommendations: Avoid direct sun radiation on the crown and camera. The best conditions are met when the sky is homogeneously cloudy (as this provides a homogeneous background), or at least when the sunlight is shaded by clouds.

S2: Protocol for the summer sampling campaign

WATSON Sampling Instructions – Summer 2023 campaign

Before you go out:

- Make sure that you have **permission** to access the site and take samples. We prefer well **established sites** with existing data above new sites. We hope that everyone who participated in the first spring sampling campaign will participate again but also welcome people from selected countries who could not participate in the spring.
- Select a sampling day with nice weather and sample in "dry conditions", i.e. in the absence of rain or fog so that trees transpire actively. Avoid sampling during dusk and dawn.
- **Check and update metadata:** We have now updated our metadata sheet so that is suits the next sampling campaign. So please fill out the remaining "gaps" if possible using the following google doc: XXX
- Make sure that you have the necessary **equipment** (0.5 cm wood corer, exetainers, labelling tape and marker, soil auger or shovel, as well as a measurement tape to measure the depth of the soil sample and if you are participating for the first time the DBH of the trees), GPS (or map), tools for estimating tree height, as well as spirit or bubble level and mobile phone. 12 ml exetainers are supplied by Labco: XXX
- Packages with exetainers (and wood corer) are on the way those contributors, who had no exetainer during the first campaign! If you cannot organise all the equipment such as the 0.5 cm wood corer or exetainers from colleagues in your country or nearby, send asap a "**NEED EQUIPMENT**" email to X and Y.

During sampling in the field:

Make sure that your hands are dry during sampling and that you do this as quickly as possible to avoid evaporation from the stem and soil samples.

Tree stem sapwood samples: Take two to three stem sapwood samples of ~5 cm with a 0.5 cm wood corer from 3 spruce (*Picea abies*) trees and/or 3 beech (*Fagus sylvatica*) trees at breast height (i.e. we expect three vials (one for each tree) with two to three 5 cm cores inside each). A minimum of two cores (more the better) are needed to get enough water for isotope analysis and to avoid isotope fractionations related to cryogenic extraction. The trees should be -representative trees for the site with a diameter at breast height (DBH) of at least 10 cm. **Remove the outer/inner bark** of the tree cores with a knife **but** make sure to **include the tissue of the outer tree rings**! Avoid sampling the heartwood! If you can, please keep the **core intact** because we plan to determine isotope in the 2023-ring.

Soil samples: Take a maximum of 5 soil samples at 0-10, 10-20, 20-30, 50-60, 80-90 cm at a location between the 3 (or 6) trees that you sampled. Litter should be removed for the soil sample at 0-10cm. Fill the exetainers for 50-80% with soil. In the case of a maximum soil depth of 30 cm, simply take 3 samples as indicated above. In the case of a maximum soil depth of 50 cm, take an additional 10 cm sample between 30 to 50 cm and note the exact depth (4 samples in total). In the case of maximum soil depth of 80 cm, take an additional 10 cm sample between 60 to 80 cm and note the exact depth (5 samples in total).

Close the sample vial: Please make sure the exetainer caps are tightly screwed on the vials. Hand tight is fine but check that the rubber sealing in the cap is not overly bend. Seal the cap additionally with parafilm (or if you don't have parafilm use tape). Remember, evaporation is the enemy!

Label the sample: Please make sure that your samples are clearly labelled. The label should include country (2-letter), site code (3-letter), sampling date (yymmdd), soil/tree species, and depth/number (e.g. CH_WSL_230525_Soil_20-30, or CH_WSL_230525_Beech_1). Sticky labels on top (first 3rd of the exetainer, underneath the cap) are preferred. Avoid handwriting with a text marker directly on the glass vial to avoid losing the "label" during sample handling. Double-check with metadata.

Take photos (optional): Only perform this task if you are new to the WATSON sampling campaign or if there was a significant change in the vegetation on your site between spring and summer. However, new fun pictures or site pictures are always welcome as we can use them for various presentations! Double-check with metadata.

For all pictures, please use your mobile phone. Please use the back and not the front camera (the latter typically provides photos at lower resolution compared to the one on the back)! Take a (1) representative landscape photo of each site, (2) representative photos of each tree, as well as (3) representative photos of the canopy. The latter will be analysed by us to obtain the crown gap fraction as a rough estimate of tree vitality on your site (description below). And of course, take pictures of yourself .

Label and upload photos: Please make sure that your photos are clearly labelled for landscape (e.g. CH_WSL_230525_Beech_Landscape), trees (CH_WSL_230525 _Beech1), canopy (CH_WSL_230525_Beech_Lab or CH_WSL_230525_Beech_1m_N) and yourself (CH_WSL_230525_Beech_Fun1). Upload your photos on google drive: XXX.

After sampling:

- Store all samples in a fridge (~4°C). Don't freeze them!
- Please **pack them nicely** in a box with some bubble wrap and double check that the labels are readable. Add a paper copy of the **import licence (attached to email)**.
  Send your vials as soon as possible to the following address: XXX
- Double-check again the metadata and tick the box for "sent".
- Double-check whether all "gaps" in the metadata are filled and all pictures are uploaded.

Instructions for taking canopy photos (Optional)

In the office/lab:

We need to know the field of view of your mobile phone camera. Put your phone horizontally with the back camera upward at 1 meter distance from a ruler and take a photo. Use a smartphone app or a physical bubble level to achieve a prober level. Make sure that meter divisions are clearly visible in the photo.

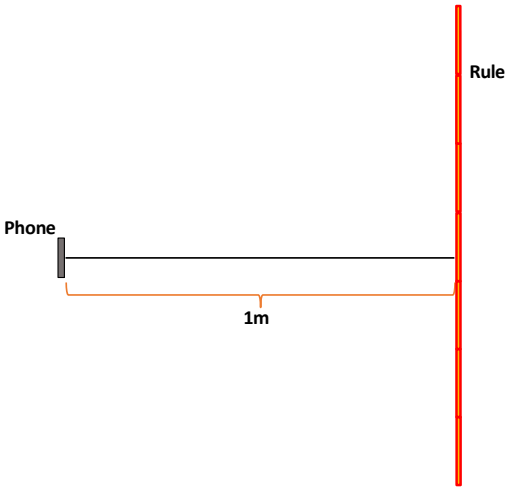

In the field:

Put your phone horizontally with the back camera upward underneath a representative tree of each site and species, at approximately 1 m above the soil surface. Use a smartphone app or a physical bubble level to achieve a proper level. Take photos at 1- and 5-meters distance to the stem. Repeat this procedure for 3 opposite directions (North, South, East or West). In total, a **minimum of 6 photos** are needed (i.e., 2 photos per direction). To improve the estimate, additional photos at 3-, 7- or 9-meters distance to the stem or at the fourth direction are highly welcome.

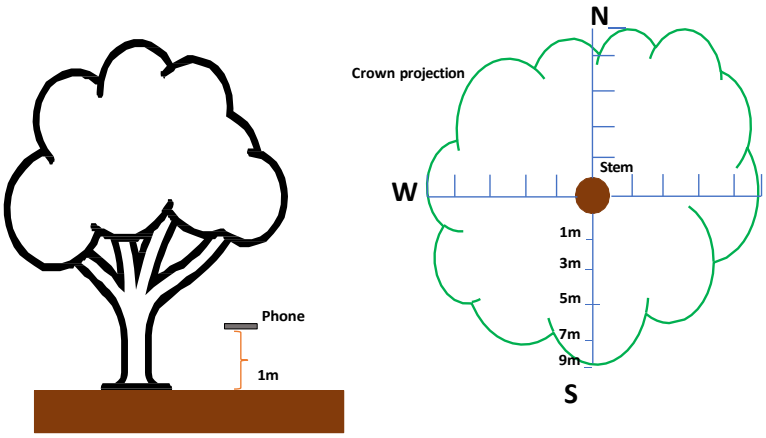

Recommendations: Avoid direct sun radiation on the crown and camera. The best conditions are met when the sky is homogeneously cloudy (as this provides a homogeneous background), or at least when the sunlight is shaded by clouds.

S3: Determination of the canopy gap fraction and canopy cover

The average canopy cover, i.e., the proportion of the forest floor that is covered by the vertical projection of the tree crown, was determined for each sampling site from non-hemispherical photographs taken with a phone camera that was levelled with a spirit level. For each tree, photos were generally taken at different distances from the tree (1, 3, 5 m from the stem) in 2 to 4 opposite directions (North, East, South, West). Most of the pictures were taken during the spring campaign but for some sites, pictures were taken during the summer campaign or during both campaigns.

To standardize the photos from different devices, the field of view (F_{oV}) for each phone was measured by taking a photo of a ruler placed one meter away from the camera. F_{oV} is given by:

$$F_{oV}=2 \tan^{-1} (L) \qquad \text{Eq. 1}$$

where L is the length of the ruler [m] in the picture.

Using the F_{oV}, a circular area with a radius of one meter was selected in the center of the image (to avoid overlap between the different pictures). The blue band (b) was extracted from each RGB image to differentiate between the pixels of the sky (high values of the blue band) and biomass (lower values of the blue band). The threshold to distinguish between pixels of the sky and biomass was set manually for each picture. The blue band images were converted to binary images with a value of 0 for biomass, and a values of 1 for the sky. Canopy cover (C) was then calculated via based on the difference in the number of biomass pixels with a value of 0 (P_0) and the number of pixels with the sky with a value of 1 (P_1) (Llorens and Gallart, 2000):

$$C = P_0/(P_0+P_1) \qquad \text{Eq. 2}$$

S4: Weights and details of different Exetainer types. Exetainer refers here to gas-tight 12 mL glass vials produced by Labco (Lampeter, UK). Label refers to the sticker affixed to the outside of the vial. The variable vial_id represents the product ID derived from Labco, while vial_type refers to the vial ID from Labco. vial_neck and vial_bottom describe the shape or characteristics of the vial's neck and bottom, respectively. vial_label indicates whether the vials were labeled. cap_type is the cap ID from Labco, cap_size describes the cap length, and cap_septum refers to the thickness of the septum. vial_mg is the mean weight in milligrams of approximately thirty vials, and cap_mg is the mean weight in milligrams of approximately thirty caps with septum. label_mg is the estimated mean weight of the label in milligrams. Finally, exe_weight is the total weight in milligrams, calculated as the sum of vial_mg, cap_mg, and label_mg.

exe_type	vial_id	vial_type	vial_neck	vial_bottom	vial_label	cap_type	cap_size	cap_septum	vial_mg	cap_mg	label_mg	exe_weight	labco.links
2	938W	3B	narrow	round	no	VC309	short	thin	11456.8	1301		12757.8	Exetainer® 12ml Vial - Round Bottom
4	939W	3B	narrow	round	yes	VC309	short	thin	11479.0	1301	120	12900.0	Exetainer® 12ml Vial - Round Bottom - Labelled
5	738W/W	3W	wide	flat	no	VC309	short	thin	11784.0	1301		13085.0	Exetainer® 12ml Vial - Wide Body - Flat Bottom
6	738W	3	narrow	flat	no	VC309	short	thin	11452.7	1301		12753.8	Exetainer® 12ml Vial - Flat Bottom
7	739W/W	3W	wide	flat	yes	VC309	short	thin	11784.0	1301	120	13205.0	Exetainer® 12ml Vial - Wide Body - Flat Bottom - Labelled
8	739W	3	narrow	flat	yes	VC309	short	thin	11452.7	1301	120	12873.8	Exetainer® 12ml Vial - Flat Bottom - Labelled
9	736W	3	narrow	flat	no	VC329	long	thick	11459.5	1599		13058.5	Exetainer® 12ml Vial - Flat Bottom - DW Cap
10	737W	3	narrow	flat	yes	VC329	long	thick	11459.5	1599	120	13178.5	Exetainer® 12ml Vial - Flat Bottom - Labelled - DW Cap

7.6 Partitioning and dynamics of mobile and tightly bound soil water

The study *Isotopic insights into the dynamics of soil water pools along an elevation gradient* (Kocum et al., submitted) employed a uniquely designed experimental setup to investigate how the dynamics of distinct soil water pools, specifically mobile versus tightly bound water, vary along an elevational gradient, and how reduced snow accumulation at lower elevations influences soil water distribution compared to higher-altitude sites.

The novelty of this study lies in the number of simultaneously studied locations spanning a well-defined elevation gradient, and in the methodological approach used to separate soil water pools. Unlike previous studies, mobile water was not compared with bulk soil water, but rather with the tightly bound water fraction selectively extracted from the soil matrix. This approach enabled a more precise characterization of water compartments relevant to plant water uptake.

Although the isotopic composition of tightly bound water and bulk water showed only minor average differences, pronounced seasonal variability was observed, especially during spring and autumn, when the isotopic offset and the relative proportion of mobile to tightly bound water were greatest. These findings underscore the need to account for seasonal dynamics in studies, especially in short-term or single-time-point studies, that rely on comparisons between soil and xylem water for plant source water attribution. The results provide valuable insights for future research exploring the interactions between soil water pool dynamics, vegetation type, rooting depth, and changes in precipitation regimes under ongoing climate change.

Manuscript review stage

The manuscript was submitted to Hydrology and Earth System Sciences on 11 August 2025.

Isotopic insights into the dynamics of soil water pools along an elevation gradient

Jiri Kocum[1,2], Kristyna Falatkova[1], Vaclav Sipek[1], Karel Patek[1,3], Jan Hnilica[1], Michal Jenicek[2], Martin Sanda[4], Lukas Trakal[5], and Lukas Vlcek[1]

[1] Institute of Hydrodynamics of the Czech Academy of Sciences, Prague, 160 00, Czech Republic
[2] Department of Physical Geography and Geoecology, Faculty of Science, Charles University, Prague, 128 00, Czech Republic
[3] Department of Water Resources and Environmental Modeling, Faculty of Environmental Sciences, Czech University of Life Sciences, Prague, 165 00, Czech Republic
[4] Department of Landscape Water Conservation, Faculty of Civil Engineering, Czech Technical University in Prague, Prague, 166 29, Czech Republic
[5] Department of Environmental Geosciences, Faculty of Environmental Sciences, Czech University of Life Sciences, Prague, 165 00, Czech Republic

Correspondence to: Jiri Kocum (kocum@ih.cas.cz)

Abstract. In recent years, research on the soil–plant–atmosphere continuum has gained renewed importance with the development of novel methodological approaches, particularly the use of stable hydrogen and oxygen isotopes in water, which allow for tracing water movement and plant responses at much finer spatial and temporal scales. These techniques provide valuable insights into plant adaptation to changing environmental conditions associated with climate change. A key focus of this research is the understanding of soil water dynamics and their sensitivity to declining snow cover, changes in precipitation phase, rising mean temperatures, and an increased frequency of extreme weather events such as intense rainfall and prolonged drought. In this study, we employed a uniquely designed experimental setup to examine how the dynamics of distinct soil water pools—mobile versus tightly bound water—vary along an elevational gradient, and how the absence of snow accumulation in lowland areas affects water distribution within the soil profile compared to higher elevations. Our results indicate a prolonged residence time of winter-derived soil water in lowland sites, in contrast to a rapid turnover at the highest elevation, where the winter water signal dissipated shortly after snowmelt. Given the projected continued decline in snow cover at higher elevations in Central Europe, these findings are critical for improving predictions of soil water storage and, consequently, the availability of water for plants under future climatic conditions. A key innovation of this study lies in the use of an experimental method enabling the selective extraction of tightly bound soil water for isotopic analysis—offering a more targeted and process-specific alternative to conventional bulk water sampling.

1 Introduction

Soil drought is becoming increasingly prevalent due to climate change, which alters air temperature, total amount of precipitation and its intra-annual distribution (Gebrechorkos et al., 2025; Samaniego et al., 2018). These shifts have contributed to a sustained decline in vegetation-accessible water over the past three decades (Jiao et al., 2021). In response, there has been

growing interest in the role of snowpack water storage and runoff generation in snow-dominated catchments, which are essential for groundwater recharge and soil moisture replenishment (Jenicek et al., 2020, 2021; Šípek et al., 2021; Musselman et al., 2017). Numerous studies project a continued decline in snow cover across mountainous regions as a consequence of rising air temperatures (Musselman et al., 2017; Marty et al., 2017; Jenicek et al., 2018; Willibald et al., 2020), accompanied by a shift from snowfall to rainfall during the winter season (Harpold et al., 2017; Safeeq et al., 2016). The implications of these changes in snow storage for the annual water balance remain a critical and unresolved question in hydrological research. Equally important are the downstream consequences for plant-available water in lowland ecosystems, particularly during the latter part of the growing season when drought stress is most acute (Büntgen et al., 2021; Qin et al., 2020; Mankin et al., 2019). A comprehensive understanding of the soil–plant–atmosphere continuum, a concept originally introduced by Gradmann (1928) and later formalized by van den Honert (1948), is therefore crucial for predicting vegetation dynamics and adaptive responses under increasingly frequent and severe drought conditions.

The relationship between plant water use and local hydrology has been studied since the early 20th century (Bates et al., 1921). Pioneering studies on water transport through soils and plants were subsequently summarized in comprehensive reviews (e.g., Tinker, 1976; Weatherley, 1976; Molz, 1981). A major shift in perspective occurred when Dawson and Ehleringer (1991) demonstrated that some riparian trees primarily access deeper groundwater, rather than the more readily available stream water. However, later work by Bond et al. (2002) appeared to challenge this finding by demonstrating diel fluctuations in stream baseflow attributable to plant transpiration, demonstrating clear interactions between transpiration and streamflow. Despite this apparent contradiction, Brooks et al. (2010) showed that mobile water (represented by stream water) and tightly bound soil water (represented by the plant water) are isotopically distinct. Their results suggested that, especially during the dry season, mobile water traveling through macropores or pipes bypasses tightly bound soil water, which is instead more likely to be taken up by plants and not contribute to streamflow.

This conceptual breakthrough formed the basis for the ecohydrological separation framework, later termed the "Two Water Worlds" (TWW) hypothesis (McDonnell, 2014). Since then, the TWW hypothesis has stimulated widespread debate, with numerous studies supporting (e.g., Goldsmith et al., 2012; Evaristo et al., 2015; Hervé-Fernandez et al., 2016) or challenging (e.g., Geris et al., 2015; Vargas et al., 2017; Dubbert et al., 2019) the existence of isotopically distinct water pools for vegetation use and runoff generation. Despite ongoing refinements, the hydrological connectivity between plant-accessible water and mobile water remains a central, unresolved question in ecohydrology.

Due to inconsistencies in the aforementioned studies, a new way forward has been proposed (Berry et al., 2017). Key priorities for future research include investigating internal water cycling within the phloem and xylem, identifying potential sampling and methodological biases, and improving both the spatial and temporal resolution of sampling strategies. Dubbert et al. (2019) further highlight the need to develop a standardized sampling protocol to harmonize methodologies across research groups and thus improve the comparability of results. Such a protocol has recently been proposed by Ceperley et al. (2024).

However, the vast majority of studies comparing soil water and xylem water (e. g., Zapater et al., 2011; Meunier et al., 2017; Vargas et al., 2017; Barbeta et al., 2019, 2020; Liu et al., 2021; Brighenti et al., 2024; Benettin et al., 2024) rely on

mobile and so-called bulk soil water for comparison. Mobile water is typically extracted using suction lysimeters or other vacuum-based systems. The water obtained in this manner—usually under tension of -60 kPa (Brooks et al., 2010; Berry et al., 2017; Sprenger et al. 2018)—originates primarily from macropores and preferential flow paths. In contrast, bulk soil water encompasses the total soil water content, including both gravitational and capillary pore water. During dry periods, when macropores are emptied and suction lysimeters cannot collect water, bulk soil water reliably represents the tightly bound water fraction. However, during wet conditions, when gravitational pores are partially or fully saturated, a significant portion of the bulk soil water may also consist of mobile water. Under such circumstances, bulk water may no longer serve as a representative of the tightly bound fraction and may not be as suitable for direct comparison with xylem water, particularly under the assumption that plants preferentially utilize tightly bound soil water (McDonell, 2014).

This study investigated the distinction between tightly bound soil water (TBW) and mobile soil water (MW). The TBW, extracted using a novel experimental approach, was further compared with the potential composition of bulk soil water (BW) to assess whether these two components can be used interchangeably without significant differences in their isotopic composition. The experiment was conducted simultaneously at four sites spanning an elevation gradient of more than 1000 meters. The focus on different elevations is especially important in areas in the rain-snow transition zone, which are widely affected by changes in snow storage due to increasing air temperature. The site selection aimed to capture the influence of declining snow cover and duration and reduced total precipitation on the isotopic behaviour of soil water. For this purpose, sites with similar soil texture were chosen, as soil texture strongly affects the proportion of macropores and capillary pores. The sampling campaign was conducted at two-week intervals from February to November 2023, except at the highest elevation site, which was accessible only from May onwards. The primary objectives of the study were to:

a. Determine whether there is a significant difference in the isotopic composition of tightly bound and mobile soil water
b. Evaluate the annual course of the isotopic composition of soil water across the elevation gradient with regard to the decrease in snow cover and precipitation in general
c. Identify the sources of tightly bound soil water
d. Determine whether replacing bulk soil water with tightly bound water can lead to different results

2 Study sites

The experiment was conducted in Czechia at four experimental plots (Tab. 1) strategically selected to span a pronounced elevation gradient, thereby capturing corresponding variations in temperature, precipitation, and snow cover extent and duration (Fig. 1). The study sites ranged from the fertile agricultural lowlands of the Elbe River Basin—Zvěřínek (185 m a.s.l.)—through the highlands and foothills—Trhové Dušníky (430 m a.s.l.) and the Liz catchment (870 m a.s.l.)—to the upper montane zone of the Bohemian Forest—Rokytka catchment (1,260 m a.s.l.). Throughout the manuscript, these locations are referred to by the abbreviations ZV, TD, LI, and RO, respectively.

Although the soil types varied due to the natural pedogenetic context of each site (Regosol, Gleyc Fluvisol, Cambisol, and Podzol), all plots exhibited similar soil texture (loamy sand or sandy loam). This minimized confounding effects from differences in clay content, allowing for a more direct assessment of elevation-related influences on soil water behaviour. Owing to the pronounced elevation differences, it was not feasible to maintain identical vegetation cover across all sites. However, vegetation at each location was representative of typical plant communities found at the corresponding elevation zones in Central Europe—ranging from agricultural land in the lowlands, to meadows, spruce forest, and beech forest at higher elevations. The agricultural land at the lowest elevation lacked vegetation cover from February to March, with post-harvest stubble remaining from October onward.

Table 1. Detailed characteristics of selected experimental areas. Climatic data (total annual precipitation and mean annual temperature) are for 2023. Snow data and climate classification (Köppen system) follow Tolasz et al. (2007). Further details for individual locations are provided in the cited references.

Name of the location		Zvěřínek	Trhové Dušníky		Liz		Rokytka	
Coordinates		50° 9' 20" N 15° 0' 37" E	49° 43' 12" N 14° 0' 46" E		49° 4' 0.2" N 13° 40' 49" E		49° 1' 22" N 13° 24' 23" E	
Elevation (m a. s. l.)		185	430		870		1,260	
Total precipitation (mm year^{-1})		631	680		931		1,380	
Average annual temperature (°C)		9.2	7		6.7		4.8	
Max snow depth (cm)		< 15	20 – 30		50 – 70		> 150	
Days with snow cover		< 30	60 – 80		100 – 120		> 160	
Climate classification		Cfb	Cfb		Dfb		Dfc	
Land cover		Agricultural land (*Sinapis alba*)	Meadow (*Agrostis capillaris, Festuca rubra*)		Forest (*Picea abies L.*)		Forest (*Fagus sylvatica L.*)	
Soil type		Regosol	Gleyc Fluvisol		Cambisol		Podzol	
Soil texture		Loamy sand	Sandy loam		Loamy sand		Loamy sand	
Retention curve parameters	Depth	20	20	40	20	40	20	40
	θ_r	0.05	0	0	0.18	0.18	0.10	0.06
	θ_s	0.39	0.50	0.50	0.51	0.52	0.65	0.45
	α	0.05	0.08	0.06	0.05	0.05	0.34	0.50
	n	1.74	1.20	1.18	1.37	1.70	1.45	1.34
	m	0.42	0.17	0.15	0.27	0.41	0.31	0.26
Reference		Seyedsadr et al. (2022)	Šípek et al. (2019)		Zelíková et al. (2024)		Vlček et al. (2021)	

Throughout the year, groundwater levels at most sites remain at least four meters below the soil surface. The only exception is the TD site, where groundwater rises to approximately one meter below the surface during the spring months, potentially influencing the isotopic composition of the overlying soil profile. However, due to the sandy texture of the soil, capillary rise is limited, and this influence is therefore assumed to be confined to the lower soil layer sampled.

Each site was equipped with a meteorological station (Fiedler, Czechia) with rainfall gauges (Meteoservis, Czechia), Palmex precipitation collectors (Palmex Ltd., Zagreb, Croatia), and a tensiometer-regulated vacuum lysimeter system (VS-Pro, UMS, Germany) for mobile soil water sampling. Precipitation amounts, soil moisture, and air temperature were measured in 10-minute steps and calculated on daily basis.

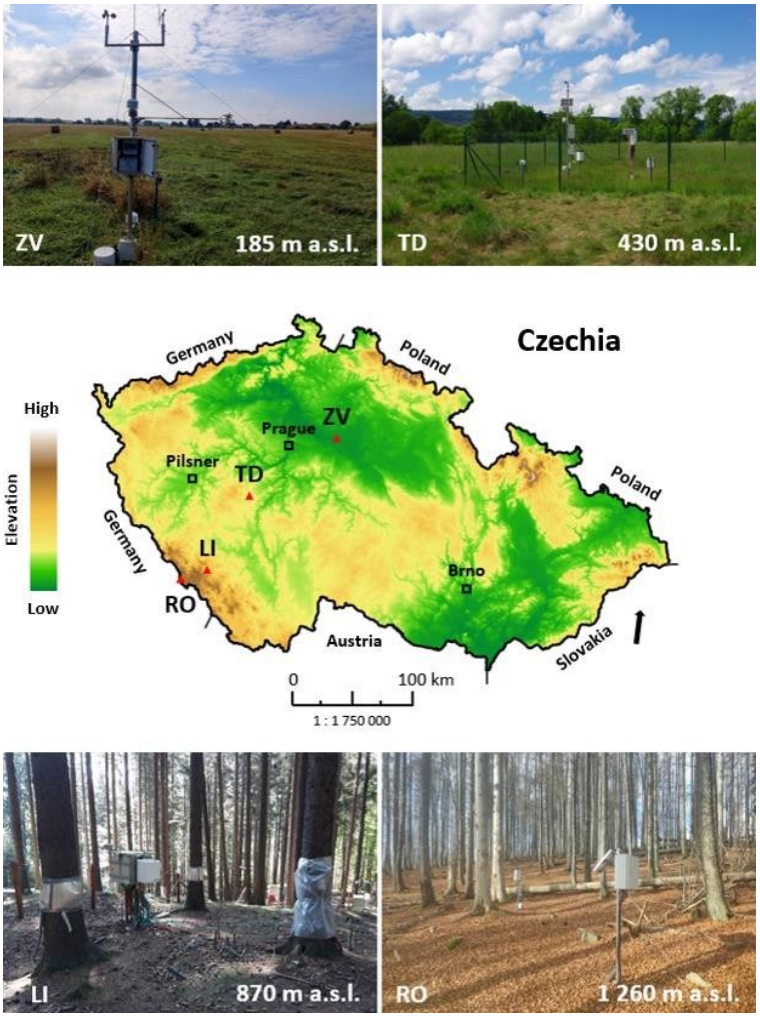

Figure 1. Location of selected experimental areas. Panels: top left – Zvěřínek; top right – Trhové Dušníky; bottom left – Liz; bottom right – Rokytka. Map data: Digital Vector Database of the Czech Republic ArcČR® version 4.3 (ARCDATA PRAHA, s.r.o., 2024).

3 Data and methods

3.1 Field sampling

At all study sites, samples of precipitation, mobile water (MW), and soil cores were collected at two-week intervals for the stable isotope analysis from February to November 2023. The exception was the RO location, which was only accessible from May 2023 onwards due to its remote location in the heart of the Bohemian Forest National Park, as well as heavy snow conditions during winter and early spring. For the extraction of MW, the tensiometer-controlled vacuum system (VS-Pro) was employed with a maximum applied tension of -60 kPa (Brooks et al., 2010; Berry et al., 2017; Sprenger et al., 2018). The extraction was conducted from two depths, specifically 20 cm and 40 cm, which often play a significant role in root water uptake (Hackmann et al., 2025). Throughout the manuscript, these depths are referred to as shallow and deep layers, respectively. In both cases, the extracted samples represented a composite of water collected over the preceding two weeks.

For the TBW extraction, undisturbed soil cores (100 cm^3) were collected from the same two depths, with five replicates per depth. The soil cylinders were wrapped in Parafilm® and stored in a portable refrigerator for transport to the laboratory. A total of 805 soil cores, 329 MW samples, and 108 precipitation samples were collected during the sampling period (Tab. 2).

Table 2. Overview of samples collected at individual locations

	Zvěřínek	Trhové Dušníky	Liz	Rokytka
Soil cores	220	230	215	140
Mobile soil water	101	150	57	21
Precipitation	20	30	44	14
Groundwater	-	9	-	-

3.2 Laboratory processing of soil samples

To obtain TBW the soil cores were inserted into the pressure plate apparatus for retention curve determination (5 Bar Pressure Plate Extractor, Soil Moisture Equipment Corp., CA, USA) with a 1 bar pressure plate cell was used. A pressure of 60 kPa (~ pF 2.4) for a two-week period was chosen to get rid of the MW fraction. Then, the top and bottom of the soil core were removed, and for further extraction, only the inner soil core was used (approx. 50 g of soil sample).

For the subsequent extraction of TBW, the mass balance mixing method was selected due to its accessibility, simplicity and high throughput (Fig. 2). Briefly, the soil sample was placed in a glass vial (volume of 60 mL) with a plastic cap and silicone sealing. Roughly 20-25 mL of a traced water was added to the sample, and the remaining space was filled with glass balls (5 mm in diameter) to remove the presence of air. Then, the samples were placed on a laboratory-constructed rotating device and continuously spun for 16 hours at a fixed speed of 15 rpm. Subsequently, they were stored in a refrigerator to allow sedimentation, after which 0.75 mL of the mixture was collected and filtered through a 0.45 µm mixed cellulose ester

membrane. The rest of the sample was dried at 105 °C for 48 hours and weighed to calculate the soil water content of the soil sample.

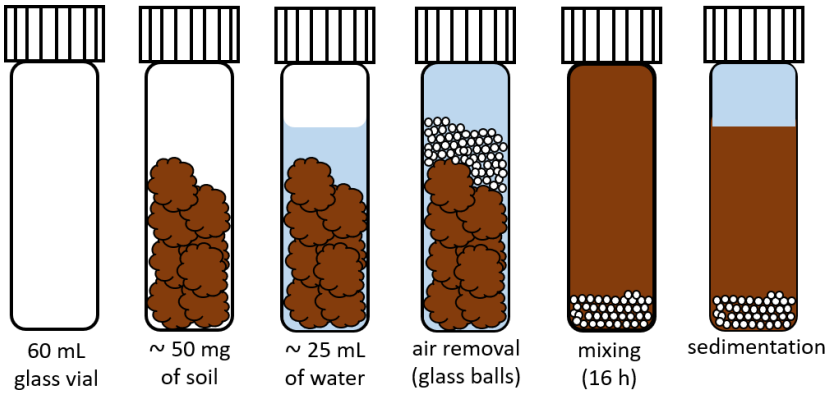

Figure 2. Sample processing procedure during the mixing extraction method.

Prior to using this procedure, conventional spike experiments with labelled water were conducted to verify the accuracy of the extraction methods. This allows us to assess the method's performance for specific soil types collected from our study sites. The resulting isotopic shift relative to labelled water (0.35 ± 0.15 and 3.02 ± 1.50 ‰ for $\delta^{18}O$ a $\delta^{2}H$, respectively) was then incorporated into data correction procedures by subtracting this error from the final isotopic values, and the associated standard deviations were incorporated into the reported measurement uncertainties (together with the standard deviation of the real data and the measurement uncertainty of the isotope analyser).

3.3 Isotope analysis and calculations

Stable isotope analyses were performed at the Institute of Hydrodynamics (Czech Academy of Sciences) with the L2140-*i* isotope analyser (Picarro Inc., Santa Clara, US). Standard mode (precision of ± 0.03 ‰ and ± 0.15 ‰ for $\delta^{18}O$ and $\delta^{2}H$, respectively) was used with 6 injections per sample, with the first 3 injections discarded. The isotope ratios are reported in per mil (‰) relative to Vienna Standard Mean Ocean Water (VSMOW) ($\delta^{2}H$ or $\delta^{18}O = (R_{sample}/R_{standard}-1) \times 1000$ ‰, where R_{sample} is the isotope ratio of the sample and $R_{standard}$ is the known reference value (i.e., VSMOW) (Craig, 1961)).

The isotopic composition of TBW was then calculated according to the mass balance mixing model (Eq. 1, 2).

$$\delta^{18}O_S = \frac{m_M}{m_S} \cdot \delta^{18}O_M - \frac{m_T}{m_S} \cdot \delta^{18}O_T \quad (1)$$

$$\delta^{2}H_S = \frac{m_M}{m_S} \cdot \delta^{2}H_M - \frac{m_T}{m_S} \cdot \delta^{2}H_T \quad (2)$$

where the sub-indices represent mixture (M), TBW (S), and traced water (T), m is the weight of those waters and $\delta^{18}0$ and $\delta^{2}H$ represent the stable isotopic composition of the sample.

Following the estimation of TBW, the same mass-balance mixing model was applied to calculate the potential stable isotopic composition of BW. In this approach, BW was represented as a mixture of MW, obtained from suction lysimeters, and TBW, as derived in the previous step. The relative proportions of these two components were determined based on measurements from the pressure plate apparatus.

Furthermore, the line-condition excess (lc-excess; Landwehr and Coplen, 2006) was calculated (Eq. 3) to identify and exclude data contaminated during the water extraction process.

$$lc - excess = \delta^2H - a \cdot \delta^{18}O - b \quad (3)$$

where a and b are the coefficients of the local meteoric water line (LMWL) from individual experimental plots. This contamination was manifested by abnormally high lc-excess values relative to the rest of the dataset. The methodological nature of the error was further supported by the observation that these anomalous values appeared randomly across different sites and sampling dates, with the only consistent factor being that the affected samples were processed together within the same run of the overpressure apparatus. In total, 6 out of 32 extraction runs of TBW, corresponding to approximately 98 out of 805 soil samples, had to be discarded due to this methodological error and significant sample contamination.

For the seasonal comparison of the stable isotopic composition of mobile and tightly bound soil water, seasons were defined as follows: winter (F), spring (MAM), summer (JJA), and autumn (SON).

3.4 Data fitting

To visualize the stable isotope data and characterize their seasonal variability, a sine function was fitted to the data using the iteratively reweighted least squares (IRLS) regression method with externally supplied weights in case of precipitation data (Eq. 4), a technique commonly applied to characterize the seasonal cycle of precipitation, streamflow, soil water, and groundwater (Kirchner, 2016; Zuecco et al., 2024; Floriancic et al., 2024; Xia et al., 2024). From the Eq. 4, the amplitude can then be determined according to the Eq. 5:

$$c(t) = a \cdot cos(2\pi ft) + b \cdot \sin(2\pi ft) + k \quad (4)$$

$$A = \sqrt{a^2 + b^2} \quad (5)$$

where t is the time, $c(t)$ represents the isotopic time series of the dataset, a and b are the cosine and sine coefficients determined by the IRLS regression, f is the frequency of annual isotopic fluctuation (f = 1 yr^{-1} for a seasonal cycle), k is the vertical shift of the sine wave, and A is the amplitude of the fitted sine wave.

Since the soil water and groundwater often lack a consistent seasonal signal, it is hard to fit them with a fixed sine wave, especially when spanning multiple seasons (Xia et al., 2024). Therefore, in some cases a weighted third-degree polynomial fit was used to provide a clear visualization of the stable isotopic composition throughout the year.

To establish the LMWLs and regression lines for soil water isotopic compositions, reduced major axis (RMA) regression was applied (Harper, 2016) instead of conventional linear regression. This approach was selected because

uncertainties in both δ^2H and $\delta^{18}O$ measurements are equally significant, whereas ordinary least squares regression assumes all error is confined to the y-axis and ignores uncertainty in the x-axis.

The slope (Eq. 6) of the RMA regression was calculated as the ratio of the standard deviations of δ^2H and $\delta^{18}O$, scaled by the sign of their Pearson correlation coefficient. The intercept was then calculated according to Eq. 7:

$$\beta_{RMA} = sign(r) \cdot \frac{\sigma_{\delta^2 H}}{\sigma_{\delta^{18} O}} \quad (6)$$

$$\alpha_{RMA} = \overline{\delta^2 H} - \beta_{RMA} \cdot \overline{\delta^{18} O} \quad (7)$$

where α_{RMA} and β_{RMA} are the intercept and slope of the RMA, respectively, r is Pearson correlation coefficient between δ^2H and $\delta^{18}O$, and $\sigma_{\delta 2H}$, $\sigma_{\delta 18O}$ are their standard deviations. This method minimizes the orthogonal distances between data points and the fitted line, making it more suitable for hydrological isotope data where both variables are subject to analytical and natural variability.

3.5 Seasonal Origin Index (SOI)

To characterize whether the extracted soil water originated from winter or summer precipitation, we calculated the SOI (Eq. 8) (Allen et al., 2019) for individual seasons, as well as for individual months, to provide a more detailed representation of gradual changes in water origin resulting from mixing with newly infiltrating water.

$$SOI = \begin{cases} \frac{\delta_x - \delta_{annP}}{\delta_{summerP} - \delta_{annP}}, if\ \delta_x > \delta_{annP} \\ \frac{\delta_x - \delta_{annP}}{\delta_{annP} - \delta_{winterP}}, if\ \delta_x < \delta_{annP} \end{cases} \quad (8)$$

where δ_x are the $\delta^{18}O$ isotopic values of soil water, and δ_{annP}, $\delta_{winterP}$, and $\delta_{summerP}$, are the $\delta^{18}O$ isotopic values of volume-weighted annual precipitation, typical winter (δ_{annP} – fitted amplitude), and typical summer (δ_{annP} + fitted amplitude) precipitation. The SOI ranges from -1 to 1, where values close to -1 represent water predominantly derived from winter precipitation, and values approaching 1 reflecting a dominant contribution from summer precipitation.

3.6 Statistical evaluation

To statistically assess the differences in annual courses of isotopic composition of individual waters (MW, TBW), it was necessary to consider the uncertainty in the coefficients of the regression models. Therefore, following the approach of Davison and Hinkley (1997), bootstrap residual resampling was performed as follows:

1. Regression models f_A and f_B were fitted to datasets A and B (Y; e.g., MW and TBW), and residuals (r_A, r_B) were calculated (Eq. 9, 10).

$$r_{A,i} = f_{A,i} - Y_{A,i} \quad (9)$$

$$r_{B,i} = f_{B,i} - Y_{A,i} \quad (10)$$

2. The following steps were repeated 10,000 times:

a. Synthetic datasets were generated (Eq. 11, 12).

$$Y_{A,boot,i} = f_{A,i} + r_{A,rand} \quad (11)$$

$$Y_{B,boot,i} = f_{B,i} + r_{B,rand} \quad (12)$$

where r_A,rand and r_B,rand are randomly sampled residuals (with replacement).

b. New regression curves f_A,boot and f_B,boot were fitted to the synthetic datasets.

c. The difference between the curves was computed and stored (Eq. 13).

$$d = \int |f_{A,boot} - f_{B,boot}| \quad (13)$$

3. A 95% confidence interval for the curve difference was derived as a range between the 0.025 and 0.975 quantiles of the resampled differences.
4. The samples were considered significantly different if the confidence interval did not contain zero.

4 Results

4.1 Precipitation and soil water data

Given the geographical proximity of the study sites, the slopes of the LMWLs were similar across all locations (Fig. 3), ranging from 7.7 to 8. In contrast, the y-intercepts varied considerably, from 4.2 to 11.5. Both parameters reflected the elevation gradient, with the lowest values recorded at the lowland ZV site and the highest at the mountainous location RO. The narrower isotopic range observed at the RO site was likely due to the incomplete dataset, as sampling was limited to the period between May and November.

Mobile soil water (MW) closely tracked the LMWLs, with slopes ranging from 7.4 to 8.1 and intercepts from 2 to 14, suggesting minimal isotopic alteration by evaporation or condensation. However, its isotopic range was narrower and often more depleted than that of precipitation. This depletion likely resulted from the absence of winter precipitation data (December and January), which typically exhibits more negative isotopic values. Similar to precipitation, an elevation trend was also apparent in the isotopic composition of MW.

In contrast, no consistent elevation pattern was observed for TBW. Unlike MW and precipitation, TBW exhibited clear signs of evaporative enrichment and isotopic modification due to condensation and internal mixing processes within the soil matrix. These effects were reflected in lower slopes (ranging from 5.9 to 7.5) and a broader dispersion of data around the respective soil water evaporation lines.

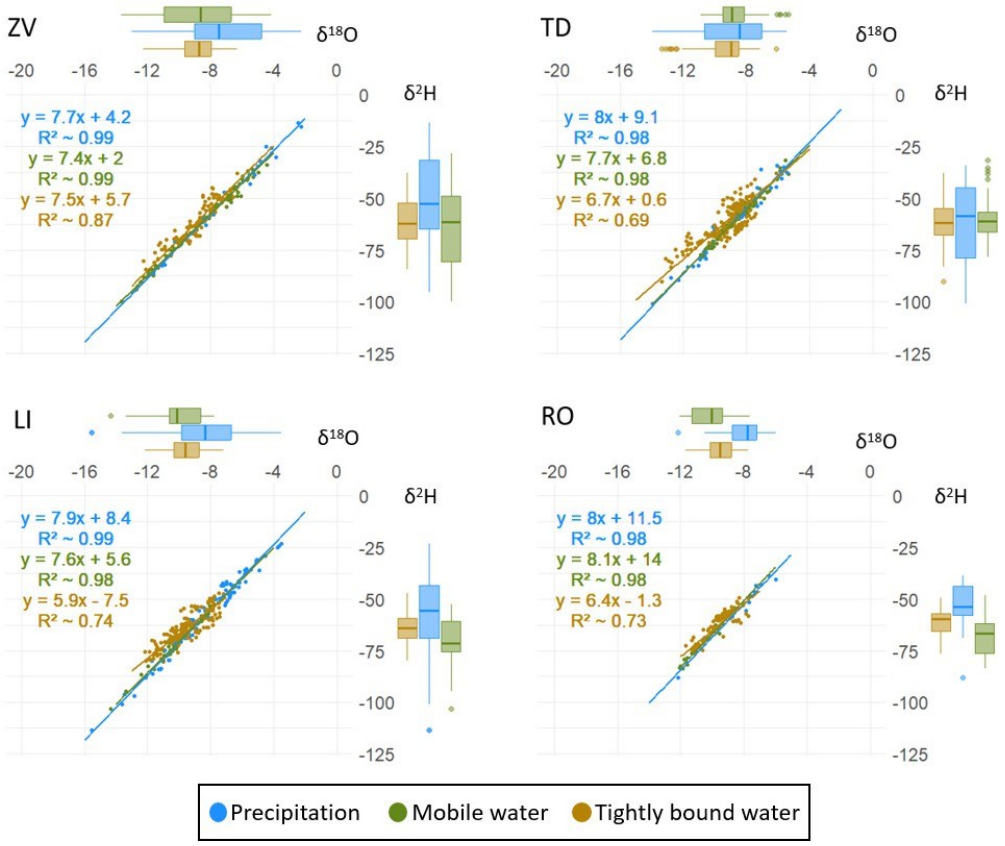

Figure 3. Dual-isotope plots of all water samples collected in this study, with corresponding regression lines. Panels: top left – Zvěřínek; top right – Trhové Dušníky; bottom left – Liz; bottom right – Rokytka. Precipitation is shown in blue, mobile soil water in green, and tightly bound soil water in brown.

4.2 Comparison of mobile and tightly bound soil water

A difference in stable isotopic composition of MW and TBW was observed across experimental sites (Fig. 4). Among all components, shallow MW exhibited the greatest annual isotopic variability. However, this variability diminished with increasing elevation. In lowland areas, deep soil water tended to be more isotopically depleted compared to shallow layers, but this trend weakened or even reversed at higher elevations.

The most pronounced contrasts between MW and TBW were recorded in spring and autumn, and to a lesser extent during summer at the TD site. At the ZV site, isotopic differences between shallow and deep soil water, both MW and TBW, became evident primarily in the second half of the year when shallow soil water was being replaced by the summer precipitation. In contrast, at the mountainous sites (LI, RO), the largest differences between shallow and deep MW occurred in the first half of the year, while the isotopic composition of TBW remained relatively stable throughout the study period.

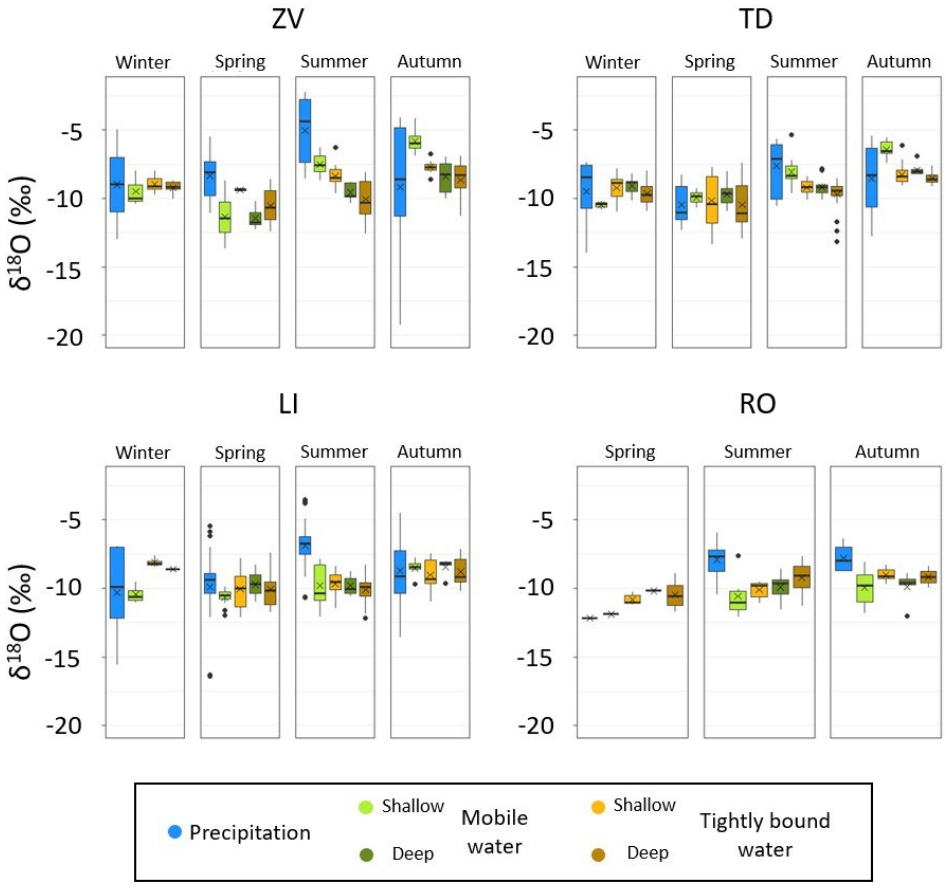

Figure 4. Seasonal comparison of the stable isotopic compositions of mobile and tightly bound soil water at the study sites. Panels: top left – Zvěřínek; top right – Trhové Dušníky; bottom left – Liz; bottom right – Rokytka. Seasons are defined as follows: winter (F), spring (MAM), summer (JJA), and autumn (SON). Boxplots are presented in the same order across panels, except for winter at the Liz site, where deep tightly bound soil water data are missing.

In most cases, the isotopic composition of soil water closely reflected that of precipitation during the corresponding time period. A notable exception was observed at the ZV site, where the response time of soil water to precipitation exceeded three months, making it the slowest among all sites. Another distinct anomaly was detected at the LI site during the summer, where soil water showed no clear isotopic response to recent rainfall. This lack of response is attributed to an intense precipitation event (>100 mm in two hours), which had an isotopic composition of approximately -10‰ for $\delta^{18}O$, and effectively stabilized the isotopic signature of soil water around this value.

4.3 Influence of the elevation gradient on the lag in soil water pool dynamics

Significant differences between MW and TBW were observed across the elevation gradient, both in their absolute quantities and their stable isotopic composition. With increasing elevation and precipitation amounts, the volumetric soil water content increased across the study sites (Fig. 5). At the lowest elevation sites (ZV, TD), the average water content was approximately 23 g per 100 cm^3 of soil at both, 20 cm and 40 cm depths, with slightly higher values in 20 cm, whereas at the highest site (RO) it reached up to 47 g per 100 cm^3 at both depths, again with slightly higher values in the upper layer. Furthermore, the influence of snow cover, increased precipitation, and lower temperatures (resulting in a delayed onset of the growing season and generally reduced evapotranspiration) was reflected in a gradual increase in soil water content during spring and early summer at higher-elevation sites. In contrast, in lowland areas, soil water content tended to plateau after the winter season due to full saturation of the soil profile. Following the onset of the growing season, accompanied by increased evapotranspiration and progressive soil drying, the soil water content began to decline at all sites.

In terms of stable isotopic composition, significant phase shifts between precipitation and various soil water pools were observed both among the study sites and within individual locations over the course of the year. The most pronounced lag between precipitation and shallow MW occurred at the ZV site, where the temporal offset exceeded three months (Fig. 5). This lag decreased along the elevation gradient by shortening to approximately six weeks at the mid-altitude site and becoming negligible at the highest-elevation site.

Furthermore, at all locations except the RO site, a distinct phase shift between shallow MW and TBW was observed between February and May, with the magnitude of this shift decreasing with increasing elevation. Deep soil water compartments generally exhibited similar temporal dynamics and phase lags as shallow tightly bound water, although they tended to be more isotopically depleted, hence contained more water from winter precipitation. An exception was found at the TD site, where the isotopic compositions of deep MW and TBW were different. Moreover, we hypothesize that the seasonal pattern of shallow TBW at the RO site would resemble that of the deep soil water pools. However, due to the limited number of data points available, all fitting approaches applied (both weighted and unweighted sine functions, as well as polynomial models) yielded comparable results, as illustrated in Fig. 5.

Following the onset of the dry season, the isotopic differences among soil water pools gradually diminished. By the end of the year, amplitude peaks became synchronized, resembling the pattern of shallow MW, though with attenuated isotopic signals. This attenuation likely resulted from mixing between newly infiltrated precipitation and residual water from previous periods. Despite this homogenization, a temporal offset between precipitation and MW remained evident. The negligible lag observed at the highest site was likely due to the high annual precipitation (~1,400 mm), which rapidly flushed the saturated soil profile.

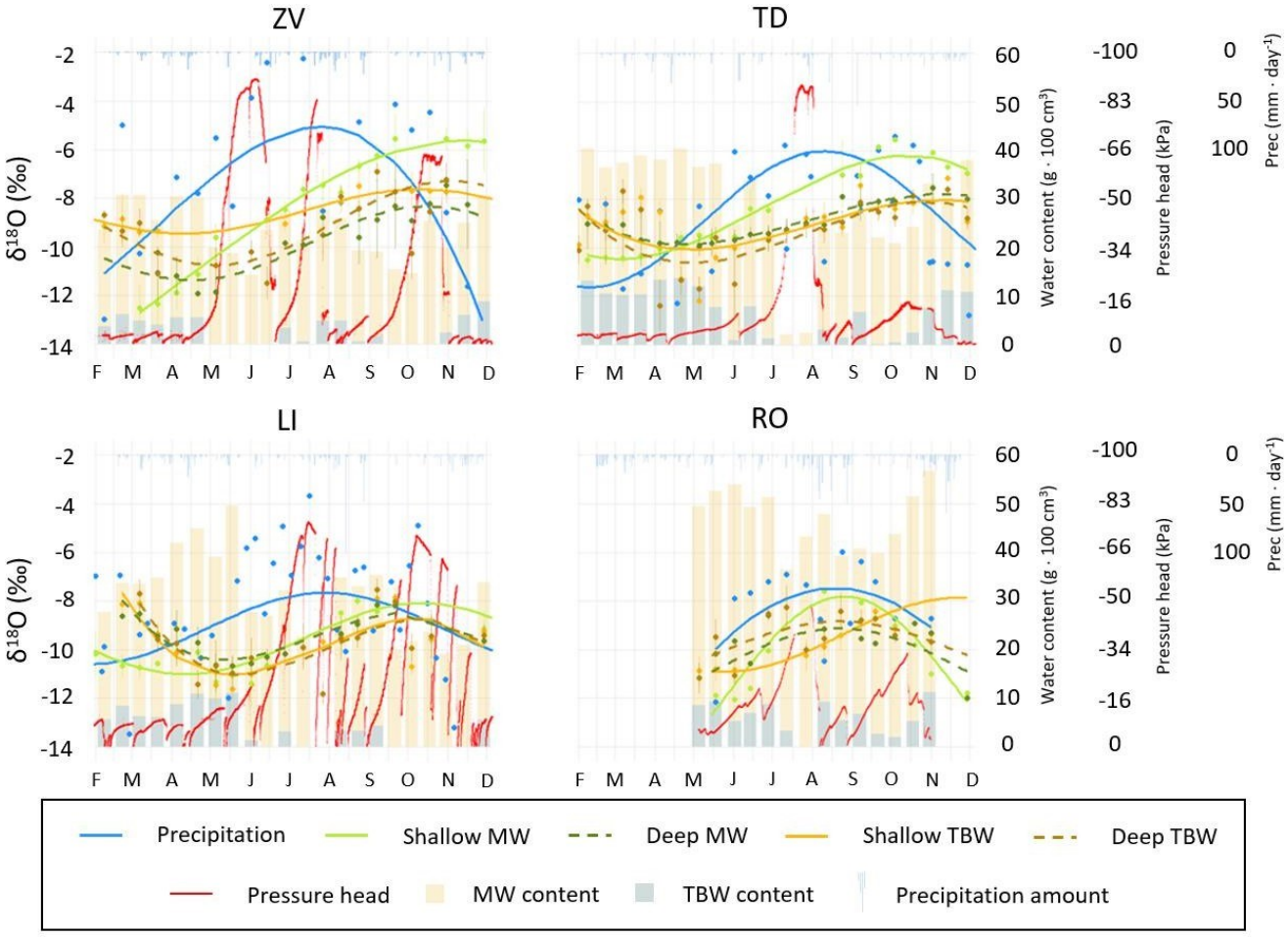

Figure 5. Annual variation in the isotopic composition of soil water in relation to soil water content, pressure head, and precipitation amounts. Both soil water content and pressure head refer to a depth of 20 cm. Panels: top left – Zvěřínek; top right – Trhové Dušníky; bottom left – Liz; bottom right – Rokytka.

The influence of the elevation gradient was further supported by the bootstrap residual analysis, which revealed statistically significant differences in the seasonal dynamics of the stable isotopic composition of soil water pools. These differences were more pronounced in lowland areas (Table 3). Among the four pairwise comparisons assessed (shallow MW vs. TBW; deep MW vs. TBW; shallow vs. deep MW; and shallow vs. deep TBW), the most consistent differences were observed between shallow and deep MW. This contrast was statistically significant in three out of four cases, with the exception of the LI site, where—despite apparent differences early in the year—the statistical test did not confirm significance.

For the comparison between deep MW and TBW at the ZV and TD sites, no statistically significant differences were detected; however, the null hypothesis was rejected only marginally, with the critical zero threshold exceeded by just -0.07 and 0.03, respectively.

In the case of shallow MW vs. TBW at the ZV site, a statistical difference was not confirmed, despite clearly distinct isotopic signatures (Fig. 5). This outcome likely reflects a limitation of the applied statistical method, which lacks sensitivity to detect differences in symmetrically distributed data. A similar limitation may also affect the comparison between shallow and deep MW at the RO site. However, the two instances confirming the null hypothesis at this site were more likely due to a lack of the TBW data and their unrepresentative interpolation using a sine curve (Fig. 5).

Table 3. The results of the bootstrap residual resampling analysis. H_0: Fitted sine functions are statistically different. The H_0 is rejected if the interval between q025 and q975 contains zero.

Compared combinations	Quantiles	Locations			
		Zvěřínek	Trhové Dušníky	Liz	Rokytka
Shallow MW	q025	-0.44	-1.19	-0.20	1.42
vs.	q975	0.40	-0.29	1.40	2.62
Shallow TBW	Result	False	True	False	True
Deep MW	q025	-0.07	-0.83	-0.69	-0.82
vs.	q975	1.11	0,03	0.76	1.25
Deep TBW	Result	False	False	False	False
Shallow MW	q025	0.65	0.33	-1.27	-2.33
vs.	q975	1.68	0.80	0.23	-0.67
Deep MW	Result	True	True	False	True
Shallow TBW	q025	0.12	-0.36	-0.69	-0.58
vs.	q975	1.15	0.83	0.83	1.13
Deep TBW	Result	True	False	False	False

4.4 Origin of the soil water

The results of water origin analyses revealed distinct temporal patterns in the SOI across the study sites. Among the soil water components, shallow MW showed the highest isotopic variability, with the magnitude of fluctuations decreasing along the elevation gradient. Within the soil profile, the lowest SOI values, indicating a predominant contribution of winter precipitation, were typically recorded in spring, whereas the highest values, reflecting a dominant influence of summer precipitation, occurred in autumn (Fig. 6).

The influence of winter precipitation remained detectable in the soil profile until late summer at all sites except the highest-elevation site, RO. This pattern was evident across all soil water compartments except shallow MW, which was already affected by summer precipitation during the summer months. At the RO site, the data obtained indicate that influence of winter

precipitation had already diminished by May. Although this assessment may be influenced by the absence of data from previous months.

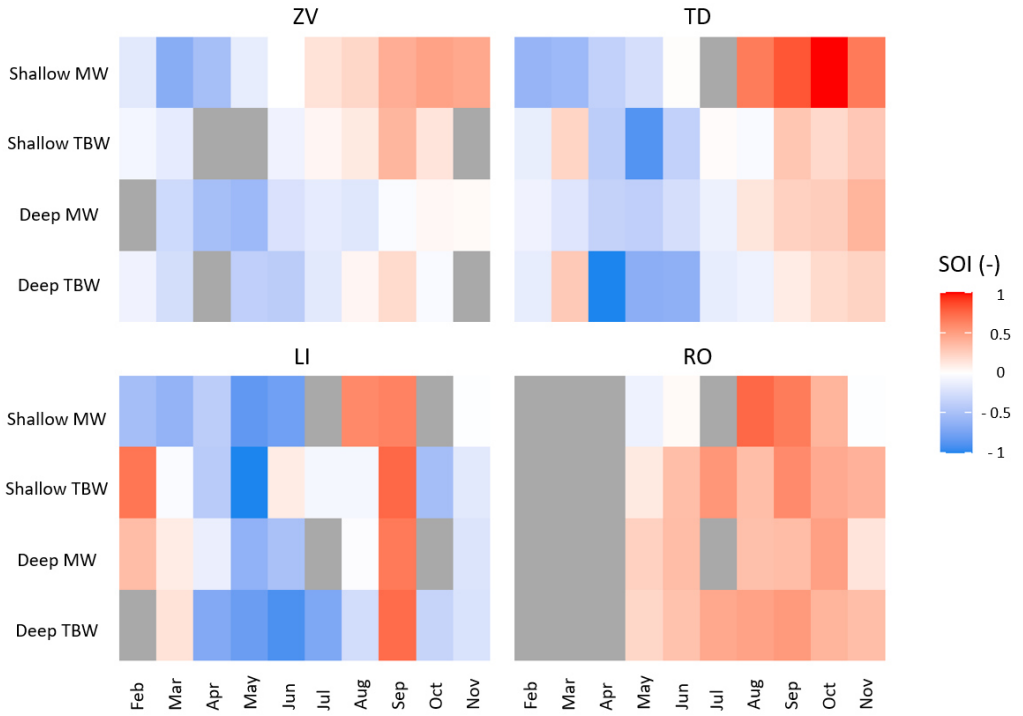

Figure 6. Seasonal origin index (SOI) values for individual sites and months. The abbreviations MW and TBW refer to mobile and tightly bound soil water, respectively. Values near -1 indicate a predominant contribution from winter precipitation, whereas values approaching 1 reflect a dominant contribution from summer precipitation. Grey areas indicate missing data for the respective period. Panels: top left – Zvěřínek; top right – Trhové Dušníky; bottom left – Liz; bottom right – Rokytka.

The highly positive SOI values observed in autumn at the TD site were attributed to a period of severe drought in July, which desiccated the upper soil layers (Fig. 5), followed by rewetting from late-summer rainfall. SOI values increased steadily from August to October and subsequently declined, closely mirroring the isotopic composition of precipitation during this period. Conversely, the strongly negative SOI values recorded in spring were likely caused by a rising groundwater table. This would explain their earlier appearance in deeper soil layers and delayed onset in shallower horizons. Notably, despite the fact that the proportion of MW in the deeper soil layer reached up to 64% relative to TBW at the beginning of the year, there was no isotopic homogenization between these two water pools, and both components remained isotopically distinct. Furthermore, we attribute the alternation of negative and positive SOI values at the TD site early in the year to preferential flow, which may have influenced the February samples of tightly bound water. We further hypothesize that the isotopic composition during this

period would resemble that at the LI site, where water from the previous summer and autumn was retained and delayed within the soil profile.

The markedly positive SOI values observed in September at the LIZ site were linked to the second most intense precipitation event of the year, nearly 50 mm, characterized by an isotopic composition of -6.55‰ for $\delta^{18}O$ and -43.36‰ for $\delta^{2}H$, which saturated the otherwise relatively dry soil profile.

4.5 Bulk soil water

Although BW was not directly sampled in this study, we present a conceptual illustration of its potential isotopic composition based on the obtained data. The results showed, that the stable isotopic composition of BW, estimated indirectly using a mass-balance mixing model (Eq. 1, 2), may vary statistically from TBW for both $\delta^{18}O$ and $\delta^{2}H$. Unpaired t-test ($P < 0.05$) revealed this difference on at least one sampling date at both lowland study site (ZV, TD), with no difference observed at higher elevations. During the summer drought period, however, when soil desiccation removed almost all MW from the soil profile, BW effectively represented TBW alone.

Since the isotopic signature of BW depends on both, the relative proportions of MW and TBW and the isotopic contrast between them, the greatest deviations were observed during the spring and autumn seasons. During these periods, both the isotopic difference between water pools and the proportion of MW in the soil reached their annual maxima (Fig. 5). At the ZV site, the discrepancy between BW and TBW was primarily driven by the pronounced isotopic contrast between mobile and tightly bound fractions, despite the low proportion of MW in the profile. In contrast, at the TD site, the difference was mainly attributed to a higher proportion of MW, while the isotopic contrast between the components was less pronounced.

In cases where BW and TBW differed, the average isotopic offset was 0.41‰ for $\delta^{18}O$ and 2.29‰ for $\delta^{2}H$, with maximum differences reaching 1.48‰ and 7.99‰, respectively. When BW values were used to calculate the SOI, only minimal or no differences between BW and TBW were observed from a broader perspective (Fig. 7). Notable deviations, however, occurred during individual sampling campaigns in April and May. In these instances, the SOI difference between BW and TBW reached up to 0.3.

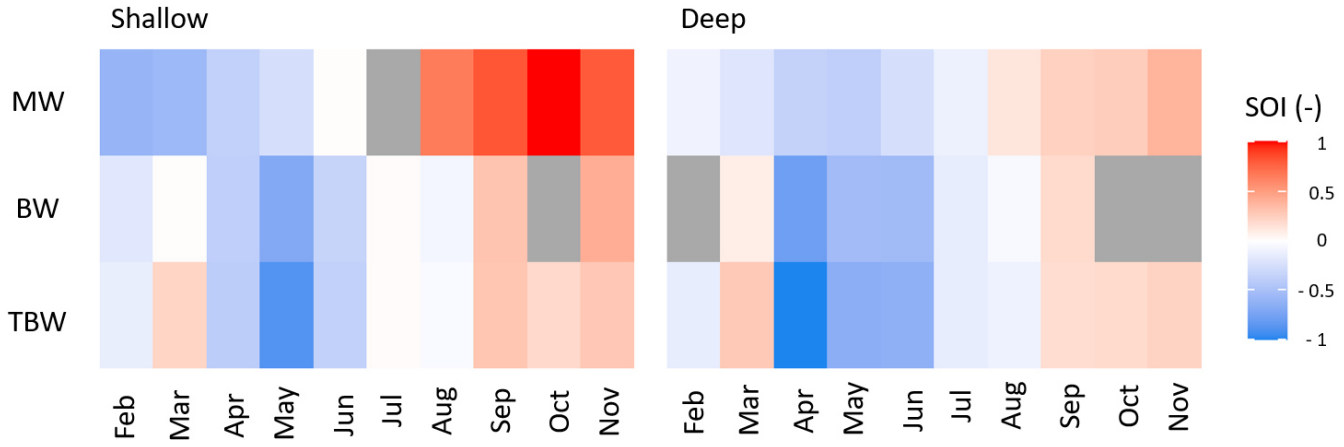

Figure 7. Comparison of the difference in SOI calculations using mobile (MW), bulk (BW) and tightly bound (TBW) soil water at the Trhové Dušníky site. Values near -1 indicate a predominant contribution from winter precipitation, whereas values approaching 1 reflect a dominant contribution from summer precipitation. Grey areas indicate missing data for the respective period.

5 Discussion

5.1 Isotopic changes due to soil properties and precipitation amount

All soil samples obtained in this study fell close to or directly on the LMWL, indicating their meteoric origin and suggesting minimal influence of the selected extraction procedures on isotopic composition. Consistent with previous studies (e.g., Hervé-Fernández et al., 2016; Sprenger et al., 2018), MW was closely aligned with the LMWL, whereas TBW exhibited a lower slope and greater variability. This reflects its longer residence time in the soil profile and mixing with water of varying ages. Interestingly, the isotopic characteristics of TBW in our study were similar to those reported for xylem water in several studies (Oliveira, et al., 2025; Floriancic et al., 2024; Brighenti et al., 2024; Yang et al., 2023; Goldsmith et al., 2019).

Despite the occurrence of extreme drought during the sampling year, which should leave an isotopically enriched signal in soil water (Dubbert et al., 2019), no such enrichment was observed at any of the study sites, regardless of precipitation regime or land cover. This was most likely due to the sampling depth (20 and 40 cm), as isotopic enrichment from evaporation typically occurs at shallower depths, between 5 and 15 cm (Dubbert et al., 2019). However, while Floriancic et al. (2024) reported no evaporative effect even at 10 cm depth, Brooks et al. (2010) observed significant evaporative enrichment down to 30 cm. This discrepancy may be attributed to differences in soil texture or extraction methodologies and their associated, often unquantified, errors, particularly under low soil moisture conditions during drought periods.

In agreement with Kleine et al. (2020), we observed a longer mean transit time, inferred from the phase shift of individual isotopic data, in non-forested areas. This phase shift also increased with soil depth, particularly for MW. In contrast,

the phase shift observed in TBW remained similar between shallow and deep layers. The greater lag observed in non-forested areas is likely driven by two main factors. The first is precipitation amount (Hervé-Fernández et al., 2016) for which higher rainfall can enhance leaching, thereby diminishing the isotopic distinction between MW and TBW. The second is vegetation cover, because, both soil texture and vegetation significantly influence the velocity of the wetting front (Xue et al., 2024). Preferential flow pathways promote deeper and more rapid infiltration in forested areas, whereas under bare soil or grass, water infiltration proceeds more slowly and diffusively.

The unexpectedly rapid turnover in isotopic composition at our highest-elevation site (RO) contrasts with results from other studies. For example, Floriancic et al. (2024) reported significant differences in soil water isotopic composition within the top 40 cm, even at forested sites with vegetation cover and precipitation amounts similar to those at our highest-elevation site. These discrepancies may be explained by differences in elevation, mean annual temperature, and soil texture. Lower elevations combined with higher temperatures can prolong the vegetation growing season, thereby increasing interception and evapotranspiration and reducing the infiltration of precipitation into the soil profile. In addition, the slightly higher silt content at their site likely enhances capillary water retention. Such capillary pores can hold water more effectively and may be bypassed by preferential flow paths, in contrast to the coarse sandy soils at our sites. This comparison suggests that vegetation cover and soil properties may exert a stronger influence on soil water dynamics than precipitation amount alone.

5.2 Bulk soil water

Bulk soil water is commonly used as a proxy for the immobile fraction of soil water and is frequently employed in comparisons with xylem water (e. g. Oliveira et al., 2025; Floriancic et al., 2024; Brighenti et al., 2024; Benettin et al., 2024; Barbeta et al., 2019, 2020; Goldsmith et al., 2019; Dubbert et al., 2019). Our results demonstrate that BW can differ significantly from TBW at certain times of the year. This isotopic divergence was observed primarily at the onset of the growing season. Following this period, all four study sites experienced substantial drought, which led to progressive drying of the soil profile and a consequent reduction or complete depletion of the MW fraction.

Historical data of MW from one of the experimental sites (Fig. 8, left), however, indicate that in years without severe drought, isotopic phase shifts within the soil profile, particularly in the MW fraction, can persist throughout the whole year. This persistence may result in subtle but consistent differences between BW and TBW even outside the early spring transition period.

Surprisingly, at the highest elevation RO site (where an unexpectedly rapid replacement of water with predominant contribution from winter precipitation was observed), previously collected mobile water data from 2021 to 2023 revealed a consistent pattern (Fig. 8, right), regardless of interannual variability in precipitation and temperature. Assuming that TBW exhibits similar behaviour, the difference between TBW and BW across years is expected to be negligible.

From a long-term perspective, substituting TBW with BW does not lead to substantially different isotopic interpretations. Furthermore, due to the methodological challenges associated with TBW extraction, this approach is generally unsuitable for routine applications. However, it may be considered in short-term or one-off experiments (e.g., Lehmann et al.,

2024), especially when the soil type and environmental conditions indicate a higher proportion of MW. In such cases, isotopic differences can occur—as demonstrated by the 0.3 difference in SOI between BW and TBW—which may result in underestimation of the role of winter precipitation.

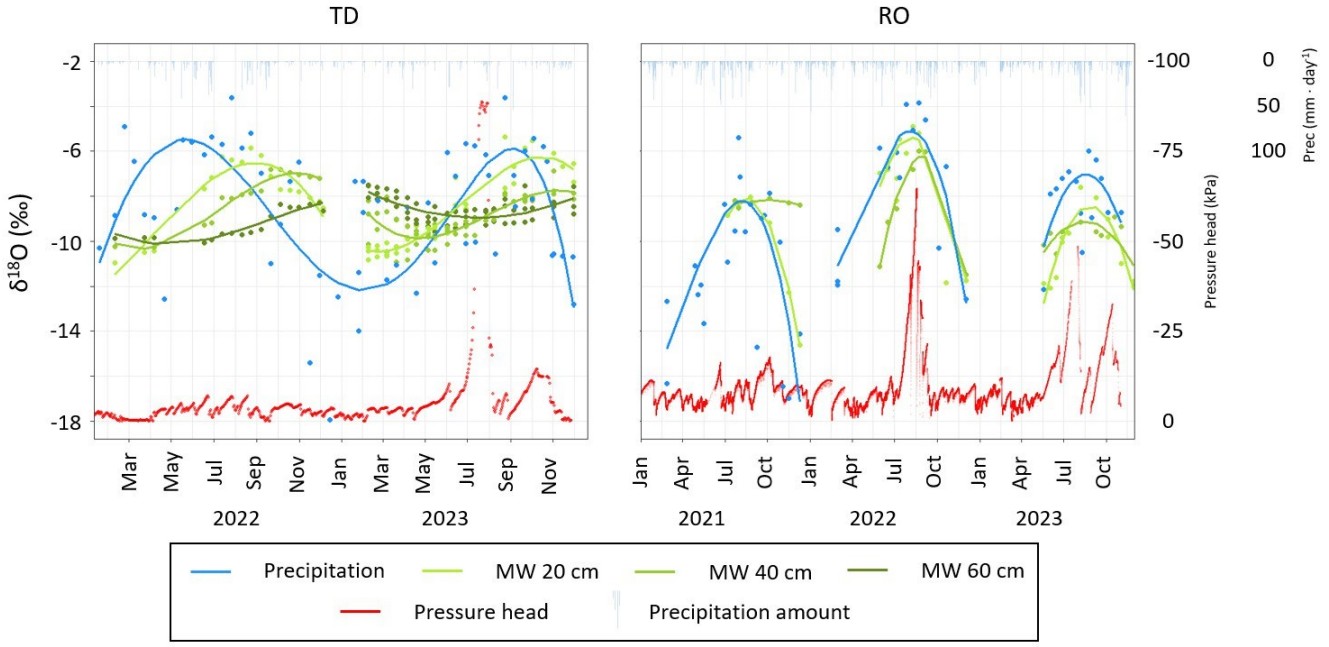

Figure 8. Annual cycle of isotopic composition of precipitation (blue) and mobile soil water (shades of green) at the Trhové Dušníky site in 2022-2023 (left) and the Rokytka site in 2021-2023 (right). MW was sampled up to three depths (20, 40, and 60 cm), where darker colour corresponds to greater depths. The red colour represents the suction pressure head at 20 cm depth, and the blue columns at the top of the graph show total precipitation.

5.3 The importance of winter precipitation

We hypothesized that winter-derived water would persist longest in soil profiles at higher elevations, where thicker snowpack melts later, compared with lowland areas characterized by transient snow cover and predominantly rainfall-based winter precipitation. This hypothesis was supported by soil water content (SWC) patterns: in lowland sites, SWC remains relatively constant during the first quarter of the year until the onset of the vegetation period or the occurrence of the first dry spe lls, whereas at higher elevations a distinct snowmelt-induced saturation signal is observed. In the latter case, increasing SWC coincides with gradual snow cover depletion and minimal or absent transpiration, conditions that limit soil moisture loss. Our results show that, with increasing elevation (except at the RO site), the presence of winter-derived water in the soil profile is progressively delayed into later months of the year.

The above elevation-dependent delay was also evident in the isotopic signatures of various soil water pools. The most rapid response was observed in MW, which exhibited its most isotopically depleted values in lowland sites as early as March,

whereas the minimum values in high-elevation sites occurred approximately one month later. This was followed by changes in shallow TBW, with isotopic minima occurring in April in the lowlands and in May at higher elevations. Winter water appeared last in the deeper soil layers (both MW and TBW), with signals emerging from April to May at low elevations and from May to June at the LI site.

However, at the highest-elevation site, which receives the greatest total precipitation and maintains the most persistent snow cover, we observed, despite limited data and a less pronounced dry season relative to other sites, a consistent pattern in which the isotopic composition of soil water closely mirrors that of precipitation. In this setting, winter water is rapidly displaced from the soil profile by subsequent rainfall events. While isotopically light values of shallow soil water in May and June reflect residual snowmelt, the influence of summer precipitation becomes increasingly evident during the vegetation period. This finding, at least with respect to water in deeper soil layers, contradicts our original hypothesis, which posited that summer precipitation would infiltrate into these layers only during the late summer and autumn months, due to elevated interception and evapotranspiration earlier in the season.

5.4 Tightly bound water extraction

To obtain TBW, the mobile fraction first had to be removed. There are several studies, that tried to extract soil water held in the soil matrix at different tensions (Geris et al., 2019; Bowers et al., 2020; Orlowski et al., 2020). The results of these studies show different isotopic compositions of individual water pools, both with laboratory-prepared (Orlowski et al., 2020; Bowers et al., 2020) and real soil samples (Geris et al., 2015). In this study, we use the pressure plate apparatus, similar to Orlowski et al. (2020), but with a different procedure. In their study, a spike experiment was performed, after which a pressure of 15 bar was applied, and the outflowing water was collected for isotopic analysis. Although labelled water was recovered during a specific time window, the initial and final stages of the experiment yielded water with isotopic signatures differing from the input. This method presents several limitations that hinder its applicability to natural soil samples. First, the true isotopic composition of soil water is typically unknown, making it difficult to determine whether the observed isotopic composition already corresponds to soil water. This ambiguity arises from mixing between the soil water and the water used to saturate the ceramic plates within the apparatus, making the collected outflow likely a composite of both sources. Second, for the method to be valid, each ceramic plate would have to be conditioned exclusively with samples from a single location and soil depth, to prevent internal mixing of different water sources. This requirement greatly reduces the practicality and scalability of the approach.

In our study, the pressure plate apparatus was employed in a modified configuration. Collected soil samples were subjected to a pressure of 0.6 bar, corresponding to the operational threshold for mobile water typically targeted by field-based suction lysimeters (Brooks et al., 2010; Berry et al., 2017; Sprenger et al., 2018). Unlike previous approaches that rely on collecting the outflow water (Orlowski et al., 2020), our method involved a subsequent extraction from pre-dried soil samples. This modification enabled the simultaneous processing of up to 24 samples from various depths and locations within a single run.

In line with the work of Geris et al. (2015), we observed (until the onset of drought) different isotopic compositions between MW and TBW, especially in the upper part of the profile, with these differences decreasing or disappearing with depth due to longer residence times. Despite the absence of data on cation exchange capacity (CEC), given the very low clay content at all four sites, it can be assumed that fractionation due to high clay CEC (Araguás-Araguás et al., 1995; Meiβner et al., 2013; Oerter et al., 2014) was negligible and that differences in isotopic composition were mainly due to different water retention times in macro- and capillary pores.

To eliminate the influence of the pressure apparatus on the isotopic composition, another potential approach would involve extracting the BW from a subset of samples, while using the pressure plate apparatus on the remaining samples to determine the proportion of MW and TBW. Based on the known isotopic composition of the BW (laboratory extraction) and MW (obtained via suction lysimeters), the isotopic composition of the TBW could then be estimated using the same mixing equation.

5.5 Data correction

Numerous studies have attempted to compare soil water (including both BW and MW) with xylem water (e.g., Zapater et al., 2011; Meunier et al., 2017; Vargas et al., 2017; Barbeta et al., 2019, 2020; Liu et al., 2021). To enable a meaningful comparison between soil water and xylem water, it is essential to employ an extraction technique that minimizes isotopic alteration of the sample. However, it is well known that no currently available extraction method can extract soil water from all soil types and moisture contents without introducing some degree of isotopic bias (Sprenger et al., 2015; Orlowski et al., 2018; Kocum et al., 2025).

For this reason, various corrections are often applied to the measured data, although not universally. These include, for instance, adjustments to account for the presence of organic compounds (Martín-Gómez et al., 2015), or corrections based on Rayleigh-type fractionation models (Araguás-Araguás et al., 1995).

There is, however, another critical yet frequently overlooked limitation. While each newly developed extraction method is typically validated using soils of different textures and moisture contents (Dalton, 1988; Revesz and Woods, 1990; Leaney et al., 1993; Scrimgeour, 1995; Wassenaar et al., 2008), the outcomes of these validation efforts often show a wide range of method-specific inaccuracies. These inaccuracies are commonly expressed as the shift ± standard deviation in ‰ from the known isotopic value of labelled water used in the test. Although useful for method comparison, these deviations are generally not applied as corrections to real measured data.

The correction employed in this study, which we consider essential for enabling meaningful comparison between individual water samples, relies on conducting spike experiments using the selected extraction method. This allows us to assess the method's performance for specific soil types collected from our study sites. Given that soil texture and moisture content significantly influence extraction outcomes (Hendry et al., 2015; Orlowski et al., 2016), such validation experiments should be performed separately for each soil type involved, ideally across a range of moisture conditions. The resulting isotopic deviations (relative to labelled water) should then be incorporated into data correction procedures for actual samples.

Ultimately, the use of different extraction methods across laboratories, each associated with varying degrees of systematic error, does not necessarily constitute a critical limitation. If these methods produce results with low standard deviations, even in the presence of systematic offsets, such biases can be quantified and subsequently corrected. Such calibration should allow meaningful comparisons across studies and research groups.

6 Conclusions

This study demonstrated that soil water stable isotope dynamics vary systematically along an elevational gradient. Despite the absence of snow cover at lowland sites, these areas exhibited longer residence times, whereas high-elevation sites—with substantial winter snow accumulation—showed more rapid isotopic turnover. All soil water samples plotted close to the respective local meteoric water lines, confirming their meteoric origin and indicating minimal isotopic bias introduced by the applied extraction methods. Mobile soil water most closely mirrored the isotopic composition of precipitation, while tightly bound water showed slight signatures of evaporative enrichment and potential mixing with older water, likely due to its longer residence time. Although tightly bound and bulk soil water exhibited only minor isotopic differences on average, seasonal variability increased—particularly in spring and autumn—when differences in isotopic composition and the proportion of mobile to tightly bound water were most pronounced. These findings highlight the importance of accounting for such variability, especially in short-term or single-time-point studies comparing soil and xylem water for plant source attribution. Future research should further explore how these dynamics interact with vegetation type, rooting depth, and changes in precipitation regimes under ongoing climate change.

Code availability. The code is available from the corresponding author upon request.

Data availability. Tha data from this study are available from the corresponding author upon request.

Author contributions. Concept: JK, LV. Methodology: JK, LV, MS. Investigation: JK, KF, VS, LV. Formal analysis: JK, JH. Resources: VS, MJ, LT, LV. Visualization: JK, KP. Writing (original draft preparation): JK, KF, VS. Writing (review and editing): JK, KP, KF, VS, JH, MJ, MS, LT, LV. Supervision: LV.

Competing interests. The authors declare that they have no conflict of interest.

Acknowledgements. The authors warmly thank David Pěsta for assistance with soil sampling.

Financial support. This work was supported by the Czech Academy of Sciences (grant no. RVO 67985874), the research programme Strategy AV21 Water for Life, the Czech Science Foundation (grant no. GA CR 23-06859K), and the Faculty of Science of Charles University in Prague (grant no. SVV 244-2606941).

References

Allen, S. T., Kirchner, J. W., Braun, S., Siegwolf, R. T. W., and Goldsmith, G. R.: Seasonal origins of soil water used by trees, Hydrology and Earth System Sciences, 23, 1199–1210, https://doi.org/10.5194/hess-23-1199-2019, 2019.

Araguás-Araguás, L., Rozanski, K., Gonfiantini, R., and Louvat, D.: Isotope effects accompanying vacuum extraction of soil water for stable isotope analyses, Journal of Hydrology, 168, 159–171, https://doi.org/10.1016/0022-1694(94)02636-P, 1995.

Barbeta, A., Gimeno, T. E., Clavé, L., Fréjaville, B., Jones, S. P., Delvigne, C., Wingate, L., and Ogée, J.: An explanation for the isotopic offset between soil and stem water in a temperate tree species, New Phytologist, 227, 766–779, https://doi.org/10.1111/nph.16564, 2020.

Barbeta, A., Jones, S. P., Clavé, L., Gimeno, T. E., Fréjaville, B., Wohl, S., and Ogée, J.: Unexplained hydrogen isotope offset complicate the identification and quantification of tree water sources in a riparian forest. Hydrology and Earth System Sciences, 23, 2129–2146, https://doi.org/10.5194/hess-23-2129-2019, 2019.

Bates, C. G.: First results in the streamflow experiment, Wagon Wheel Gap, Colorado, Journal of Forestry, 19, 402–408, 1921.

Benettin, P., Tagliavini, M., Adreotti, C., di Villahermosa F. S. M., Verdone, M., Dani, A., and Penna, D.: Ecohydrological Dynamics and Temporal Water Origin in a European Mediterranean Vineyard, Ecohydrology, 18, e2711, https://doi.org/10.1002/eco.2711, 2024.

Berry, Z. C., Evaristo, J., Moore, G., Poca, M., Steppe, K., Verrot, L., Asbjornsen, H., Borma, L. S., Bretfeld, M., Hervé - Fernández, P., Seyfried, M., Schwendenmann, L., Sinacore, K., De Wispelaere, L., and McDonell, J. J.: The two water worlds hypothesis: Addressing multiple working hypotheses and proposing a way forward, Ecohydrology, 11, e1843, https://doi.org/10.1002/eco.1843, 2017.

Bond, B. J., Jones, J. A., Moore, G., Phillips, N., Post, D., and McDonell, J. J.: The zone of vegetation influence on baseflow revealed by diel patterns of streamflow and vegetation water use in a headwater basin, Hydrological Processes, 16, 1671–1677, https://doi.org/10.1002/hyp.5022, 2002.

Bowers, W. H., Mercer, J. J., Pleasants, M. S., and Williams, D. G.: A combination of soil water extraction methods quantifies the isotopic mixing of waters held at separate tensions in soil, Hydrology and Earth System Sciences, 24, 4045–4060, https://doi.org/10.5194/hess-24-4045-2020, 2020.

Brighenti, S., Obojes, N., Bertoldi, G., Zuecco, G., Censini, M., Cassiani, G., Penna, D., and Francesco, C.: Snowmelt and subsurface heterogeneity control tree water sources in a subalpine forest, Ecohydrology, 17, e2695, https://doi.org/10.1002/eco.2695, 2024.

Brooks, J., Barnard, H., Coulombe, R., and McDonell, J. J.: Ecohydrologic separation of water between trees and streams in a Mediterranean climate, Nature Geoscience, 3, 100–104, https://doi.org/10.1038/ngeo722, 2010.

Büntgen, U., Urban, O., Krusic, P. J., Rybníček, M., Kolář, T., Kyncl, T., Ač, A., Koňasová, E., Čáslavský, J., Esper, J., Wagner, S., Saurer, M., Tegel, W., Dobrovolný, P., Cherubini, P., Reining, F., and Trnka, M.: Recent European drought extremes beyond Common Era background variability, Nature Geoscience, 14, 190–196, https://doi.org/10.1038/s41561-021-00698-0, 2021.

Ceperley, N., Gimeno, T. E., Jacobs, S. R., Beyer, M., Dubbert, M., Fischer, B., Geris, J., Holko, L., Kübert, A., Le Gall, S., Lehmann, M. M., Llorens, P., Millar, C., Penna, D., Prieto, I., Radolinski, J., Scandellari, F., Stockinger, M., Stumpp, C., Tetzlaff, D., van Meerveld, I., Werner, C., Yildiz, O., Zuecco, G., Barbeta, A., Orlowski, N., and Rothfuss, Y.: Toward a common methodological framework for the sampling, extraction, and isotopic analysis of water in the Critical Zone to study vegetation water use, WIREs Water, 11, e1727, https://doi.org/10.1002/wat2.1727, 2024.

Craig, H.: Standard for reporting concentrations of deuterium and oxygen-18 in natural waters, Science, 133, 1833–1834, https://doi.org/10.1126/science.133.3467.1833, 1961.

Dalton, F. N.: Plant root water extraction studies using stable isotopes, Plant Soil, 111, 217–221, https://doi.org/10.1007/BF02139942, 1988.

Davison, A. C., and Hinkley, D. V.: Bootstrap Methods and their Application, Cambridge University Press, Cambridge, United Kingdom, https://doi.org/10.1017/CBO9780511802843, 1997.

Dawson, T. E., and Ehleringer, J. R.: Streamside trees that do not use stream water, Nature, 350, 335–337, https://doi.org/10.1038/350335a0, 1991.

Dubbert, M., Caldeira, M. C., Dubbert, D., and Werner, C.: A pool-weighted perspective on the two-water-worlds hypothesis, New Phytologist, 222, 1271–1283, https://doi.org/10.1111/nph.15670, 2019.

Evaristo, J., Jasechko, S., and McDonell, J. J.: Global separation of plant transpiration from groundwater and streamflow, Nature, 525, 91–94, https://doi.org/10.1038/nature14983, 2015.

Floriancic, M. G., Allen, S. T. and Kirchner, J. W.: Isotopic evidence for seasonal water sources in tree xylem and forest soils, Ecohydrology, 17, e2641, https://doi.org/10.1002/eco.2641, 2024.

Gebrechorkos, S. H., Sheffield, J., Vicente-Serrano, S. M., Funk, C., Miralles, D. G., Peng, J., Dyer, E., Talib, J., Beck, H. E., Singer, M. B., and Dadson, S. J.: Warming accelerates global drought severity, Nature, 642, 628–635, https://doi.org/10.1038/s41586-025-09047-2, 2025.

Geris, J., Tetzlaff, D., McDonell, J. J., Anderson, J., Paton, G., and Soulsby, C.: Ecohydrological separation in wet, low energy northern environments? A preliminary assessment using different soil water extraction techniques, Hydrological Processes, 15, 5139–5152, https://doi.org/10.1002/hyp.10603, 2015.

Goldsmith, G., Allen, S., Braun, S., Engbersen, N., González-Quijano, C. R., Kirchner, J. W., and Siegwolf, R. T. W.: Spatial variation in throughfall, soil, and plant water isotopes in a temperate forest, Ecohydrology, 12, 1–11, https://doi.org/10.1002/eco.2059, 2019.

Goldsmith, G. R., Muñoz-Villers, L. E., Holwerda, F., McDonell, J. J., Asbjornsen, H., and Dawson, T. E.: Stable isotopes reveal linkages among ecohydrological processes in a seasonally dry tropical montane cloud forest, Ecohydrology, 5, 779–790, https://doi.org/10.1002/eco.268, 2012.

Gradmann, H.: Untersuchungen über die Wasserverhältnisse des Bodens als Grundlage des Pflanzenwachstums, Jahrbücher für wissenschaftliche Botanik, 69,1-100, 1928.

Hackmann, C. A., Paligi, S. S., Mund, M., Hölscher, D., Leuschner, C., Pietig, K., and Ammer, C.: Root water uptake depth in temperate forest trees: species-specific patterns shaped by neighbourhood and environment, Plant biology, Advance online publication, https://doi.org/10.1111/plb.70058, 2025.

Harper, W. V.: Reduced Major Axis Regression: Teaching Alternatives to Least Squares, Wiley StatsRef: Statistics Reference Online, https://doi.org/10.1002/9781118445112.stat07912, 2016.

Harpold, A. A., Kaplan, M. L., Klos, P. Z., Link, T., McNamara, J. P., Rajagopal, S., Schumer, R., and Steele, C. M.: Rain or snow: hydrologic processes, observations, prediction, and research needs, Hydrology and Earth System Sciences, 21, 1–22, https://doi.org/10.5194/hess-21-1-2017, 2017.

Hendry, M. J., Schmeling, E., Wassenaar, L. I., Barbour, S. L., Pratt, D.: Determining the stable isotope composition of pore water from saturated and unsaturated zone core: improvements to the direct vapour equilibration laser spectrometry method, Hydrology and Earth System Sciences, 19, 4427–4440, https://doi:10.5194/hess-19-4427-2015, 2015.

Hervé-Fernández, P., Oyarzún, C., Brumbt, C., Bodé, H. S., Verhoest, N. E. C., and Boeckx, P.: Assessing the 'two water worlds' hypothesis and water sources for native and exotic evergreen species in south central Chile, Hydrological Processes, 15, 4227–4241, https://doi.org/10.1002/hyp.10984, 2016.

Jenicek, M., Hnilica, J., Nedelcev, O., Sipek, V.: Future changes in snowpack will impact seasonal runoff and low flows in Czechia, Journal of Hydrology: Regional Studies, 37, 100899, https://doi.org/10.1016/j.ejrh.2021.100899, 2021.

Jenicek, M., and Ledvinka, O.: Importance of snowmelt contribution to seasonal runoff and summer low flows in Czechia, Hydrology and Earth System Sciences, 24, 3475–3491, https://doi.org/10.5194/hess-24-3475-2020, 2020.

Jenicek, M., Seibert, J., and Staudinger, M.: Modeling of Future Changes in Seasonal Snowpack and Impacts on Summer Low Flows in Alpine Catchments, Water Resources Research, 54, 538–556, https://doi.org/10.1002/2017WR021648, 2018.

Jiao, W., Wang, L., Smith, W. K., Chang, Q., Wang, H., and D'Odorico, P.: Observed increasing water constraint on vegetation growth over the last three decades, Nature Communication, 12, 3777, https://doi.org/10.1038/s41467-021-024016-9, 2021.

Kirchner, J. W.: Aggregation in environmental systems – Part 1: Seasonal tracer cycles quantify young water fractions, but not mean transit times, in spatially heterogeneous catchments, Hydrology and Earth System Sciences, 20, 279–297, https://doi.org/10.5194/hess-20-279-2016, 2016.

Kleine, L., Tetzlaff, D., Smith, A., Wang, H., and Soulsby, C.: Using water stable isotopes to understand evaporation, moisture stress, and re-wetting in catchment forest and grassland soils of the summer drought of 2018, Hydrology and Earth System Sciences, 24, 3737–3752, https://doi.org/10.5194/hess-24-3737-2020, 2020.

Kocum, J., Haidl, J., Gebousky, O., Falatkova, K., Sipek, V., Sanda, M., Orlowski, N., and Vlcek, L.: Technical note: A new laboratory approach to extract soil water for stable isotope analysis from large soil samples, Hydrology and Earth System Sciences, 29, 2863–2880, https://doi.org/10.5194/hess-29-2863-2025, 2025.

Landwehr, J. M., and Coplen, T. B.: Line-condition excess: A new method for characterizing stable hydrogen and oxygen isotope ratios in hydrologic systems, Isotopes in Environmental Studies, Edition: 1, IAEA, ISBN: 92-0-111305-X, 2006.

Leaney, F. W., Smettem, K. R. J., and Chittleborough, D. J.: Estimating the contribution of preferential flow to subsurface runoff from a hillslope using deuterium and chloride, Journal of Hydrology, 147, 83–103, https://doi.org/10.1016/0022-1694(93)90076-L, 1993.

Lehmann, M. M., Geris, J., van Meerveld, I., Penna, D., Rothfuss, Y., Verdone, M., Ala-Aho, P., Babre, M. A. A., Balandier, P., Bernhard, F., Butorac, L., Carrière, S. D., Ceperley, N. C., Chen, Z., Correa, A., Diao, H., Dubbert, D., Dubbert, M., Ercoli, F., Floriancic, M. G., Gimeno, T. E., Gounelle, D., Hagedorn, F., Hissler, C., Huneau, F., Iraheta, A., Jakovljević, T., Kazakis, N., Kern, Z., Knaebel, K., Kobler, J., Kocum, J., Koeber, C., Koren, G., Kübert, A., Kupka, D., Le Gall, S., Lehtonen, A., Leydier, T., Malagoli, P., Manca di Villahermosa, F. S., Marchina, C., Martínez-Carreras, N., Martin-StPaul, N., Marttila, H., Oliveira, A. M., Monvoisin, G., Orlowski, N., Palmik-Das, K., Persoiu, A., Popa, A., Prikaziuk, E., Quantin, C., Rinne-Garmston, K. T., Rohde, C., Sanda, M., Saurer, M., Schulz, D., Stockinger, M. P., Stumpp, C., Venisse, J. S., Vlcek, L., Voudouris, S., Weeser, B., Wilkinson, M. E., Zuecco, G., and Meusburger, K.: Soil and stem xylem water isotope data from two pan-European sampling campaigns, Earth System Science Data, [preprint], https://doi.org/10.5194/essd-2024-409, in review, 2024.

Liu, J., Si, Z., Wu, L., Chen, J., Gao, Y., and Duan, A.: Using stable isotopes to quantify root water uptake under a new planting pattern of high-low seed beds cultivation in winter wheat, Soil and Tillage Research, 205, 104816, https://doi.org/10.1016/j.still.2020.104816, 2021.

Mankin, J. S., Seager, R., Smerdon, J. E., Cook, B. I., and Williams, A. P.: Mid-latitude freshwater availability reduced by projected vegetation responses to climate change, Nature Geoscience, 12, 983–988, https://doi.org/10.1038/s41561-019-0480-x, 2019.

Martín-Gómez, P., Barbeta, A., Voltas, J., Peñuelas, J., Dennis, K., Palacio, S., Dawson, T. E., and Ferrio, J. P.: Isotope-ratio infrared spectroscopy: a reliable tool for the investigation of plant-water sources?, New Phytologist, 207, 914–927, https://doi.org/10.1111/nph.13376, 2015.

Marty, C., Tilg, A. M., and Jonas, T.: Recent Evidence of Large-Scale Receding Snow Water Equivalents in the European Alps, Journal of Hydrometeorology, 18, 1021–1031, https://doi.org/10.1175/JHM-D-16-0188.1, 2017.

McDonell, J. J.: The two water worlds hypothesis: ecohydrological separation of water between streams and trees?, WIREs Water, 1, 323–329, https://doi.org/10.1002/wat2.1027, 2014.

Meißner, M., Köhler, M., Schwendenmann, L., Hölscher, D., and Dyckmans, J.: Soil water uptake by trees using water stable isotopes (δ^2H and $\delta^{18}O$)-a method test regarding soil moisture, texture and carbonate, Plant Soil, 376, 327–335, https://doi.org/10.1007/s11104-013-1970-z, 2024.

Meunier, F., Rothfuss, Y., Bariac, T., Biron, P., Richard, P., Durand, J. L., Couvreur, V., Vanderborght, J., and Javaux, M.: Measuring and Modeling Hydraulic Lift of *Lolium multiflorum* Using Stable Water Isotopes, Vadose Zone Journal, 17, 1–15, https://doi.org/10.2136/vzj2016.12.0134, 2017.

Molz, J. F.: Models of water transport in the soil-plant system: A review, Water Resources Research, 17, 1245–1260, https://doi.org/10.1029/WR017i005p01245, 1981.

Musselmann, K. N., Clark, M. P., Liu, C., Ikeda, K., and Rasmussen, R.: Slower snowmelt in a warmer world, Nature Climate Change, 7, 214–219, https://doi.org/10.1038/nclimate3225, 2017.

Oerter, E., Finstad, K., Schaefer, J., Goldsmith, G. R., Dawson, T., and Amundson, R.: Oxygen isotope fractionation effects in soil water via interaction with cations (Mg, Ca, K, Na) adsorbed to phyllosilicate clay minerals, Journal of Hydrology, 515, 1–9, https://doi.org/10.1016/j.jhydrol.2014.04.029, 2014.

Oliveira, A. M., Floriancic, M., Gianasi, F. M., Herbstritt, B., Pompeu, P. V., Araújo, F. C., Silva-Sene, A. M., Reis, M. G., Farrapo, C. L., Ferreira, L. A. S., dos Santos, R. M., and van Meerveld, I.: Isotopic Composition of Soil and Xylem Water Across Six Seasonal Floodplain Forests in Southeastern Brazil, Ecohydrology, 18, e70076, https://doi.org/10.1002/eco.70076, 2025.

Orlowski, N., and Breuer, L.: Sampling soil water along pF curve for δ^2H and $\delta^{18}O$ analysis, Hydrological Processes, 34, 4959–4972, https://doi.org/10.1002/hyp.13916, 2020.

Orlowski, N., Breuer, L., Angeli, N., Boeckx, P., Brumbt, C., Cook, C. S., Dubbert, M., Dyckmans, J., Gallagher, B., Gralher, B., Herbstritt, B., Hervé-Fernández, P., Hissler, C., Koeniger, P., Legout, A., Macdonald, C. J., Oyarzún, C., Redelstein, R., Seidler, C., Siegwolf, R., Stumpp, C., Thomsen, S., Weiler, M., Werner, C., and McDonnell, J. J.: Inter-laboratory comparison of cryogenic water extraction systems for stable isotope analysis of soil water, Hydrology and Earth System Sciences., 22, 3619–3637, https://doi.org/10.5194/hess-22-3619-2018, 2018.

Orlowski, N., Breuer, L., and McDonell, J. J.: Critical issues with cryogenic extraction of soil water for stable isotope analysis, Ecohydrology, 9, 3–10, https://doi.org/10.1002/eco.1722, 2016.

Qin, Y., Abatzoglou, J. T., Siebert, S., Huning, L. S., AghaKouchak, A., Mankin, J. S., Hong, C., Tong, D., Davis, S. J., and Mueller, N. D.: Agricultural risks from changing snowmelt, Nature Climate Change, 10, 459–465, https://doi.org/10.1038/s41558-020-0746-8, 2020.

Revesz, K., and Woods, P. H.: A method to extract soil water for stable isotope analysis, Journal of Hydrology, 115, 397–406, https://doi.org/10.1016/0022-1694(90)90217-L, 1990.

Safeeq, M., Shukla, S., Arismendi, I., Grant, G. E., Lewis, S. L., and Nolin, A.: Influence of winter season climate variability on snow-precipitation ratio in the western United States, International Journal of Climatology, 36, 3175–3190, https://doi.org/10.1002/joc.4545, 2015.

Samaniego, L., Thober, S., Kumar, R., Wanders, N., Rakovec, O., Pan, M., Zink, M., Sheffield, J., Wood, E. F., and Marx, A.: Anthropogenic warming exacerbates European soil moisture droughts, Nature Climate Change, 8, 421–426, https://doi.org/10.1038/s41558-018-0138-5, 2018.

Scrimgeour, C. M.: Measurement of plant and soil water isotope composition by direct equilibration methods, Journal of Hydrology, 172, 261–274, https://doi.org/10.1016/0022-1694(95)02716-3, 1995.

Seyedsadr, S., Šípek, V., Jačka, L., Sněhota, M., Beesley, L., Pohořelý, M., Kovář, M., and Trakal, L.: Biochar considerably increases the easily available water and nutrient content in low-organic soils amended with compost and manure, Chemosphere, 293, 133586, https://doi.org/10.1016/j.chemosphere.2022.133586, 2022.

Šípek, V., Jenicek, M., Hnilica, J., and Zelíková, N.: Catchment Storage and its Influence on Summer Low Flows in Central European Mountainous Catchments, Water Resources Management, 35, 2829–2843, https://doi.org/10.1007/s11269-021-02871-x, 2021.

Šípek, V., Jačka, L., Seyedsadr, S., and Trakal, L.: Manifestation of spatial and temporal variability of soil hydraulic properties in the uncultivated Fluvisol and performance of hydrological model, Catena, 182, 104119, https://doi.org/10.1016/j.catena.2019.104119, 2019.

Sprenger, M., Tetzlaff, D., Buttle, J., Laudon, H., Leistert, H., Mitchell, C. P. J., Snelgrove, J., Weiler, M., and Soulsby, C.: Measuring and Modeling Stable Isotopes of Mobile and Bulk Soil Water, Vadose Zone Journal, 17, 1–18, https://doi.org/10.2136/vzj2017.08.0149, 2018.

Sprenger, M., Herbstritt, B., and Weiler, M.: Established methods and new opportunities for pore water stable isotope analysis, Hydrological Processes, 29, 5174–5192, https://doi.org/10.1002/hyp.10643, 2015.

Tinker, P. B.: Transport of water to plant root in soil, Philosophical Transactions of the Royal Society of London, 273, 445–461, https://doi.org/10.1098/rstb.1976.0024, 1976.

Tolasz, R., Míková, T., Valeriánová, A., and Voženílek, V.: Climate atlas of Czechia. 1. vyd., 255s., Praha: Český hydrometeorologický ústav; Olomouc: Univerzita Palackého v Olomouci. ISBN: 978-80-86690-26-1, 2007.

van den Honert, T. H.: Water transport in plats as a catenary process, Discussions of the Faraday Society, 3, 146–153, https://doi.org/10.1039/DF9480300146, 1948.

Vargas, A. I., Schaffer, B., Yuhong, L., and Sternberg, L. S. L.: Testing plant use of mobile vs immobile soil water sources using stable isotope experiments, New Phytologist, 215, 582–594, https://doi.org/10.1111/nph.14616, 2017.

Vlček, L., Šípek, V., Kofroňová, J., Kocum, J., Doležal, T., and Janský, B.: Runoff formation in a catchment with Peat bog and Podzol hillslopes, Journal of Hydrology, 593, 125633, https://doi.org/10.1016/j.jhydrol.2020.125633, 2021.

Wassenaar, L. I., Hendry, M. J., Chostner, V. L., and Lis, G. P.: High Resolution Pore Water δ^2H and $\delta^{18}O$ Measurements by $H_2O_{(liquid)}$-$H_2O_{(vapor)}$ Equilibration Laser Spectroscopy, Environmental Science & Technology, 42, 9262–9267, https://doi.org/10.1021/es802065s, 2008.

Weatherley, P. E.: Introduction: Water movement through plants, Philosophical Transactions of the Royal Society of London, 273, 435–444, https://doi.org/10.1098/rstb.1976.0023, 1976.

Willibald, F., Kotlarski, S., Grêt-Regamey, A., and Ludwig, R.: Anthropogenic climate change versus internal climate variability: impacts on snow cover in the Swiss Alps, The Cryosphere, 14, 2909–2924, https://doi.org/10.5194/tc-14-2909-2020, 2020.

Xia, C., Zuecco, G., Marchina, C., Penna, D., and Borga, M.: Effects of Short-Term Climate Variations on Young Water Fraction in a Small Pre-Alpine Catchment, Water Resources Research, 60, e2023WR036245, https://doi.org/10.1029/2023WR036245, 2024.

Xue, D., Tian, J., Zhang, B., Kang, W., Zhou, Y., and He, C.: Effects of vegetation types on soil wetting pattern and preferential flow in arid mountainous areas of northwest China, Journal of Hydrology, 642, 131849, https://doi.org/10.1016/j.jhydrol.2024.131849, 2024.

Yang, B., Dossa, G. G. O., Hu, Y. H., Liu, L. L., Meng, X. J., Du, Y. Y., Li, J. Y., Zhu, X. A., Zhang, Y. J., Singh, A. K., Yuan, X., Wu, J. E., Zakari, S., Liu, W. J., and Song, L.: Uncorrected soil water isotopes through cryogenic vacuum distillation may lead to a false estimation on plant water sources, Methods in Evology and Evolution, 14, 1443–1456, https://doi.org/10.1111/2041-210X.14107, 2023.

Zapater, M., Hossann, C., Bréda, N., Bréchet, C., Bonal, D., and Granier, A.: Evidence of hydraulic lift in a young beech and oak mixed forest using ^{18}O soil water labelling, Trees, 25, 885–894, https://doi.org/10.1007/s00468-011-0563-9, 2011.

Zelíková, N., Toušková, J., Kocum, J., Vlček, L., Tesař, M., Bouda, M., and Šípek, V.: Divergent water balance trajectories under two dominant tree species in montane forest catchment shifting from energy- to water-limitation, Hydrology and Earth System Sciences, [preprint], https://doi.org/10.5194/hess-2024-244, in review, 2024.

8 Conclusions

More frequent drought periods and an increasing number of extreme precipitation events are just some apparent manifestations of ongoing climate change. These hydroclimatic transformation affect runoff generation, groundwater recharge, or the availability of soil water for plants, which are forced to adapt their strategies to cope with these changing conditions. A better understanding of soil water dynamics, runoff formation, and soil–plant–atmosphere interactions is essential for improving predictions of extreme events such as droughts and flash floods. Such knowledge is critical for effective water resource management under evolving hydroclimatic conditions.

The first part of this study focused on the soil–plant relationship using a 22-year dataset of air temperature, precipitation, and soil moisture under two forest types: Norway spruce (*Picea abies* L.) and European beech (*Fagus sylvatica* L.). The results estimate that under increasing water limitation, forests will be dominated by deeper-rooted and more anisohydric species, which would deplete deep water storage. The combined effects of climate and changes in forest species composition may therefore intensify soil drought and spring drying. On the other hand, increasing the proportion of deciduous species may enhance winter recharge due to lower interception compared to conifers. These insights can improve the development of next-generation models and projections, thereby supporting both ecosystem and water resource management in a changing climate.

The second part of the study focused on the evaluation of waterlogged soil (peat) in catchment hydrological processes. Using tracers such as spring temperature and stable isotopes, it was found that runoff from peaty soils and their water balance are more sensitive to droughts and summer rain distribution compared to mineral soils. The findings indicate that peat bogs play a key role in generating rapid runoff during intense rainfall events, while groundwater stored in mineral soils dominates baseflow during dry periods. Moreover, mineral soils accumulate water from snow melt more effectively and support the spring yields. These results illustrate how these ecosystems are sensitive to increasing climatic fluctuations, such as a lack of precipitation or its state (solid/liquid).

Further parts of this work focused on the analysis of the isotopic composition of soil water. For this purpose, a novel method for soil water extraction was developed, including a custom-built apparatus specifically designed for this task. In parallel, an experimental protocol

was applied to isolate the tightly bound fraction of soil water. This fraction plays a crucial role in understanding soil water dynamics—both macropore and capillary components—and is essential for determining rooting depths, the origin of water taken up by plants, water residence time within the soil profile, and the relative contributions of winter and summer precipitation to soil water recharge and storage. Given the projected continued decline in snow cover at higher elevations across Central Europe, these findings are significant for improving predictions of soil water storage and, ultimately, the availability of water for plants under future climatic scenarios.

The experience gained during the development of this study, particularly in the application of stable hydrogen and oxygen isotopes in ecohydrological research, enabled a contribution to a pan-European effort to establish a unique, openly accessible dataset of soil and xylem water. This dataset is intended to support a wide range of ecohydrological applications, including the identification of factors controlling tree water uptake depth and seasonal water sources, the calibration and validation of isotope-enabled ecohydrological models, and the development of isoscape models.

High-quality water resources are indispensable for the sustainable development of human society and the functioning of ecosystems. The results of this study provide insights that can enhance ecohydrological models and projections, thereby improving the prediction of extreme events such as droughts and flash floods. These advancements can inform more effective strategies for ecosystem protection and for the management of water resources in agriculture and forestry, particularly in the context of ongoing climate change.

9 References

Allen, S. T., Kirchner, J. W., Braun, S., Siegwolf, R. T. W., and Goldsmith, G. R.: Seasonal origins of soil water used by trees, Hydrology and Earth System Sciences, 23, 1199–1210, https://doi.org/10.5194/hess-23-1199-2019, 2019.

Allen, S. T., Kirchner, J. W., and Goldsmith, G. R.: Predicting spatial patterns in precipitation isotope (δ^2H and $\delta^{18}O$) seasonality using sinusoidal isoscapes, Geophysical Research Letters, 45, 4859–4868, https://doi.org/10.1029/2018GL077458, 2018.

Anderson, A. E., Weiler, M., Alila, Y., and Hudson, R. O.: Dye staining and excavation of a lateral preferential flow network, Hydrology and Earth System Sciences, 13, 935–944, https://doi.org/10.5194/hess-13-935-2009, 2009.

Araguás-Araguás, L., Rozanski, K., Gonfiantini, R., and Louvat, D.: Isotope Effects Accompanying Vacuum Extraction of Soil Water for Stable Isotope Analyses, Journal of Hydrology, 168, 159–171, https://doi.org/10.1016/0022-1694(94)02636-P, 1995.

Bachmair, S., Weiler, M., and Nützmann, G.: Controls of land use and soil structure on water movement: Lessons for pollutant transfer through the unsaturated zone, Journal of Hydrology, 369, 241–252, https://doi.org/10.1016/j.jhydrol.2009.02.031, 2009.

Bao, H., Cao, X., and Hayles, J. A.: Triple Oxygen Isotopes: Fundamental Relationship and Applications. Annual Review of Earth and Planetary Sciences, 44, 463–492, https://doi.org/10.1146/annurev-earth-060115-012340, 2016.

Bao, H., Fairchild, I., Wynn, P. M., and Spötl, Ch.: Stretching the Envelope of Past Surface Environments: Neoproterozoic Glacial Lakes from Svalbard. Science, 323, 119–122, https://doi.org/ 10.1126/science.1165373, 2009.

Barrow, N. J., and Whelan, B. R.: A Study of a Method for Displacing Soil Solution by Centrifuging with an Immiscible Liquid. Journal of Environmental Quality, 9, 315–319, https://doi.org/10.2134/jeq1980.00472425000900020031x, 1980.

Bates, C. G.: First results in the streamflow experiment, Wagon Wheel Gap, Colorado, Journal of Forestry, 19, 402–408, 1921.

Batley, G. and Giles, M.: Solvent displacement of sediment interstitial waters before trace metal analysis, Water Research, 13, 879–886, https://doi.org/10.1016/0043-1354(79)90223-9, 1979.

Berry, Z. C., Evaristo, J., Moore, G., Poca, M., Steppe, K., Verrot, L., Asbjornsen, H., Borma, L. S., Bretfeld, M., Hervé-Fernández, P., Seyfried, M., Schwendenmann, L., Sinacore, K., De Wispelaere, L., and McDonell, J. J.: The two water worlds hypothesis: Addressing multiple working hypotheses and proposing a way forward, Ecohydrology, 11, e1843, https://doi.org/10.1002/eco.1843, 2017.

Bhaskar, A. S., Harvey, J. W., and Henry, E. J.: Resolving hyporheic and groundwater components of streambed water flux using heat as a tracer. Water Resources Research, 48, https://doi.org/10.1029/2011WR011784, 2012.

Bianchin, M., Smith, L., and Beckie, R.: Quantifying hyporheic exchange in a tidal river using temperature time series, Water Resources Research, 46, W07507, https://doi.org/10.1029/2009WR008365, 2010.

Birkel, C., Soulsby, C., and Tetzlaff, D.: Developing a Consistent Process-based Conceptualization of Catchment Functioning Using Measurements of Internal State Variables. Water Resources Research, 50, 3,481–3,501, https://doi.org/10.1002/2013WR014925, 2014.

Birkinshaw, S. J. and Webb, B.: Flow pathways in the Slapton Wood catchment using temperature as a tracer, Journal of Hydrology, 383, 269–279, https://doi.org/10.1016/j.jhydrol.2009.12.042, 2010.

Blunier, T., Bender, M. L., Barnett, B., and von Fischer, J. C.: Planetary Fertility During the Past 400 ka Based on the Triple Isotope Composition of O_2 in Trapped Gases from the Vostok Ice Core. Climate of the Past, 8, 1,509–1,526, https://doi.org/10.5194/cp-8-1509-2012, 2012.

Blunier, T., Barnett, B., Bender, M. L., and Hendricks, M. B.: Biological Oxygen Productivity During the Last 60,000 Years from Triple Oxygen Isotope Measurements. Global Biogeochemical Cycles, 16, 3–13, https://doi.org/10.1029/2001GB001460, 2002.

Bond, B. J., Jones, J. A., Moore, G., Phillips, N., Post, D., and McDonell, J. J.: The zone of vegetation influence on baseflow revealed by diel patterns of streamflow and vegetation water use in a headwater basin, Hydrological Processes, 16, 1671–1677, https://doi.org/10.1002/hyp.5022, 2002.

Böttcher, G., Brumsack, H.-J., Heinrichs, H., and Pohlmann, M.: A new high-pressure squeezing technique for pore fluid extraction from terrestrial soils, Water Air Soil Pollution, 94, 289–296, https://doi.org/10.1007/BF02406064, 1997.

Bowling, D. R., Schulze, E. S., and Hall, S. J.: Revisiting streamside trees that do not use stream water: can the two water worlds hypothesis and snowpack isotopic effects explain a missing water source? Ecohydrology, 10, e1771, https://doi.org/10.1002/eco.1771, 2017.

Brinkmann, N., Seeger, S., Weiler, M., Buchmann, N., Eugster, W., and Kahmen, A.: Employing stable isotopes to determine the residence times of soil water and the temporal origin of water taken up by Fagus sylvatica and Picea abies in a temperate forest, New Phytologist, 219, 1300–1313, https://doi.org/10.1111/nph.15255, 2018.

Brocca, L., Camici, S., Melone, F., Moramarco, T., Martínez-Fernández, J., Didon-Lescot, J. F., and Morbidelli, R.: Improving the representation of soil moisture by using a semi-analytical infiltration model, Hydrological Processes, 28, 2103–2115, https://doi.org/10.1002/hyp.9766, 2014.

Brocca, L., Melone, F., and Moramarco, T.: On the estimation of antecedent wetness conditions in rainfall-runoff modelling, Hydrological Processes, 22, 629–642, https://doi.org/10.1002/hyp.6629, 2008.

Brooks, J., Barnard, H., Coulombe, R., and McDonell, J. J.: Ecohydrologic separation of water between trees and streams in a Mediterranean climate, Nature Geoscience, 3, 100–104, https://doi.org/10.1038/ngeo722, 2010.

Brown, L. E. and Hannah, D. M.: Alpine stream temperature response to storm events. Journal of Hydrometeorology, 8, 952–967, https://doi.org/10.1175/JHM597.1, 2007.

Ceperley, N., Gimeno, T. E., Jacobs, S. R., Beyer, M., Dubbert, M., Fischer, B., Geris, J., Holko, L., Kübert, A., Le Gall, S., Lehmann, M. M., Llorens, P., Millar, C., Penna, D., Prieto, I., Radolinski, J., Scandellari, F., Stockinger, M., Stumpp, C., Tetzlaff, D., van Meerveld, I.,

Werner, C., Yildiz, O., Zuecco, G., Barbeta, A., Orlowski, N., and Rothfuss, Y.: Toward a common methodological framework for the sampling, extraction, and isotopic analysis of water in the Critical Zone to study vegetation water use, WIREs Water, 11, e1727, https://doi.org/10.1002/wat2.1727, 2024.

Chen, S., and Yuan, X.: The Timing of Detectable Increases in Seasonal Soil Moisture Droughts Under Future Climate Change, Earth's Future, 12, e2023EF004174, https://doi.org/10.1029/2023EF004174, 2024.

Chiang, F., Mazdiyasni, O., and AghaKouchak, A.: Evidence of anthropogenic impacts on global drought frequency, duration, and intensity, Nature Communications, 12, 2754, https://doi.org/10.1038/s41467-021-22314-w, 2021.

Combe, M., de Arellano, J. V. G., Ouwersloot, H. G., and Peters, W.: Plant water-stress parameterization determines the strength of land–atmosphere coupling, Agricultural and Forest Meteorology, 217, 61–73, https://doi.org/10.1016/j.agrformet.2015.11.006, 2016.

Corbin, J. D., Thomsen, M. A., Dawson, T. E., and D'Antonio, C. M.: Summer Water Use by California Coastal Prairie Grasses: Fog, Drought, and Community Composition, Oecologia, 145, 511–521, https://doi.org/ 10.1007/s00442-005-0152-y, 2005.

Craig, H.: Standard for reporting concentrations of deuterium and oxygen-18 in natural waters, Science, 133, 1833–1834, https://doi.org/10.1126/science.133.3467.1833, 1961.

Criss, R. E., and Farquhar, J.: Abundance, Notation, and Fractionation of Light Stable Isotopes, Reviews in Mineralogy and Geochemistry, 68, 15–30, https://doi.org/10.2138/rmg.2008.68.3, 2008.

Dalton, F. N.: Plant root water extraction studies using stable isotopes, Plant Soil, 111, 217–221, https://doi.org/10.1007/BF02139942, 1988.

Dansgaard, W.: Stable isotopes in precipitation, Tellus, 16, 436–468, https://doi.org/10.1111/j.2153-3490.1964.tb00181.x, 1964.

Dawson, T. E., and Ehleringer, J. R.: Streamside trees that do not use stream water, Nature, 350, 335–337, https://doi.org/10.1038/350335a0, 1991.

Dubbert, M., Caldeira, M. C., Dubbert, D., and Werner, C.: A pool-weighted perspective on the two-water-worlds hypothesis, New Phytologist, 222, 1271–1283, https://doi.org/10.1111/nph.15670, 2019.

Dütsch, M., Pfahl, S., and Sodemann, H.: The Impact of Nonequilibrium and Equilibrium Fractionation on Two Different Deuterium Excess Definitions. Journal of Geophysical Research: Atmospheres, 122, 12,732–12,746, https://doi.org/10.1002/2017JD027085, 2017.

Eggemeyer, K. D., Awada, T., Harvey, F. E., Wedin, D. A., Zhou, X., and Zanner, C.W.: Seasonal Changes in Depth of Water Uptake for Encroaching Trees *Juniperus Virginiana* and *Pinus Ponderosa* and Two Dominant C_4 Grasses in a Semiarid Grassland, Tree Physiology, 29, 157–169, https://doi.org/10.1093/treephys/tpn019, 2009.

Engel, M., Frentress, J., Penna, D., Andreoli, A., van Meerveld, I., Zerbe, S., Tagliavini, M., and Comiti, F.: How do geomorphic characteristics affect the source of tree water uptake in restored river floodplains? Ecohydrology, 15, e2443, https://doi.org/10.1002/eco.2443, 2022.

Evaristo, J., Jasechko, S., and McDonell, J. J.: Global separation of plant transpiration from groundwater and streamflow, Nature, 525, 91–94, https://doi.org/10.1038/nature14983, 2015.

Falatkova, K., Šípek, V., Vlček, L., Kocum, J., and Pivokonský, M.: Hydrological balance and runoff from a montane peat bog traced by water temperature, Hydrological Sciences Journal, 69, 393–406, https://doi.org/10.1080/02626667.2024.2320392, 2024.

Falátková, K., Šobr, M., Slavík, M., Bruthans, J., and Janský, B.: Hydrological characterization and connectivity of proglacial lakes to a stream, Adygine ice-debris complex, northern Tien Shan. Hydrological Sciences Journal, 65, 610–623, https://doi.org/10.1080/02626667.2020.1711913, 2020.

Floriancic, M. G., Allen, S. T., and Kirchner, J. W.: Isotopic evidence for seasonal water sources in tree xylem and forest soils, Ecohydrology, 17, e2641, https://doi.org/10.1002/eco.2641, 2024.

Froehlich, K., Gibson, J. J., and Aggarwal, P. K.: Deuterium Excess in Precipitation and its Climatological Significance (IAEA-CSP—13/P). International Atomic Energy Agency (IAEA), ISBN 92-0-116402-5, 2002.

Gaj, M., Kaufhold, S., and McDonnell, J. J.: Potential limitation of cryogenic vacuum extractions and spiked experiments, Rapid Communication in Mass Spectroscopy, 31, 821–823, https://doi.org/10.1002/rcm.7850, 2017.

Gat, J. R.: Oxygen and Hydrogen Isotopes in the Hydrologic Cycle. Annual Review of Earth and Planetary Sciences, 24, 225–262, https://doi.org/10.1146/annurev.earth.24.1.225, 1996.

Garvelmann, J., Külls, C., and Weiler, M.: A Porewater-Based Stable Isotope Approach for the Investigation of Subsurface Hydrological Processes. Hydrological and Earth System Science, 16, 631–640, https://doi.org/10.5194/hess-16-631-2012, 2012.

Gebrechorkos, S. H., Sheffield, J., Vicente-Serrano, S. M., Funk, C., Miralles, D. G., Peng, J., Dyer, E., Talib, J., Beck, H. E., Singer, M. B., and Dadson, S. J.: Warming accelerates global drought severity, Nature, 642, 628–635, https://doi.org/10.1038/s41586-025-09047-2, 2025.

Genthon, P., Bataille, A., Fromant, A., D'Hulst, D., and Bourges, F.: Temperature as a marker for karstic waters hydrodynamics. Inferences from 1 year recording at La Peyrére cave (Ariège, France). Journal of Hydrology, 311, 157–171, https://doi.org/10.1016/j.jhydrol.2005.01.015, 2005.

Geris, J., Tetzlaff, D., McDonell, J. J., Anderson, J., Paton, G., and Soulsby, C.: Ecohydrological separation in wet, low energy northern environments? A preliminary assessment using different soil water extraction techniques, Hydrological Processes, 15, 5139–5152, https://doi.org/10.1002/hyp.10603, 2015.

Gessler, A., Bachli, L., Freund, E. R., Treydte, K., Schaub, M., Haeni, M., Weiler, M., Seeger, S., Marshall, J., Hug, C., Zweifel, R., Hagedorn, F., Rigling, A., Saurer, M., and Meusburger, K.: Drought reduces water uptake in beech from the drying topsoil, but no compensatory uptake occurs from deeper soil layers, New Phytologist, 233, 194–206, https://doi.org/10.1111/nph.17767, 2022.

Goebel, T. S., and Lascano, R. J.: System for High Throughput Water Extraction from Soil Material for Stable Isotope Analysis of Water. Journal of Analytical Sciences, Methods and Instrumentation, 2, 203–207, https://doi.org/ 10.4236/jasmi.2012.24031, 2012.

Goldsmith, G. R., Muñoz-Villers, L. E., Holwerda, F., McDonell, J. J., Asbjornsen, H., and Dawson, T. E.: Stable isotopes reveal linkages among ecohydrological processes in a seasonally dry tropical montane cloud forest, Ecohydrology, 5, 779–790, https://doi.org/10.1002/eco.268, 2012.

Gosling, S. N. and Arnell, N. W.: A global assessment of the impact of climate change on water scarcity. Climatic Change, 134, 371–385, https://doi.org/10.1007/s10584-013-0853-x, 2016.

Gradmann, H.: Untersuchungen über die Wasserverhältnisse des Bodens als Grundlage des Pflanzenwachstums, Jahrbücher für wissenschaftliche Botanik, 69,1-100, 1928.

Gronevelt, P. H., and Grant, C. D.: A new model for the soil-water retention curve that solves the problem of residual water contents, European Journal of Soil Science, 55, 479–485, https://doi.org/10.1111/j.1365-2389.2004.00617.x, 2004.

Gupta, R. S.: Hydrology and hydraulic systems. Waveland Press, Long Grove, ISBN 1-4786-3091-4, 2016.

Hackmann, C. A., Paligi, S. S., Mund, M., Hölscher, D., Leuschner, C., Pietig, K., and Ammer, C.: Root water uptake depth in temperate forest trees: species-specific patterns shaped by neighbourhood and environment, Plant biology, Advance online publication, https://doi.org/10.1111/plb.70058, 2025.

Harper, W. V.: Reduced Major Axis Regression: Teaching Alternatives to Least Squares, Wiley StatsRef: Statistics Reference Online, https://doi.org/10.1002/9781118445112.stat07912, 2016.

Harpold, A. A., Kaplan, M. L., Klos, P. Z., Link, T., McNamara, J. P., Rajagopal, S., Schumer, R., and Steele, C. M.: Rain or snow: hydrologic processes, observations, prediction, and research needs, Hydrology and Earth System Sciences, 21, 1–22, https://doi.org/10.5194/hess-21-1-2017, 2017.

Hendry, M. J., Schmeling, E., Wassenaar, L. I., Barbour, S. L., and Pratt, D.: Determining the stable isotope composition of pore water from saturated and unsaturated zone core: improvements to the direct vapour equilibration laser spectrometry method, Hydrology and Earth System Sciences, 19, 4427–4440, https://doi.org/10.5194/hess-19-4427-2015, 2015.

Hervé-Fernández, P., Oyarzún, C., Brumbt, C., Bodé, H. S., Verhoest, N. E. C., and Boeckx, P.: Assessing the ‘two water worlds‘ hypothesis and water sources for native and exotic evergreen species in south central Chile, Hydrological Processes, 15, 4227–4241, https://doi.org/10.1002/hyp.10984, 2016.

Hossein, T.: Climate change impact on flood and extreme precipitation increases with water availability, Scientific Reports, 10, 13768, https://doi.org/10.1038/s41598-020-70816-2, 2020.

Hsieh, J. C. C., Savin, S. M., Kelly, E. F., and Chadwick, O. A.: Measurement of soil-water $\delta^{18}O$ values by direct equilibration with CO_2, Geoderma, 82, 255–268, https://doi.org/10.1016/S0016-7061(97)00104-3, 1998.

Iglesias, A., Garrote, L., Flores, F., and Moneo, M.: Challenges to manage the risk of water scarcity and climate change in the Mediterranean. Water Resources Management, 21, 775–788, https://doi.org/10.1007/s11269-006-9111-6, 2007.

Ignatev, A., Velivetckaia, T., Sugimoto, A., and Ueta, A.: A soil water distillation technique using He-purging for stable isotope analysis, Journal of Hydrology, 498, 265–273, https://doi.org/10.1016/j.jhydrol.2013.06.032, 2013.

James, E. R., Manga, M., Rose, T. P., and Hudson, G. B.: The use of temperature and the isotopes of O, H, C, and noble gases to determine the pattern and spatial extent of groundwater flow, Journal of Hydrology, 237, 100–112, https://doi.org/10.1016/S0022-1694(00)00303-6, 2000.

Jarvis, P.G.: The interpretation of the variations in leaf water potential and stomatal conductance found in canopies in the field, Philosophical Transactions of the Royal Society B, 273, 593–610, https://doi.org/10.1098/rstb.1976.0035, 1976.

Jenicek, M., Hnilica, J., Nedelcev, O., Sipek, V.: Future changes in snowpack will impact seasonal runoff and low flows in Czechia, Journal of Hydrology: Regional Studies, 37, 100899, https://doi.org/10.1016/j.ejrh.2021.100899, 2021.

Jenicek, M., and Ledvinka, O.: Importance of snowmelt contribution to seasonal runoff and summer low flows in Czechia, Hydrology and Earth System Sciences, 24, 3475–3491, https://doi.org/10.5194/hess-24-3475-2020, 2020.

Jenicek, M., Seibert, J., and Staudinger, M.: Modeling of Future Changes in Seasonal Snowpack and Impacts on Summer Low Flows in Alpine Catchments, Water Resources Research, 54, 538–556, https://doi.org/10.1002/2017WR021648, 2018.

Jenicek, M., Seibert, J., Zappa, M., Staudinger, M., and Jonas, T.: Importance of maximum snow accumulation for summer low flows in humid catchments, Hydrology and Earth System Sciences, 20, 859–874, https://doi.org/10.5194/hess-20-859-2016, 2016.

Jiao, W., Wang, L., Smith, W. K., Chang, Q., Wang, H., and D'Odorico, P.: Observed increasing water constraint on vegetation growth over the last three decades, Nature Communication, 12, 3777, https://doi.org/10.1038/s41467-021-024016-9, 2021.

Jouzel, J., and Merlivat, L.: Deuterium and Oxygen 18 in Precipitation: Modeling of the Isotopic Effects During Snow Formation. Journal of Geophysical Research: Atmospheres, 89, 11,749–11,757, https://doi.org/10.1029/JD089iD07p11749, 1984.

Jusserand, C.: Pore water extraction from sediment and soil: Oxygen-18 abundances comparisons between different techniques. First results, Catena, 7, 87–96, https://doi.org/10.1016/S0341-8162(80)80006-3, 1980.

Käss, W.: Tracing Technique in Geohydrology, Balkema, Rotterdam, 602 p., https://doi.org/10.1201/9780203735282, 1998.

Kelln, C. J., Wassenaar, L. I., and Hendry, M. J.: Stable Isotopes ($\delta^{18}O$, $\delta^{2}H$) of Pore Waters in Clay-Rich Aquitards: A Comparison and Evaluation of Measurement Techniques, Ground Water Monitoring and Remediation, 21, 108–116, https://doi.org/10.1111/j.1745-6592.2001.tb00306.x, 2001.

Karl, T. R., Gleason, B. E., Menne, M. J., McMahon, J. R., Heim Jr., R. R., Brewer, M. J., Kunkel, K. E., Arndt, D. S., Privette, J. L., Bates, J. J., Groisman, P. Y., and Easterling, D.

R.: U.S. temperature and drought: Recent anomalies and trends, Eos, 93, 473–474, https://doi.org/10.1029/2012EO470001, 2012.

Kendall, C., and Coplen, T. B.: Distribution of Oxygen-18 and Deuterium in River Waters Across the United States. Hydrological Processes, 15, 1,363–1,393, https://doi.org/10.1002/hyp.217, 2001.

Kendall, C. and Coplen, T. B.: Multi-sample conversion of water to hydrogen by zinc for stable isotope determination, Analytical Chemistry Journal, 57, 1437–1440, https://doi.org/10.1021/ac00284a058, 1985.

Keys, W. S. and Brown, R. F.: The use of temperature logs to trace the movement of injected water, Groundwater, 16, 32–48. https://doi.org/10.1111/j.1745-6584.1978.tb03201.x, 1987.

Kinzinger, L., Mach, J., Haberstroh, S., Schindler, Z., Frey, J., Dubbert, M., Seeger, S., Seifert, T., Weiler, M., Orlowski, N., Werner, C., and Meinzer, F.: Interaction between beech and spruce trees in temperate forests affects water use, root water uptake pattern and canopy structure, Tree Physiology, 44, tpad144, https://doi.org/10.1093/treephys/tpad144, 2024.

Kirchner, J. W.: Aggregation in environmental systems – Part 1: Seasonal tracer cycles quantify young water fractions, but not mean transit times, in spatially heterogeneous catchments, Hydrology and Earth System Sciences, 20, 279–297, https://doi.org/10.5194/hess-20-279-2016, 2016a.

Kirchner, J. W.: Aggregation in environmental systems – Part 2: Catchment mean transit times and young water fractions under hydrologic nonstationarity, Hydrology and Earth System Sciences, 20, 299–328, https://doi.org/10.5194/hess-20-299-2016, 2016b.

Kocum, J., Haidl, J., Gebousky, O., Falatkova, K., Sipek, V., Sanda, M., Orlowski, N., and Vlcek, L.: Technical note: A new laboratory approach to extract soil water for stable isotope analysis from large soil samples, Hydrology and Earth System Sciences, 29, 2863–2880, https://doi.org/10.5194/hess-29-2863-2025, 2025.

Koehler, G., Wassenaar, L. I., and Hendry, M. J.: An Automated Technique for Measuring δD and $\delta^{18}O$ Values of Porewater by Direct CO_2 and H_2 Equilibration, Analytical Chemistry, 72, 5,659–5,664, https://doi.org/10.1021/ac000498n, 2000.

Koeniger, P., Marshall, J. D., Link, T., and Mulch, A.: An Inexpensive, Fast and Reliable Method for Vacuum Extraction of Soil and Plant Water for Stable Isotope Analysis by Mass Spectrometry. Rapid Communication in Mass Spectrometry, 25, 3,041–3,048, https://doi.org/10.1002/rcm.5198, 2011.

Landwehr, J. M., and Coplen, T. B.: Line-condition excess: A new method for characterizing stable hydrogen and oxygen isotope ratios in hydrologic systems, Isotopes in Environmental Studies, Edition: 1, IAEA, ISBN: 92-0-111305-X, 2006.

Lin, G., Stenberg, L. da S. L.: Hydrogen Isotopic Fractionation by Plant Roots During Water Uptaken in Costal Wetland Plants, Stable Isotopes and Plant Carbon-water Relations, 31, 497–510, https://doi.org/10.1016/B978-0-08-091801-3.50041-6, 1993.

Liu, Q., Peng, C., Schneider, R., Cyr, D., McDowell, N. G., and Kneeshaw, D.: Drought-induced increase in tree mortality and corresponding decrease in the carbon sink capacity of Canada's boreal forests from 1970 to 2020, Global Change Biology, 29, 2274–2285, https://doi.org/10.1111/gcb.16599, 2023.

Liu, Y., Pan, Z., Zhuang, Q., Miralles, D. G., Teuling, A. J., Zhang, T., An, P., Dong, Z., Zhang, J., He, D., Wang, L., Pan, X., Bai, W., and Niyogi, D.: Agriculture intensifies soil moisture decline in Northern China, Scientific reports, 5, 11261, https://doi.org/10.1038/srep11261, 2015.

Lopez, M. G., Vis, M., Jenicek, M., Griessinger, N., and Seibert, J.: Assessing the degree of detail of temperature-based snow routines for runoff modelling in mountainous areas in central Europe, Hydrology and Earth System Sciences, 24, 4441–4461, https://doi.org/10.5194/hess-24-4441-2020, 2020.

Lüthi, M. P.: Stream gauge calibration of a cave stream using water temperature variability as a tracer, Water Resources Research, 55, 5738–5750, https://doi.org/10.1029/2018WR023762, 2019.

Majoube, M.: Oxygen-18 and Deuterium Fractionation Between Water and Steam. Journal de chimie physique et physico-chimie biologique, 68, 1,423–1,436, https://doi.org/10.1051/jcp/1971681423, 1971.

Mancosu, N., Synder, R. L., Kyriakakis, G., and Spano, D.: Water scarcity and future challenges for food production, Water, 7, 975–992, https://doi.org/10.3390/w7030975, 2015.

Mankin, J. S., Seager, R., Smerdon, J. E., Cook, B. I., and Williams, A. P.: Mid-latitude freshwater availability reduced by projected vegetation responses to climate change, Nature Geoscience, 12, 983–988, https://doi.org/10.1038/s41561-019-0480-x, 2019.

Marty, C., Tilg, A. M., and Jonas, T.: Recent Evidence of Large-Scale Receding Snow Water Equivalents in the European Alps, Journal of Hydrometeorology, 18, 1021–1031, https://doi.org/10.1175/JHM-D-16-0188.1, 2017.

Matsuhisa, Y., Goldsmith, J. R., and Clayton, R. N.: Mechanism of Hydrothermal Crystallization of Quartz at 250 °C and 15 kbar. Geochimica et Cosmochimica Acta, 42, 173–182, https://doi.org/10.1016/0016-7037(78)90130-8, 1978.

McDonnell, J. J., McGuire, K., Aggarwal, P., Beven, K. J., Biondi, D., Destouni, G., Dunn, S., James, A., Kirchner, J., Kraft, P., Lyon, S., Maloszewski, P., Newman, B., Pfister, L., Rinaldo, A., Rodhe, A., Sayama, T., Seibert, J., Solomon, K., Soulsby, C., Stewart, M., Tetzlaff, D., Tobin, C., Troch, M., Weiler, M., Western, A., Wörman, A., and Wrede, S.: How Old is Streamwater? Open Questions in Catchment Transit Time Conceptualization, Modeling and Analysis. Hydrological Processes, 24, 1,745–1,754, https://doi.org/10.1002/hyp.7796, 2010.

McDonnell, J.J.: The Two Water Worlds Hypothesis: Ecohydrological Separation of Water Between Streams and Trees? Wiley Interdisciplinary Reviews, 1, 323–329, https://doi.org/10.1002/wat2.1027, 2014.

McGuire, K. J., and McDonell, J. J.: A Review and Evaluation of Catchment Transit Time Modeling, Journal of Hydrology, 330, 543–563, https://doi.org/10.1016/j.jhydrol.2006.04.020, 2006.

McKee, T. B., Doesken, N. J., and Kleist, J.: The relationship of drought frequency and duration to time scales, 8th Conference on Applied Climatology, Anaheim, 17-22 January 1993, 179–184, 1993.

McMahon, S. M., Arellano, G., and Davies, S. J.: The importance and challenges of detecting changes in forest mortality rates, Ecosphere, 10, e02615, https://doi.org/10.1002/ecs2.2615, 2019.

Mekonnen, M. M. and Hoekstra, A. Y.: Four billion people facing severe water scarcity. Science Advances, 2, e1500323, https://doi.org/10.1126/sciadv.1500323, 2016.

Molz, J. F.: Models of water transport in the soil-plant system: A review, Water Resources Research, 17, 1245–1260, https://doi.org/10.1029/WR017i005p01245, 1981.

Mubarak, A. and Olsen, R.: Immiscible displacement of soil solution by centrifugation, Soil Science Society of America Journal, 40, 329–331, 1976.

Mueller, M. H., Alaoui, A., Kuells, C., Leistert, H., Meusburger, K., and Stumpp, C.: Tracking Water Pathways in Steep Hillslopes by $\delta^{18}O$ Depth Profiles of Soil Water. Journal of Hydrology, 519, 340–352, https://doi.org/10.1016/j.jhydrol.2014.07.031, 2014.

Munksgaard, N. C., Cheesman, A. W., Wurster, C. M., Cernusak, L. A., and Bird, M. I.: Microwave extraction–isotope ratio infrared spectroscopy (ME-IRIS): a novel technique for rapid extraction and in-line analysis of $\delta^{18}O$ and $\delta^{2}H$ values of water in plants, soils and insects, Rapid Communication in Mass Spectroscopy, 28, 2151–2161, https://doi.org/10.1002/rcm.7005, 2014.

Musselmann, K. N., Clark, M. P., Liu, C., Ikeda, K., and Rasmussen, R.: Slower snowmelt in a warmer world, Nature Climate Change, 7, 214–219, https://doi.org/10.1038/nclimate3225, 2017.

Noone, D., Risi, C., Bailey, A., Berkelhammer, M., Brown, D. P., Buenning, N., Gregory, S., Nusbaumer, J., Schneider, D., Sykes, J., Vanderwende, B., Wong, J., Meillier, Y., and Wolfe, D.: Determining Water Source in the Boundary Layer from Tall Tower Profiles of Water Vapor and Surface Water Isotope Ratios after a Snowstorm in Colorado. Atmospheric Chemistry and Physics, 12, 16,327-16,375, https://doi.org/10.5194/acp-13-1607-2013, 2013.

Orlowski, N., and Breuer, L.: Sampling Soil Water Along pF Curve for $\delta^{2}H$ and $\delta^{18}O$ Analysis. Hydrological Processes, 34, 4,959–4,972, Hydrological Precesses, https://doi.org/10.1002/hyp.13916, 2020.

Orlowski, N., Breuer, L., Angeli, N., Boeckx, P., Brumbt, C., Cook, C. S., Dubbert, M., Dyckmans, J., Gallagher, B., Gralher, B., Herbstritt, B., Hervé-Fernández, P., Hissler, C., Koeniger, P., Legout, A., Macdonald, C. J., Oyarzún, C., Redelstein, R., Seidler, C., Siegwolf, R., Stumpp, C., Thomsen, S., Weiler, M., Werner, C., and McDonnell, J. J.: Inter-laboratory comparison of cryogenic water extraction systems for stable isotope analysis of soil water, Hydrology and Earth System Sciences, 22, 3619–3637, https://doi.org/10.5194/hess-22-3619-2018, 2018.

Orlowski, N., Breuer, L., and McDonell, J. J.: Critical issues with cryogenic extraction of soil water for stable isotope analysis, Ecohydrology, 9, 3–10, https://doi.org/10.1002/eco.1722, 2016.

Orlowski, N., Frede, H. G., Brüggemann, N., and Breuer, L.: Validation and Application of a Cryogenic Vacuum Extraction System for Soil and Plant Water Extraction for Isotope Analysis. Journal of Sensors and Sensor Systems, 2, 179–193, https://doi.org/10.5194/jsss-2-179-2013, 2013.

Padrón, R.S., Gudmundsson, L., Decharme, B., Ducharne, A., Lawrence, D. M., Mao, J., Peano, D., Krinner, G., Kim, H., and Seneviratne, S. I.: Observed changes in dry-season water availability attributed to human-induced climate change. Nature Geoscience, 13, 477–481, https://doi.org/10.1038/s41561-020-0594-1, 2020.

Peleg, N., Koukoula, M., and Marra, F.: A 2°C warming can double the frequency of extreme summer downpours in the Alps, npj Climate and Atmospheric Science, 8, 216, https://doi.org/10.1038/s41612-025-01081-1, 2025.

Penna, D., Geris, J., Hopp, L., and Scandellari, F.: Water sources for root water uptake: Using stable isotopes of hydrogen and oxygen as a research tool in agricultural and agroforestry systems, Agriculture Ecosystems Environment, 291, https://doi.org/10.1016/j.agee.2019.106790, 2020.

Penna, D., and van Meerveld, H. J.: Spatial Variability in the Isotopic Composition of Water in Small Catchments and its Effect on Hydrograph Separation, WIREs Water, 6, e1367, https://doi.org/10.1002/wat2.1367, 2019.

Peters, L. I., and Yakir, D.: A Direct and Rapid Leaf Water Extraction Method for Isotopic Analysis, Rapid Communication in Mass Spectrometry, 22, 2,929–2,936, https://doi.org/10.1002/rcm.3692, 2008.

Plavcová, L., Hronková, M., Šimková, M., Květoň, J., Vráblová, M., Kubásek, J., and Šantrůček, J.: Seasonal variation of $\delta^{18}O$ and $\delta^{2}H$ in leaf water of *Fagus sylvatica* L. and related water compartments, Journal of Plant Physiology, 227, 56–65, https://doi.org/10.1016/j.jplph.2018.03.009, 2018.

Pokhrel, Y., Felfelani, F., Satoh, Y., Boulange, J., Burek, P., Gädeke, A., Gerten, D., Gosling, S. N., Grillakis, M., Gudmundsson, L., Hanasaki, N., Kim, H., Koutroulis, A., Liu, J., Papadimitriou, L., Schewe, J., Schmied, H. M., Stacke, T., Telteu, C. E., Thiery, W., Veldkamp, T., Zhao, F., and Wada, Y.: Global terrestrial water storage and drought severity under climate change, Nature Climate Change, 11, 226–233, https://doi.org/10.1038/s41558-020-00972-w, 2021.

Powell, T. L., Galbraith, D. R., Christoffersen, B. O., Harper, A., Imbuzeiro, H. M. A., Rowland, L., Almeida, S., Brando, P. M., da Costa, A. C. L., Costa, M. H., Levine, N. M., Malhi, Y., Saleska, S. R., Sotta, E., Williams, M., Meir, P., and Moorcroft, P. R.: Confronting model predictions of carbon fluxes with measurements of Amazon forests subjected to experimental drought, New Phytologist, 2, 350–365, https://doi.org/10.1111/nph.12390, 2013.

Qin, Y., Abatzoglou, J. T., Siebert, S., Huning, L. S., AghaKouchak, A., Mankin, J. S., Hong, C., Tong, D., Davis, S. J., and Mueller, N. D.: Agricultural risks from changing snowmelt, Nature Climate Change, 10, 459–465, https://doi.org/10.1038/s41558-020-0746-8, 2020.

Revesz, K. and Woods, P. H.: A method to extract soil water for stable isotope analysis, Journal of Hydrology, 115, 397–406, https://doi.org/10.1016/0022-1694(90)90217-L, 1990.

Rossatto, D. R., Silva, L. de C. R., Villalobos-Vega, R., Sternberg L. da S. L., and Franco, A. C.: Depth of water uptake in woody plants relates to groundwater level and vegetation structure along a topographic gradient in a neotropical savanna, Envirnmental and Experimental Botany, 77, 259–266, https://doi.org/10.1016/j.envexpbot.2011.11.025, 2012.

Rothfuss, Y., Merz, S., Vanderborght, J., Hermes, N., Weuthen, A., Pohlmeier, A., Vereecken, H., and Brüggemann, N.: Long-term and high-frequency non-destructive monitoring of

water stable isotope profiles in an evaporating soil column, Hydrology and Earth System Sciences, 19, 4067–4080, https://doi.org/10.5194/hess-19-4067- 2015, 2015.

Rothfuss, Y., Vereecken, H., and Brüggemann, N.: Monitoring water stable isotopic composition in soils using gas-permeable tubing and infrared laser absorption spectroscopy, Water Resources Research, 49, 1–9, https://doi.org/10.1002/wrcr.20311, 2013.

Rothfuss, Y., Braud, I., Le Moine, N., Biron, P., Durand, J. L., Vauclin, M., and Bariac, T.: Factors Controlling the Isotopic Partitioning Between Soil Evaporation and Plant transpiration: Assessment Using a Multi-Objective Calibration of SiSPATIsotope Under Controlled Conditions. Journal of Hydrology, 442–443, 75–88, https://doi.org/10.1016/j.jhydrol.2012.03.041, 2012.

Roudier, P., Ducharne, A., and Feyen, L.: Climate change impacts on runoff in West Africa: a review, Hydrology and Earth System Sciences, 18, 2789–2801, https://doi.org/10.5194/hess-18-2789-2014, 2014.

Rozanski, K., Araguás-Araguás, L., and Gonfiantini, R.: Isotopic Patterns in Modern Global Precipitation, Climate Change in Continental Isotopic Records, 78, https://doi.org/10.1029/GM078p0001, 1993.

Safeeq, M., Shukla, S., Arismendi, I., Grant, G. E., Lewis, S. L., and Nolin, A.: Influence of winter season climate variability on snow-precipitation ratio in the western United States, International Journal of Climatology, 36, 3175–3190, https://doi.org/10.1002/joc.4545, 2015.

Samaniego, L., Thober, S., Kumar, R., Wanders, N., Rakovec, O., Pan, M., Zink, M., Sheffield, J., Wood, E. F., and Marx, A.: Anthropogenic warming exacerbates European soil moisture droughts, Nature Climate Change, 8, 421–426, https://doi.org/10.1038/s41558-018-0138-5, 2018.

Šantrůček, J., Šantrůčková, H., Kaštovská, E. and Vráblová, M.: Stabilní izotopy biogenních prvků: Použití v biologii a ekologii. Academia, 175 s., ISBN 978-80-200-2772-6, 2018.

Schneider, P., Pool, S., Strouhal, L., and Seibert, J.: True colors – experimental identification of hydrological processes at a hillslope prone to slide, Hydrol. Earth Syst. Sci., 18, 875–892, https://doi.org/10.5194/hess-18-875-2014, 2014.

Scrimgeour, C. M.: Measurement of plant and soil water isotope composition by direct equilibration methods, Journal of Hydrology, 172, 261–274, https://doi.org/10.1016/0022-1694(95)02716-3, 1995.

Seneviratne, S. I., Corti, T., Davin, E. L., Hirschi, M., Jaeger, E. B., Lehner, I., Orlowsky, B., and Teuling, A. J.: Investigating soil moisture–climate interactions in a changing climate: A review, Earth-Science Reviews, 99, 125–161, https://doi.org/10.1016/j.earscirev.2010.02.004, 2010.

Seyedsadr, S., Šípek, V., Jačka, L., Sněhota, M., Beesley, L., Pohořelý, M., Kovář, M., and Trakal, L.: Biochar considerably increases the easily available water and nutrient content in low-organic soils amended with compost and manure, Chemosphere, 293, 133586, https://doi.org/10.1016/j.chemosphere.2022.133586, 2022.

Shanley, J. B. and Peters, N. E.: Preliminary observations of streamflow generation during storms in a forested Piedmont watershed using temperature as a tracer, Journal of

Contaminant Hydrology, 3, 349–365, https://doi.org/10.1016/0169-7722(88)90040-X, 1988.

Sheffield, J., Wood, E. F., and Roderick, M. L.: Little change in global drought over the past 60 years, Nature, 491, 435–438, https://doi.org/10.1038/nature11575, 2012.

Shukla, S., and Wood, A. W.: Use of a standardized runoff index for characterizing hydrologic drought, Geophysical Research Letters, 35, https://doi.org/10.1029/2007GL032487, 2008.

Šípek, V., Jenicek, M., Hnilica, J., and Zelíková, N.: Catchment Storage and its Influence on Summer Low Flows in Central European Mountainous Catchments, Water Resources Management, 35, 2829–2843, https://doi.org/10.1007/s11269-021-02871-x, 2021.

Šípek, V., Jačka, L., Seyedsadr, S., and Trakal, L.: Manifestation of Spatial and Temporal Variability of Soil Hydraulic Properties in the Uncultivated Fluvisol and Performance of Hydrological Model, Catena, 182, 104119, https://doi.org/10.1016/j.catena.2019.104119, 2019.

Soulsby, C., Malcolm, R., Helliwell, R., Ferrier, R. C., and Jenkins, A.: Isotope hydrology of the Allt a'Mharcaidh catchment, Cairngorms, Scotland, implications for hydrologic pathways and residence times, Hydrological Processes, 14, 747–762 https://doi.org/10.1002/(SICI)1099-1085(200003)14:4<747::AID-HYP970>3.0.CO;2-0, 2000.

Sprenger, M., Stumpp, C., Weiler, M., Aeschbach, W., Allen, S. T., Benettin, P., Dubbert, M., Hartmann, A., Hrachowitz, M., Kirchner, J. W., McDonell, J. J., Orlowski, N., Penna, D., Pfahl, S., Rinderer, M., Rodriguez, N., Schmidt, M., and Werner, C.: The Demographics of Water: A Review of Water Ages in the Critical Zone, Review of Geophysics, 57, 800–834, https://doi.org/10.1029/2018RG000633, 2019.

Sprenger, M., Tetzlaff, D., Buttle, J., Laudon, H., Leistert, H., Mitchell, C. P. J., Snelgrove, J., Weiler, M., and Soulsby, C.: Measuring and Modeling Stable Isotopes of Mobile and Bulk Soil Water. Vadose zone journal, 17, 1–18, https://doi.org/10.2136/vzj2017.08.0149, 2018.

Sprenger, M., Herbstritt, B., and Weiler, M.: Established Methods and New Opportunities for Pore Water Stable Isotope Analysis, Hydrological Processes, 29, 5,174–5,192, https://doi.org/10.1002/hyp.10643, 2015a.

Sprenger, M., Volkmann, T. H. M., Blume, T., and Weiler. M.: Estimating Flow and Transport Parameters in the Unsaturated Zone with Pore Water Stable Isotopes. Hydrology and Earth System Sciences, 19, 2,617–2,635, https://doi.org/10.5194/hess-19-2617-2015, 2015b.

Starostová, M.: Měření srážek totalizátory na Šumavě (Precipitation measurement with rain gauges at the Bohemian Forest). Meteorologické zprávy, 65, 180–183. (In Czech), 2012.

Stewart, M. K.: Stable Isotope Fractionation due to Evaporation and Isotopic Exchange of Falling Waterdrops: Applications to Atmospheric Processes and Evaporation of Lakes. Journal of Geophysical Research: Atmospheres, 80, 1,133–1,146, https://doi.org/10.1029/JC080i009p01133, 1975.

Stratton, L., Goldstein, G., and Meinzer, F. C.: Stem water storage capacity and efficiency of water transport: their functional significance in a Hawaiian dry forest, Plant, Cell and Environment, 23, 99–106, https://doi.org/10.1046/j.1365-3040.2000.00533.x, 2001.

Teuling, A. J., van Loon, A. F., Seneviratne, S. I., Lehner, I., Aubinet, M., Heinesch, B., Bernhofer, C., Grünwald, T., Prasse, H., and Spank, U.: Evapotranspiration amplifies

European summer drought, Geophysical Research Letters, 40, 2071–2075, https://doi.org/10.1002/grl.50495, 2013.

Thiemens, M. H., Chakraborty, S., and Dominguez, G.: The Physical Chemistry of Mass-Independent Isotope Effects and their Observation in Nature. Annual Review of Physical Chemistry, 63, 155–177, https://doi.org/10.1146/annurev-physchem-032511-143657, 2012.

Thiemens, M. H., and Heidenreich, J. E.: The Mass-Independent Fractionation of Oxygen: A Novel Isotope Effect and its Possible Cosmochemical Implications. Science, 219, 1,073–1,075, https://doi.org/10.1126/SCIENCE.219.4588.1073, 1983.

Thorburn, P. J., Walker, G. R., and Brunel, J. P.: Extraction of Water form Eucalyptus Trees for Analysis of Deuterium and Oxygen-18: Laboratory and Field Techniques, Plant, Cell & Environment, 16, 269–277, https://doi.org/10.1111/j.1365-3040.1993.tb00869.x, 1993.

Tinker, P. B.: Transport of water to plant root in soil, Philosophical Transactions of the Royal Society of London, 273, 445–461, https://doi.org/10.1098/rstb.1976.0024, 1976.

Tolasz, R., and Byštýřová, H.: Atlas podnebí Česka. Český hydrometeorologický ústav. Univerzita Palackého v Olomouci. Olomouc. 255 s. ISBN: 978-80-86690-26-1, 2007.

Trenberth, K. E., Dai, A., van der Schrier, G., Jones, P. D., Barichivich, J., Briffa, K. R., and Sheffield, J.: Global warming and changes in drought, 4, 17–22, https://doi.org/10.1038/nclimate2067, 2014.

Trnka, M., Brázdil, R., Možný, M., Štěpánek, P., Dobrovolný, P., Zahradníček, P., Balek, J., Semerádová, D., Dubrovský, M., Hlavinka, P., Eitzinger, J., Wardlow, B., Svoboda, M., Hayes, M., and Žalud, Z.: Soil moisture trends in the Czech Republic between 1961 and 2012, International Journal of Climatology, 35, 3733–3747, https://doi.org/10.1002/joc.4242, 20115.

Unkovich, M., Pate, J., McNeill, A., and Gibbs, J.: Stable Isotope Techniques in the Study of Biological Processes and Functioning of Ecosystems, Annals of Botany, 89, 499–500, https://doi.org/10.1093/aob/mcf058, 2002.

van Genuchten, M. T.: A Closed-form Equation for Predicting the Hydraulic Conductivity of Unsaturated Soils, Soil Science Society of America Journal, 44, 892–898, https://doi.org/10.2136/sssaj1980.03615995004400050002x, 1980.

van den Honert, T. H.: Water transport in plats as a catenary process, Discussions of the Faraday Society, 3, 146–153, https://doi.org/10.1039/DF9480300146, 1948.

van Vliet, M. T., Franssen, W. H. P., Yearsley, J. R., Ludwig, F., Haddeland, I., Letternmaier, D. P., and Kabat, P.: Global river discharge and water temperature under climate change, Global Environmental Change, 23, 450–464, https://doi.org/10.1016/j.gloenvcha.2012.11.002, 2013.

Vargas, A. I., Schaffer, B., Yuhong, L., and Sternberg, L. S. L.: Testing plant use of mobile vs immobile soil water sources using stable isotope experiments, New Phytologist, 215, 582–594, https://doi.org/10.1111/nph.14616, 2017.

Verhoef, A., and Egea, G.: Modeling plant transpiration under limited soil water: Comparison of different plant and soil hydraulic parameterizations and preliminary implications for their use in land surface models, Agricultural and Forest Meteorology, 191, 22–32, https://doi.org/10.1016/j.agrformet.2014.02.009, 2014.

Vicente-Serrano, S. M., Beguería, S., and López-Moreno, J. I.: A Multiscalar Drought Index Sensitive to Global Warming: The Standardized Precipitation Evapotranspiration Index, Journal of Climate, 23, 1696–1718, https://doi.org/10.1175/2009JCLI2909.1, 2010.

Vlček, L., Šípek, V., Kofroňová, J., Kocum, J., Doležal, T., and Janský, B.: Runoff formation in a catchment with Peat bog and Podzol hillslopes, Journal of Hydrology, 593, 125633, https://doi.org/10.1016/j.jhydrol.2020.125633, 2021.

Vlček, L., Falátková, K., and Schneider, P.: Identification of runoff formation with two dyes in a mid-latitude mountain headwater, Hydrology and Earth System Sciences, 21, 3025–3040, https://doi.org/10.5194/hess-21-3025-2017, 2017.

Voelker, S. L., Brooks, J. R., Meinzer, F. C., Roden, J., Pazdur, A., Pawelczyk, S., Hartsough, P., Snyder, K., Plavcová, L., and Šantrůček, J.: Reconstructing relative humidity from plant $\delta^{18}O$ and δD as deuterium deviations from the global meteoric water line. Ecological Applications, 25, 960–975, https://doi.org/10.1890/13-0988.1, 2014.

Volkmann, T. H. M., and Weiler, M.: Continual in Situ Monitoring of Pore Water Stable Isotopes in the Subsurface. Hydrological and Earth System Science, 18, 1,819–1,833, https://doi.org/10.5194/hess-18-1819-2014, 2014.

Wassenaar, L. I., Hendry, M. J., Chostner, V. L., and Lis, G. P.: High Resolution Pore Water $\delta 2H$ and $\delta 18O$ Mea- surements by $H_2O_{(liquid)}$-$H_2O_{(vapor)}$ Equilibration Laser Spectroscopy, Environ. Sci. Technol., 42, 9262–9267, https://doi.org/10.1021/es802065s, 2008.

Walker, C. D., and Richardson, S. B.: The Use of Stable Isotopes of Water In Characterising the Source of Water in Vegetation. Chemical Geology, Isotope Geoscience Section, 94, 145–158, https://doi.org/10.1016/0168-9622(91)90007-J, 1991.

Wang, X. F., and Yakir, D.: Using Stable Isotopes of Water in Evapotranspiration Studies, Hydrological Processes. 14, 1,407–1,421, https://doi.org/10.1002/1099-1085(20000615)14:8<1407::AID-HYP992>3.0.CO;2-K, 2000.

Weatherley, P. E.: Introduction: Water movement through plants, Philosophical Transactions of the Royal Society of London, 273, 435–444, https://doi.org/10.1098/rstb.1976.0023, 1976.

Weiler, M. and Flühler, H.: Inferring flow types from dye patterns in macroporous soils, Geoderma, 120, 137–153, https://doi.org/10.1016/j.geoderma.2003.08.014, 2004.

Weiler, M., McGlynn, B. L., McGuire, K. J., and McDonell, J. J.: How Does Rainfall Become Runoff? A Combined Tracer and Runoff Transfer Function Approach. Water Resources Research, 39, 1,315, https://doi.org/10.1029/2003WR002331, 2003.

Wershaw, R. L., Friedman, I., Heller, S. J., and Frank, P. A.: Hydrogen isotopic fractionation of water passing through trees, in: Advances in Organic Geochemistry: Proceedings of the Third International Congress, edited by: Hobson, F. and Speers, M., Pergamon Press Ltd., Elsevier, New York, USA, 55–67, https://doi.org/10.1016/B978-0-08-012758-3.50007-4, 1966.

West, A. G., Patrickson, S. J., and Ehleringer, J. R.: Water Extraction Times for Plant and Soil Materials Used in Stable Isotope Analysis, Rapid Communication in Mass Spectrometry, 20, 1,317–1,321, https://doi.org/10.1002/rcm.2456, 2006.

Wheeler, T. and Von Braun, J.: Climate change impacts on global food security. Science, 341, 508–513, https://doi.org/10.1126/science.1239402, 2013.

White, J. W. C., Cook, E. R., Lawrence, J. R., and Wallace, S. B.: The D/H Ratios of Sap in Trees: Implications for Water Sources and Tree Ring D/H Ratios, Geochimica et Cosmochimica Acta, 49, 237–246, https://doi.org/10.1016/0016-7037(85)90207-8, 1985.

Whitehead, P.G., Wilby, R. L., Battarbee, R. W., Kernan, M., and Wade, J.: A review of the potential impacts of climate change on surface water quality. Hydrological Sciences Journal, 54, 101–123, https://doi.org/10.1623/hysj.54.1.101, 2009.

Wienhöfer, J., Germer, K., Lindenmaier, F., Färber, A., and Zehe, E.: Applied tracers for the observation of subsurface stormflow at the hillslope scale, Hydrol. Earth Syst. Sci., 13, 1145–1161, https://doi.org/10.5194/hess-13-1145-2009, 2009.

Williams, D. G., and Ehleringer, J. R.: Intra- and Interspecific Variation for Summer Precipitation Use in Pinyon-Juniper Woodlands, Ecological Monographs, 70, 517–537, https://doi.org/10.1890/0012-9615(2000)070[0517:IAIVFS]2.0.CO;2, 2000.

Willibald, F., Kotlarski, S., Grêt-Regamey, A., and Ludwig, R.: Anthropogenic climate change versus internal climate variability: impacts on snow cover in the Swiss Alps, The Cryosphere, 14, 2909–2924, https://doi.org/10.5194/tc-14-2909-2020, 2020.

Worden, J., Noone, D.,and Bowman, K.: Importance of Rain Evaporation and Continental Convection in the Tropical Water Cycle, Nature, 445, 528–532, https://doi.org/10.1038/nature05508, 2007.

Xia, C., Zuecco, G., Marchina, C., Penna, D., and Borga, M.: Effects of Short-Term Climate Variations on Young Water Fraction in a Small Pre-Alpine Catchment, Water Resources Research, 60, e2023WR036245, https://doi.org/10.1029/2023WR036245, 2024.

Yang, Y., Peng, B., Guan, K., Pan, M., Franz, T. E., Cosh, M. H., and Bernacchi, C. J.: Within-field soil moisture variability and time-invariant spatial structures of agricultural fields in the US Midwest, Vadose Zone Journal, 23, e20337, https://doi.org/10.1002/vzj2.20337, 2024.

Yang, B., Dossa, G. G. O., Hu, Y. H., Liu, L. L., Meng, X. J., Du, Y. Y., Li, J. Y., Zhu, X. A., Zhang, Y. J., Singh, A. K., Yuan, X., Wu, J. E., Zakari, S., Liu, W. J., and Song, L.: Uncorrected soil water isotopes through cryogenic vacuum distillation may lead to a false estimation on plant water source, Method. Ecol. Evol., 6, 1443–1456, https://doi.org/10.1111/2041-210X.14107, 2023.

Yang, H., Auerswald, K., Bai, Y., and Han, X.: Complementarity in Water Sources Among Dominant Species in Typical Steppe Ecosystems of Inner Mongolia, China, Plant Soil, 340, 303–313, https://doi.org/10.1007/S11104-010-0307-4, 2011.

Young, E. D., Galy, A., and Nagahara, H.: Kinetic and Equilibrium Mass-Dependent Isotope Fractionation Laws in Nature and their Geochemical and Cosmochemical Signifikance, Geochimica et Cosmochimica Acta, 66, 1,095–1,104, https://doi.org/10.1016/S0016-7037(01)00832-8, 2002.

Yuan, X., and Wood, E. F.: Multimodel seasonal forecasting of global drought onset, Geophysical Research Letters, 40, 4900–4905, https://doi.org/10.1002/grl.50949, 2013.

Zajíček, A., Pomije, T., and Kvítek, T.: Event water detection in tile drainage runoff using stable isotopes and a water temperature in small agricultural catchment in Bohemian-Moravian Highlands, Czech Republic. Environmental Earth Sciences, 75, 1–13, https://doi.org/10.1007/s12665-016-5561-1, 2016.

Žák, K., Rohovec, J., and Navrátil, T.: Fluxes of Heavy Metals from a Highly Polluted Watershed During Flood Events: A Case Study of the Litavka River, Czech Republic, Water Air and Soil Pollution, 203, 343–358, https://doi.org/10.1007/s11270-009-0017-9, 2009.

Zhang, Q., Shao, M., Jia, X., and Wei, X.: Relationship of Climatic and Forest Factors to Drought- and Heat-Induced Tree Mortality, Plos, 12, e0169770, https://doi.org/10.1371/journal.pone.0169770, 2017.

Zhu, Q. Z., Sun, Q., Su, Z. G., Xie, M.-M., Song, J. Y., Shan, Y. B., Wang, N., and Chu, G. Q.: A Soil Water Extraction Method with Accelerated Solvent Extraction Technique for Stable Isotope Analysis, Chinese J. Anal. Chem., 42, 1270–1275, https://doi.org/10.1016/S1872-2040(14)60766-0, 2014.